

AD-A130 043

NUMERICAL SIMULATION OF SPACECRAFT CHARGING PHENOMENA
AT HIGH ALTITUDE...(U) YORK UNIV DOWNSVIEW (ONTARIO)
CENTRE FOR RESEARCH IN EXPERIME..

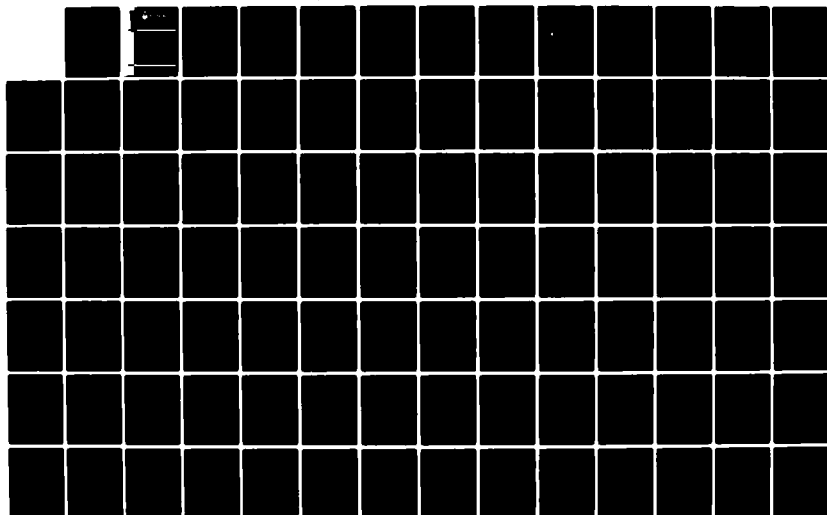
1/2

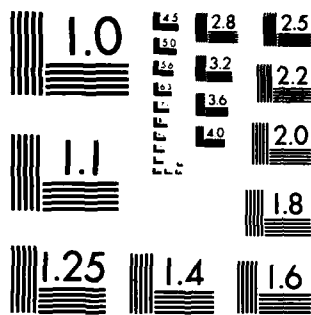
UNCLASSIFIED

J G LAFRAMBOISE ET AL. 10 AUG 82

F/G 22/2

NL





MICROCOPY RESOLUTION TEST CHART
NATIONAL BUREAU OF STANDARDS-1963-A

10



YORK
UNIVERSITY

ADA130049

NUMERICAL SIMULATION OF SPACECRAFT CHARGING
PHENOMENA AT HIGH ALTITUDE

J.G. Laframboise, M. Kamitsuma, S.M.L. Prokopenko,
Jen-Shih Chang, and R. Godard

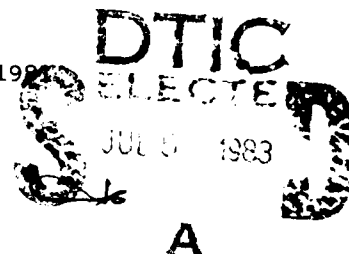
Physics Department and Centre for Research in Experimental Space Science
York University
Toronto, Canada M3J 1P3
10 August 1982

Approved for public release;
distribution unlimited.

FINAL REPORT

1 March 1976 through 31 August 1982

Grant AFOSR-76-2962



Prepared for
Air Force Office of Scientific Research (AFSC)
Bolling Air Force Base, D.C., U.S.A. 20332

83 07 01 023

Unclassified

SECURITY CLASSIFICATION OF THIS PAGE (When Data Entered)

REPORT DOCUMENTATION PAGE		READ INSTRUCTIONS BEFORE COMPLETING FORM
1. REPORT NUMBER AFOSR-TR- 83-0549	2. GOVT ACCESSION NO. AD-A130043	3. RECIPIENT'S CATALOG NUMBER
4. TITLE (and Subtitle) NUMERICAL SIMULATION OF SPACECRAFT CHARGING PHENOMENA AT HIGH ALTITUDE		5. TYPE OF REPORT & PERIOD COVERED Final Report 1 March 1976 - 31 August 1981
		6. PERFORMING ORG. REPORT NUMBER
7. AUTHOR(s) J.G. Laframboise, M. Kamitsuma, S.M.L. Prokopenko, Jen-Shih Chang, and R. Godard		8. CONTRACT OR GRANT NUMBER(s) AFOSR-76-2962
9. PERFORMING ORGANIZATION NAME AND ADDRESS York University, Toronto, Canada M3J 1P3		10. PROGRAM ELEMENT, PROJECT, TASK AREA & WORK UNIT NUMBERS 61102F 2311/A1
11. CONTROLLING OFFICE NAME AND ADDRESS Air Force Office of Scientific Research (AFSC) Bolling Air Force Base, D.C., U.S.A. 20332 Monitor/H. Radoski/NP		12. REPORT DATE 10 August 1982
14. MONITORING AGENCY NAME & ADDRESS (if different from Controlling Office)		13. NUMBER OF PAGES
		15. SECURITY CLASS. (of this report) Unclassified
		15a. DECLASSIFICATION DOWNGRADING SCHEDULE
15. DISTRIBUTION STATEMENT (of this Report) Approved for public release; distribution unlimited.		
17. DISTRIBUTION STATEMENT (of the abstract entered in Block 20, if different from Report)		
18. SUPPLEMENTARY NOTES		
19. KEY WORDS (Continue on reverse side if necessary and identify by block number) Numerical Simulation, Spacecraft Charging, Spacecraft - Environment Interactions		
20. ABSTRACT (Continue on reverse side if necessary and identify by block number) This report describes work done under grant AFOSR-76-2962. This work has included the development of computer programs for simulating spacecraft charging at three levels of complexity: LOCHG, a relatively simple local-charging calculation; CYLVIA, a two-dimensional simulation program for treating cylindrical spacecraft cross-sections, and XYCIC, a simulation program for the treatment of a larger variety of two-dimensional geometries. This work has also included studies of two physical phenomena which are fundamental to an improved understanding of spacecraft charging: the "threshold temperature" effect (over)		

DD FORM 1 JAN 73 1473

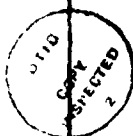
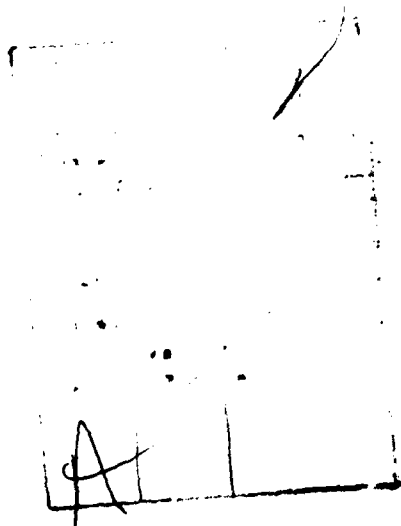
Unclassified

SECURITY CLASSIFICATION OF THIS PAGE (When Data Entered)

Unclassified

SECURITY CLASSIFICATION OF THIS PAGE(When Data Entered)

and the "barrier" effect. Also included is a derivation of two results which appear likely to be of use in future simulation studies: an analytic expression for photoelectron currents on surfaces with variable illumination in electric fields, and a perturbation technique for calculating space-charge density and flux along particle orbits.



Unclassified

SECURITY CLASSIFICATION OF THIS PAGE(When Data Entered)

NUMERICAL SIMULATION OF SPACECRAFT CHARGING

PHENOMENA AT HIGH ALTITUDE

J.G. Laframboise, M. Kamitsuma, S.M.L. Prokopenko,

Jen-Shih Chang, and R. Godard

Physics Department and Centre for Research in Experimental Space Science

York University

Toronto, Canada M3J 1P3

10 August 1982

Final Report

1 March 1976 through 31 August 1981

Grant AFOSR-76-2962

AIR FORCE OFFICE OF SCIENTIFIC RESEARCH (AFSC)
NOTICE OF TRANSMITTAL TO DTIC
This technical report has been reviewed and is
approved for distribution under AFM 190-12.
Distribution is unlimited.

MATTHEW J. KENNEDY
Chief, Technical Information Division

Prepared for

Air Force Office of Scientific Research (AFSC)

Bolling Air Force Base, D.C., U.S.A. 20332

TABLE OF CONTENTS

	PAGE
Acknowledgments	iii
Abstract	iv
1. Introduction	1
2. LOCHG: a local-charging calculation	4
2.1 Introduction	4
2.2 Theory	6
2.3 Results and discussion: shaded cavities and multiple floating potentials	12
2.4 Prediction of ion drift effects on spacecraft floating potentials	18
2.4.1 Introduction	18
2.4.2 Theory of local ion collection on a unipotential sphere	20
2.4.3 Results and discussion	22
3. Multiple floating potentials, and the "threshold material temperature for high-voltage charging".	24
3.1 Introduction	24
3.2 The threshold-temperature property	26
3.3 Calculation of threshold temperatures; discussion	30
4. CYLVIA: a two-dimensional charging simulation for cylindrical spacecraft cross-sections with angle-dependence.	34
4.1 Introduction; the quasistatic iteration method	34
4.2 Use of approximate space-charge density expressions	35
4.3 Approximate inclusion of finite-cylinder-length (three-dimensional) effects in Poisson's equation	37
4.4 Orbit integration and current calculations	39
4.5 Results and discussion	43
4.6 The barrier effect	46
5. XYCIC: a simulation for general planar-symmetric (two-dimensional) spacecraft geometries	50
5.1 Introduction	50
5.2 Preliminary results	51
6. An analytic calculation of surface photocurrents	53
6.1 Introduction	53
6.2 Theory	53
6.3 Comparison with a numerical result from CYLVIA.	57
7. Flux and Density Calculation for Collisionless Particle Orbits	59
References	66
Tables	73
Figures	75

Appendix A:	Listing of LOCHG	A1
Appendix B:	Listing of threshold temperatures program	B1
Appendix C:	Listing of CYLVIA	C1
Appendix D:	Listing of Plotting program used with CYLVIA	D1
Appendix E:	Listing of XYCIC	E1


ACKNOWLEDGMENTS

We are indebted to H.I. Cohen, L.W. Parker, and A.D. Stauffer for valuable discussions, and to M. Mandell for providing unpublished data used in Fig. 4.7 and discussed in Sec. 4.5. One of us (J.G. Laframboise) wishes to acknowledge the contributions of co-authors to specific sections of this Report, as follows: M. Kamitsuma (Secs. 3, 4, 5, and 6.3; Appendices B, D, and E), S.M.L. Prokopenko (Secs. 2 and 4; Appendices A, C, and D), Jen-Shih Chang (Sec. 2), and R. Godard (Secs. 2, 4, and 6.3; Appendices C and D). We wish to thank the computer center of Air Force Geophysics Laboratory for the provision of computer time, and the Department of Computer Services of York University for the use of its facilities. Special thanks are due to S. Bredesen of AFGL for much assistance with computing arrangements. We are grateful to the National Center for Atmospheric Research for the provision of computer software.

This work was supported by the U.S. Air Force Office of Scientific Research under grant number AFOSR-76-2962.

ABSTRACT

This report describes work done under grant AFOSR-76-2962. This work has included the development of computer programs for simulating spacecraft charging at three levels of complexity: LOCHG, a relatively simple local-charging calculation; CYLVIA, a two-dimensional simulation program for treating cylindrical spacecraft cross-sections, and XYCIC, a simulation program for the treatment of a larger variety of two-dimensional geometries. This work has also included studies of two physical phenomena which are fundamental to an improved understanding of spacecraft charging: the "threshold temperature" effect and the "barrier" effect. Also included is a derivation of two results which appear likely to be of use in future simulation studies: an analytic expression for photoelectron currents on surfaces with variable illumination in electric fields, and a perturbation technique for calculating space-charge density and flux along particle orbits.



1. INTRODUCTION

The performance of many satellites in geostationary orbit has been degraded by anomalous events which include frequent spurious spacecraft commands and in some cases permanent damage [Rosen, 1975; McPherson and Schober, 1976]. These events invariably appear to involve electrical discharges caused by differential charging of spacecraft surfaces to large relative potentials. The latter condition is known to result from the large average energies (up to a few keV) of the charged-particle environment at geostationary-orbit altitude, particularly in disturbed magnetospheric conditions. In order to be able to design spacecraft in future which do not suffer from such difficulties, it is important to be able to make reliable predictions of them on proposed spacecraft configurations. The ability to make such predictions requires improved understanding of the plasma sheath which connects a spacecraft with its environment in such conditions. This sheath is more complex in many ways than those which usually surround lower-altitude spacecraft because at geostationary-orbit altitude, the fluxes of incident electrons, secondary and backscattered electrons, and photoelectrons can all have comparable magnitudes and usually vary by large amounts over the surface of a spacecraft, and the relative weakness of space-charge shielding (large Debye length) means that electric fields due to charging of one part of a spacecraft surface can readily extend around the spacecraft to other parts, including those on its other sides, exerting strong influences on charged-particle collection by them and hence on their charging.

Because of the magnitude of the spacecraft-charging problem, a joint USAF-NASA programme was commenced during the 1970-1980 decade to study it, including the launching of the P78-2 (SCATHA) satellite, which was specifically devoted to the study of the high-altitude charging process, and also including theoretical work on the nature of the spacecraft-environment interface problem: this work was to be closely coordinated with analysis of SCATHA observations.

The work described in this report is part of this theoretical effort.

This work has been conducted using a number of different approaches. In Sec. 2, we describe a relatively simple local-current-balance calculation of charging which formed the first phase of it, and led to the discovery that floating potentials (voltages) of many spacecraft surface materials can have more than one possible value in certain, frequently-occurring, space environments; the possibility that this might occur had been earlier predicted by Whipple (1965). Attempts to gain further understanding of the conditions in which this might occur led to the realization that this was one of several closely-related phenomena which could all be explained in terms of a newly-defined property of spacecraft surface materials, the threshold material temperature for high-voltage charging (Sec. 3). We present herein a table of these threshold temperatures, calculated for a variety of spacecraft surface materials. A second phase of our effort was the development of a more elaborate, two-dimensional spacecraft charging simulation program called CYLVIA, which treats the regions around circular spacecraft cross-sections (Sec. 4). We have also begun development of another two-dimensional simulation program, called XYCIC (Sec. 5), which treats a wider class of two-dimensional geometries than does CYLVIA. The effort to develop CYLVIA, together with efforts by other workers (Sec. 4.6), led gradually to an understanding of the importance of the barrier effect, an example of which is presented in Sec. 4.6.

A related phase of our work has been an effort to develop efficient numerical techniques, and analytical replacements for some numerical procedures, which will be of general use not only in our own simulation programs but also in other spacecraft-charging simulations. To this end, we have developed an analytic expression for the electric current produced by photoelectron migration on a surface with spatially-varying illumination in an electric field (Sec. 6), and a perturbation technique for calculating current

density and space-charge density carried by collisionless charged-particle orbits (Sec. 7).

Listings of computer programs developed as part of this work appear in Appendices A-E.

2. LOCHG: A LOCAL-CHARGING CALCULATION

2.1 INTRODUCTION

In order for high-voltage differential charging of a spacecraft to occur, some of its surfaces must charge to large (usually negative) potentials (voltages) relative to space. The amount of such "absolute" charging, for the surface at the largest potential, is generally simpler to estimate than are the differential potentials between this surface and others. On the sunlit side of a spacecraft, photoelectron emission tends to compensate for incident electron fluxes. Sunlit-side surface potentials therefore are generally less negative than shaded-side potentials, and may be slightly positive if photoemission flux $>$ ambient random electron flux. Therefore, an approximate upper bound on differential charging magnitudes can be obtained by simply calculating floating potentials of electrically-isolated shaded surfaces, relative to space potential. In the present work, we have attempted to obtain upper bounds on these floating potentials, which in cases of interest are usually highly negative, because these bounds constitute "worst cases" for design purposes, and also because unlike more exact calculations, they can be obtained from simple current-balance calculations. Furthermore, it is sufficient to consider local current balance only, because this corresponds to an electrically-isolated surface element, which is also a "worst case" for differential charging. To calculate these bounds, we have constructed a computer program called LOCHG (LOCAL CHARGING), which extends a previous calculation by Knott [1972], of the floating potential of a spherically-symmetric geostationary-altitude satellite in eclipse. A listing of LOCHG appears in Appendix A. To investigate geometrical effects, we have replaced Knott's use of the Mott-Smith and Langmuir [1926] orbit-limited current expression for collection of Maxwellian ions by a unipotential sphere, by the corresponding expression for an infinite cylinder;

both expressions have been shown [Laframboise and Parker, 1973] to be upper bounds for collisionless ion collection as a function of local surface potential, for three- and two-dimensional collectors, respectively, regardless of collector shape, sheath potential, or potential of other parts of the collector. This replacement causes a large decrease in ion collection and a correspondingly large increase in negative shaded-side floating potentials (Sec. 2.3). Another important ion-current restriction may be caused by "effective-potential barrier" or "angular-momentum selection" effects [Bernstein and Rabinowitz, 1959; Laframboise, 1966; Laframboise and Parker, 1973], in which the presence of less-negative sunlit-side potentials produces dipole and higher moments in the sheath potential [Fahleson, 1973], causing steepening and contraction of the potential well surrounding the shaded side (Fig. 2.1). A similar steepening effect will also occur if an isolated shaded surface element is surrounded by adjacent shaded surfaces which for any reason have less-negative potentials (Fig. 2.2). The most extreme possibility would be a potential profile which was equal to space potential almost to the spacecraft surface, then fell discontinuously to surface potential. This limit would correspond to a "planar sheath" situation in which the ion collection on any shaded convex surface would be given by just the ion random flux. This amounts to a further ion-current restriction which produces even larger increases in negative shaded-side floating potentials (Sec. 2.3). This situation corresponds to a velocity-space cutoff boundary for incident ions which is "one-dimensional"; the cutoff boundaries corresponding to spherical and infinite cylindrical collectors are, respectively, "three-dimensional" and "two-dimensional" (Sec. 2.2) [Laframboise and Parker, 1973].

We also show (Sec. 2.3) that if shaded cavities containing isolated surfaces exist on a spacecraft, negative potentials on such surfaces may surpass even these predictions. In some cases, more than one possible floating potential results from the calculation. This has several implications (Sec. 2.3), including the possibility

(a) of "bifurcation phenomena" in which adjacent isolated surfaces of the same material may arrive at different floating potentials as a result of differences in their charging histories (b) that large and relatively sudden changes in surface potentials may result from gradual changes in ambient velocity distributions (c) that such changes may also result from relatively gradual changes in beam emission currents in a beam experiment. In Sec. 2.4 we calculate effects of ion drift motion on floating potentials.

We have also modified Knott's calculation in another way, by including currents due to electron backscattering (Sec. 2.2). These currents will tend to decrease net electron collection, thereby making floating potentials less negative than otherwise (Sec. 2.3). A process not included by either Knott or ourselves is secondary electron emission due to ion impacts; this will also tend to make floating potentials less negative. Ion-produced secondaries have been included in a calculation by DeForest [1972] of the floating potential of a shaded aluminum surface. However, no direct comparison is possible between his result and ours (Sec. 2.3) because we have used different ambient velocity distributions than his.

2.2 THEORY

The ambient electron energy distributions used in the present work are a model quiet-time spectrum (Knott [1972], Figure 1) and a model disturbed spectrum (Knott [1972], Figure 2b) based on measurements by Shield and Frank [1970] and DeForest and McIlwain [1971], respectively. Both of these distributions, and also the ambient ion distribution, are assumed isotropic. The disturbed spectrum was chosen from the three used by Knott because it has a higher average electron energy (~ 4 keV) than the others. In using it, we have changed it as follows: in the energy ranges $0.5 \text{ keV} \leq E \leq 10 \text{ keV}$ and $10 \text{ keV} \leq E \leq 40 \text{ keV}$, we have replaced Knott's differential energy spectrum by $\sqrt{2} \times 10^8 E^{-1/2}$ and $\sqrt{2} \times 10^9 E^{-3/2}$ electrons/cm² sec steradian keV, respectively, where E is

energy. These relations are simpler than those indicated by Knott, and they also bring the model spectrum into closer agreement with the data on which it is based. We therefore believe that they may have been the ones actually used by Knott, and that the corresponding parts of Figure 2b in his paper may be incorrectly plotted. For any spacecraft surface having a negative potential $\phi_s < 0$, or for a three-dimensional (e.g. spherical) surface having $\phi_s > 0$, the orbit-limited flux (particle current density) J_e of ambient electrons is given by [Laframboise and Parker, 1973]:

$$\begin{aligned}
 J_e &= \int f v_n d^3 \vec{v} \\
 &= \int_{E=\max(0, -e\phi_s)}^{E=\infty} \int_{\theta=0}^{\theta=\pi/2} \int_{\psi=0}^{\psi=2\pi} f(E) (v \cos \theta) (v^2 \sin \theta dv d\theta d\psi) \\
 &= \int_{\max(0, -e\phi_s)}^{\infty} (1 + e\phi_s/E) (dJ_{eo}/dE) dE \quad (2.1)
 \end{aligned}$$

where e is magnitude of unit electronic charge, ϕ_s is local surface potential, dJ_{eo}/dE is the ambient energy-differential flux incident on one side of an arbitrarily oriented surface element, v_n is the inward velocity component normal to the same surface element, (v, θ, ψ) are spherical coordinates in velocity space with v_n as polar axis, and $E = \frac{1}{2} m_e v^2 - e\phi$. dJ_{eo}/dE is π times the energy-differential flux per steradian used by Knott [1972], and is given in terms of the ambient electron velocity distribution $f = d^3 N_{\infty} / d^3 \vec{v}$ by the relation $dJ_{eo}/dE = 2\pi f E / m_e^2$, where m_e is electron mass and N_{∞} is ambient ion or electron number density. Since f is isotropic, $f \equiv f(E)$. The factor $(1 + e\phi_s/E)$ in (2.1), which appears to have been neglected by Knott, leads to a divergent integration in (2.1) if $\phi_s > 0$, unless $dJ_{eo}/dE \rightarrow 0$ as $E \rightarrow 0$, i.e. $f(E)$ remains finite as $E \rightarrow 0$. This implies that the differential fluxes in Knott's Figures 1-3 must approach zero linearly with E at E values smaller than those shown in these Figures. In the present work we have introduced a linear rise in dJ_{eo}/dE from 0 to 1 eV. We have also introduced a sharp upper cutoff at 50 keV in the quiet-time spectrum, also in order to avoid a divergent integration when calculating average energy for use in backscattering calculations (see below). The resulting values of N_{∞} are 5.43 cm^{-3} and 5.39 cm^{-3} for the quiet-time

and disturbed spectra, respectively. These values are consistent with those quoted by Knott [1972] for the corresponding spectra. The resulting values of the average ambient electron energy \bar{E} are 0.176 keV and 4.17 keV, respectively. The incorporation of these changes has a relatively minor influence on Knott's results [Prokopenko and Laframboise, 1977, Table 1].

In order to obtain the orbit-limited electron flux expression for an arbitrary cylindrical collector, the lower integration limit in (2.1) must be replaced by the two-dimensional velocity-space cutoff boundary $E_1 = \max(0, -e\phi_s)$, where E_1 is the total energy of transverse motion $\frac{1}{2}m_e(v_x^2 + v_y^2) - e\phi$, and we have chosen a z coordinate perpendicular to the cylinder cross-section. If $\phi_s > 0$, this complicates the integration in (2.1), which may then be done in either of two ways. The first [Laframboise and Parker, 1973, Eq. (6)] is to convert (2.1) into an integration using cylindrical coordinates in velocity space. A more convenient method [Mott-Smith and Langmuir, 1926; Polychronopoulos, 1973] is as follows. We choose rectangular coordinates (v_n, v_t, v_z) in velocity space, such that v_n is the velocity component in the inward normal direction at the collector surface. Then v_t and v_z become tangential coordinates, with v_t in the plane of the cylinder cross-section. We then transform to spherical coordinates (v, θ, ψ) with v_z as polar axis. Then: $v_z = v \cos \theta$, $v_n = v \sin \theta \cos \psi$, and $v_t = v \sin \theta \sin \psi$. The condition $E_1 \geq 0$ is equivalent to $\sin \theta \geq [e\phi_s / (E + e\phi_s)]^{1/2}$. For $\phi_s > 0$, Eq. (2.1) is then replaced by:

$$\begin{aligned}
 J_e &= \int f v_n d^3 \vec{v} \\
 &= 2 \int_{E=0}^{\infty} \int_{\psi=-\pi/2}^{\pi/2} \int_{\theta=\text{Arc sin}[e\phi_s/(E+e\phi_s)]^{1/2}}^{\pi/2} f(E) (v \sin \theta \cos \psi) (v^2 \sin \theta dv d\theta d\psi) \\
 &= \int_0^{\infty} \frac{2}{\pi} \left[\text{Arc sin} \left(\frac{E}{E+e\phi_s} \right)^{1/2} + \frac{(Ee\phi_s)^{1/2}}{E+e\phi_s} \right] \left(1 + \frac{e\phi_s}{E} \right) \frac{dJ_{e0}}{dE} dE. \quad (2.2)
 \end{aligned}$$

In comparison with Eq. (2.1), we see that the integrand in (2.2) contains an extra, energy-dependent weighting factor, which arises from integration of v_n over the fractional solid angle over which ambient electrons can reach the collector at each energy.

A similar procedure is advantageous in obtaining the one-dimensional (Sec. 2.1) orbit-limited flux expression. In this case, the lower limit in (2.1) must be replaced by: $E_n = \max(0, -e\phi_s)$, where $E_n = \frac{1}{2} m_e v_n^2 - e\phi$. This time we transform (v_n, v_t, v_z) to spherical coordinates (v, θ, ψ) with v_n as polar axis. The condition $E_n \geq 0$ is equivalent to $\cos \theta \geq [e\phi_s / (E + e\phi_s)]^{1/2}$. For $\phi_s > 0$, Eq. (2.1) is now replaced by:

$$J_e = \int_{E=0}^{E=\infty} \int_{\theta=\text{Arc cos}[e\phi_s/(E+e\phi_s)]^{1/2}}^{\theta=\text{Arc cos}[e\phi_s/(E+e\phi_s)]^{1/2}} f(E) (v \cos \theta) (2\pi v^2 \sin \theta dv d\theta) \\ = \int_0^{\infty} \frac{dJ_{e0}}{dE} dE \quad (2.3)$$

independently of collector potential, as expected.

The corresponding expressions for ion flux J_i are simpler because the ions are assumed to be Maxwellian. Corresponding to the three-, two-, and one-dimensional velocity-space cutoffs described above, we obtain, respectively [Mott-Smith and Langmuir, 1926; Laframboise and Parker, 1973], for ion-attracting surface potentials $\chi_{is} > 0$:

$$J_i = J_{i0} \begin{cases} (1 + \chi_{is}) & (2.4) \\ [2(\chi_{is}/\pi)^{1/2} + \exp(\chi_{is}) \text{erfc}(\chi_{is}^{1/2})] & (2.5) \\ (1) & (2.6) \end{cases}$$

where $\chi_{is} = -e\phi_s/kT_i$, k is Boltzmann's constant, T_i is ion temperature and J_{i0} is the ion random flux $N_{\infty}(kT_i/2\pi m_i)^{1/2}$. For ion-retarding surface potentials $\chi_{is} < 0$, we obtain:

$$J_i = J_{i0} \exp(\chi_{is}). \quad (2.7)$$

We have assumed, following Knott [1972], that $T_i = 1$ keV, and that the random ion-to-electron flux ratio $J_{io}/J_{eo} = 0.025$. Making these two assumptions simultaneously causes ambient charge neutrality to be violated in general. Large apparent violations of charge neutrality are frequently observed in measurements made by particle energy analyzers. Such discrepancies are believed to result from failure to measure particles outside the energy ranges of these analyzers, especially at energies of a few volts or less [DeForest and McIlwain, 1971]. Our calculations therefore neglect any current contributions which may be made by such particles.

For the secondary electron fractional yield $\delta(E)$, we have used, following Knott [1972], the relation of Sternglass [1954a]:

$$\delta(E) = 7.4 \delta_{\max} (E/E_{\max}) \exp[-2(E/E_{\max})^2]. \quad (2.8)$$

We have used values of δ_{\max} and E_{\max} from Gibbons [1966], Hachenberg and Brauer [1959], and Willis and Skinner [1973].

The process of electron backscattering, which was not included in Knott's calculations, becomes important at incident electron kinetic energies larger than those for which secondary emission is dominant. For the backscattered electron fractional yield η , we have fitted the results of Sternglass [1954b] and Palluel [1947] with a relation of the form:

$$\eta(E) = A - B \exp(-CE) \quad (2.9)$$

where the coefficients A , B , and C are functions of the atomic number Z of the surface material. We have evaluated A , B and C for each surface material considered (Sec. 2.3) by substituting Sternglass' and Palluel's values of η at 0, 1 and 16 keV, into Eq. (2.9). For compound surface materials, we have used an atomic number given by a weighted average of those of each constituent. There exist more recent measurements of η [Thomas and Pattinson, 1970; Darlington and Cosslett, 1972] which give generally larger values than those of Sternglass or Palluel, especially for electrons having near-tangential incidence.

Increased values of δ have also been measured for electrons having non-normal incidence [Allen, 1939; Dekker, 1958]. In a separate calculation (Sec. 3), we have included angle-of-incidence effects on η and δ , but here we have ignored these. We have therefore underestimated both δ and η , and our predicted floating potentials in Sec. 2.3 will therefore be somewhat more negative than more realistic corresponding values.

When $\phi_s > 0$, not all secondary and backscattered electrons will escape. To calculate flux escaping, we assume [Sternglass, 1954b; Chung and Everhart, 1974] that both secondary and backscattered electrons are emitted with Maxwellian velocity distributions having thermal energies $E_{\text{sec}} = kT_{\text{sec}} = 3 \text{ eV}$, and $E_{\text{scat}} = kT_{\text{scat}} = (0.45 + 2 \times 10^{-3}Z)(E + e\phi_s) \text{ eV}$, respectively, regardless of the form of the incident velocity distribution. Here, $(E + e\phi_s)$ is the average incident electron kinetic energy. We further assume that escape of emitted electrons is orbit-limited, i.e. that no barriers of effective potential [Bernstein and Rabinowitz, 1959; Laframboise, 1966; Laframboise and Parker, 1973] or negative barriers of electric potential exist on the shaded side. {Fahleson [1973] has pointed out that such a barrier is likely to exist on the sunlit side independently of any space-charge effects, if substantial shaded-sunlit differences exist in ϕ_s . Such a barrier would cause most electrons emitted from the sunlit side to be recollected, driving sunlit-side potential just negative enough to almost destroy the barrier [Sec. 4.5]; [Katz et al, 1979, Figs. 17-21]}). The expressions for the escaping secondary and backscattered fluxes J_{sec} and J_{scat} therefore are:

$$J_{\text{sec}} = \int_{-e\phi_s}^{\infty} \delta(E + e\phi_s) (1 + e\phi_s/E) (dJ_{e0}/dE) dE \quad (2.10)$$

$$J_{\text{scat}} = \int_{-e\phi_s}^{\infty} \eta(E + e\phi_s) (1 + e\phi_s/E) (dJ_{e0}/dE) dE \quad (2.11)$$

if $\phi_s < 0$. If $\phi_s > 0$, the three-, two-, and one-dimensional cases must be considered separately. We define $\chi_{\text{sec}} = e\phi_s/kT_{\text{sec}}$ and $\chi_{\text{scat}} = e\phi_s/kT_{\text{scat}}$. For brevity, we consider only the secondary fluxes; the corresponding results for backscattered fluxes may be obtained by replacing δ by η and χ_{sec} by χ_{scat} throughout. If J_s is the emitted flux of secondaries,

then their velocity distribution at the surface is $f_s = (J_s/2\pi)(m_e/kT_{sec})^{-2} \exp(-\frac{1}{2}m_e v^2/kT_{sec})$. In the three-dimensional case, the cutoff condition for their escape is $E = \frac{1}{2}m_e v^2 - e\phi_s > 0$. We redefine v_n as velocity component in the outward normal direction, and we use spherical coordinates as defined in connection with (2.3). We obtain, for the escaping secondary flux:

$$\begin{aligned} J_{sec} &= \int f_s v_n d^3\vec{v} \\ &= \frac{J_s}{2\pi} \left(\frac{m_e}{kT_{sec}} \right)^2 \int_{E=0}^{\infty} \int_{\theta=0}^{\pi/2} \exp(-\frac{1}{2}m_e v^2/kT_{sec}) (v \cos \theta) (2\pi v^2 \sin \theta dv d\theta) \\ &= (1 + \chi_{sec}) \exp(-\chi_{sec}) \int_0^{\infty} \delta(E + e\phi_s) (1 + e\phi_s/E) (dJ_{eo}/dE) dE. \quad (2.12) \end{aligned}$$

The factor $(1 + \chi_{sec})$ is noteworthy, because it is specific to three-dimensional, as opposed to planar, sheath geometry. In the two-dimensional case, the cutoff condition for escape is $\frac{1}{2}m_e(v_n^2 + v_t^2) - e\phi_s > 0$, and the integral for J_s contains the extra weighting factor which appears in Eq. (2.2). It is convenient to use spherical coordinates as defined in connection with (2.2). We obtain:

$$\begin{aligned} J_{sec} &= \left[2(\chi_{sec}/\pi)^{1/2} + \exp(\chi_{sec}) \operatorname{erfc}(\chi_{sec}^{1/2}) \right] \exp(-\chi_{sec}) \\ &\quad \times \int_0^{\infty} \frac{2}{\pi} \left[\operatorname{Arc sin} \left(\frac{E}{E + e\phi_s} \right)^{1/2} + \frac{(Ee\phi_s)^{1/2}}{E + e\phi_s} \right] \left(1 + \frac{e\phi_s}{E} \right) \delta(E + e\phi_s) \frac{dJ_{eo}}{dE} dE. \quad (2.13) \end{aligned}$$

In the one-dimensional case, the escape condition is $\frac{1}{2}m_e v_n^2 - e\phi_s > 0$, and we again use spherical coordinates as defined in connection with (2.3). We obtain:

$$J_{sec} = \exp(-\chi_{sec}) \int_0^{\infty} \delta(E + e\phi_s) (dJ_{eo}/dE) dE. \quad (2.14)$$

The floating potential(s) of an isolated shaded surface element is (are) now given by the zero(s) of the function:

$$J_{net} = J_i - J_e + J_{sec} + J_{scat}. \quad (2.15)$$

2.3 RESULTS AND DISCUSSION: SHADED CAVITIES AND MULTIPLE FLOATING POTENTIALS

Table 1 shows floating potential values obtained using the program LOCHG, which performs numerical solution of the equation $J_{net} = 0$, where J_{net} is given by Eq. (2.15). An important feature of Table 1 is the very

large floating potentials which are evident in disturbed conditions in the presence of the two- and one-dimensional velocity-space cutoffs. The dramatic differences among these results are evidence that spacecraft geometry and sheath potential shape are important influences in determining floating potentials. As floating potential becomes more negative, it also becomes more sensitive to the presence of small amounts of high-energy electrons. This means that if a spacecraft should encounter conditions that are "more disturbed" than those given by Knott's spectrum 2b, the values in Table 1 most likely to be significantly exceeded are those for the one-dimensional cutoff. This implies that for design purposes in which worst-case information is desired, it is important to do calculations with the "most disturbed" electron spectra available. In obtaining these results, we have made no attempt to calculate the charging times involved.

Also evident in Table 1 are situations in which the current-voltage characteristic of the surface has three roots. For these to occur, it is necessary that δ_{\max} be substantially greater than one, and that the ambient electron spectrum be at least slightly non-Maxwellian (Sec. 3). The latter requirement arises because if the incident electrons are Maxwellian and ion-produced secondaries are ignored, the ratio of total secondary emission current to incident electron current will then be independent of ϕ_s for $\phi_s < 0$, and the total secondary emission will therefore be a monotonic function of ϕ_s for $\phi_s < 0$. (An exception to this, in which a triple-root situation occurs with Maxwellian ambient electrons, has been found by Meyer-Vernet (1982), but this exception applies only when $T_e < T_{\text{sec}}$, a condition which is not applicable here; see also Sec. 3). The centre root never represents a possible floating potential, because it is "unstable" in the sense that a small change in surface potential would cause a net current collection of a sign which would drive the surface potential away from this root to one on either side. Various consequences of such a situation are discussed later in this Section. A similar phenomenon in electronic image storage devices has been discussed by Kazan and Knoll [1968, pp. 17-19].

In comparison with the results of Knott [1972], Table 1 includes the further addition of backscattered electron flux (Sec. 2.2). In most cases, the effect is a moderate reduction of negative floating potentials. In some cases, the reduction is large, as in the case of a gold surface

exposed to the "quiet" spectrum. In several other cases, all associated with the quiet spectrum, backscattering changes a multiple-root to a single-root situation [Prokopenko and Laframboise, 1977]. As indicated in Sec. 2.2, we have probably underestimated secondary and backscattered fluxes caused by electron impacts, and we have also (Sec. 2.1) ignored secondary electron emission caused by ion impacts. Both of these effects would tend to further reduce negative potentials. For ion-produced secondaries, fractional yields at energies from 5 to 50 keV are generally of order unity to several times unity for metallic surfaces [Cousinie et al, 1959; Ray and Barnett, 1971; Baragiola et al, 1979] so substantial reductions due to this cause can be expected whenever ion collection plays an important role in total current balance. In comparison with the results of Table 1, potentials reaching -19 kV on the ATS 6 spacecraft in eclipse have been observed (E.C. Whipple, Jr., private communication).

Figures 2.3 - 2.7 show current-voltage characteristics for some of the situations in Table 1. Figure 2.3 shows a "typical" single-root situation in which secondary and backscatter contributions do not change the general shape of the net current curve. Figure 2.4 shows the above-mentioned case of gold exposed to the quiet spectrum, in which the backscatter contribution changes a large predicted negative floating potential to a much smaller value. Figure 2.5 shows a triple-root situation. Figure 2.6 shows the disappearance of a triple-root situation because of backscatter. In Fig. 2.7, secondary electron current is sufficient by itself to prohibit a negative floating potential.

We now examine situations which may arise in the case of spacecraft which have shaded cavities containing electrically-isolated interior surfaces. Figure 2.8 shows an idealization of such a spacecraft. We wish to show that the effects of surface concavity may cause ion collection to be reduced more than net electron collection at an interior point such as B, relative to an exterior point A; such a situation would result in floating potentials more negative than those of Table 1. To demonstrate this possibility, we first note that in the presence of an isotropic ambient plasma, incident fluxes to any surface depend only [Laframboise and Parker, 1973] on the locations, in velocity space, of

the cutoff boundaries inside of which the orbits of ambient particles can connect "from infinity" to the surface. Figure 2.8 shows a set of the associated "cutoff orbits". We see from Fig. 2.8 that the included angle between cutoff orbits has been reduced in going from A to B for ions but not for electrons, for which orbits tangential to the surface are shown as reaching both A and B and the range of allowable directions remains 180° . Accordingly, the incident ion current contribution for the energy shown will also be reduced, but the electron contribution will not. This picture is invalid for higher-energy electrons at B, whose orbits are straighter and will have a greater tendency to connect back to the interior surfaces of the cavity. Even though such higher-energy orbits will generally have lower populations than lower-energy orbits, it is not clear whether the relative current reduction at B will be greater for ions or for electrons. Therefore, this argument demonstrates only the possibility that the bounds in Table 1 will be exceeded. On the other hand, this possibility will be enhanced by the effects of secondary and backscattered electrons, which will tend to be recollected inside any cavity, rather than escaping into space, thus tending to increase net electron collection and driving floating potentials more negative. This effect will be strongest for backscattered electrons because their higher emission energies will cause them to have straighter orbits. The detailed numerical simulation required to draw firm conclusions remains to be done. An additional feature of cavities is their generally higher outgassing pressures, which will increase any tendencies for arcing to occur. More negative floating potentials may also result if the ambient electron distribution contains beam-like constituents [DeForest, 1977] which happen to be directed into a cavity. Severe arcing problems are known to have occurred between electronic components mounted inside a cavity at one end of the DSCS spacecraft.

Finally, we discuss some further implications of the multiple-root results shown in Table 1 and Fig. 2.5. We first consider a situation involving a shaded, isolated spacecraft surface whose external conditions change with time, as in the case of time-varying ambient distributions,

in such a way as to produce an evolution from a multiple-root to a single-root situation. If a spacecraft surface were floating at a potential corresponding to a root which disappeared, a large and relatively sudden change in surface potential would occur, even if external changes were gradual. In many situations, rapid redistribution of potentials on other parts of the spacecraft would result. In order to examine this situation in more detail, we illustrate it schematically in Fig. 2.9.

In Fig. 2.9a, the current-voltage curve at an earlier time t_1 has three roots. The two roots furthest apart, ϕ_{1a} and ϕ_{1b} , correspond to stable floating surface potentials; these are typically from one to ten kilovolts apart. As a result of a changing environment, this curve evolves continuously into the one shown for the later time t_2 , which has only the single root ϕ_2 . If the surface happened to be floating at the voltage ϕ_{1a} at time t_1 , then a sudden positive change in surface voltage, toward the voltage ϕ_2 , would occur as soon as the two left-hand roots disappeared.

In Fig. 2.9b, a spacecraft surface floating at the more positive root (at ϕ_{1b}) would undergo a sudden negative change in voltage, toward ϕ_2 , as soon as the two right-hand roots disappeared. Sudden voltage changes have been observed both on the SCATHA (P78-2) satellite and in numerical simulations (Sec. 3.1; Schnuelle et al, 1981; Stannard et al, 1982).

Similar sudden changes could occur on a spacecraft which was emitting a changing ion or electron gun current, if an increase or decrease in gun current were to provide enough net current to a surface to cause it to change from one stable floating potential to another. Again, such a change would be relatively sudden even if beam current changes were gradual.

A different effect could arise if the situation evolved in reverse fashion, so that t_2 were now the earlier time. Consider a spacecraft whose rotation carries a number of independently-floating surface panels from sunlight into shade, one after another. Suppose the situation evolves as in Fig. 2.9b. A surface already in the shade when the environment changed would go from voltage ϕ_2 to ϕ_{1a} . However, a surface which was

still in the sun, and whose photoemission current held its voltage close to ϕ_{1b} , would go to ϕ_{1b} when it entered the shade. As a result, two adjacent surfaces made of the same material could easily come to quite different voltages in the same environment, with a resulting danger of arcing between them.

In Sec. 3, we examine in detail the conditions in which multiple roots can occur.

2.4 PREDICTION OF ION DRIFT EFFECTS ON SPACECRAFT FLOATING POTENTIALS

2.4.1 INTRODUCTION

The plasma environment of high-altitude spacecraft has been observed to involve ion velocity anisotropies which sometimes become comparable to ion mean thermal speeds. These anisotropies are varied in nature, but a qualitative estimate of their effects on spacecraft charging may be obtained by considering the effects of a relatively simple anisotropy, namely the addition of a drift to a Maxwellian velocity distribution. Such drifts may cause an electrically-isolated spacecraft surface to float at a substantially increased negative potential if it is simultaneously shaded and downstream relative to the drift direction. In this Section, we present a calculation of upper and lower bounds on such potentials for a spherical spacecraft, based on the fact that ion collection on the spacecraft at its downstream point is bounded above by the corresponding current which would be collected if the spacecraft were an equipotential (i.e. were more attractive for ions elsewhere on its surface than it is in reality) and bounded below by the corresponding result for a sphere at space potential. The results show that (1) the ion speed ratio at which drift effects become "important" (i.e. change the floating potential by at least 10%) can be as low as 0.1, and may be decreased if the ambient electrons are non-Maxwellian; (2) the effects of ion speed ratio increase with increasing ion-to-electron temperature ratio; (3) negative floating potentials for drifting Maxwellian ion velocity distributions with speed ratio unity are typically about twice as large as the corresponding potentials for nondrifting conditions. We now examine the effects of ion drift in detail.

If a spacecraft is exposed to ambient ions whose drift velocity U is comparable to or larger than their most probable thermal speed [ion speed ratio $S_i = U/(2kT_i/m_i)^{1/2} \gtrsim 1$, where k is Boltzmann's constant and m_i and T_i are ion mass and assumed ion temperature], a large decrease in ion flux J_i to downstream surfaces will occur. Unless such surfaces are able to expel surplus incident electron fluxes, e.g. by photoemission,

2.4 PREDICTION OF ION DRIFT EFFECTS ON SPACECRAFT FLOATING POTENTIALS

2.4.1 INTRODUCTION

The plasma environment of high-altitude spacecraft has been observed to involve ion velocity anisotropies which sometimes become comparable to ion mean thermal speeds. These anisotropies are varied in nature, but a qualitative estimate of their effects on spacecraft charging may be obtained by considering the effects of a relatively simple anisotropy, namely the addition of a drift to a Maxwellian velocity distribution. Such drifts may cause an electrically-isolated spacecraft surface to float at a substantially increased negative potential if it is simultaneously shaded and downstream relative to the drift direction. In this Section, we present a calculation of upper and lower bounds on such potentials for a spherical spacecraft, based on the fact that ion collection on the spacecraft at its downstream point is bounded above by the corresponding current which would be collected if the spacecraft were an equipotential (i.e. were more attractive for ions elsewhere on its surface than it is in reality) and bounded below by the corresponding result for a sphere at space potential. The results show that (1) the ion speed ratio at which drift effects become "important" (i.e. change the floating potential by at least 10%) can be as low as 0.1, and may be decreased if the ambient electrons are non-Maxwellian; (2) the effects of ion speed ratio increase with increasing ion-to-electron temperature ratio; (3) negative floating potentials for drifting Maxwellian ion velocity distributions with speed ratio unity are typically about twice as large as the corresponding potentials for nondrifting conditions. We now examine the effects of ion drift in detail.

If a spacecraft is exposed to ambient ions whose drift velocity U is comparable to or larger than their most probable thermal speed [ion speed ratio $S_i = U / (2kT_i/m_i)^{1/2} \gtrsim 1$, where k is Boltzmann's constant and m_i and T_i are ion mass and assumed ion temperature], a large decrease in ion flux J_i to downstream surfaces will occur. Unless such surfaces are able to expel surplus incident electron fluxes, e.g. by photoemission,

their floating potentials will become substantially more negative as a result. If the ambient electron temperature T_e is simultaneously large, or more generally the ambient electron energy distribution has a significant high-energy component, then large absolute increases in negative floating potentials will occur, with correspondingly increased arcing hazards. Even if T_e is relatively small, such effects may influence surface potentials enough to disturb particle and field measurements. S_i values of order unity may be reached in the Earth's outer magnetosphere (Mauk 1975; DeForest 1977, Figs. 6 and 8); larger values are likely in the outer Jovian magnetosphere and magnetosheath (Goldstein and Divine 1977), and in the solar wind (Dessler 1967; Axford 1968; Manka 1973). In both outer magnetospheres, electron distributions having substantial high-energy components have been observed (DeForest and McIlwain 1971; Goldstein and Divine 1977).

A calculation of ion drift effects on the floating potential of the lunar surface has been done by Manka (1973), using a local-current-balance formulation. Parker (1978) has done exact numerical calculations of floating surface potentials for nonconductive finite cylindrical objects, including photoemission due to illumination of one end and ion drift parallel to the axis of symmetry.

In this Section we have done an approximate calculation of ion drift effects on the floating potential of a shaded, downstream, electrically-isolated surface element on a spherical spacecraft (Fig. 2.10), using a local-current-balance formulation which yields upper and lower bounds on such potentials. This formulation is an adaptation of that of Secs. 2.1 to 2.3. The basis of the calculation is as follows: if one compares, on one hand, a situation wherein the entire spacecraft is at the same potential as the surface element in question, with, on the other hand, a more realistic situation wherein the rest of the spacecraft is at a less negative potential (Fig. 2.11), then in the latter case, the potential well surrounding the surface element will be steeper and less spatially extended, and the ion collection will in general be

decreased. When $S_i \neq 0$, this argument is subject to qualifications not present in the nondrifting case, for which it is rigorously true in a wide range of conditions (Laframboise and Parker 1973; Laframboise and Godard 1974). In particular, one can envision hypothetical asymmetric sheath potentials which would cause a high-speed-ratio ambient ion distribution to be focused onto the downstream point. We exclude such cases in what follows.

The most extreme example of steepening would be a potential profile which was equal to space potential almost to the spacecraft surface, then fell discontinuously to surface potential. In this limit, the surface element in question would collect just the downstream space-potential current corresponding to the given ion speed ratio. The downstream-point current-density values corresponding to a unipotential sphere at, respectively, the potential of the surface element and space potential may therefore be regarded as upper and lower bounds on the actual current collection at that potential, the upper bound being subject to the above-mentioned qualifications. The resulting values of local floating surface potential may correspondingly be regarded as upper and lower bounds on more realistic values of this quantity. The above-mentioned upper and lower bounds on current correspond, respectively, to the "three-dimensional" and "one-dimensional" velocity-space cutoffs considered in Secs. 2.1 to 2.3 for nondrifting situations.

2.4.2 THEORY OF LOCAL ION COLLECTION ON A UNIPOTENTIAL SPHERE

We assume a collisionless plasma with a drifting Maxwellian ion velocity distribution and negligible magnetic field, containing a fully charge-absorbing, unipotential, spherical electrode. We assume that Debye length $\lambda_D \gg$ electrode radius r_s . In the resulting spherically-symmetric Laplace potential $\phi(r) = \phi_s r_s/r$, the nondimensional ion current density at the electrode surface is (Godard 1975, p. 31)

$$j_i = \int_{\max(0, \chi_s)}^{\infty} \int_0^{3-\chi_s} \exp(-\beta - 2S_i \beta^2 \cos \mu \cos \theta - S_i^2) I_0(2S_i \beta^2 \sin \mu \sin \theta) d\Omega d\beta \quad (2.16)$$

where $\chi_s = q\phi_s/kT$, $\beta = E/kT$, $\Omega = L^2/(2mr_s^2kT)$, $j = J/[N_\infty q(kT/2\pi m)^{1/2}]$,

I_0 is the modified Bessel function of zero order, N_∞ is number density far from the electrode, μ is angular surface position coordinate measured from the upstream direction, θ is change in direction of the radius vector of a particle as it moves from infinity to radial distance r_s , and θ is related to particle energy E , angular momentum L , charge q and the potential profile $\phi(r)$ by the following expression (Goldstein 1950, Ch. 3):

$$\theta = \int_{r_s}^{\infty} Ldr / \{r^2 [2mE - 2mq\phi(r) - L^2/r^2]\}^{1/2} \quad (2.17)$$

We have computed j_i by integrating Eq. (2.16) numerically. For the given Laplace potential, Eq. (2.17) can be integrated analytically. We obtain:

$$\theta = \sin^{-1} [(2\Omega + \chi_s)/(\chi_s^2 + 4\Omega)^{1/2}] - \sin^{-1} [\chi_s/(\chi_s^2 + 4\Omega)^{1/2}] \quad (2.18)$$

For space potential ($\chi_s = 0$), Eq. (2.16) can be integrated analytically. The result is (Tsien 1946)

$$j_i = \pi^{1/2} S_i \cos \mu [1 + \operatorname{erf}(S_i \cos \mu)] + \exp(-S_i^2 \cos^2 \mu) \quad (2.19)$$

Figure 2.12 shows results obtained for the ion current density $j_{i\pi}$ at the downstream point $\mu = \pi$, as a function of S_i , with χ_s as a parameter, where $\chi_s = e\phi_s/kT_i \leq 0$ and $e \equiv q_i$. As expected, $j_{i\pi}$ decreases with increasing S_i and increases with increasing $|\chi_s|$. In Figure 2.13 the same results are graphed logarithmically as functions of χ_s . Figure 2.13 shows that these results may be approximated with an error $\lesssim 5\%$ by power-law relations of the form

$$j_{i\pi}(\chi_s) = j_{i\pi}(\chi_s = 0) + A_\pi |\chi_s|^{\alpha_\pi}; \quad \chi_s \leq 0 \quad (2.20)$$

The resulting S_i dependence of the coefficients A_π , α_π and $B_\pi \equiv j_{i\pi}(\chi_s = 0)$ is shown in Fig. 2.14.

2.4.3 RESULTS AND DISCUSSION

Upper and lower bounds on negative downstream-point floating potentials for a shaded, isolated surface element, obtained by numerical solution of the equation $J_i + J_e = 0$, are shown in Fig. 2.15 for various ion-to-electron temperature ratios $\epsilon = T_i/T_e$. Here we have assumed that ambient electrons are Maxwellian, and that J_i is given alternatively by Eq. (2.20) with Fig. 2.14 and by Eq. (2.19), yielding upper and lower bounds on ion current, corresponding respectively to "three-dimensional" and "one-dimensional" ion velocity-space cutoffs (Sec. 2.4.1). We have also assumed that secondary, backscattered, and photoemitted electron currents are zero. The lower-bound results are subject to the qualifications noted in Sec. 2.4.1. The dashed lines in Fig. 2.15 represent floating potentials for the nondrifting case $S_i = 0$. At ion speed ratios larger than those shown, the situation becomes complicated by electron speed ratio effects, especially at larger values of ϵ . In Fig. 2.15 we see that at larger values of ϵ , effects of S_i become important at smaller S_i values.

In Fig. 2.16, upper and lower bounds are shown which are similar to those of Fig. 2.15, except that instead of Maxwellian electron velocity distributions, we have used the "quiet" and "disturbed" electron distributions measured by Shield and Frank (1970) and DeForest and McIlwain (1971) respectively in the Earth's outer magnetosphere, and approximated by Knott (1972), as described in Sec. 2.2; see also Prokopenko and Laframboise (1977) and Laframboise and Prokopenko (1978). The ion temperatures used are 111.6 eV and 2.43 keV, respectively. These values were obtained by integrating the electron velocity distributions to find $N_{e\infty}$, equating $N_{i\infty}$ to the result, then assuming that the ions were Maxwellian and that the ratio of ion to electron random fluxes was 0.025. This procedure differs from that used by Knott (1972) and in Secs. 2.1 - 2.3 in which an ion-to-electron random flux ratio of 0.025 and an ion temperature of 1 keV were assumed simultaneously, thereby violating ambient charge neutrality in general. The corresponding electron mean energies are 270 eV and 8.78 keV. The method used for calculating electron currents is described in Sec. 2.2. We see that S_i effects become important at smaller S_i values in "quiet" magnetospheric conditions. The ratio of ion to electron mean energies implied by the

above data is also larger in "quiet" conditions, corresponding to the dependence of S_i effects on ϵ noted in Fig. 2.15. The "quiet" and "disturbed" distributions also differ substantially in shape (Knott, 1972, Figs. 1 and 2b). The onset of "significant" drift effects (i.e. floating potential changes $\gtrsim 10\%$) is seen to occur at S_i values as low as 0.1, depending on conditions. It occurs at lower S_i values in the presence of the "quiet" distribution than in any of the other cases shown in Figs. 2.15 and 2.16. In Figs. 2.15 and 2.16, negative floating potentials for $S_i = 1$ are in most cases about twice as large as the corresponding potentials for nondrifting situations.

3. MULTIPLE FLOATING POTENTIALS, AND THE "THRESHOLD MATERIAL TEMPERATURE FOR HIGH-VOLTAGE CHARGING"

3.1 INTRODUCTION

The high-voltage charging behaviour of spacecraft surfaces, especially in outer-magnetospheric plasma conditions, displays a variety of unexpectedly complex features.

These features are most evident in the absence of photoemission (as on shaded surfaces of a spacecraft). One of them is the existence of multiple roots (zeros) in the current-voltage characteristic of various spacecraft materials exposed to certain kinds of ambient plasma environments. An example of such a current-voltage characteristic was shown in Fig. 2.5. In this illustration, only the right- and left-hand roots, which are located at +1.9 and -4100 volts, respectively, represent stable floating surface potentials, because the centre root is an unstable one, in the sense that any voltage excursion from the indicated value (-500V) would result in a net current of a sign which would cause the voltage excursion to increase, ultimately driving the voltage to the right- or left-hand roots.

The possibility of such triple-root situations was first proposed by Whipple (1965, pp. 4-7). Prokopenko and Laframboise (1977, 1980) calculated current-voltage characteristics of various surface materials in outer-magnetospheric (including geostationary-orbit) plasma environments, and found numerous examples in which triple-root characteristics were actually obtained. Sanders and Inouye (1979) did calculations to examine the ranges of conditions in which such characteristics would occur. Besse (1981) examined the mechanisms underlying them. Meyer-Vernet (1982) showed that they may also occur on dust grains in space, such as those in Saturn's rings. It is now generally recognized that in triple-root situations, the stable floating potential near space potential is the result primarily of a current balance between incident "primary" electrons and emitted (secondary and backscattered) electrons,

with incident ion current making only a minor contribution, while at the more negative stable potential, the current balance is primarily between incident ion and electron currents, even though in this case also, both of these may be substantially modified by secondary or backscattered electron emission.

Another feature of the high-voltage charging phenomenon is the occurrence of "sensitivity" effects in the numerical prediction of spacecraft potentials (Stannard et al, 1981), in which relatively small changes in assumed surface properties or ambient conditions can cause large changes in spacecraft floating potentials. Evidently, this phenomenon may frustrate attempts to make reliable predictions of spacecraft charging, and it is important to identify the parameter ranges in which such sensitivity effects occur.

This phenomenon is closely related to that of "threshold" effects, both predicted (Stannard et al, 1981), and observed (Gussenhoven and Mullen, 1982), in which no high-voltage charging occurs over a large range of environmental or surface conditions, but a small further change in conditions then results in a large change in surface potential from a small value (relative to space) to a value typically several kilovolts negative.

Another closely-related effect is that of sudden large changes in surface potential in response to relatively slow temporal changes in ambient plasma conditions (Sec. 2.3). This phenomenon was predicted by Prokopenko and Laframboise (1980) and Besse (1981), and subsequently observed both on the SCATHA (P78-2) satellite and in numerical simulations made using the NASA Charging Analyzer Program (NASCAP) (Schnuelle et al, 1981; Stannard et al, 1982).

In Secs. 3.2 and 3.3, we introduce the concept of threshold temperature as a property of a spacecraft surface material, and we show that all of the above-mentioned phenomena are unified and explained by this concept.

A separate phenomenon, which often controls the differential charging of other surfaces, including sunlit ones, relative to the most highly-charged surface, is the "barrier" effect; we discuss this in Sec. 4.5.

3.2 THE THRESHOLD-TEMPERATURE PROPERTY.

A typical secondary-electron yield curve is shown in Fig. 3.1(a). For most commonly-used spacecraft surface materials, there exists a region of this yield curve in which more than one secondary is produced on average per primary. This generally occurs for incident electron kinetic energies of a few hundred eV. In Fig. 3.1(b), energy-differential incident-electron flux (particle current density) curves are shown for Maxwellian electron velocity distributions at two representative values of electron temperature T_e . In the example shown, the peak of the lower-temperature curve is at almost the same energy as that of the secondary yield curve. In this situation, there is a large production of secondaries; in fact, the total secondary flux, which is given by an integral involving the product of these two functions [Eq. (2.10); Prokopenko and Laframboise (1977, 1980, Eq. 10)], will be greater than the incident primary flux if the maximum secondary yield δ_{\max} per primary is greater than about 1.16 (Besse, 1981, Fig. 2). In contrast, the peak of the higher-temperature curve does not coincide closely with that of the secondary-emission curve, and in this case, the total secondary flux will be less than the incident flux. Evidently, a critical value of T_e must exist, intermediate between the two values indicated, at which emitted flux would exactly balance incident flux (H.I. Cohen, 1982, private communication). (There will also be another such critical temperature, below the peak of the secondary yield curve, but this is not of importance here.)

Maxwellian ambient distributions also have the special property that if they are retarded by a repelling (negative) surface potential, the distribution of particle kinetic energies reaching the surface is independent of the value of this potential. Therefore, for a Maxwellian ambient distribution, the preceding conclusions have a special property: they are independent of spacecraft surface potential (Besse, 1981; H.I. Cohen, private communication, 1982) as long as this potential is negative (with respect to space). Therefore, if the ambient electrons were Maxwellian at the critical temperature, incoming and outgoing fluxes would balance each other for all negative values of surface potential, and the surface then "would not know at what potential to float", i.e. the surface potential would become indeterminate, except for the (relatively small) current contribution from ambient ions. It is therefore evident that very large (negative) increases in floating potential will result for very small increases in ambient electron temperature in the neighbourhood of this critical value, which is a property of the surface material only. We will therefore refer to this critical value as the threshold material temperature T^* for high-voltage charging. In terms of this property, the first four effects mentioned in Sec. 3.1 can be immediately explained, as follows.

(1) Triple-root current-voltage characteristics have a simple explanation if the ambient electron velocity distribution can be approximated by a double Maxwellian. Such an approximation, although empirically-based, is often a very good one (Garrett and DeForest, 1979 ; Garrett et al, 1981). In this case, a characteristic will have three roots if (i) the temperature T_1 of one Maxwellian is less than T^* , but the other one T_2 is greater than T^* , and (ii) the total emitted electron (secondary and backscattered) flux at space potential is greater than the incident flux.

This can be proven as follows. The roots of the current-voltage characteristic are given by the zeros of the function:

$$J_{\text{net}} = J_i - J_e + J_{\text{sec}} + J_{\text{scat}} \quad (3.1)$$

where J_i , J_e , J_{sec} and J_{scat} are particle current densities (fluxes) for incident (ambient) ions and electrons, secondary electrons and backscattered electrons, respectively. Except at relatively large negative surface potentials ϕ_s relative to space, J_i is relatively small, and will be neglected in what follows. For $\phi_s < 0$, we then have, in this approximation:

$$\begin{aligned}
 J_{net} &= (J_{sec,1} + J_{scat,1} - J_{e,1}) \exp(e\phi_s/kT_1) \\
 &\quad + (J_{sec,2} + J_{scat,2} - J_{e,2}) \exp(e\phi_s/kT_2) \\
 &\approx J_{net,1} \exp(e\phi_s/kT_1) + J_{net,2} \exp(e\phi_s/kT_2)
 \end{aligned} \tag{3.2}$$

where $e > 0$ is the elementary charge, k is Boltzmann's constant, and all double-subscripted J are space-potential values. A triple-root characteristic must have an unstable root, i.e. a value of ϕ_s such that (a) $J_{net} = 0$, and (b) $dJ_{net}/d\phi_s > 0$. This can happen only for $\phi_s < 0$ because J_{sec} and J_{scat} both decrease rapidly at positive potentials (an exception to this, applicable at very small electron temperatures, has been found by Meyer-Vernet (1982)). Condition (a) requires that $J_{net,1}$ and $J_{net,2}$ have opposite signs, i.e. T^* is between T_1 and T_2 . Condition (b) implies that $J_{net} > 0$ for all ϕ_s values between this root and zero; this in turn implies that $J_{net,1} + J_{net,2} > 0$. This completes the proof of (i) and (ii). Even though this proof is only approximate for real velocity distributions, it will still be generally valid in terms of "temperatures" related in the usual way ($\bar{E} = \frac{3}{2} kT$) to the mean energies obtained from a double-Maxwellian fit. Meyer-Vernet (1982) has shown that triple roots can also occur with Maxwellian electrons, when the electron temperature is less than the "temperature" of emission of secondary electrons. The unstable root then occurs at a positive rather than negative value of ϕ_s .

(2) For T (or $2\bar{E}/3k$) close to T^* , most current-voltage characteristics will have both a very small value and small slope over a large range of potentials, and the floating potential(s) will then be subject to large changes when only small changes in conditions occur. This explains "sensitivity" effects.

(3) For T slightly less than T^* , $J_{\text{sec}} + J_{\text{scat}} > J_e$ if $\phi_p < 0$, and the floating potential will generally be slightly positive. For T slightly greater than T^* , $J_{\text{sec}} + J_{\text{scat}} < J_e$ and the floating potential will generally be very negative. Clearly T^* is the temperature at which "threshold" effects may be expected.

(4) For a distribution which is (nearly) Maxwellian and has $T \approx T^*$, small (or gradual) changes in ambient conditions can cause the sign of $J_{\text{sec}} + J_{\text{scat}} - J_e$ to change, resulting in large, sudden changes in floating potential. For a distribution which may not be near-Maxwellian but which leads to a triple-root characteristic, changes in ambient conditions may cause two of the three roots to coalesce and disappear, also producing large, sudden potential changes (Sec. 2.3; Prokopenko and Laframboise, 1980; Besse, 1981; Meyer-Vernet, 1982).

3.3 CALCULATION OF THRESHOLD TEMPERATURES; DISCUSSION

We have calculated threshold-temperature values (Table 2) for a variety of spacecraft surface materials; a listing of our computer program for doing this appears in Appendix B. In order to do this, we have calculate $J_{\text{sec}} + J_{\text{scat}} - J_e$ as a function of T for Maxwellian incident distributions, and searched numerically for the value T^* at which this function changes from positive to negative as T increases.

For ambient electrons normally incident to a surface, we have used the secondary and backscattered flux expressions given by Prokopenko and Laframboise (1977, 1980), together with data given by Dekker (1958), Haenenberg and Brauer (1959, 1962), Gibbons (1966), Willis and Skinner (1973), Katz et al (1977, p. 38), Schnuelle et al (1979), Leung et al (1981), and Krainsky et al (1981).

The increased yields for electrons incident at other angles have an important influence on our results (last three columns of Table 2). For both secondary (Dekker, 1958; Salehi and Flinn, 1981; Krainsky et al, 1981) and backscattered (Darlington and Cosslett, 1972; Krainsky et al, 1981) electrons, it is found experimentally that the dependence of yield (average number of emitted electrons per incident electron) $\delta(E, \theta)$ on angle of incidence θ relative to the surface normal can be usefully approximated by a relation of the form

$$\ln \delta(E, \theta) = \ln \delta(E, 0) + \beta(1 - \cos \theta). \quad (3.3)$$

For secondary emission, the coefficient β appears to depend primarily on E/E_{max} , where E_{max} is the energy at which δ is largest when $\theta = 0^\circ$. For backscattered emission, β appears to depend most strongly on the atomic number Z of the surface material, and only weakly on incident energy E . Also, available information on E dependence is fragmentary, and in any case, secondary emission predominates over backscattered emission at smaller values of E . For these reasons, we have ignored the E dependence.

The dependence given by Eq. (3.3) has the special advantage that for any isotropic ambient velocity distribution, the integration over angle in the emitted flux expression can be done analytically. In this case, we have:

$$\begin{aligned}
 J_{\text{sec}} \text{ or } J_{\text{scat}} &= \int f \delta v_n d^3\vec{v} \\
 &= \iiint f(E) \delta(E, \theta) (v \cos \theta) (v^2 \sin \theta dv d\theta d\phi) \\
 &= 2\pi \int_0^\infty f(E) \delta(E, 0) v^3 dv \int_0^{1/2\pi} e^{\beta(E)(1-\cos \theta)} \cos \theta \sin \theta d\theta
 \end{aligned} \quad (3.4)$$

where (v, θ, ϕ) are spherical coordinates in velocity space with polar axis normal to the surface, $f \equiv d^6N/d^3\vec{r} d^3\vec{v}$ is the velocity distribution of ambient electrons, $E = \frac{1}{2}mv^2$, and v_n is the normal component of incident electron velocity.

The integral over θ yields $[\exp(\beta) - \beta - 1]/\beta^2$, which has the value $\frac{1}{2}$ when $\beta = 0$. After β is specified as a function of E , multiplication of $\delta(E, 0)$ by the factor $\Gamma = (2/\beta^2)[\exp(\beta) - \beta - 1]$ then corrects $\delta(E, 0)$ to include angle-dependence of the secondary or backscattered yield [see also Whipple, 1981, Eq. (3.11)]. To obtain the resulting dependence of $\delta \equiv \delta_{\text{sec}} + \delta_{\text{scat}}$ on E , we require that E_{max} and δ_{max} for normal-incidence secondary yield be specified, together with Z . Our complete yield algorithm then is:

$$\xi = \ln(E/E_{\text{max}}); \quad \eta = 0.2755(\xi - 1.658) - \sqrt{[0.2755(\xi - 1.658)]^2 + 0.0228};$$

$$\beta_{\text{sec}} = e^\eta; \quad \Gamma_{\text{sec}} = (2/\beta_{\text{sec}}^2) [\exp(\beta_{\text{sec}}) - \beta_{\text{sec}} - 1]; \quad (3.5)$$

$$\beta_{\text{scat}} = 7.37Z^{-0.56875}; \quad \Gamma_{\text{scat}} = (2/\beta_{\text{scat}}^2) [\exp(\beta_{\text{scat}}) - \beta_{\text{scat}} - 1]$$

where the above expressions for β_{sec} and β_{scat} have been obtained by fits to the data of Dekker (1958), Darlington and Cosslett (1972), Salehi and Flinn (1981), and Krainsky et al (1981). Finally:

$$S(E) = \left[7.4 \delta_{\max} \frac{E}{E_{\max}} \exp\left(-2\sqrt{\frac{E}{E_{\max}}}\right) \right] \Gamma_{\text{sec}} + [A - B e^{-CE}] \Gamma_{\text{scat}} \quad (3.6)$$

where the factors multiplying Γ_{sec} and Γ_{scat} are, respectively, the secondary-yield curve of Sternglass (1954a), and an empirical factor given by Eq. 2.9 (See also Prokopenko and Laframboise, 1980, Eq. (9)), in which the coefficients A, B, and C are functions of Z obtained from the data of Sternglass (1954b) and Palluel (1947). These coefficients are also displayed in Table 2. $J_{\text{sec}} + J_{\text{scat}}$ is then given by 2π times the integral over v in (3.4) with f replaced by the Maxwellian distribution corresponding to temperature T , or more generally, by Eqs. (2.10) - (2.14). $J_e = n_e (kT/2\pi m_e)^{1/2}$, i.e. the usual random flux for a Maxwellian distribution (where n_e is ambient electron density and m_e is electron mass), or more generally, is given by Eqs. (2.1) - (2.3).

The resulting threshold temperatures T^* (labeled "TC3") appear in the last column of Table 1. Corresponding values of T^* for simplified forms of $\delta(E)$ as indicated (labeled "TC1" and "TC2") appear in the two adjacent columns. It is clear from these results that angle-dependence of δ_{sec} and δ_{scat} has an important effect on values of T^* . The values labeled "TC1" can also be inferred from Fig. 2 of Besse (1981).

Clearly, those surface materials having the largest values of T^* will be the "most resistant" to high-voltage charging (leaving aside the effects of material conductivity) because the ambient environment will exceed their threshold temperature the least often. From this viewpoint, and using the data of Table 1, MgF_2 is the "most resistant" material, followed by activated beryllium-copper, gold, and NASCAP 'BOOMAT', a spatially-averaged representation of a composite surface consisting of kapton partly covered with platinum strips, used on the SCATHA satellite (Schnuelle et al, 1979). The zero entries for T^* in Table 1 are those for which $J_{\text{sec}} + J_{\text{scat}} < J_e$ at all values of T .

Our discussion so far has been almost completely concerned with "absolute" or "overall" surface charging, and has been based only on calculations of local currents to and from surfaces. Calculations of this type are usually sufficient to determine the floating potential of the most highly (usually negatively) charged portion of a spacecraft surface, which is usually in a shaded or partly-shaded region of the spacecraft. However, the most damaging effects of high-voltage charging are "differential" effects involving large potential differences between adjacent parts of a spacecraft. These effects are frequently dominated by non-local phenomena, an example of which we present in Sec. 4.6.

4. CYLVIA: A TWO-DIMENSIONAL CHARGING SIMULATION FOR CYLINDRICAL SPACECRAFT CROSS-SECTIONS WITH ANGLE-DEPENDENCE.

4.1 INTRODUCTION: THE QUASISTATIC ITERATION METHOD

We have constructed a numerical simulation program called CYLVIA (CYLinder Voltages in Ionosphere and Above) which combines the following features:

a) infinite circular cylindrical geometry with angle-dependence. We have chosen this geometry for the following reasons: A realistic model must be at least two-dimensional because the asymmetry between sunlit and shaded surfaces, or between surfaces with large and small secondary-electron emission currents, is a key feature of the differential charging problem. Cylindrical geometry is the simplest two-dimensional geometry, and it is also a useful approximation to many spacecraft shapes, including the DSCS and SCATHA mainframes, which are finite circular cylinders. Effects of finite cylinder length (three-dimensionality) on sheath potential profiles, which tend to cause a more rapid decrease of potential with radius, can be approximated by using a modified form of Poisson's equation (Sec. 4.3).

b) Quasistatic time-dependent iteration (Laframboise and Prokopenko, 1977). In this procedure, sheath potential changes during particle transit times are ignored. This leads to the following iteration scheme: a distribution of surface potentials is chosen. Poisson's equation is then solved to provide a radius- and angle-dependent static sheath potential [see (c) below]. Particle orbits are then followed numerically in this potential, yielding net surface charging rate as a function of surface position. Using this information, the surface potentials are updated. This process is repeated until a steady-state floating condition is obtained or in order to follow temporal changes in external conditions, such as spacecraft rotation or eclipse passage.

c) use of simplified space-charge density expressions (Sec. 4.2; Laframboise and Prokopenko, 1977), rather than numerical orbit-following,

in solving Poisson's equation for sheath potentials. Approximations of this type are good ones for geostationary-orbit situations, in which the Debye length of the ambient plasma is generally large enough that space-charge effects are almost negligible. They also yield an important saving of computer time.

Features (b) and (c) are now also used in the NASCAP (Katz et al, 1977, 1979) simulation program.

A listing of CYLVIA appears in Appendices C and D. The numerical solution of Poisson's equation in CYLVIA calculations uses the subroutines POIS, POISGN, POINIT, TRID, TRIDP, and NCHECK written by Swarztrauber and Sweet (1975).

4.2 USE OF APPROXIMATE SPACE-CHARGE DENSITY EXPRESSIONS

At geostationary-orbit altitude, the Debye length λ_D for ambient particles is usually ~ 10 m, so for satellites of ordinary size, effects of ambient space charge on sheath potentials will be relatively small. Any reasonably realistic approximation of this space charge can therefore be expected to produce only negligible errors in solving Poisson's equation for sheath potentials. Furthermore, large savings in computer time can be expected to result if one can avoid exact density calculations involving numerical orbit-following. In calculations using CYLVIA, only a relatively small amount of orbit-following is done, in order to calculate surface currents (Sec. 4.4).

A more significant space-charge effect near the spacecraft may be caused by emitted photoelectrons or secondary electrons (Soop, 1972; Schröder, 1973), because of their relatively low velocities compared to ambient values. However, effects of these are likely also to be small enough that any reasonably realistic approximations for their densities will yield good accuracy (Lafon, 1976). Such approximations must ultimately be verified by comparison with exact calculations. It is advantageous if such approximations depend on local potential only (rather than potentials at many locations), together with a relatively small number of other parameters, such as spacecraft potentials and potential barrier heights and locations. Laframboise and Prokopenko (1977) have developed such an approximation. Here we develop three

approximate expressions for ambient space-charge density [Eqs. (4.1)-(4.3)], based on the use of exact density expressions developed for collisionless, Maxwellian particles in the presence of obstacle-free potential wells of arbitrary shape by Laframboise and Parker (1973). The appropriate expression for our purposes is the result given by their Eq. (2) for three-dimensional wells. This is true even for an "infinite", that is, very long cylindrical spacecraft geometry, because of particle entry at the ends of such a geometry. For definiteness, we consider a negative well given by $\phi(x,y,z) \leq 0$, with $\phi \rightarrow 0$ as $x^2 + y^2 + z^2 \rightarrow \infty$, where ϕ is electric potential. If only ambient particles are considered, Poisson's equation is:

$$\nabla^2 \phi = \frac{e}{\epsilon_0} (N_e - N_i) \quad (4.1)$$

where e is magnitude of unit electron charge, ϵ_0 is permittivity of space, and N_e , N_i are electron and ion number densities, respectively. Since positive ions are the attracted species in this well, we use Eq. (2) of Laframboise and Parker (1973) for ion density, and the usual Boltzmann factor for electron density. If $\lambda_{De} = (\epsilon_0 k T_e / e^2 N_\infty)^{1/2}$, N_∞ is electron or ion density far from the spacecraft, L is a characteristic spacecraft length, $\tilde{\nabla} = L \nabla$, $\chi = e\phi / k T_e < 0$, k is Boltzmann's constant and T is temperature, Eq. (4.1) becomes:

$$\tilde{\nabla}^2 \chi = \left(\frac{L}{\lambda_{De}} \right)^2 \left\{ e^\chi - \frac{2}{\sqrt{\pi}} \left[(-\chi T_e / T_i)^{1/2} + g(-\chi T_e / T_i)^{1/2} \right] \right\} \quad (4.2)$$

where $g(s) = \frac{1}{2} \sqrt{\pi} \exp(s^2) \operatorname{erfc}(s) = \exp(s^2) \int_s^\infty \exp(-t^2) dt$. An efficient method for calculating $\operatorname{erfc}(s)$ has been given by Shepherd and Laframboise (1981).

The important feature of Eq. (4.2) for our purposes is that its right-hand side is a function of χ only. For small χ , Eq. (4.2) reduces to:

$$\tilde{\nabla}^2 \chi = (1 + T_e / T_i) (L / \lambda_{De})^2 \chi \quad (4.3)$$

where terms of order $\chi^{3/2}$ and higher have been ignored. The linear form of (4.3) permits the use of direct Poisson-solvers for finding χ . Another simplified form can be obtained by rederiving Eq. (4.2) with monoenergetic instead of Maxwellian ions assumed. The appropriate monoenergetic velocity

distribution (Chen, 1965; Laframboise, 1966, p. 14) is:

$$f = \frac{d^3 N}{d^3 \vec{v}} = \frac{m_i^2 N}{4\pi} \frac{\delta(E - E_1)}{(2m_i E_1)^{1/2}} \quad (4.4)$$

where $E_1 = 4kT_i/\pi$ and m_i is ion mass; this distribution duplicates the ambient number density and flux values of a Maxwellian at temperature T_i . Rederivation of (2) using this distribution yields the computationally simpler form:

$$\nabla^2 \chi = \left(\frac{L}{\lambda_{De}}\right)^2 \left[e^\chi - \left(1 - \frac{\pi}{4} \frac{T_e}{T_i} \chi\right)^{1/2} \right]. \quad (4.5)$$

If any regions exist where $\chi > 0$, the roles of ions and electrons are interchanged, and Eqs. (4.2) - (4.5) must be modified accordingly.

The essential approximation contained in Eqs. (4.2) - (4.5) is the neglect of orbit depletion due to intersection with the spacecraft. The densities of ambient ions and electrons will therefore both be overestimated near the spacecraft in these results. As long as the spacecraft is at least moderately smaller than λ_{De} , the effects of this overestimate will be small. The attracted-species density will be overestimated by the greater amount for reasons involving the curvatures of attracted and repelled particle orbits. The sheath profiles predicted by (4.2) or (4.5) will therefore be steeper than real profiles, if electron emission effects are ignored. Laframboise and Prokopenko (1977, Secs. 2.4.2 and 2.4.3) have also discussed space-charge density approximations based on symmetric potentials and on equivalent potential wells, for ambient and emitted electrons.

4.3 APPROXIMATE INCLUSION OF FINITE-CYLINDER - LENGTH (THREE-DIMENSIONAL) EFFECTS IN POISSON'S EQUATION.

Effects of finite spacecraft length on sheath potential profiles can be included in either of two approximate ways which lead to modifications of the two-dimensional Poisson equation to be solved. We include here a description of these methods. The first method is derived by pretending that the circular inner boundary of the computation grid, which

represents the spacecraft surface, is no longer a cross-section of an infinite cylinder, but rather is a cross-section through the equatorial plane of a prolate spheroid of polar-to-equatorial axis ratio $L \geq 1$.

We also assume that the sheath potential is (for some unspecified reason) independent of the latitude coordinate perpendicular to this plane.

This leads to a modified Poisson equation of the form

$$\tanh^2 \xi \frac{\partial^2 \chi}{\partial \xi^2} + \tanh \xi \frac{\partial \chi}{\partial \xi} + \frac{\partial^2 \chi}{\partial \theta^2} = \frac{\sinh^2 \xi}{\sinh^2 \xi_s} \left(\frac{R_s}{\lambda_D} \right)^2 (n_e - n_i) \quad (4.6)$$

where $\chi = e\phi/kT_e$, ξ is a radial coordinate in the equatorial plane and is related to nondimensional radius $r = R/R_s$, defined in the same plane, by the relation

$r = (L^2 - 1)^{1/2} \sinh \xi$, $\xi_s = \frac{1}{2} \ln [(L+1)/(L-1)]$, θ is angular coordinate in the same plane, R_s is spacecraft radius, λ_D is Debye length, and n_e and n_i are the nondimensional electron and ion densities $N_e/N_{e\infty}$ and $N_i/N_{i\infty}$, where N_0 is ambient density of either species. Use of Eq. (4.6) in place of the usual polar-coordinate Poisson equation would result in sheath potential profiles which became increasingly steeper as L decreased, thus allowing for approximate estimates of sheath potentials around finite cylinders. The limiting case $L=1$ would correspond to an assumed spherical geometry without latitude dependence; the limit $L \rightarrow \infty$ leads to recovery of infinite cylindrical geometry.

The transformation $s = \ln \coth \frac{1}{2} \xi$ leads to the alternative form

$$\frac{1}{\cosh^3 \xi} \frac{\partial^2 \chi}{\partial s^2} + \frac{\partial^2 \chi}{\partial \theta^2} = \frac{\sinh^2 \xi}{\sinh^2 \xi_s} \left(\frac{R_s}{\lambda_D} \right)^2 (n_e - n_i) \quad (4.7)$$

which contains no first-order terms. For small ξ , s varies logarithmically with r ; for large ξ , s varies as r^{-1} .

The second method is derived by first writing the nondimensional Poisson equation for cylindrical coordinates, which has the form

$$\frac{\partial^2 \chi}{\partial z^2} + \frac{1}{r} \frac{\partial \chi}{\partial r} + \frac{1}{r^2} \frac{\partial^2 \chi}{\partial \theta^2} + \frac{\partial^2 \chi}{\partial z^2} = \left(\frac{R_s}{\lambda_D} \right)^2 (n_e - n_i) \quad (4.8)$$

We then assume that $\chi(r, \theta, z)$ is periodic in z , such that values of χ repeat after nondimensional distance 2ℓ parallel to the z axis. In particular, we assume that $\chi(r, \theta, z) = \text{some given dependence } \chi_2(r, \theta)$,

and that $\chi(r, \theta, 0) = \chi_0(r, \theta)$ to be found. We further assume that $\partial\chi/\partial z = 0$ at $z = 0$, $z = \pm l$, $z = \pm 2l$, etc, and that only the lowest Fourier component of the z dependence of χ is present. Then

$$\chi(r, \theta, z) = \frac{1}{2}[\chi_0(r, \theta) + \chi_l(r, \theta)] + \frac{1}{2}[\chi_0(r, \theta) - \chi_l(r, \theta)] \cos\left(\frac{\pi z}{l}\right) \quad (4.9)$$

and, at $z = 0$, we have

$$\frac{\partial^2 \chi_0}{\partial z^2} = \frac{1}{2} \left(\frac{\pi}{l}\right)^2 [\chi_l(r, \theta) - \chi_0(r, \theta)] \quad (4.10)$$

The Poisson equation for $\chi_0(r, \theta)$ now becomes

$$\frac{\partial^2 \chi_0}{\partial r^2} + \frac{1}{r} \frac{\partial \chi_0}{\partial r} + \frac{1}{r^2} \frac{\partial^2 \chi_0}{\partial \theta^2} - \frac{1}{2} \left(\frac{\pi}{l}\right)^2 \chi_0 = \left(\frac{R_s}{\lambda_D}\right)^2 (n_e - n_i) - \frac{1}{2} \left(\frac{\pi}{l}\right)^2 \chi_l(r, \theta) \quad (4.11)$$

We see that in this Poisson equation, effects of z -dependence are represented by a homogeneous "Helmholtz" term and a fictitious space charge contribution. The z -dependence incorporated into this equation could represent approximately the effects on sheath potentials of finite spacecraft length and/or features such as conductive circumferential bands. Equations (4.7) and (4.11) are both solvable by standard methods; both are linear. Both contain only two (radius and angle) independent variables.

4.4 ORBIT INTEGRATION AND CURRENT CALCULATION

CYLVIA uses a form of the particle orbit equations in which particle total energy is explicitly conserved. This formulation was adopted because of a difficulty which arose when using more standard methods to integrate photoelectron orbits. Accumulation of numerical errors was occasionally found to change the total energy of an orbit by amounts large compared to the assumed thermal energy of emission (1.5V), especially near points where orbits were "reflected" by a potential barrier; this in turn produced large errors in calculations of photoelectron currents reimpacting spacecraft surfaces.

In order to derive the orbit equations, we consider the motion of a particle in a plane. We let (r, θ) and (v_r, v_θ) represent its position and

velocity components in polar coordinates (Fig. 4.1). We let s represent arc length along its orbit, and \hat{u} and \hat{n} represent unit tangent and unit normal vectors at a point on the orbit, the latter directed toward its local centre of curvature. We let ρ represent its local radius of curvature. We let q, m , and E represent particle charge, mass, and total energy, and $\phi(r, \theta)$ represent electric potential. The equation of motion $m \, d\vec{v}/dt = -q\nabla\phi$ reduces to:

$$v \frac{dv}{ds} \hat{u} + \frac{v^2}{\rho} \hat{n} = \frac{q}{m} \left(-\hat{n} \frac{\partial \phi}{\partial n} - \hat{u} \frac{\partial \phi}{\partial s} \right) \quad (4.12)$$

We equate respective components of Eq. (4.12) and use the relations $ds = \rho d(\alpha + \theta)$, $dr = \cos(\alpha) ds$, and $r \, d\theta = \sin(\alpha) ds$. We then obtain the orbit equations in the following form:

$$\begin{aligned} \frac{d\alpha}{ds} &= - \frac{q}{mv^2} \left(\frac{\cos \alpha}{r} \frac{\partial \phi}{\partial \theta} - \sin \alpha \frac{\partial \phi}{\partial r} \right) - \frac{\sin \alpha}{r} \\ \frac{dr}{ds} &= \cos \alpha \\ \frac{d\theta}{ds} &= \frac{\sin \alpha}{r} \\ v^2 &= \frac{2}{m} \left[E - q\phi(r, \theta) \right] \end{aligned} \quad (4.13)$$

This system is reduced from fourth to third order because the last equation appears in integrated form. At points where particle reflection from potential barriers produces cusps or near-cusps in an orbit ($d\alpha/ds$ becomes singular or large), a segment of the orbit is replaced by a parabolic arc.

We illustrate the current calculation method used by CYLVIA by first considering photoelectrons which arrive at a point on the surface whose normal makes an angle θ with the sunward direction, each of them having originated at some other surface location θ_0 (Fig. 4.2a) and forced to return to the surface by a potential barrier which surrounds the spacecraft. Their current density at the surface location given by θ is:

$$J(\theta) = \int_{v=0}^{v=\infty} \int_{\omega=0}^{\omega=\pi} \hat{f}(v, \omega) (v \sin \omega) (v \, dv \, d\omega) \quad (4.14)$$

where $v = (v_r^2 + v_\theta^2)^{1/2}$ and $\omega = \tan^{-1}(v_r/v_\theta)$ are polar coordinates in incident velocity space at the surface location θ , $\hat{f} \equiv d^2N/dv_r dv_\theta$ is the two-dimensional velocity distribution of photoelectrons, and N is their number density. By Liouville's theorem, \hat{f} is constant along a particle orbit. Assuming that photoelectrons are emitted with a Maxwellian distribution corresponding to a temperature T , their emission flux $J_{ph}(\theta_0)$ is related to \hat{f} as follows:

$$\hat{f} = \frac{1}{\sqrt{2\pi}} J_{ph}(\theta_0) \left(\frac{m}{kT} \right)^{3/2} e^{-mv_0^2/2kT} \quad (4.15)$$

If the sunlit side of the spacecraft has uniform material properties, then

$J_{ph}(\theta_0) = J_{ph}(0) \cos \theta_0$. We introduce dimensionless variables as follows:

$$\chi = q\phi/kT; \quad u = v(m/2kT)^{1/2} \quad (4.16)$$

Since $\frac{1}{2}mv^2 + q\phi = \frac{1}{2}mv_0^2 + q\phi_0$, (4.15) and (4.14) become:

$$\hat{f} = \frac{1}{\sqrt{2\pi}} J_{ph}(\theta_0) \left(\frac{m}{kT} \right)^{3/2} e^{\chi_0 - \chi} e^{-u^2} \quad (4.17)$$

$$J(\theta) = \frac{2}{\sqrt{\pi}} \int_{u=0}^{u=\infty} du \, u^2 \, e^{-u^2} \int_{\omega=0}^{\omega=\pi} d\omega \sin \omega \left[J_{ph}(\theta_0) e^{\chi_0 - \chi} \right] \quad (4.18)$$

The factor in square parentheses in (4.18) is evaluated for each u and ω by integrating the corresponding photoelectron orbit backward to its origin to find θ_0 and χ_0 . To do the integrations in (4.18) we set up a polar-coordinate grid in velocity space at the surface location θ , as shown in fig. 4.2b, where we have defined $u_n = -u_r$, $u_t = -u_\theta$. We approximate $F(u, \omega) \equiv (2/\sqrt{\pi}) J_{ph}(\theta_0) \exp(\chi_0 - \chi)$ in each cell $u_i \leq u \leq u_{i+1}$, $\omega_j \leq \omega \leq \omega_{j+1}$ by $(A + Bu)(C + D\omega)$ where A, \dots, D can be determined if the values of F at its four corners are found, again by integrating orbits backward. Equation (4.18) then becomes:

$$J(\theta) = \sum_{i,j} \int_{u_i}^{u_{i+1}} du u^2 e^{-u^2} (A_{ij} + B_{ij}u) \int_{\omega_j}^{\omega_{j+1}} d\omega \sin \omega (C_{ij} + D_{ij}\omega), \quad (4.19)$$

a form in which all integrals can be evaluated analytically. This method for evaluating $J(\theta)$ is essentially equivalent to the "inside-out" method of Parker and Whipple (1967). The factor $\exp(\chi_0 - \chi)$ in $F(u, \omega)$ may vary strongly within individual cells. The potential barrier which surrounds a spacecraft is always of finite height, permitting some photoelectrons to escape and ambient electrons to reach it. This means that the integration in (4.19) must be performed over two regions of velocity space, labelled I and II in Fig. 4.2b, containing photoelectrons (and secondary and backscattered electrons), and ambient electrons, respectively. In general, \hat{f} will contain a discontinuity at the boundary between I and II (Whipple, 1976) which can produce large errors in the evaluation of $J(\theta)$. The integration method used in CYLVIA treats these discontinuities explicitly, using bisection searches to find points such as those circled in Fig. 4.2b. If the ambient electron velocity distribution is isotropic, then F in region II will be independent of ω .

4.5 RESULTS AND DISCUSSION

Figure 4.3 shows a CYLVIA calculation of equipotential contours surrounding a cylindrical spacecraft cross-section whose surface consists of two independently floating conductive sectors, the smaller of which is shaded and subtends an angle of 90° . In this calculation the ambient ion and electron velocity distributions are double Maxwellians with the following properties:

$N_{i1} = 1 \text{ cm}^{-3}$	$N_{e1} = 1 \text{ cm}^{-3}$
$T_{i1} = 20 \text{ eV}$	$T_{e1} = 500 \text{ eV}$
$N_{i2} = 1 \text{ cm}^{-3}$	$N_{e2} = 1 \text{ cm}^{-3}$
$T_{i2} = 10^4 \text{ eV}$	$T_{e2} = 5000 \text{ eV}$

The photoelectron charge flux eJ_{ph} is $45 \times 10^{-6} \text{ A/m}^2$ at normal sunlight incidence. $T_{ph} = 1.5 \text{ eV}$. Secondary and backscattered electron fluxes are assumed zero. Ambient ion and electron and photoelectron currents are calculated using numerical orbit-following as described in Sec. 4.4. The computation grid in (r, θ) contains 65×48 intervals. In this and subsequent calculations, the computation grid in (u, ω) contains 8×16 intervals for each Maxwellian component of each particle species, apart from bisection searches (Sec. 4.4) which give finer resolution. Linear space charge is assumed [Sec. 4.2; Laframboise and Prokopenko, 1977, Eq. (3)]. The above-mentioned plasma parameters imply an ambient Debye length of 32.5 meters; spacecraft radius r_s is 1 meter. The outer boundary of the computation grid is at $e^5 r_s \approx 148 r_s$. The most noteworthy feature of Fig. 4.3 is a negative saddle-point potential barrier which surrounds the larger sector, and whose height varies from about 2 volts at the sunward point to several hundred volts near the edges of this sector. The potential of the 270° sector (-2.265 kV) is controlled by blocking of electron escape caused by this barrier; this mechanism is discussed in more detail in Sec. 4.6. In Sec. 6.5, surface photocurrents obtained from this calculation are compared with values given by an analytic approximation. In this and subsequent calculations, calculated surface potentials are all within 10 volts of the values at which the residual currents change sign.

Figure 4.4 shows a CYLVIA calculation of equipotential contours around a spacecraft cross-section divided into four 90° sectors, two covered with aluminum and two with quartz. The aluminum sectors are electrically connected to each other. In this calculation the ambient velocity distributions are single Maxwellians with $N_i = N_e = 3\text{cm}^{-3}$ and $T_i = T_e = 1\text{ keV}$. Photoelectron fluxes at normal sunlight incidence are 42 and $32\text{ }\mu\text{A/m}^2$ for aluminum and quartz, respectively. $T_{ph} = 1.5\text{ eV}$ for both. Secondary and backscattered fluxes are assumed zero. The computation grid in (r, θ) contains 65×16 intervals. The outer boundary of this grid is at $e^7 \times 1097$ spacecraft radii. The above-mentioned plasma parameters imply an ambient Debye length of 96 meters; spacecraft radius r_s is 1 meter. As in Fig. 4.3, a saddle-point barrier is present on the sunward side of the spacecraft (see Sec. 4.6), and controls the potential of the sunlit quartz sector and the two aluminum sectors.

In a separate calculation, which is not shown, we included secondary and backscattered electron emission; the calculated surface potentials then were all between 0 and +10V. This result can be readily interpreted in terms of the threshold material temperatures for high-voltage charging defined in Sec. 3 and listed in Table 2. Although the value of T_e for this case is greater than the threshold temperature of aluminum (Table 2), the aluminum sectors are partly sunlit, and photoemit enough to balance their ambient electron collection current. The threshold temperature of quartz is greater than T_e , so secondary and backscattered electron emission from these sectors is therefore enough to balance their ambient electron collection current. Thus in this case, no negative charging occurs on any sector. If T_e were made substantially larger than the threshold temperature of quartz (Table 2), then high-voltage negative charging of the shaded quartz sector would again occur.

In Fig. 4.5, the same spacecraft cross-section as in Fig. 4.4 has been rotated by 90° relative to the sunward direction. In this case the most negative potentials are those on the shaded regions of the quartz sectors, which float separately from the sunlit regions because the quartz is nonconductive. In this situation it is possible that

breakdown of orbit-limitation of the collection of ambient ions (Sec. 2.1) could occur, especially near the edges of these shaded regions, and this would restrict ion collection and cause their floating potentials to become even more negative than we have calculated, but the rather coarse θ -interval of our computational grid has prevented us from resolving this question in this calculation.

Also in Fig. 4.5, we have this time a saddle-point barrier on the shaded side of the spacecraft; if the calculation had included secondary and backscattered electrons, this barrier would have controlled their escape. In this case a negative current flows from the shaded to the sunlit aluminum sector, so the sunlit sector floats at a much more negative potential than it would otherwise.

Figure 4.6 shows the distribution of surface potentials corresponding to the calculations of Figs. 4.4 and 4.5, together with the calculated surface potential distribution of a completely nonconductive ("quartz" but with secondary and backscattered electron emission not included) cylinder which is placed in the same environment.

Figure 4.7 shows again the same surface potential distribution for a nonconductive cylinder as in Fig. 4.6, together with another distribution for conditions which are unchanged except that the outer boundary r_B of the calculation is moved inward to 12 spacecraft radii r_S . A third calculation is shown, which has been done not using CYLVIA but using a program called TWOD, which combines the physical assumptions of the NASCAP program with circular cylindrical geometry (M. Mandell, Systems, Science and Software Inc., private communication). Except as noted, the physical situations treated in the CYLVIA and TWOD calculations are the same; in both cases $r_B = 12 r_S$, zero secondary and backscattered emission is assumed, and a 16-point angular discretization is used. In the TWOD calculation, zero space charge is assumed, but since $\lambda_D = 96 r_S$ in the CYLVIA calculation, the comparison shown is probably unaffected by this

difference. In the TWOD calculation, photoelectron temperature and normal-incidence flux are 2 eV and $20 \mu\text{A}/\text{m}^2$, whereas for CYLVIA, the corresponding parameters are 1.5 eV and $45 \mu\text{A}/\text{m}^2$.

We see that rough agreement exists between the CYLVIA and the TWOD calculations. Either our higher photoemission flux, or the rather coarse angular discretization used in both calculations, may account for the differences; we have not yet investigated this question with further calculations. Even though the barrier which surrounds the sunlit side of the cylinder prevents almost all photoelectron escape in the (two) regions $60^\circ \leq \theta < 90^\circ$ where the largest disagreement occurs, our larger assumed flux permits greater surface migration of photoelectrons (Sec. 6), and the resulting surface current will drain excess negative charge from these regions (to an extent which we have so far not determined). The large difference between the two CYLVIA calculations for $r_B = 12r_S$ and $r_B = e^7 r_S$ is symptomatic of the great sensitivity which two-dimensional Laplace-potential (or nearly Laplace-potential, as in our case) calculations have to outer-boundary position generally. On the other hand, tests with CYLVIA have indicated that $r_B \gtrsim e^5 r_S$ is sufficient to overcome this sensitivity, especially when a small amount of linear (or other) space charge is included, as we have done.

4.6 THE BARRIER EFFECT

As we have seen (Secs. 2 and 3), charging calculations based on local-current-balance considerations are usually sufficient to determine the floating potential of the most highly (usually negatively) charged portion of a spacecraft surface, which is usually in a shaded or partly-shaded region of the spacecraft. However, the most damaging effects of high-voltage charging are "differential" effects involving large potential differences between adjacent parts of a spacecraft. These effects are frequently dominated by non-local phenomena, several examples of which occurred in Sec. 4.5, and which we now examine in more detail.

The most important among these phenomena is the "barrier" effect, which often controls the differential charging of other surfaces, including sunlit ones, relative to the most highly-charged surface. In the "barrier" effect, a strong dipole or higher moment of the spacecraft's potential distribution produces "saddle-point" barriers over less-highly-charged portions of the spacecraft, limiting photoemitted or other electron escape from these portions and causing them to charge more negatively than otherwise. Space-charge effects are normally not important in the formation of such barriers. Their existence, and the resulting implications for differential charging, were first predicted by Fahleson (1973). Whipple (1976) presented evidence for the existence of such a barrier on the ATS-6 satellite. Other properties and consequences of these barriers were discussed by Prokopenko and Laframboise (1977,1980) and Laframboise and Prokopenko (1977). Katz et al (1979) performed a numerical simulation which showed the formation of such a barrier near a polyhedral "quasispherical" model satellite, together with the resulting effects for differential charging. Besse and Rubin (1980) developed an analytical treatment of the barrier effect for a spherical satellite. Purvis (1982) presented a variety of NASCAP numerical simulations to illustrate the prevalence of the barrier effect in high-voltage charging situations. Katz and Mandell (1982) examined mechanisms underlying the barrier effect, called by them the "field-reversal" effect, and in one particular application, the "snapover" effect. In this Section, we present results of a numerical simulation for circular cylindrical geometry, which emphasize the importance of the barrier effect for differential charging.

Using CYLVIA (Secs. 4.1 - 4.5), we have calculated the equilibrium charging state of a cylindrical spacecraft shape with a nonconductive surface in a model geostationary-orbit plasma with sunlight incident normally to the cylinder axis on one side. Figure 4.8 shows the results of a CYLVIA calculation in which we have deliberately made an important oversimplification: we have calculated the surface potential distribution on the basis of local current balance only. Because sunlight

strikes only one side of the spacecraft, photoelectrons are emitted only from this side. In this example, the escaping photoelectron flux from most of the sunlit side is sufficient to balance the ambient electron flux, so the sunlit side of the spacecraft floats at a potential of 5.1V, while the shaded side floats at -2.96 kV. As a result, the spacecraft potential has a strong dipole moment, resulting in the existence of a potential barrier which surrounds its sunlit side. The height of this barrier is -0.61 kV, while the assumed photoelectron emission temperature is only 1.5 eV, so almost all photoelectrons reflect from the barrier and return to the spacecraft, an effect which we have not taken into account in this calculation.

In Fig. 4.9 we have included this effect, and have allowed CYLVIA to converge to the resulting more-realistic steady state. As a result of photoelectron reflection from the barrier, the sunlit side of the spacecraft has charged to a more negative potential. As a result, the barrier height in the sunward direction has been reduced to -0.2V. A substantial fraction of the photo-electrons now escape over the barrier, permitting the local currents to come into balance. A further indication of this is that the saddle point has moved inward from 5.9 spacecraft radii almost to the spacecraft surface: such an inward movement was first predicted by Fahleson (1973), and is evident also in the results of Katz et al (1979, Figs. 17-21) and Besse and Rubin (1980).

The resulting changes in the potential profile along the spacecraft-sun line are shown in Fig. 4.10. The inward motion of the saddle point is again evident. Most importantly, the amount of differential charging between the sunlit and shaded sides has been reduced dramatically, from 2.96 kV to 1.19 kV. Potential-barrier formation evidently exerts a controlling effect on the differential charging. This is increasingly recognized as being the normal condition in differential-charging situations (Purvis, 1982; Katz and Mandell, 1982). Because the capacitances between various parts of a spacecraft are generally much larger than the free-space capacitance of the entire spacecraft, the

charging times for differential charging are usually much larger than those for absolute charging (Purvis, 1982).

It is clear from our example and also the examples presented in Sec. 4.5 (and also another example to be presented in Sec. 5.2), that the formation of potential barriers is very geometry-dependent. This is the case because in geostationary-orbit conditions, space-charge shielding around spacecraft of "ordinary" size (up to a few tens of meters) is a small effect (since the ambient Debye length is usually at least this large), and electric fields produced by charging on one part of a spacecraft surface readily surround other parts of it, even if these are on the other side of the spacecraft. Detailed simulations which include realistic representation of spacecraft geometry therefore appear likely to remain important for studies of spacecraft charging whenever the possibility of barrier effects exists.

In Fig. 4.11 we show another CYLVIA calculation which is discussed in detail in Sec. 5.

5. XYCIC: A SIMULATION FOR GENERAL PLANAR-SYMMETRIC (TWO-DIMENSIONAL) SPACECRAFT GEOMETRIES

5.1 INTRODUCTION

We have developed and partly tested a program called XYCIC [(X,Y) Charging Investigation Code], which is designed to permit simulation of a wider class of two-dimensional geometries than does CYLVIA. XYCIC is designed to treat any spacecraft cross-section which takes the form of one or more polygons, each of which joins a set of unit lattice points in a Cartesian plane with lines having slopes of 0, $\pm\frac{1}{2}$, ± 1 , ± 2 , or ∞ . Thus a circular cylinder can be approximated by either an octagon or a hexadecagon (16-sided polygon). At present, the geometric features, or "object-generation" portion of XYCIC, and its Poisson-solver, have been completed and tested, and program segments incorporating the same plasma simulation features as in CYLVIA (Secs. 4.1-4.4) have been written and partly tested. A listing of the present version of XYCIC appears in Appendix E.

As noted in connection with Fig. 4.7, plasma simulations in two dimensions generally involve strong sensitivity to boundary effects, unless space-charge shielding intervenes, an effect which frequently does not occur at the large Debye lengths typical of geostationary-orbit conditions. In such cases, as we have seen, it may become necessary to place the outer boundaries of computational domains very far from a (simulated) spacecraft. In order to accomplish this in XYCIC without the penalty of excessive numbers of grid points, we have constructed its computational domain as a set of nested square grids, each of which is centered in the next larger one, and such that in crossing the boundary from each to the next larger one, the grid interval is doubled. A similar succession of nested sub-domains is used in three dimensions in NASCAP (Katz et al, 1977). On the boundary of the outermost domain, the potential is assumed to be zero.

5.2 PRELIMINARY RESULTS

Figure 5.1 shows a XYCIC calculation of equipotential contours around an octagonal approximation to the circular cylindrical geometry of Fig. 4.11. As in the case of Fig. 4.11, the surface potentials in Fig. 5.1 have the imposed values shown, rather than self-consistent values. A total of 7 nested grids have been used in this calculation, with the outermost grid boundary located at 27.4 half-widths of the simulated object.

This calculation, and the CYLVIA calculation shown in Fig. 4.11, have been done for comparison with a NASCAP calculation (Olsen, 1980, p. 190; Olsen and Whipple, 1980, Fig. 16) of potentials around an octagonal-cylinder "model object" which approximates the ATS-5 satellite. The feature of greatest interest in both sets of calculations is the potentials of the four saddle points which occur outside the 50 V sections of the spacecraft surface, which represent conductive areas from which electron emission occurred on the real spacecraft. Comparison of our results, Figs. 4.11 and 5.1, with each other indicates a satisfactory level of agreement between them with regard to the potentials and locations of the saddle points. This is the case even though the CYLVIA calculation contains a small amount of linear space charge, while the XYCIC calculation contains none.

Comparison of either result with that of Olsen and Whipple indicates that our saddle points are located about twice as far from the spacecraft surface as theirs, and have larger negative potentials (-56 to -59 V) than theirs (-53 V). These differences undoubtedly result from the fact that our simulation is two-dimensional and theirs is three-dimensional, even though our geometry in Fig. 5.1 is identical with that of their cross-section. Incorporation of three-dimensionality into our calculation, using the approximate method described in Sec. 4.3, would probably bring our results into much closer agreement with theirs, but we have not yet done this. In modifying our calculation in this fashion, it would probably be advantageous to perform our calculation as the superposition

of two modified calculations of the type described by Eqs. (4.8) to (4.11). One of these would have surface potentials given by the (uniform) average (taken over surface position) of those in our Figures, and the characteristic length λ used in it would be that of the ATS-5 model object. The other would have surface potentials given by the departures from this average, and its (much smaller) value of λ would be that of the conductive patches on the ATS-5 object. The disturbance potential of the patches would then decrease more quickly with radius, in better agreement with the Olsen and Whipple calculation.

Figure 5.2 shows a XYCIC prediction of equipotentials around a composite "object" which represents a cross-section through a hypothetical spacecraft-body-and-antenna combination. Again the surface potential values are given ones; in this case they are hypothetical. Other data pertinent to this calculation are given in the figure caption. If self-consistent calculations are made in the future with a geometry similar to the one shown, the "cutout" in the spacecraft body, and the region between the spacecraft body and the antenna, would both become examples of the "shaded cavities" discussed in connection with Fig. 2.8. It would then be possible to verify the prediction, made in Sec. 2.3, that electrically-isolated surfaces inside such cavities may charge to larger negative potentials than those elsewhere on the spacecraft. It would also be possible to investigate the relative importance of the two mechanisms, discussed in Sec. 2.3, which may produce such charging.

6. AN ANALYTIC CALCULATION OF SURFACE PHOTOCURRENTS

6.1 INTRODUCTION

Photoelectron migration can be an important cause of surface currents on spacecraft in charging situations. Numerical methods of calculating photoelectron migration involve following a large number of electron orbits which will generally be short (from origin to impact point) and have large curvature. Such a procedure can be a major source of expense in operating a simulation program. A good analytic approximation for surface photocurrent can therefore be of great value. If photoelectron migration takes place over a curved surface, the sunlight incidence angle will vary over this surface and therefore so will the photoemission flux. On the other hand, if the normal component of electric force on the electrons is attractive toward the surface and is large enough, the total distance of their travel along the surface will be short enough that effects of surface curvature on their orbits can be neglected, so a model situation involving a planar surface with a photoemission gradient along it becomes appropriate. In Section 6.2, we perform an analytic calculation of surface photocurrent for such a situation. In Section 6.3, we do a partial numerical verification of our result by comparing it with a numerical result obtained using CYLVIA.

6.2 THEORY

In this Section, we derive an analytic expression for the surface current density of photoelectron migration along a plane surface $y=0$, in the presence of: (a) a uniform normal electric field $E_y > 0$, which causes photoelectrons emitted from the surface to reimpact it (Fig. 6.1) (b) a uniform tangential electric field E_x (c) a uniform photoemission current density gradient $J'_{ph} = dJ_{ph}/dx$, so that the photoemission current per unit surface area is $J_{ph}(x) = J_{ph,0} + J'_{ph} x$. This photoemission gradient, or "production gradient", would ordinarily be caused by a spatial variation in the illumination of the surface. We also assume

that photoelectrons are emitted with a Maxwellian velocity distribution corresponding to a temperature $T = T_{ph}$. In the presence of (a) and (b), all photoelectron orbits are parabolas whose axes are parallel to the resultant electric field vector (Fig. 6.1). The impact location x for a photoelectron which originates at x_0 with emission velocity components v_{x0} and v_{y0} is:

$$x = x_0 + \frac{2m}{eE_y} (v_{x0} v_{y0} - \frac{E_x}{E_y} v_{y0}^2) \quad (6.1)$$

where e is the magnitude of unit electronic charge. The surface current Γ in the x direction, per unit distance z perpendicular to the (x, y) plane, can now be found by integrating over position and velocity of emission to find the number of photoelectrons per unit z and unit time which cross the plane $x = 0$ in the direction of increasing x , then subtracting the corresponding result for decreasing x . We note that $v_{y0} \hat{f}(x_0, v_{x0}, v_{y0})$ is the number of photoelectrons produced per unit surface area per unit v_{x0} and v_{y0} , where $\hat{f} \equiv d^2N/dv_x dv_y$ is the two-dimensional velocity distribution of photoelectrons and N is their number density.

We obtain:

$$\Gamma = \int_{-\infty}^0 dx_0 \int_{-\infty}^{\infty} dv_{x0} \int_0^{\infty} dv_{y0} v_{y0} \hat{f}(x_0, v_{x0}, v_{y0}) H_+(x_0, v_{x0}, v_{y0}) - \int_0^{\infty} dx_0 \int_{-\infty}^{\infty} dv_{x0} \int_0^{\infty} dv_{y0} v_{y0} \hat{f}(x_0, v_{x0}, v_{y0}) H_-(x_0, v_{x0}, v_{y0}) \quad (6.2)$$

where $\hat{f} = (1/2\pi) J_{ph}(x) (m/kT)^{3/2} \exp(-mv_0^2/2kT)$, and H_+ and H_- are equal to 1 if the impact location x given by (6.1) is positive or negative, respectively, and equal to 0 otherwise. We define:

$$v_0^2 = v_{x0}^2 + v_{y0}^2; \quad \psi = \tan^{-1}(v_{y0}/v_{x0}); \quad \xi = \tan^{-1}(E_y/E_x). \quad (6.3)$$

Since $v_{y0} > 0$, (6.1) implies that $x \geq x_0$ if $v_{x0} \geq (E_x/E_y)v_{y0}$, or $\psi \geq \xi$.

Equation (6.2) now becomes:

$$\Gamma = \frac{1}{\sqrt{2\pi}} \left(\frac{m}{kT} \right)^{3/2} \int_0^{\infty} dv_0 v_0^2 \exp\left(-\frac{mv_0^2}{2kT}\right) \int_0^{\xi} d\psi \sin\psi \int_0^0 dx_0 (J_{ph,0} + J'_{ph} x_0) - \frac{2mv_0^2}{eE_y} (\cos\psi \sin\psi - \cot\xi \sin^2\psi) - \frac{2mv_0^2}{eE_y} (\cos\psi \sin\psi - \cot\xi \sin^2\psi) - \frac{1}{\sqrt{2\pi}} \left(\frac{m}{kT} \right)^{3/2} \int_0^{\infty} dv_0 v_0^2 \exp\left(-\frac{mv_0^2}{2kT}\right) \int_{\xi}^{\pi} d\psi \sin\psi \int_0^{\pi} dx_0 (J_{ph,0} + J'_{ph} x_0) \quad (6.4)$$

We define:

$$\begin{aligned}\Gamma_o &= J_{ph,o} kT/eE_y; \quad \gamma = \Gamma/\Gamma_o; \\ \tilde{x} &= (eE_y/kT)x; \quad j' = J'_{ph} \Gamma_o/J_{ph,o}^2; \\ u &= v_o \sqrt{m/2kT}.\end{aligned}\tag{6.5}$$

Then (6.4) becomes:

$$\begin{aligned}\gamma &= \frac{2}{\sqrt{\pi}} \int_0^\infty du u^2 e^{-u^2} \int_0^\pi d\psi \left[4u^2 (\cos \psi \sin^2 \psi - \cot \xi \sin^3 \psi) \right. \\ &\quad \left. - 8u^4 j' (\cos^2 \psi \sin^3 \psi - 2\cos \psi \sin^4 \psi \cot \xi + \cot^2 \xi \sin^5 \psi) \right] \\ &= -4\cot \xi - j'(4 + 16\cot^2 \xi).\end{aligned}\tag{6.6}$$

Using (6.3) and (6.5), we finally obtain:

$$\Gamma = -\frac{4J_{ph,o} kT}{eE_y^2} \frac{E_x}{E_y} - J'_{ph} \left(\frac{kT_{ph}}{eE_y} \right)^2 \left[4 + 16 \left(\frac{E_x}{E_y} \right)^2 \right].\tag{6.7}$$

This result contains, respectively, a potential-gradient term, a production-gradient term, and a cross-term. The effect of the cross-term can be substantial: we see that it enhances the production-gradient term five-fold if $(E_x/E_y)^2 = 1$, in comparison with its value when $E_x = 0$. This is true regardless of the sign of E_x ; in other words, surprisingly, an "opposed" electric field causes the same enhancement as an "aligned" one.

The potential-gradient term is twice that given by Eq. (14) of Pelizzari and Criswell (1978); this can be seen as follows. If one assumes that photoelectrons are emitted isotropically, corresponding to a value of zero for the parameter b in their Eqs. (13) and (14), then in our notation, their Eq. (14) is:

$$-e\Gamma = \frac{4J_{ph,o} \left(\frac{3}{2} kT_{ph} \right) E_x}{3E_y^2}\tag{6.8}$$

where our quantities $-e\Gamma$, $J_{ph,o}$, and $\frac{3}{2}kT_{ph}$ are the same as their J_a , F , and $\langle E \rangle$, respectively. It is readily seen that (6.7) with $J'_{ph} = 0$ gives a result twice as large as (6.8), as just mentioned. To see why this difference occurs, we rederive Pelizzari and Criswell's result more rigorously, as follows. From our Eq. (6.1), the contribution of E_x to particle displacement in the x direction is

$$\frac{-2mE_x v_{yo}^2}{eE_y^2} \quad (6.9)$$

which is the same as their Eqs. (9) and (11) combined. The contribution due to v_{xo} in (6.1) averages to zero. Now the surface current density Γ per unit z equals the integral over v_{xo} and v_{yo} of: photoelectron production rate per unit v_{xo} and v_{yo} per unit surface area in the (x,z) plane, times distance travelled by particles of a given v_{yo} before impact [given by (6.9)]. This production rate in turn equals number per unit volume per unit v_{xo} and v_{yo} , times the value of v_{yo} .

Therefore:

$$\begin{aligned} \Gamma &= \int_0^\infty dv_{yo} \int_{-\infty}^\infty dv_{xo} \hat{f} v_{yo} \left(-\frac{2mE_x v_{yo}^2}{eE_y^2} \right) \\ &= \frac{J_{ph,o}}{\sqrt{2\pi}} \left(\frac{m}{kT} \right)^{\frac{3}{2}} \left(-\frac{2mE_x}{eE_y^2} \right) \int_{-\infty}^\infty dv_{xo} \exp \left(-\frac{mv_{xo}^2}{2kT} \right) \int_0^\infty dv_{yo} v_{yo}^3 \exp \left(-\frac{mv_{yo}^2}{2kT} \right) \\ &= -\frac{4J_{ph,o} kT_{ph}}{eE_y^2} \quad (6.10) \end{aligned}$$

in agreement with our result [Eq. (6.7)] rather than that of Pelizzari and Criswell. The reason for the difference evidently involves the fact that we have integrated Eq. (6.9) over v_{yo} but they did not. Thus we perform an integral containing v_{yo}^3 [in the first line of (6.10)], but their procedure involves essentially an integral containing v_{yo}^2 (to evaluate their quantity $\langle E \rangle$), times a separate integral containing v_{yo} (to obtain $J_{ph,o}$ from \hat{f}). Their procedure therefore involves the use of incorrect moments of the velocity distribution function of photoemitted electrons.

6.3 COMPARISON WITH A NUMERICAL RESULT FROM CYLVIA

Figure 4.3 shows a CYLVIA calculation of equipotential contours surrounding a cylindrical spacecraft cross-section whose surface consists of two independently floating conductive sectors, the smaller of which is shaded and subtends an angle of 90° . Data pertinent to this calculation are given in Sec. 4.5. The most noteworthy feature of Fig. 4.3 is a negative saddle-point potential barrier which surrounds the larger sector, and whose height varies from about 2 volts at the sunward point to several hundred volts near the edges of this sector.

The resulting normalized current densities j_i, j_e , and j_{ph} of ambient ions, ambient electrons, and photoelectrons are shown as functions of surface position in Fig. 6.2. We have made a separate calculation of j_{ph} using Eq. (6.7) with the tangential electric field E_x set equal to zero since the spacecraft surfaces are conductive. To use (6.7), we note that the net photoelectron flux out of the surface is equal to the divergence of Γ with respect to surface coordinates. In our geometry, this means that

$$J_{ph,net\ in} \equiv J_{ph,in} - J_{ph,out} = -\frac{1}{r_s} \frac{d\Gamma}{d\theta} = \frac{4}{r_s^2} \frac{d}{d\theta} \left[\left(\frac{kT_{ph}}{eE_r} \right)^2 \frac{dJ_{ph,out}}{d\theta} \right] \quad (6.11)$$

where

$$edJ_{ph,out}/d\theta = -45 \times 10^{-8} \sin \theta \text{ A/m}^2 \left(-\frac{1}{2}\pi < \theta < \frac{1}{2}\pi \right),$$

and the radial electric field E_r is obtained from the numerical solution for $\phi(r, \theta)$ used to construct Fig. 4.3. Net photoelectron currents obtained in this way are shown as dashed curves in Fig. 6.2. We see that near $\theta = 0^\circ$, the net outward photocurrent is badly underestimated by Eq. (6.11) since the potential barrier for electrons at this location is not much higher than the photoelectron mean thermal energy, so a substantial fraction of photoelectrons escape, and this is not allowed for in Eqs. (6.7) and (6.11). However, in the interval $30^\circ \lesssim \theta \lesssim 90^\circ$, where photoelectron escape is negligible, agreement between Eq. (6.11) and the numerical result is much better. The numerical result is about 10% to 20% above that given by (6.11); the most important reason for this

difference is probably the fact that the tangential electric field, although zero at the spacecraft surface, is nonzero outside it, and the form of the cross-term in (6.7) indicates that the production-gradient current [which is the one calculated in Eq. (6.11)] is strongly sensitive to such fields. We have shown the photoelectron current as decreasing to zero almost discontinuously beyond $\theta = 90^\circ$, because the average angular distance of photoelectron migration in the electric fields at this point ($E_\theta = 0$, $E_r = 1824$ V/m) is about 0.1° .

Another noteworthy feature of Fig. 6.2 is the decrease in the flux of ambient electrons at larger θ , caused by the increasing height of the potential barrier as one moves away from the sunward point $\theta = 0^\circ$.

7. FLUX AND DENSITY CALCULATION FOR COLLISIONLESS PARTICLE ORBITS

Calculation of current density deposited on a surface by particle orbits neighbouring a given orbit is of importance in several contexts related to spacecraft charging. Examples of these are: calculation of current density deposited on one part of a spacecraft by photoelectrons, secondary electrons, or beams of charged particles emitted from another point on it, or calculation of ion current density deposited on spacecraft surfaces in the presence of either a (model) infinite or a large but finite ion speed ratio. In this Section, a simple, general procedure is described for obtaining such information essentially as a byproduct of a numerical orbit calculation. The procedure is based on a perturbation of the orbit equations, and involves finding the evolution along an orbit of the axes of a differential tube of neighbouring orbits. The positions of these axes are given in terms of a set of integrals, contributions to which are collected as the orbit is followed numerically, and whose integrands involve the space derivatives $\partial F_i / \partial x_j$ of the force components of points along it. At a surface impingement point, current density is then obtained by projecting the cross-section of this tube onto the surface tangent plane. The same formulation can also be used to obtain information about particle number density along an orbit.

In order to appreciate the usefulness of such a procedure it is instructive to compare it with the "standard" procedure which one would normally follow in calculating values of current density deposited on surfaces, and space charge density, of collisionless ions with negligible thermal motion flowing past a collecting object. The "standard" procedure is to numerically follow sets of neighbouring, initially-parallel particle orbits inward from an assumed unperturbed region far from the object, and to calculate flux and density everywhere between any two orbits by finding out how far apart they have become at their impingement points or elsewhere. This method has inherent difficulties: if the orbits chosen are too far apart initially, an orbit may eventually go off in a very different direction than the orbit next to it, making calculations of flux or density between them impossible or unrealistic. On the other hand, if they are initially too close together, inaccuracies in calculating either orbit may obscure the small difference which one is trying to calculate.

Our calculation proceeds as follows. The equations of particle motion are:

$$\frac{d^2 \vec{x}}{dt^2} = \frac{F(\vec{x}, t)}{m} \quad (7.1)$$

which is equivalent to:

$$\frac{d^2 x_i}{dt^2} = \frac{F_i(x_1, x_2, x_3, t)}{m} \quad (7.2)$$

Integration of this yields:

$$x_i(t) = x_i(0) + v_i(0)t + \int_0^t dt' \int_0^{t'} dt'' \frac{F_i[x_k(t''), t'']}{m} \quad (7.3)$$

For perturbed orbits, (7.2) is replaced by:

$$\frac{d^2}{dt^2} (x_i + \delta x_i) = \frac{F_i + \delta F_i}{m} \quad (7.4)$$

Subtraction of (7.2) from (7.4) yields:

$$\frac{d^2}{dt^2} \delta x_i = \frac{\delta F_i}{m} \quad (7.5)$$

We now assume that perturbations at any instant are small. Then:

$$\delta F_i = \sum_j \frac{\partial F_i}{\partial x_j} \delta x_j \quad (7.6)$$

i.e. we ignore $(\delta x_j)^2$, $(\delta x_j)^3$, etc.

Equations (7.5) and (7.6) now imply, after integrating twice:

$$\delta x_i(t) = \frac{1}{m} \int_0^t dt' \int_0^{t'} dt'' \sum_j \frac{\partial F_i}{\partial x_j} [x_k(t''), t''] \delta x_j(t'') + \delta x_i(0) + t \delta v_i(0) \quad (7.7)$$

where the nine quantities $\partial F_i / \partial x_j$ must be provided along the unperturbed orbit given by $x_k(t'')$ and t'' .

By noting that the region of integration in (7.7) is a triangle in (t', t'') coordinates, and then interchanging the order of integration, we can change (7.7) into the equivalent form (A.D. Stauffer, private communication):

$$\delta x_i(t) = \frac{1}{m} \int_0^t dt'' (t-t'') \sum_j \frac{\partial F_i}{\partial x_j} [x_k(t''), t''] \delta x_j(t'') + \delta x_i(0) + t \delta v_i(0) \quad (7.8)$$

which contains only a single integration.

We now consider a monokinetic particle beam having initial velocity $(v_0, 0, 0)$. This implies a zero initial perturbation velocity: $\delta \vec{v}(0) = (0, 0, 0)$. We choose two mutually orthogonal initial perturbations in position:

$$\delta_2 \vec{x}(0) = (0, 1, 0) \quad (7.9)$$

$$\delta_3 \vec{x}(0) = (0, 0, 1)$$

Since (7.8) is both linear and homogeneous in $\delta \vec{x}$, final values of $\delta_2 \vec{x}$ and $\delta_3 \vec{x}$ are proportional to initial values, as one expects for perturbation quantities.

Furthermore, if $\delta \vec{x}(0) = a \delta_2 \vec{x}(0) + b \delta_3 \vec{x}(0)$, then $\delta \vec{x}(t) = a \delta_2 \vec{x}(t) + b \delta_3 \vec{x}(t)$, where a and b are unchanged.

We now consider an initially circular differential tube of orbits defined by (7.9). As the unperturbed orbit is followed numerically, we simultaneously calculate $\delta_2 \vec{x}$ and $\delta_3 \vec{x}$ using (7.8). At the impingement point of the orbit, we project these onto the surface tangent plane (Fig. 7.1). The area of the ellipse thus generated is inversely proportional to the current density deposited on the surface.

For a monokinetic beam, this gives current density with no approximations.

The linearity of the perturbation equation (7.8) now implies that all orbits passing through A_0 (Fig. 7.1) also pass through A . Therefore the total current carried by the tube is a constant, equal to $A_0 j_0 = \frac{\pi}{4} j_0$, where j_0 is the current density through A_0 .

The area A is given by:

$$A = \frac{\pi}{4} \left| \delta_2^{\vec{x}} \times \delta_3^{\vec{x}} \right| = \frac{\pi}{4} \begin{vmatrix} \hat{i} & \hat{j} & \hat{k} \\ \delta_2^{x_1} & \delta_2^{x_2} & \delta_2^{x_3} \\ \delta_3^{x_1} & \delta_3^{x_2} & \delta_3^{x_3} \end{vmatrix} \quad (7.10)$$

where \hat{i} , \hat{j} , and \hat{k} are unit vectors along the coordinate axes.

The current density at the surface therefore varies inversely as the projected tube area given by:

$$\frac{\pi}{4} \hat{n} \cdot (\delta_2^{\vec{x}} \times \delta_3^{\vec{x}}) = \frac{\pi}{4} \begin{vmatrix} n_1 & n_2 & n_3 \\ \delta_2^{x_1} & \delta_2^{x_2} & \delta_2^{x_3} \\ \delta_3^{x_1} & \delta_3^{x_2} & \delta_3^{x_3} \end{vmatrix} \quad (7.11)$$

evaluated at the orbit impingement point on the surface, where \hat{n} is a unit vector perpendicular to the surface tangent plane (Fig. 7.1).

The current density at the surface therefore is:

$$j_{\text{surface}} = j_0 \left/ \begin{vmatrix} n_1 & n_2 & n_3 \\ \delta_2^{x_1} & \delta_2^{x_2} & \delta_2^{x_3} \\ \delta_3^{x_1} & \delta_3^{x_2} & \delta_3^{x_3} \end{vmatrix} \right|_{\text{surface}} \quad (7.12)$$

It is possible for the plane of the ellipse to be perpendicular to the surface tangent plane. This occurs when the perturbed orbits happen to cross each other at the surface. The current density at the surface will then be infinite. This can occur only for a monokinetic distribution of initial velocities, which is only an approximation to real distributions.

We can also obtain an expression for number density n along the orbit, since $n\vec{v}$ times the projection of A on a plane perpendicular to \vec{v} remains constant along the orbit.

i.e. the product $\frac{\pi}{4} n \left| \vec{v} \cdot (\delta_2 \vec{x} \times \delta_3 \vec{x}) \right|$ is constant.

We therefore obtain:

$$n = n_o v_o / \left\| \begin{array}{ccc} v_1 & v_2 & v_3 \\ \delta_2 x_1 & \delta_2 x_2 & \delta_2 x_3 \\ \delta_3 x_1 & \delta_3 x_2 & \delta_3 x_3 \end{array} \right\| \quad (7.13)$$

For a monokinetic distribution, n can also become infinite if the perturbed orbits cross each other. For the same distribution, n (and j_{surface} if a surface is present) can also become infinite if one of the vectors $\delta_2 \vec{x}$ or $\delta_3 \vec{x}$, or some linear combination of them, becomes zero. An example of this occurs on the (wake) axis of symmetry behind a sphere in a flowing collisionless plasma containing infinite-speed-ratio ions.

In two dimensions the perturbation produces a differential strip rather than tube. The corresponding results are:

$$j_{\text{surface}} = j_o / \left\| \begin{array}{cc} n_1 & n_2 \\ \delta x_1 & \delta x_2 \end{array} \right\|_{\text{surface}} \quad (7.14)$$

$$n = n_o v_o / \left\| \begin{array}{cc} v_1 & v_2 \\ \delta x_1 & \delta x_2 \end{array} \right\| \quad (7.15)$$

We can also consider velocity-space rather than position-space initial perturbations. We assume that:

$$\delta_2 \vec{x} = \delta_3 \vec{x} = 0, \text{ but } \delta_2 \vec{v} = (0,1,0), \text{ and } \delta_3 \vec{v} = (0,0,1). \quad (7.16)$$

This permits us to treat situations where the ion speed ratio is large but not infinite. We can use (7.16) to do a calculation of ion defocusing on the wake axis behind a sphere, valid to order S_i^{-1} , where S_i is the ion speed ratio. We consider the situation shown in Fig. 7.2, in which an unperturbed orbit, initially parallel to the ion drift direction, has already been computed, in the presence of some known or given electric potential distribution e.g. a Coulomb potential. This orbit crosses the z axis at a downstream point z_o . Because

all orbits having the same impact parameter r_0 cross at z_0 , the ion density at this point is "infinite" unless the ions also have some random motion (S_i is finite). In reality the resulting space charge along this axis will influence ion orbits near it, but we ignore this effect here. We assume that values of $\partial F_r / \partial r$, $\partial F_r / \partial z$, $\partial F_z / \partial r$, and $\partial F_z / \partial z$ are known along the unperturbed orbit. Our procedure is as follows. We choose two initial velocity perturbation vectors $\delta_a \vec{v}(0)$ and $\delta_b \vec{v}(0)$ in the plane of the unperturbed orbit (Fig. 7.2). We also choose $\delta_2 \vec{x}(0) = \delta_3 \vec{x}(0) = 0$ at z_0 . We now do our perturbation calculations backward, or "inside-out" along the ion orbit, even though we initially calculated the orbit forward, in the ion direction of motion. A single integration of (7.5) with (7.6) yields:

$$\delta v_i(t) = \frac{1}{m} \int_0^t dt' \sum_j \frac{\partial F_i}{\partial x_j} [x_k(t'), t'] \delta x_j(t') + \delta v_i(0). \quad (7.17)$$

For each of our two initial velocity perturbation vectors, we first integrate (7.8) from z_0 to an upstream point at which the orbit is essentially no longer affected by the electric field of the sphere. We then use the resulting values of $\delta x_j(t')$ [in this case $\delta r(t')$ and $\delta z(t')$] in (7.17) to calculate $\delta v_i(t)$ [in this case $\delta v_r(t)$ and $\delta v_z(t)$] at the same upstream point. The linearity of the perturbation calculation

already discussed, implies now that multiplying $\delta_a \vec{v}(0)$ and $\delta_b \vec{v}(0)$ by any constants a and b means that $\delta_a \vec{v}(t)$ and $\delta_b \vec{v}(t)$ are also multiplied by a and b . Suppose now that the velocity distribution at the upstream point is a drifting Maxwellian. The linearity just mentioned now implies that velocity components in the (r, z) plane at the upstream point map linearly into those on the axis at z_0 , so an integration over velocity space to find the density at z_0 is easy to perform. This now will be found to yield a finite rather than infinite result, essentially because most ions will now have a small amount of angular momentum about the axis of symmetry and will no longer be found at z_0 , and our perturbation calculation implicitly takes this into account.

As a final example, we consider the case of a nearly-monokinetic beam (the usual case for ion or electron guns on a spacecraft). We first need to calculate the five perturbation quantities $\delta_2 \vec{x}, \dots, \delta_6 \vec{x}$ resulting from choosing initial perturbations given by (7.9) and by $\delta_1 \vec{v}(0) = (1, 0, 0)$, $\delta_2 \vec{v}(0) = (0, 1, 0)$, $\delta_3 \vec{v}(0) = (0, 0, 1)$. The values of $\delta_2 \vec{x}$ and $\delta_3 \vec{x}$ then give, as before, current density or space-charge density at any point of interest, but these are now differential

quantities with respect to the velocity distribution $f \equiv d^3N/dv_1dv_2dv_3$ of the beam at its emission point; i.e. the values of these quantities found in this way are proportional to $f(v_1, v_2, v_3)dv_1dv_2dv_3$. The remaining perturbation quantities $\delta_4^{\vec{x}}$, $\delta_5^{\vec{x}}$, and $\delta_6^{\vec{x}}$ then give the required information about the spread of the beam in position space. This may itself be due or partly due to beam space-charge; if this is the case, then the force derivatives $\partial F_1/\partial x_j$ must themselves be found self-consistently, complicating the problem; in this case, calculations of the kind presented here would presumably become part of an iterative scheme.

If the beam is not nearly monokinetic (as will often be the case if it has not been deliberately accelerated) or it creates its own potential barrier around the spacecraft, so that part of it escapes and part does not, then evidently differential perturbations in velocity do not provide a realistic description of the result, and one would then need to replace calculations of $\delta_4^{\vec{x}}$, $\delta_5^{\vec{x}}$, and $\delta_6^{\vec{x}}$ by separate, non-perturbation, orbit calculations for a representative discrete sample of the particle velocities most strongly represented in the beam.

REFERENCES

- Allen, J.S., 1939, The emission of secondary electrons from metals bombarded with protons, Phys. Rev. 55, 336.
- Axford, W.I., 1968, Observations of the interplanetary plasma, Space Sci. Rev. 8, 331-365.
- Baragiola, R.A., Alonso, E.V., Florio, A.O., 1979, Electron emission from clean metal surfaces induced by low-energy light ions, Phys. Rev. B 19, 121.
- Bernstein, I.B. and Rabinowitz, I.N., 1959, Theory of electrostatic probes in a low-density plasma, Phys. Fluids 2, 112.
- Besse, A.L. 1981, Unstable Potential of Geosynchronous Spacecraft, J. Geophys. Res. 86(A4), 2443-2446.
- Besse, A.L. and Rubin, A.G., 1980, A Simple Analysis of Spacecraft Charging Involving Blocked Photoelectron Currents, J. Geophys. Res. 85 (A5), 2324-2328.
- Chen, F.F., 1965, Numerical computations for ion probe characteristics in a collisionless plasma, Plasma Phys. (J. Nucle. Ener. Part C) 7, 47-68.
- Chung, M.S., and Everhart, T.E., 1974, Simple calculation of energy distribution of low-energy secondary electrons emitted from metals under electron bombardment, J. Appl. Phys. 45, 707.
- Cousinie, P., Colombié, N., Fert, C. and Simon, R., 1959, Variation du coefficient d'émission électronique secondaire de quelques métaux avec l'énergie des ions incidents, Compt. Rend. 249, 387.
- Darlington, E.H. and Cosslett, V.E. 1972, Backscattering of 0.5 - 10keV electrons from solid targets, J. Phys. D: Appl. Phys. 5, 1969-1981.
- DeForest, S.E., 1972, Spacecraft charging at synchronous orbit, J. Geophys. Res. 77, 651.
- DeForest, S.E., 1977, The plasma environment at geosynchronous altitude, in: Proceedings of the Spacecraft Charging Technology Conference, edited by C.P. Pike and R.R. Lovell, pp. 37-52, Air Force Surveys in Geophysics, No. 364, Hanscom Air Force Base, Mass., Rep. AFGL-TR-77-0051/NASA TMX-73537.

- DeForest, S.E., and McIlwain, C.E., 1971, Plasma clouds in the magnetosphere, J. Geophys. Res. 76, 3587-3611.
- Dekker, A.J. 1958, Secondary Electron Emission, in: Solid State Physics, edited by F. Seitz and D. Turnbull, vol. 6, Academic, New York, p.251.
- Dessler, A.J., 1967, Solar wind and interplanetary magnetic field, Rev. Geophys. 5, 1-4'.
- Fahleson, U. 1973, Plasma-Vehicle Interactions in Space - Some Aspects on Present Knowledge and Future Development, in: Photon and Particle Interaction with Surfaces in Space, edited by R.J.L. Grard, D. Reidel, Dordrecht, Holland, pp. 563-569.
- Garrett, H.B. and DeForest, S., 1979, An Analytical Simulation of the Geosynchronous Plasma Environment, Planet.Space Sci. 27, 1101-1109.
- Garrett, H.B., Schwank, D.C. and DeForest, S.E., 1981, A Statistical Analysis of the Low-Energy Geosynchronous Plasma Environment - I. Electrons, Planet.Space Sci. 29, (10), 1021-1044.
- Gibbons, D.J., 1966, Secondary Electron Emission, in: Handbook of Vacuum Physics, edited by A.H. Beck, Pergamon, Oxford, p. 301.
- Godard, R., 1975, A symmetrical model for cylindrical and spherical collectors in a flowing collisionless plasma, Ph.D. Thesis, York University, Toronto.
- Goldstein, H., 1950, Classical Mechanics, Addison-Wesley Pub. Co., Reading, Massachusetts.
- Goldstein, R. and Divine, N., 1977, Plasma distribution and spacecraft charging modeling near Jupiter. In: Proc. USAF-NASA Spacecraft Charging Technology Conference, C.P. Pike and R.R. Lovell, Editors, Report No. AFGL-TR-77-0051, Air Force Geophysics Laboratory, Hanscom AFB, Massachusetts/NASA TMX-73537, Lewis Research Center, Cleveland Ohio, pp. 131-141.
- Gussenhoven, M.S. and Mullen, E.G., A "Worst Case" Spacecraft Charging Environment as Observed by SCATHA on 24 April 1979, paper No. 82-0271, Amer. Inst. Aeron. Astron. 20th Aerospace Sciences Mtg., Jan. 82, Orlando, Florida.

- Hachenberg, O. and Brauer, W., 1959, Secondary Electron Emission from Solids, Advan. Electron. Electron Phys. 11, 413.
- Hachenberg, O. and Brauer, W., 1962, Advan. Electron. Electron Phys., 16, 145.
- Katz, I., Parks, D.E., Mandell, M.J., Harvey, J.M., Brownell, D.H. Jr., Wang, S.S. and Rotenberg, M., 1977, A Three Dimensional Dynamic Study of Electrostatic Charging in Materials, NASA Contractor Report No. CR-135256, Lewis Research Center, Cleveland, Ohio.
- Katz, I., Parks, D.E., Wang, S., and Wilson, A., 1977, Dynamic modeling of spacecraft in a collisionless plasma. In: Proc. USAF-NASA Spacecraft Charging Technology Conference, C.P. Pike and R.R. Lovell, Editors, Report No. AFGL-TR-77-0051, Air Force Geophysics Laboratory, Hanscom AFB, Massachusetts/NASA TMX-73537, Lewis Research Center, Cleveland, Ohio, pp. 319-330.
- Katz, I., Cassidy, J.J., Mandell, M.J., Schnuelle, G.W., Steen, P.G., and Roche, J.C., 1979, The Capabilities of the NASA Charging Analyzer Program, in: Spacecraft Charging Technology - 1978, NASA Conference Publication 2071/Report No. AFGL-TR-79-0082, Air Force Geophysics Laboratory, Massachusetts, pp. 101-122.
- Katz, I., and Mandell, M.J., 1982, Differential Charging of High-Voltage Spacecraft: The Equilibrium Potential of Insulated Surfaces, J. Geophys. Res. 87, 4533-4541.
- Kazan, B., and Knoll, M., 1968, Electronic Image Storage, Academic Press, New York.
- Knott, K., 1972, The equilibrium potential of a magnetospheric satellite in an eclipse situation, Planet. Space Sci. 20, 1137.
- Krainsky, I., Lundin, W., Gordon, W.L. and Hoffman, R.W., 1981, Secondary Electron Emission Yields, in: Spacecraft Charging Technology 1980, NASA Conference Publication 2182/Report No. AFGL-TR-81-0270, Air Force Geophysics Laboratory, Massachusetts, pp. 179-197.
- Lafon, J.-P.J., 1976, On the sheath surrounding a conductor emitting photoelectrons in an isotropic collisionless plasma, Radio Science 11, 483-493.

- Laframboise, J.G., 1966, Theory of spherical and cylindrical Langmuir probes in a collisionless, Maxwellian plasma at rest, Univ. of Toronto, Institute for Aerospace Studies, UTIAS Rep. 100.
- Laframboise, J.G., and Parker, L.W., 1973, Probe design for orbit-limited current collection, Phys. Fluids 16, 629-636.
- Laframboise, J.G., and Godard, R., 1974, Perturbation of an electrostatic probe by a spacecraft at small speed ratios, Planet. Space Sci. 22, 1145-1155.
- Laframboise, J.G. and Prokopenko, S.M.L., 1977, Numerical Simulation of Spacecraft Charging Phenomena, in: Proc. Spacecraft Charging Technology Conference, C.P. Pike and R.R. Lovell, Eds., Report No. AFGL-TR-77-0051, Air Force Geophysics Laboratory, Massachusetts/Report No. NASA TMX-73537, Lewis Research Center, Cleveland, Ohio, pp. 309-318.
- Laframboise, J.G., and Prokopenko, S.M.L., 1978, Predictions of high-voltage differential charging on geostationary spacecraft, in: Proc. 1978 Symposium on the Effect of the Ionosphere on Space and Terrestrial Systems, paper 4.4, Naval Research Lab./Office of Naval Research, Washington.
- Leung, M.S., Tueling, M.B. and Schnauss, E.R., 1981, Effects of Secondary Electron Emission on Charging, in: Spacecraft Charging Technology 1980, NASA Conference Publication 2182/Report No. AFGL-TR-81-0270, Air Force Geophysics Laboratory, Massachusetts, pp. 163-178.
- Manka, R.H., 1973, Plasma and potential at the lunar surface. In: Photon and Particle Interactions with Surfaces in Space, R.J.L. Grard, Editor, D. Reidel Pub. Co., Dordrecht, Holland, pp. 347-361.
- Mauk, B., 1975, Magnetospheric substorm pitch angle distribution, EOS 56, 423.
- McPherson, D.A., and Schober, W.R., 1976, Spacecraft charging at high altitudes: the Scatha satellite program, in: Spacecraft Charging by Magnetospheric Plasmas, edited by A. Rosen, American Institute of Aeronautics and Astronautics, New York, and MIT Press, Cambridge, Massachusetts.

- Meyer-Vernet, N., 1982, "Flip-Flop" of Electric Potential of Dust Grains in Space, Astron. Astrophys. 105, 98-106.
- Mott-Smith, H., Jr., and Langmuir, I., 1926, The theory of collectors in gaseous discharges, Phys. Rev. 28, 727.
- Olsen, R.C., 1980, Differential and Active Charging Results from the ATS Spacecraft. Univ. of California, San Diego, Ph.D. Thesis.
- Olsen, R.C. and Whipple, E.C., 1980, Analysis of Differential and Active Charging Phenomena on ATS-5 and ATS-6. University of California, San Diego, Center for Astrophysics and Space Sciences, Rep. CASS-80-1.
- Palluel, P., 1947, Composante rediffusée du rayonnement électronique secondaire des métaux, C.R. Acad. Sci. 224, 1492.
- Parker, L.W., 1978, Potential barriers and asymmetric sheaths due to differential charging of nonconducting spacecraft. Report No. AFGL-TR-78-0045, Air Force Geophysics Laboratory, Hanscom AFB, Massachusetts.
- Parker, L.W., and Whipple, E.C., Jr., 1967, Theory of a Satellite Electrostatic Probe. Ann. Phys. 44, 126-161.
- Pelizzari, M.A., and Criswell, D.R., 1978, Differential Photoelectric Charging of Nonconducting Surfaces in Space. J. Geophys. Res. 83, 5233-5244.
- Polychronopoulos, B., 1973, Effects of non-Maxwellian electron energy distributions on the orbital limited current-voltage characteristics of cylindrical and spherical Langmuir probes under collisionless conditions, Plasma Phys. 15, 37.
- Prokopenko, S.M.L. and Laframboise, J.G., 1977, Prediction of Large Negative Shaded-Side Spacecraft Potentials, in: Proc. Spacecraft Charging Technology Conference, C.P. Pike and R.R. Lovell, Eds., Report No. AFGL-TR-77-0051, Air Force Geophysics Laboratory, Massachusetts/Report No. NASA TMX-73537, Lewis Research Center, Cleveland, Ohio, pp. 369-387.
- Prokopenko, S.M.L. and Laframboise, J.G., 1980, High-Voltage Differential Charging of Geostationary Spacecraft, J. Geophys. Res. 85, (A8), 4125-4131.

- Purvis, C., 1982, Evolution of Spacecraft Charging Technology, Paper No. 82-0273, Amer. Inst. Aeron. Astron. 20th Aerospace Sciences Mtg., Jan. 82, Orlando, Florida.
- Ray, J.A., and Barnett, C.F., 1971, Secondary electron emission of metals bombarded with 120-eV to 5-keV protons, J. Appl. Phys. **42**, 3260.
- Rosen, A., 1975, Large Arcs and Discharges on Spacecraft, Astronaut. Aeronaut., **13**, 36.
- Salehi, M. and Flinn, E.A., 1981, Dependence of Secondary-Electron Emission from Amorphous Materials on Primary Angle of Incidence, J. Appl. Phys. **52** (2), 994-996.
- Sanders, N.L. and Inouye, G.T., 1979, Secondary Emission Effects on Spacecraft Charging: Energy Distribution Considerations, in: Spacecraft Charging Technology - 1978. NASA Conference Publication 2071/Report No. AFGL-TR-79-0082, Air Force Geophysics Laboratory, Massachusetts, pp. 747-755.
- Schnuelle, G.W., Parks, D.E., Katz, I., Mandell, M.J., Steen, P.G., Cassidy, J.J. and Rubin, A., 1979, Charging Analysis of the SCATHA satellite, in: Spacecraft Charging Technology - 1978, NASA Conference Publication 2071/Report No. AFGL-TR-79-0082, Air Force Geophysics Laboratory, Massachusetts, pp. 123-143.
- Schnuelle, G.W., Stannard, P.R., Katz, I. and Mandell, M.J., 1981, Simulation of Charging Response of SCATHA (P78-2) Satellite, in: Spacecraft Charging Technology 1980, NASA Conference Publication 2182/Report No. AFGL-TR-81-0270, Air Force Geophysics Laboratory, Massachusetts, pp. 580-591.
- Schröder, H., 1973, Spherically symmetric model of the photoelectron sheath for moderately large plasma Debye lengths. In: Photon and Particle Interactions with Surfaces in Space, R.J.L. Grard, Editor, D. Reidel Pub. Co., Dordrecht, Holland, pp. 51-58.
- Shepherd, M.M., and Laframboise, J.G., 1981, Chebyshev approximation of $(1 + 2x)\exp(x^2)\operatorname{erfc}(x)$ in $0 \leq x < \infty$. Math. of Computation **36**, 249.

- Shield, M.A., and Frank, L.A., 1970, Electron observations between the inner edge of the plasma sheet and the magnetosphere, J. Geophys. Res. 75, 5401-5414.
- Soop, M., 1972, Report on photo-sheath calculations for the satellite GEOS, Planet. Space Sci. 20, 859-870.
- Stannard, P.R., Schnuelle, G.W., Katz, I., and Mandell, M.J., 1981, Representation and Material Charging Response of GEO Plasma Environments, in: Spacecraft Charging Technology 1980, NASA Conference Publication 2182/Report No. AFGL-TR-81-0270, Air Force Geophysics Laboratory, Massachusetts, pp. 560-579.
- Stannard, P.R., Katz, I., Gedeon, L., Roche, J.C., Rubin, A.G. and Tautz, M.F., 1982, Validation of the NASCAP Model Using Spaceflight Data, Paper No. 82-0269, Amer. Inst. Aeron. Astron. 20th Aerospace Sciences Mtg., Jan. 82, Orlando, Florida.
- Sternglass, E.J., 1954, Theory of Secondary Electron Emission, Sci. Pap. 1772, Westinghouse Res. Lab., Pittsburgh, Pa.
- Sternglass, E.J., 1954, Backscattering of Kilovolt Electrons from Solids, Phys. Rev. 95, 345-358.
- Swarztrauber, P., and Sweet, R., 1975, Efficient FORTRAN Subprograms for the Solution of Elliptic Partial Differential Equations, Tech. Note NCAR-TN/IA-109, National Center for Atmospheric Research, Boulder, Colorado.
- Thomas, S., and Pattinson, E.B., 1970, Range of electrons and contribution of back-scattered electrons in secondary production in aluminum, J. Phys. D: Appl. Phys. 3, 349.
- Tsien, H.S., 1946, Superaerodynamics, mechanics of rarefied gases, J. Aero. Sci. 13, 653-664.
- Whipple, E.C., Jr., 1965, The Equilibrium Electric Potential of a Body in the Upper Atmosphere and in Interplanetary Space, Ph.D. Thesis, The George Washington Univ., Washington, D.C./Report No. X-615-65-296, NASA Goddard Space Flight Center, Greenbelt, Maryland.
- Whipple, E.C. Jr., 1976, Observation of Photoelectrons and Secondary Electrons Reflected from a Potential Barrier in the Vicinity of ATS 6, J. Geophys. Res. 81 (4), 715-719.
- Whipple, E.C., 1981, Potentials of Surfaces in Space, Rep. Prog. Phys. 44, 1197-1250.
- Willis, R.F., and Skinner, D.K., 1973, Secondary electron emission yield behaviour of polymers, Solid State Comm. 13, 685.

Table 1

Floating potentials of shaded surfaces of geostationary-altitude spacecraft, using the incident velocity spectra assumed by Knott [1972], with backscattered and secondary electron emission due to electron impacts included, with three-, two-, and one-dimensional velocity-space cutoffs corresponding to orbit-limited ion collection in spherical, infinite cylindrical and planar symmetries, respectively.

Material	Secondary Electron Emission Data		Back-scatter Data $\eta(5000\text{eV})$	Spectrum 1 "Quiet"			Spectrum 2b "Disturbed"		
	δ_{max}	E_{max} (eV)		Floating Potential (volts) 3-dimen.	Floating Potential (volts) 2-dimen.	Floating Potential (volts) 1-dimen.	Floating Potential (volts) 3-dimen.	Floating Potential (volts) 2-dimen.	Floating Potential (volts) 1-dimen.
Gold	1.45	800	.42	-39.9	-40.0	-40.8	-3470	-6430	-15,450
Aluminum	.97	300	.16	-1410	-2140	-5390	-6770	-11,500	-21,770
Aluminum with Oxide Coating	2.60	300	.12	+4.6 -630* -750	+3.0 -490* -1560	+1.9 -420* -4900	-6610	-11,360	-21,610
Quartz	2.50	420	.12	+3.9	+2.5	+1.5 -640* -4120	-6310	-10,960	-21,130
Aquadag	.75	350	.08	-1560	-2380	-5890	-7090	-12,010	-22,350
Beryllium Copper	2.20	300	.31	+4.7	+2.9	+1.9 -560* -3430	-5740	-9920	-19,890
Beryllium Copper Activated	5.00	400	.31	+8.0	+5.8	+4.2	-4.3 -900* -3950	+2.9 -830* -7580	+1.6 -770* -17,670
Teflon	3.00	300	.10	+5.2	+3.6 -660* -1370	+2.3 -490* -4870	-6640	-11,430	-21,700
Kapton	2.10	150	.07	+3.9 -170* -1580	+2.5 -170* -2440	+1.4 -170* -6040	-7180	-12,130	-22,520
No secondary or backscattered electrons	—	—	—	-1860	-2830	-6680	-7550	-12,690	-23,130

* Unstable

TABLE 2

THRESHOLD TEMPERATURES T* FOR SPACECRAFT SURFACE MATERIALS
 TC1: INCLUDING SECONDARY ELECTRONS.
 TC2: INCLUDING SECONDARY AND BACKSCATTERED ELECTRONS.
 TC3: SAME AS TC2 EXCEPT THAT ANGULAR DEPENDENCE OF YIELD IS INCLUDED.

MATERIAL	SECONDARY		BACKSCATTERING				T* (keV)		
	E _{max} (keV)	δ _{max}	Z	A	B	C	TC1	TC2	TC3
GOLD	.80	1.45	79.0	.4802	.3566	.6103	1.278	2.931	4.939
ALUMINUM	.30	.97	13.0	.1569	.0303	.3431	0.000	0.000	.601
ALUMINUM OXIDE	.30	2.60	10.0	.1238	.0172	.3435	1.116	1.777	1.931
SiO ₂ (QUARTZ)	.42	2.50	10.0	.1238	.0172	.3435	1.496	1.713	2.621
FUSED SILICA	.33	3.46	10.0	.1238	.0172	.3435	1.645	1.847	2.707
ARADAG(COLLOIDAL GRAPHITE)	.35	.75	6.0	.0800	0.0000	0.0000	0.000	0.000	0.000
BERYLLIUM-COPPER	.30	2.20	29.0	.3136	.0692	.6207	.918	1.349	2.157
BERYLLIUM-COPPER(ACTIVATED)	.40	5.00	29.0	.3136	.0692	.6207	2.754	3.697	5.423
TEFLON	.30	3.00	8.0	.0900	0.0000	0.0000	1.299	1.477	2.102
KAPTON (Willis and Skinner, 1973)	.15	2.10	5.3	.0700	0.0000	0.0000	.433	.474	.769
KAPTON (Leung et al, 1981)	.25	1.80	5.3	.0700	0.0000	0.0000	.583	.647	1.096
INDIUM OXIDE	.80	1.40	24.4	.2750	.0600	.5400	1.184	2.010	3.596
MAGNESIUM	.25	.92	12.0	.1460	.0250	.3440	0.000	0.000	.441
MAGNESIUM OXIDE	.40	4.00	10.0	.1738	.0172	.3435	2.280	2.548	3.686
SILVER	.80	1.00	47.0	.3900	.2890	.6320	0.000	1.233	2.754
ITO ON KAPTON	.35	2.55	15.3	.1830	.0370	.3820	1.275	1.550	2.370
ITO ON 'FEP' TEFLON	.36	2.39	16.2	.1920	.0400	.3990	1.217	1.507	2.329
ITO ON BOROSILICATE GLASS	.35	2.35	16.9	.2000	.0420	.4100	1.160	1.456	2.254
ION-SPUTTERED ITO ON KAPTON	.39	1.52	15.3	.1830	.0370	.3820	.684	.921	1.587
MGF2	.85	6.38	10.0	.1238	.0172	.3435	7.141	7.889	11.054
NASCAP 'MPAI'	.15	2.10	5.0	.0600	0.0000	0.0000	.433	.468	.747
NASCAP 'SOLA'	.41	2.05	10.0	.1238	.0172	.3435	1.147	1.338	2.123
NASCAP 'CPAI'	.15	2.10	5.0	.0600	0.0000	0.0000	.433	.468	.747
NASCAP 'WHITEN'	.15	2.10	5.0	.0600	0.0000	0.0000	.433	.468	.747
NASCAP 'BLACKC YELLOWC'	.15	2.10	5.0	.0600	0.0000	0.0000	.433	.468	.747
NASCAP 'GOLIFD'	.72	1.03	70.1	.4560	.3380	.6120	0.000	1.392	2.857
NASCAP 'YGULDS'	.48	1.49	42.0	.3730	.2760	.6170	.810	1.392	2.444
NASCAP 'EDUHAT'	.59	1.86	63.4	.4380	.3250	.6130	1.443	2.596	4.203
NASCAP 'MLI2'	.30	1.00	6.0	.0800	0.0000	0.0000	0.000	0.000	.602

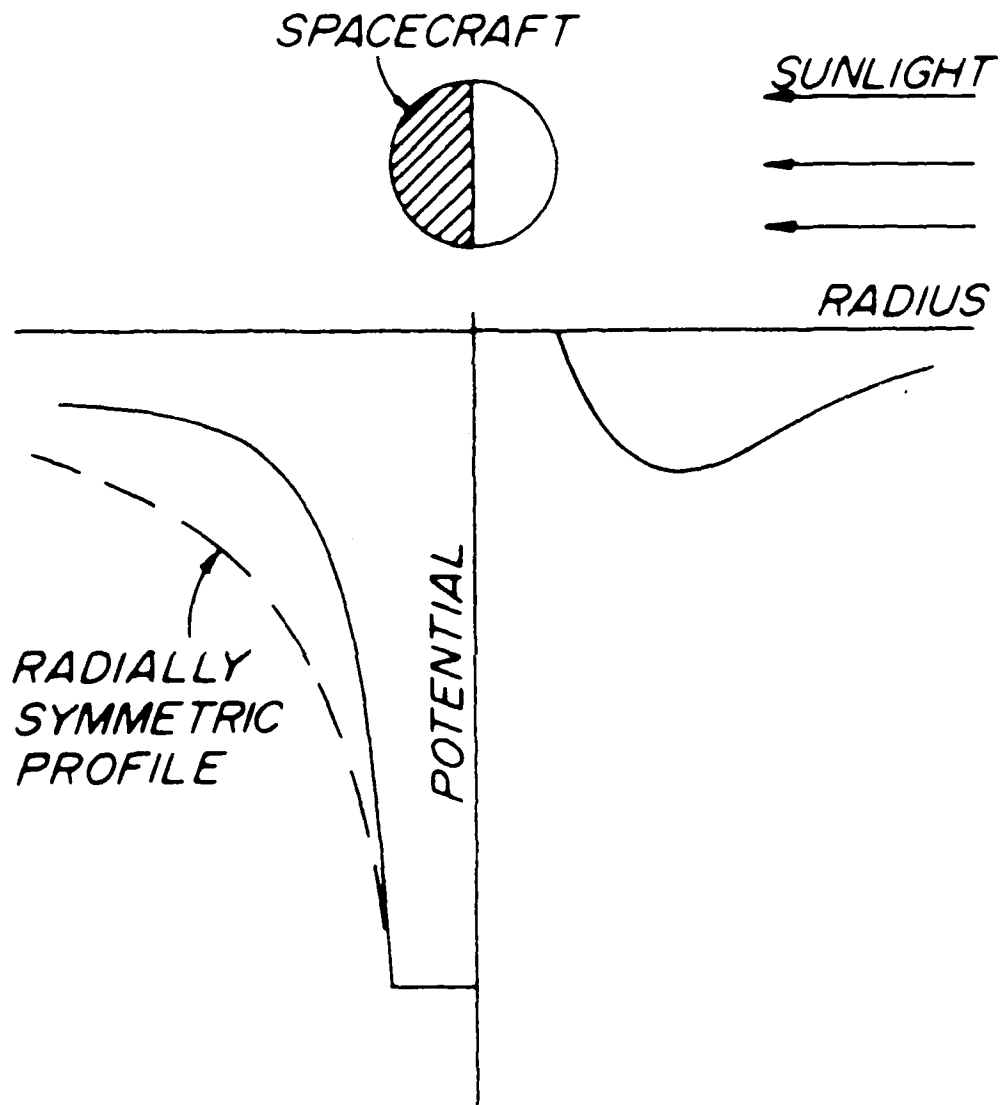


Fig. 2.1. Steepening of shaded-side potential profile, and sunlit-side potential barrier formation, caused by shaded-sunlit asymmetry on a spacecraft with an insulated surface, after Fahleson [1973].

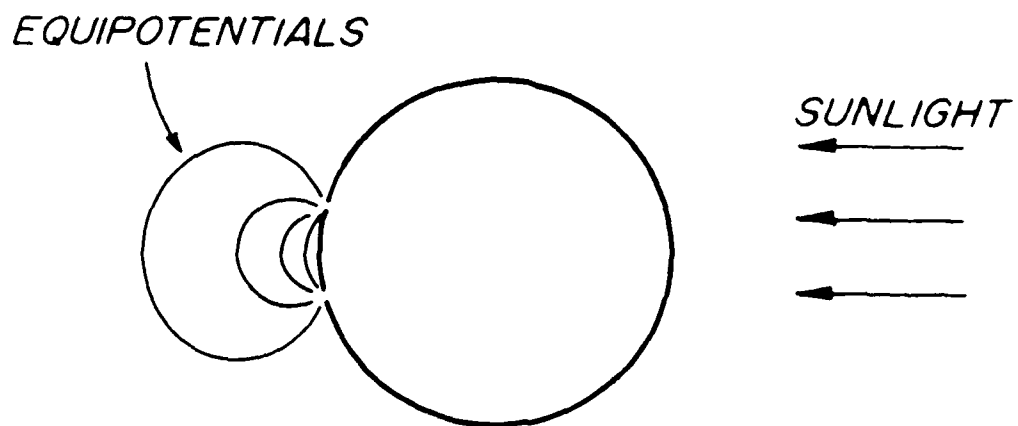


Fig.2.2. Conductive spacecraft with shaded isolated surface patch.

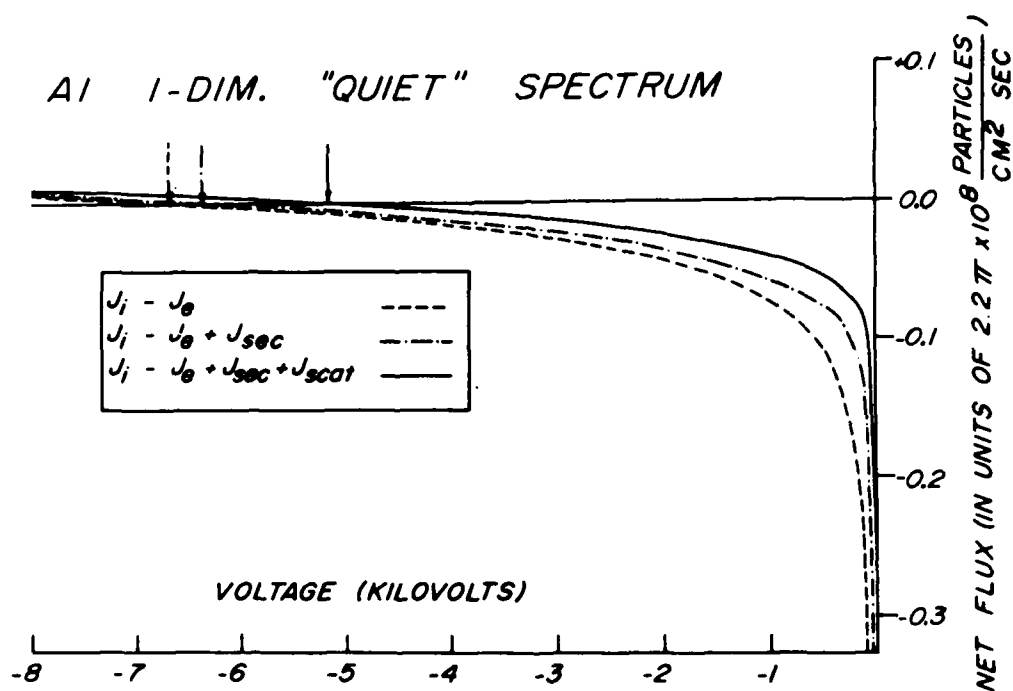


Fig. 2.3. Current-voltage characteristic for aluminum in "quiet" conditions, with a one-dimensional velocity-space cutoff. In Figures 2.3 - 2.7 the zeros of the characteristics are indicated by arrows.

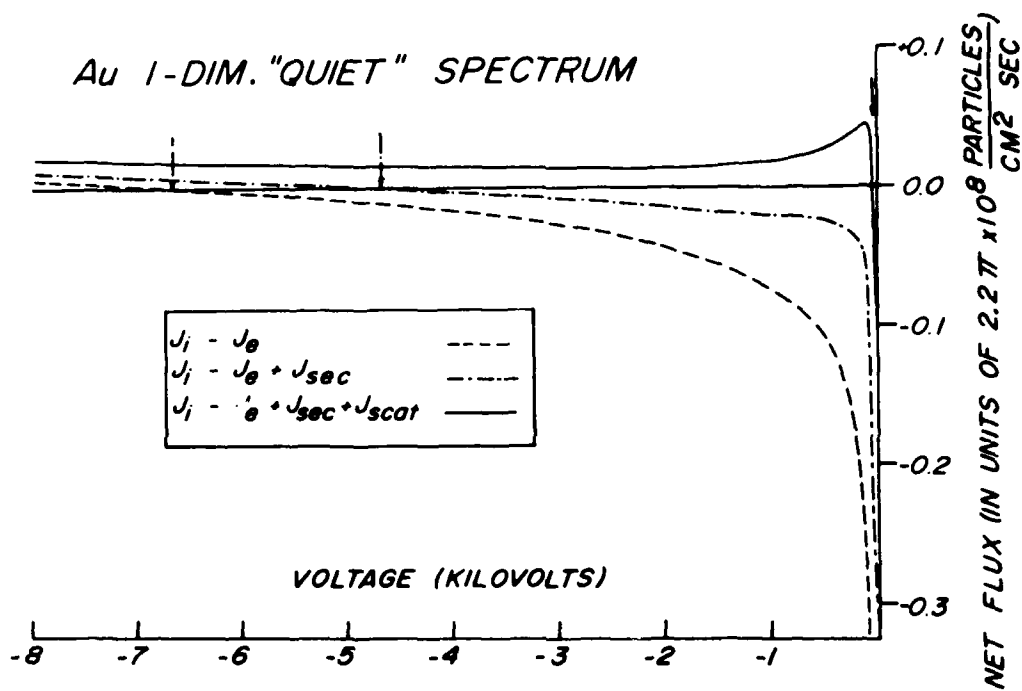


Fig. 2.4. Current-voltage characteristic for gold in "quiet" conditions, with a one-dimensional velocity-space cutoff.

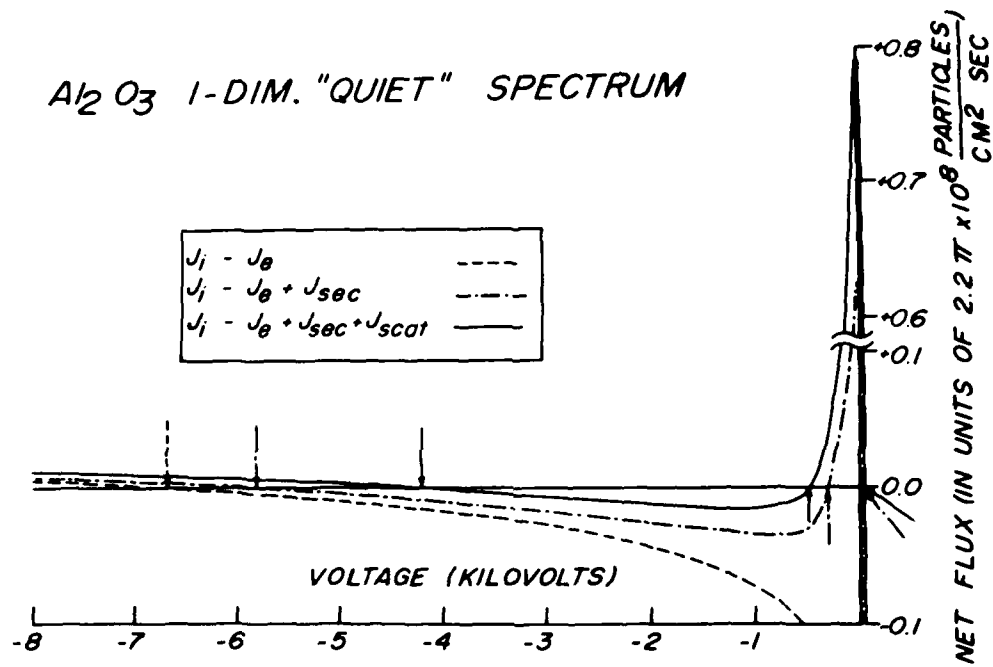


Fig. 2.5. Current-voltage characteristic for aluminum oxide in "quiet" conditions, with a one-dimensional velocity-space cutoff.

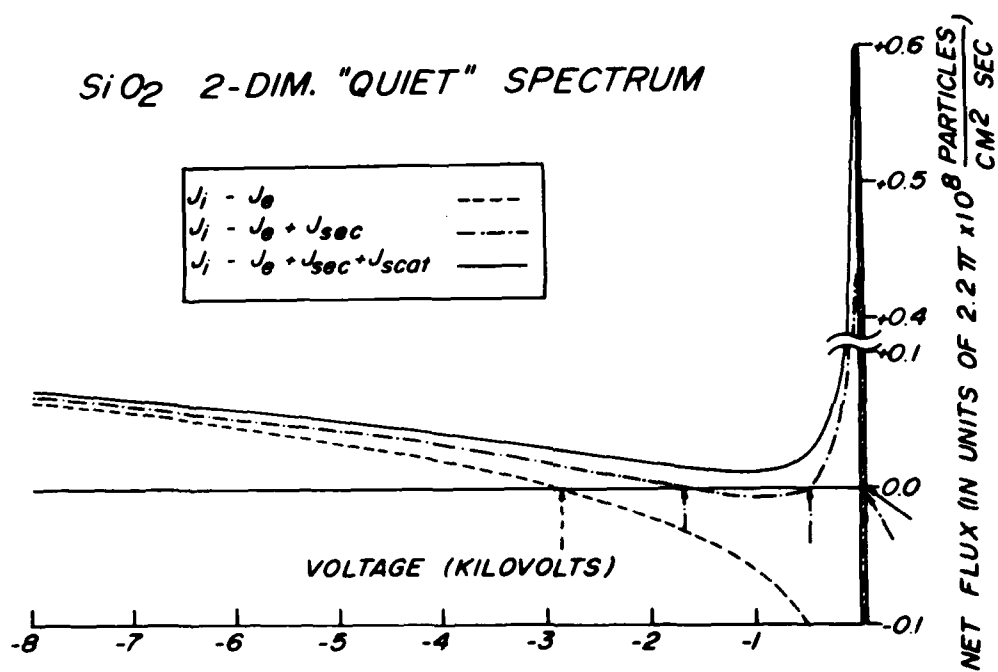


Fig. 2.6. Current-voltage characteristic for quartz in "quiet" conditions, with a two-dimensional velocity-space cutoff.

*Activated Beryllium-Copper
1-DIM. "QUIET" SPECTRUM*

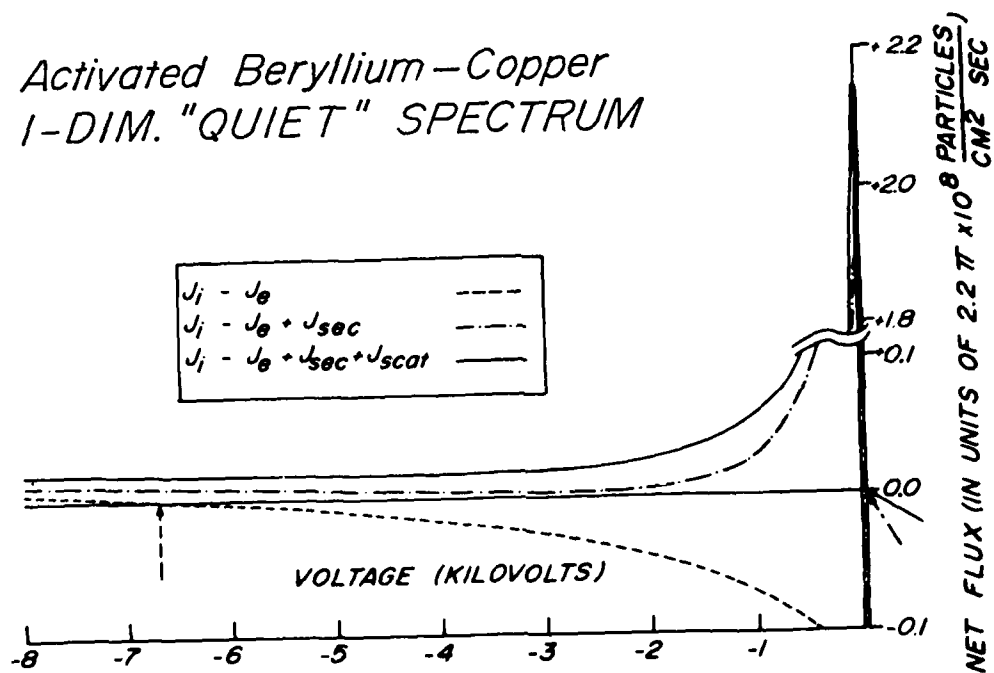


Fig. 2.7. Current-voltage characteristic for activated beryllium-copper in "quiet" conditions, with a one-dimensional velocity-space cutoff.

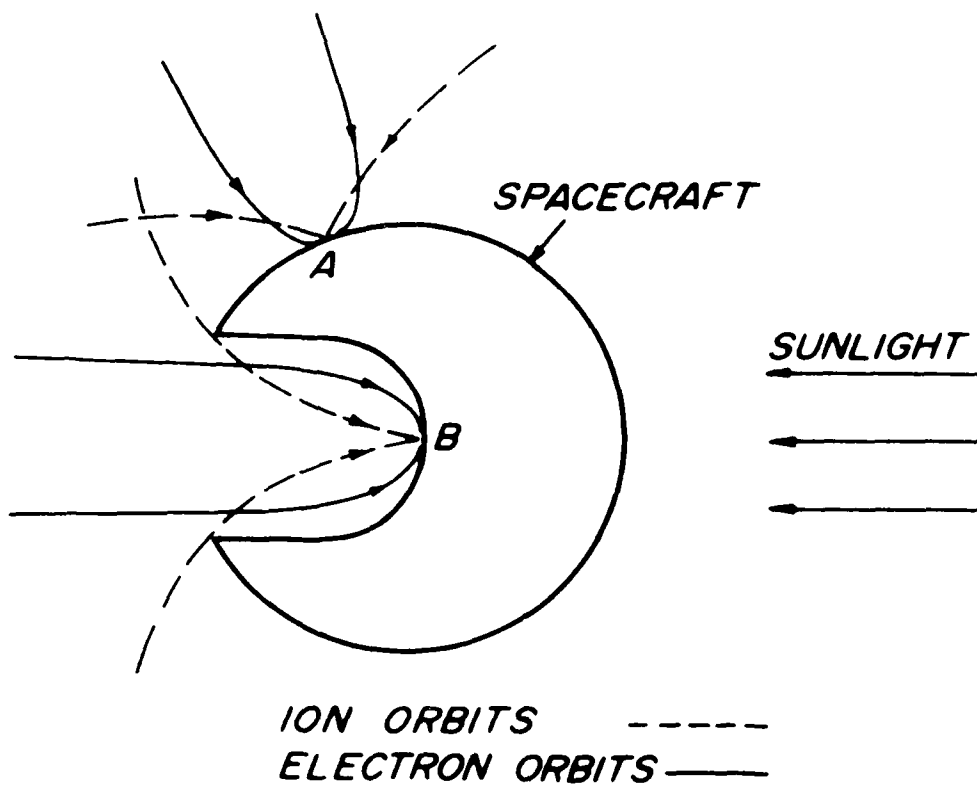


Fig. 2.8. Spacecraft with shaded isolated cavity, showing incident ion and electron orbits with energies close to the lowest for which collection of each species is possible. The orbits shown are cutoff orbits, defined as the most nearly tangential orbits for which incident particles of a given energy are able to reach a given point on the spacecraft surface, having tangential velocity component in a given direction.

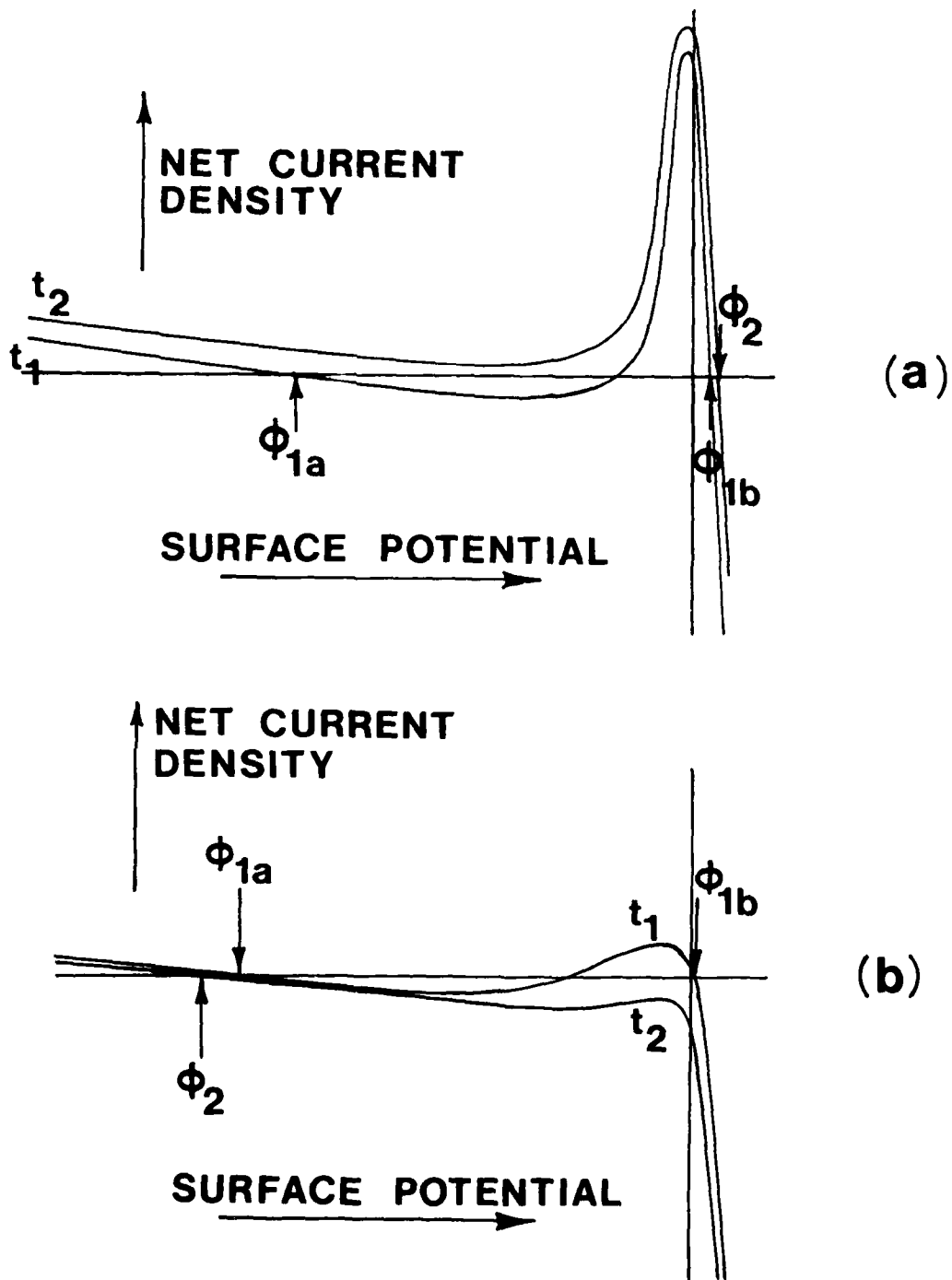


Fig. 2.9. Disappearance of multiple roots in the current-voltage characteristic of a spacecraft surface, as a result of temporal changes in ambient electron velocity distributions. These illustrations are schematic only but are representative of predicted behavior for various surface materials. Some combinations of materials and environments for which such behavior is predicted appear as clusters of three numbers in Table 1.

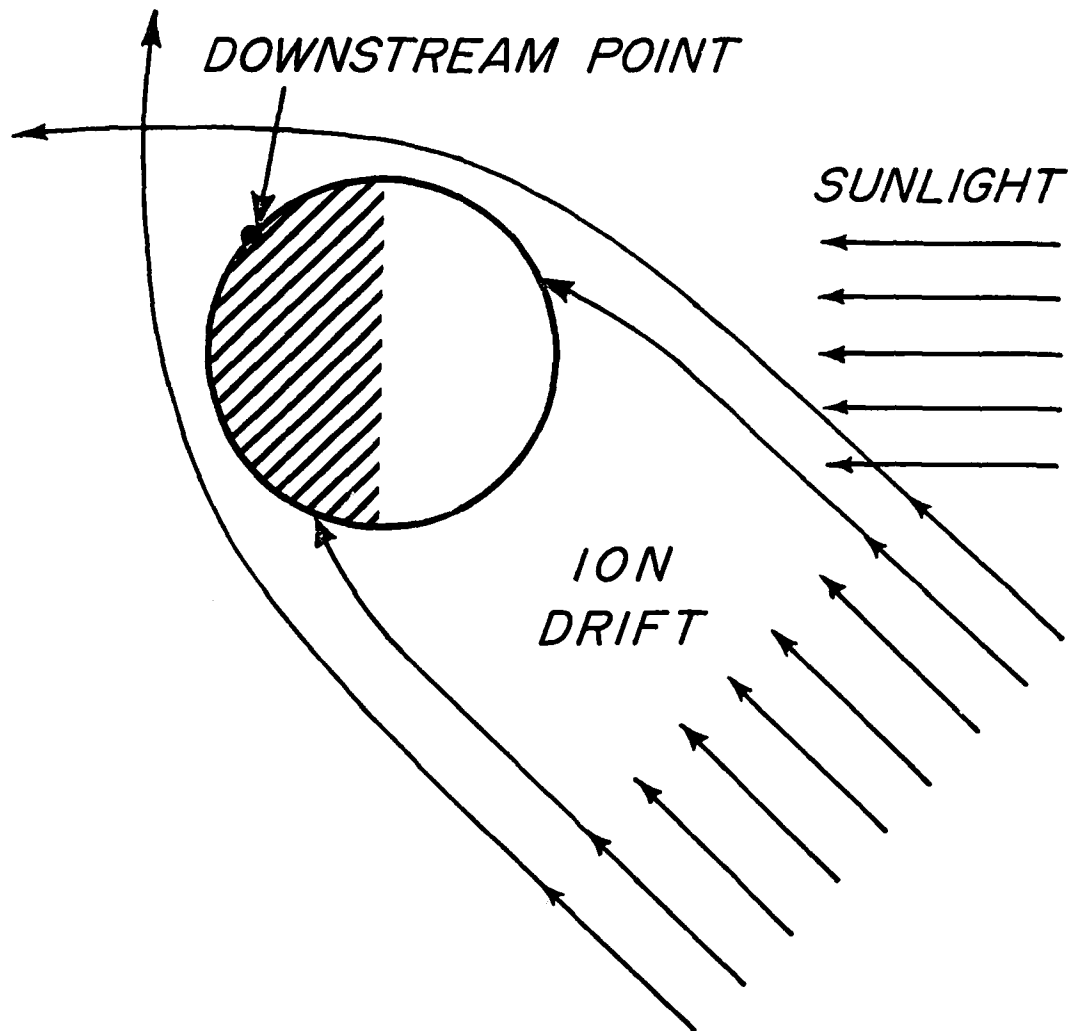


Fig. 2.10. Spherical spacecraft with downstream point (relative to ion drift direction) shaded.

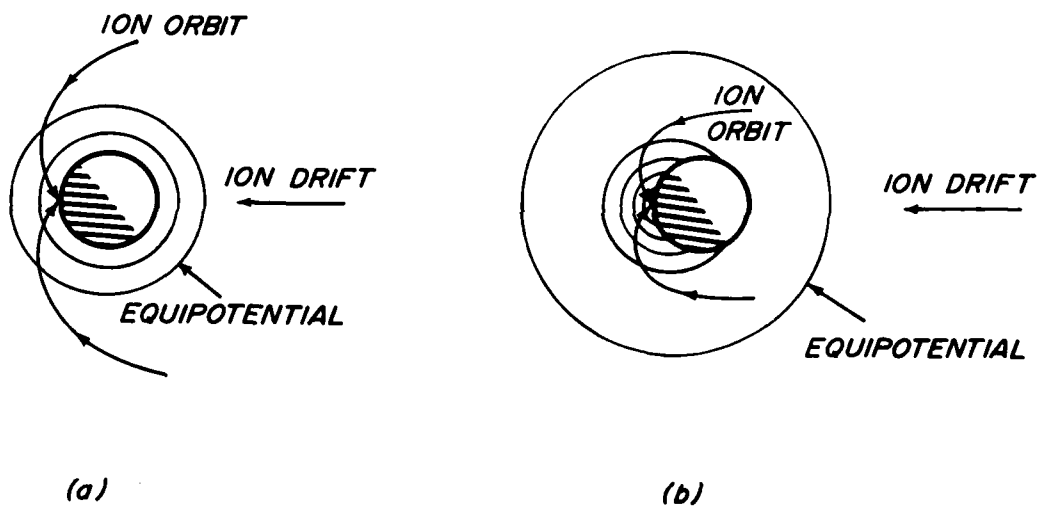


Fig. 2.11(a) Hypothetical symmetric equipotentials around a spherical spacecraft (b) nonsymmetric equipotentials around the same spacecraft.

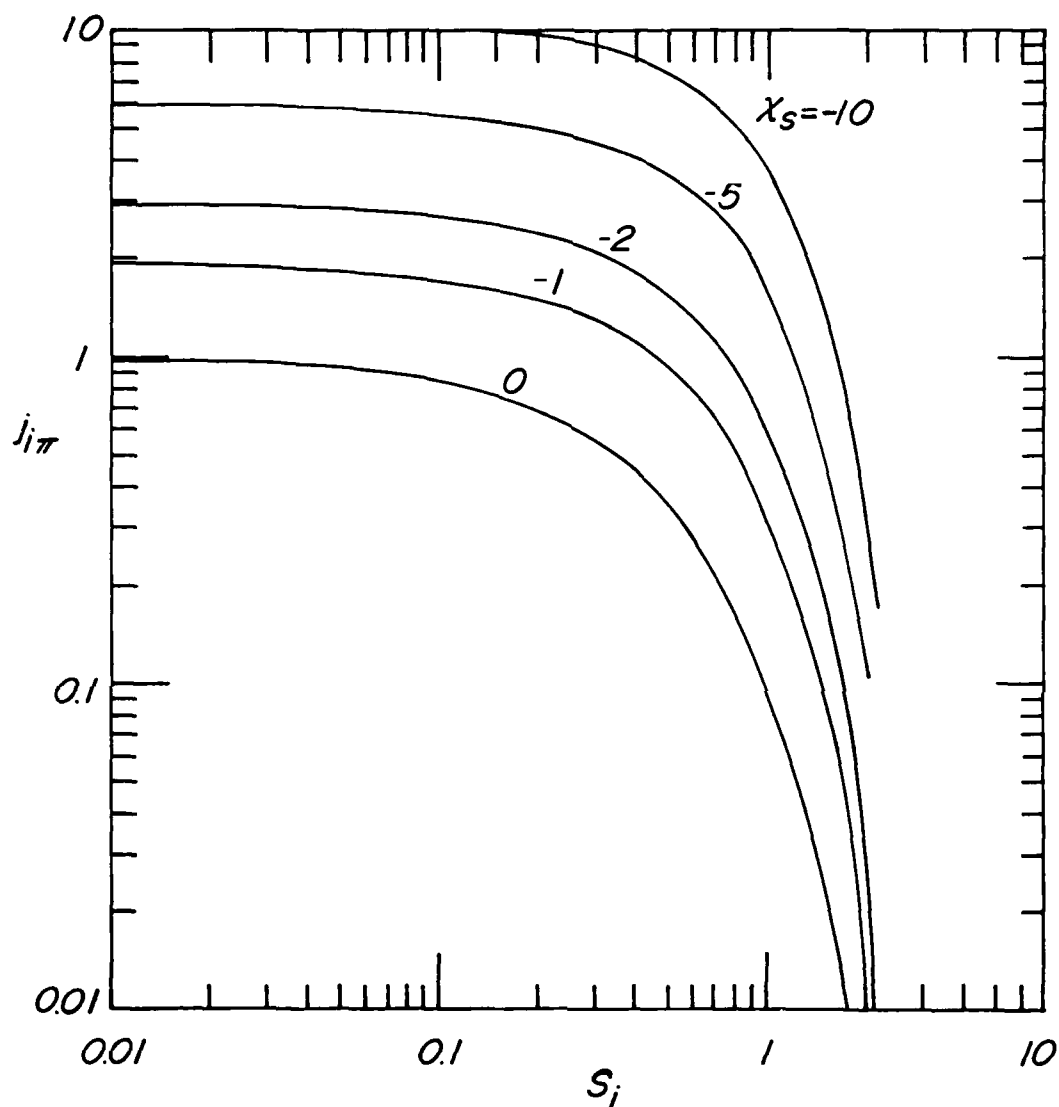


Fig. 2.12. Nondimensional downstream-point ion current density $j_{i\pi} = J_{i\pi} / [N_{\infty} e (kT_i / 2\pi m_i)^{1/2}]$ as a function of ion speed ratio $S_i = U / (2kT_i / m_i)^{1/2}$ for various nondimensional surface potentials $\chi_s = e\phi_s / kT_i$, assuming spherical geometry, zero magnetic field, uniform surface potential, collisionless large-Debye-length conditions, and drifting Maxwellian ions. For $S_i \rightarrow 0$, $j_{i\pi} \rightarrow 1 + |\chi_s|$ when $\chi_s < 0$.

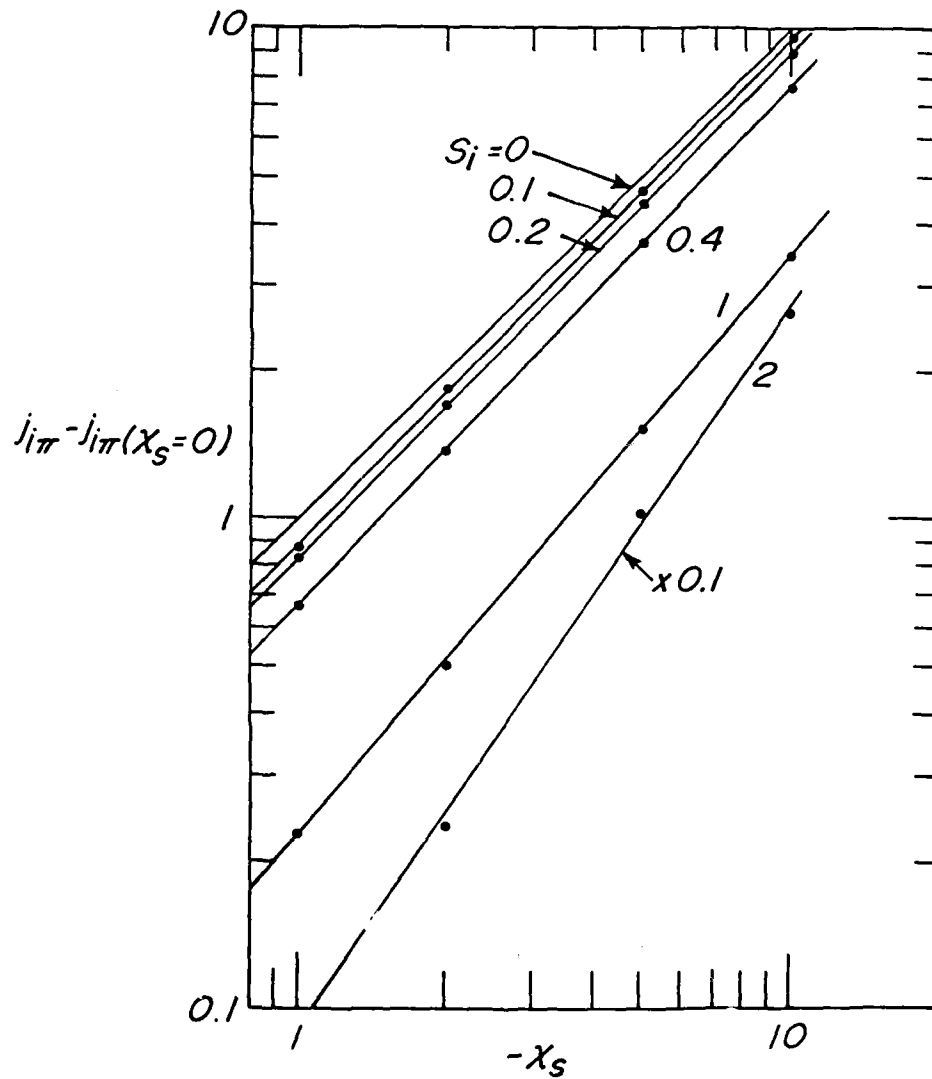


Fig. 2.13. Nondimensional downstream-point ion current density $j_{i\pi}$ as a function of surface potential X_s for various ion speed ratios S_i , for the same conditions as in Fig. 2.12. The straight lines shown are power-law approximations.

AD-A130 043

NUMERICAL SIMULATION OF SPACECRAFT CHARGING PHENOMENA
AT HIGH ALTITUDE..(U) YORK UNIV DOWNSVIEW (ONTARIO)
CENTRE FOR RESEARCH IN EXPERIME..

2/2

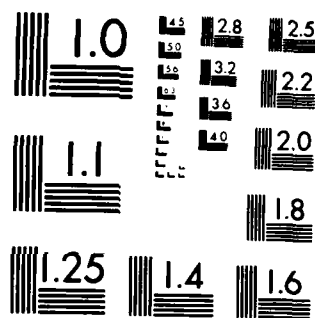
UNCLASSIFIED

J G LAFRAMBOISE ET AL. 10 AUG 82

F/G 22/2

NL

END
DATE
FILMED
7-83
DTIC



MICROCOPY RESOLUTION TEST CHART
NATIONAL BUREAU OF STANDARDS-1963 A

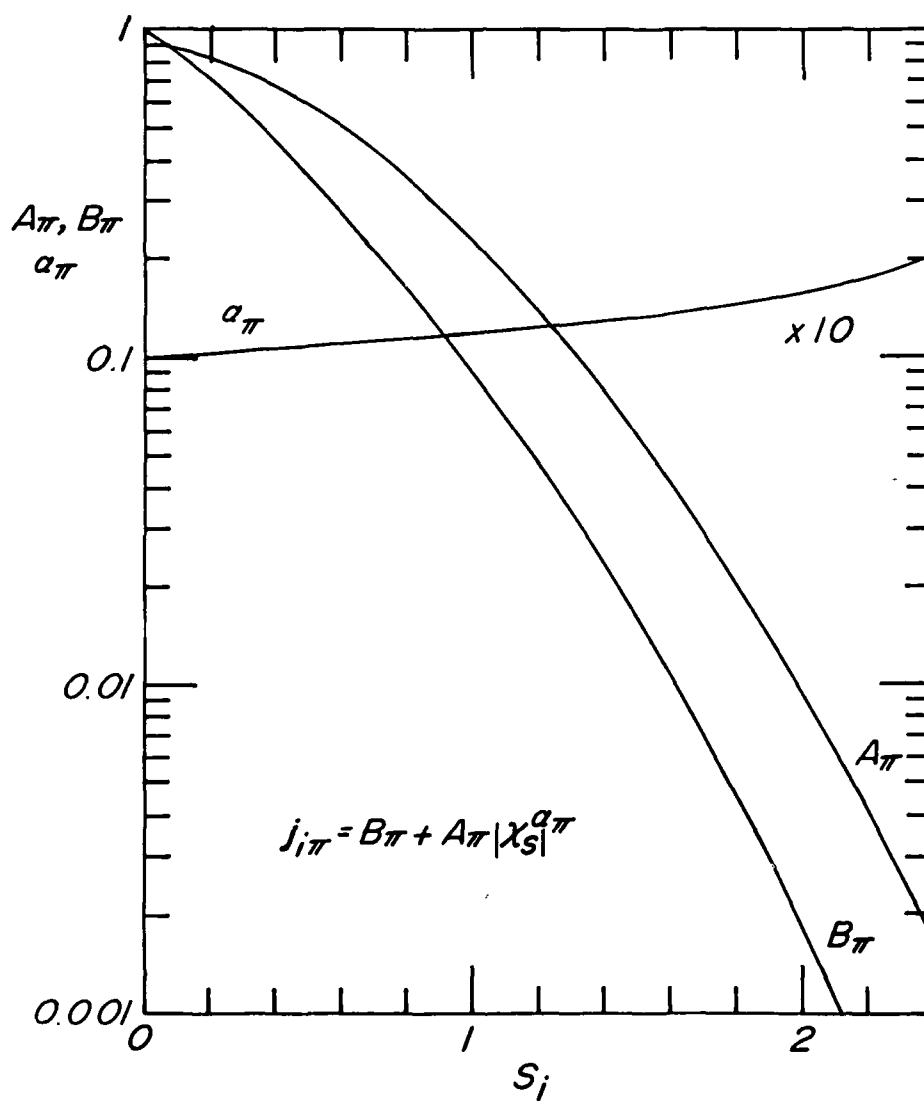


Fig. 2.14. Dependence of the power-law coefficients A_π , B_π and α_π on ion speed ratio S_i .

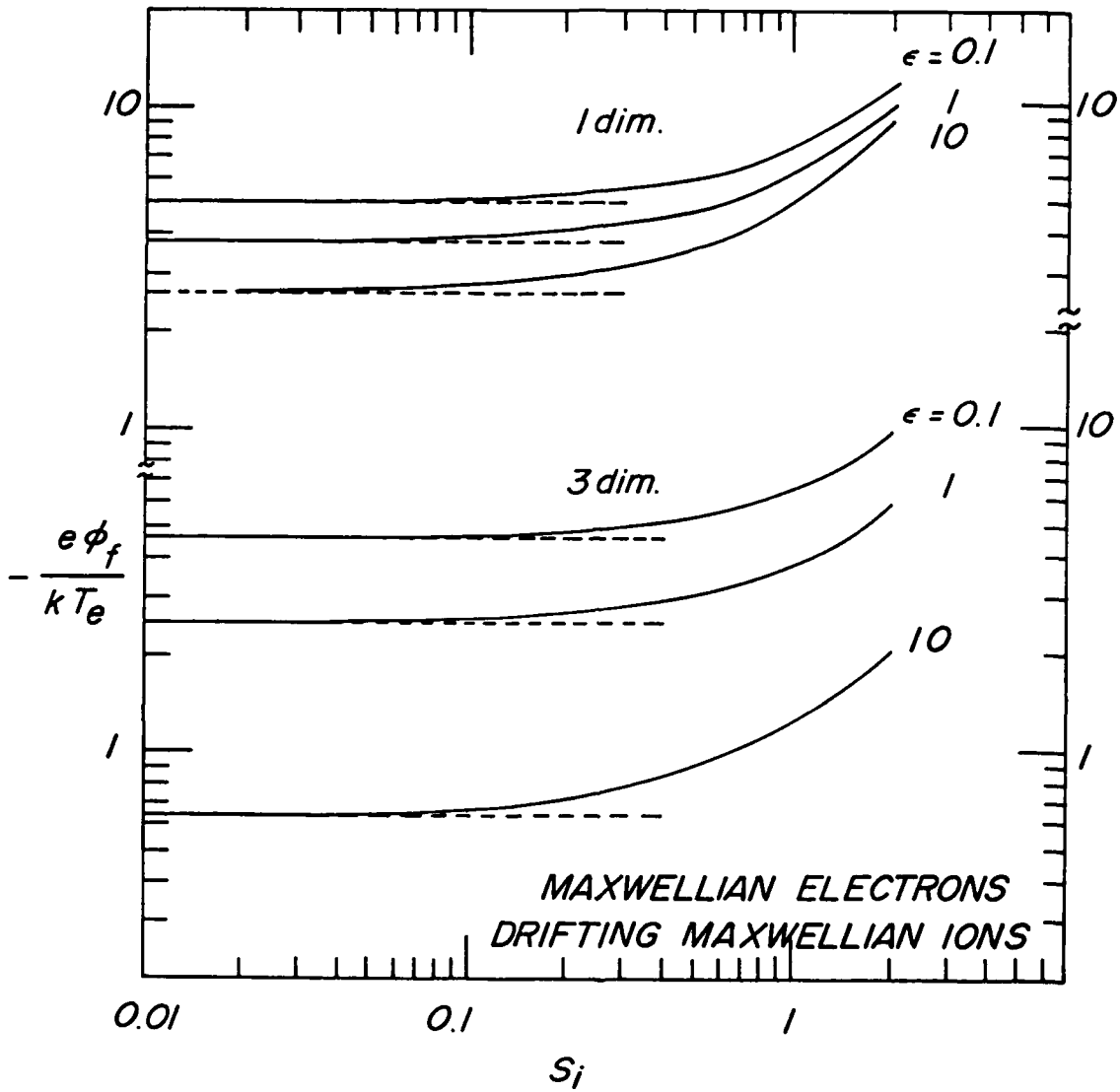


Fig. 2.15. Upper and lower bounds on floating potential ϕ_f at shaded downstream point of spacecraft, as a function of ion speed ratio S_i for various ion-to-electron temperature ratios ϵ , for Maxwellian electrons and drifting Maxwellian ions, for one-dimensional and three-dimensional ion velocity space cutoffs.

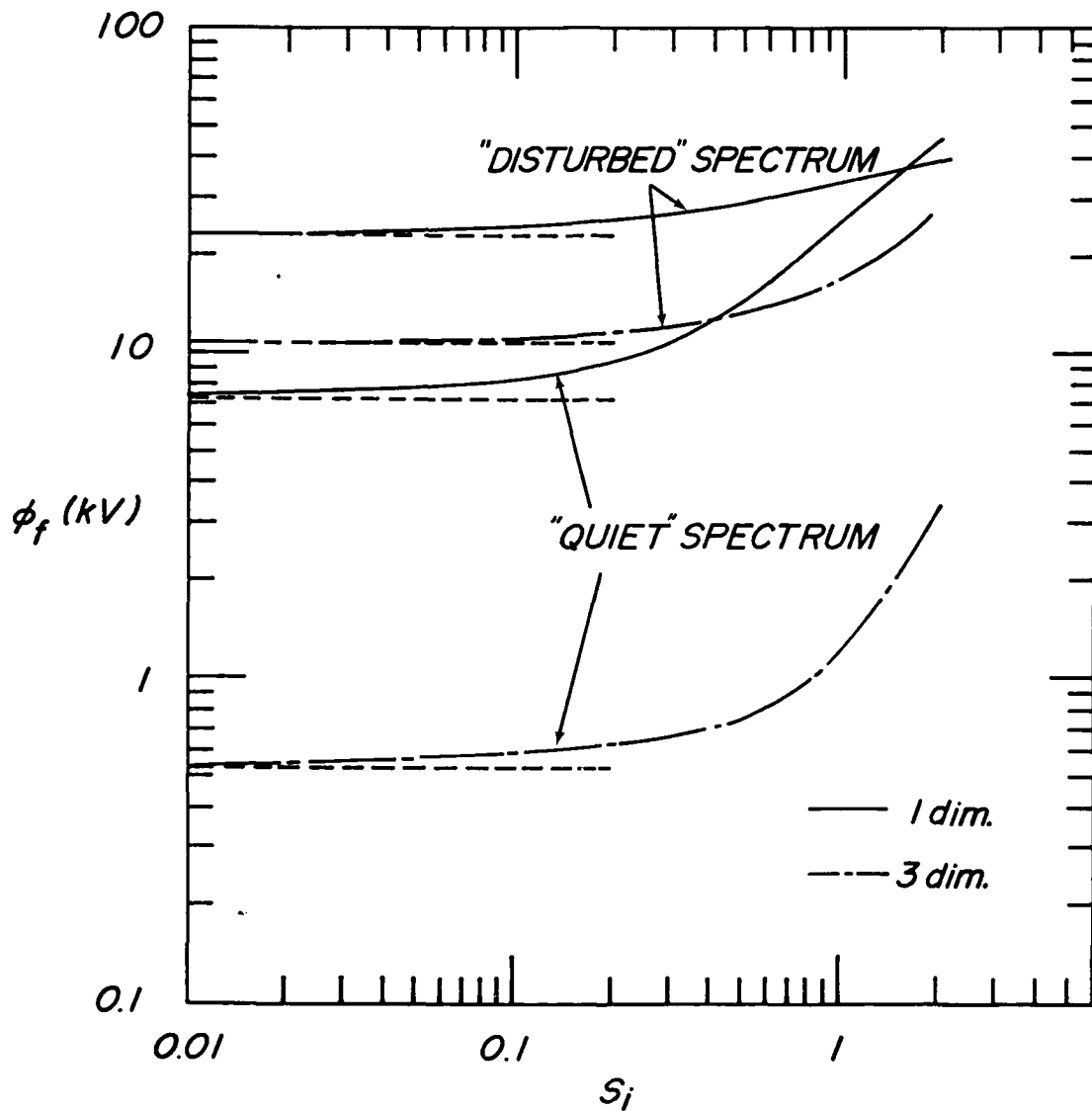


Fig. 2.16. Upper and lower bounds on floating potential ϕ_f at shaded downstream point of spacecraft, as a function of ion speed ratio S_i for "disturbed" and "quiet" electron velocity spectra representing geostationary orbit conditions, for one-dimensional and three-dimensional ion velocity space cutoffs.

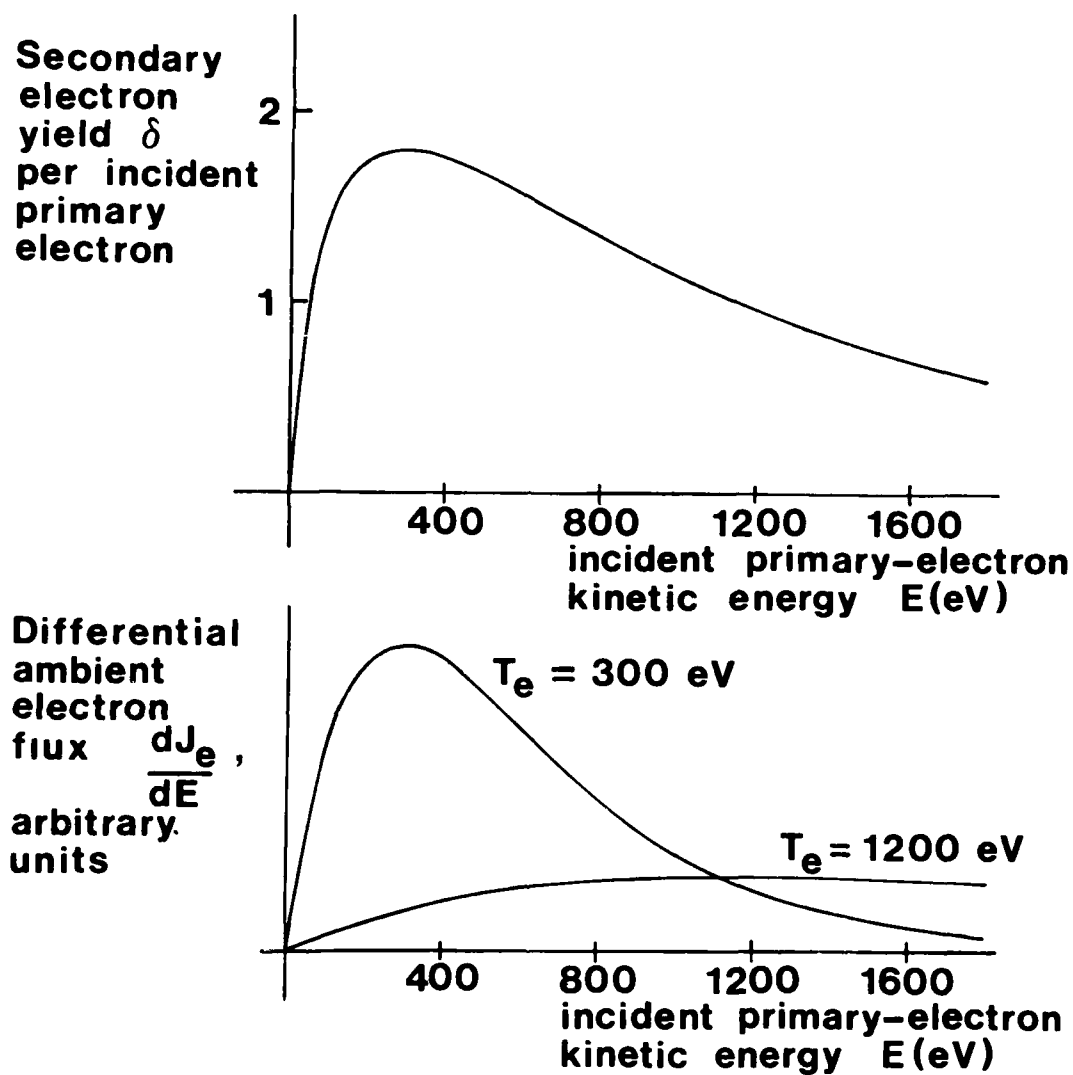


Fig. 3.1.(a) typical form of secondary-electron yield δ (secondary electrons per incident primary electron), as a function of incident primary kinetic energy E , at normal incidence (b) energy-differential electron flux dJ_e/dE for Maxwellian ambient electron velocity distributions at two different temperatures. Total secondary-electron flux is obtained by integrating the product of these two functions [multiplied by another factor given in Eq. (2.10)] over energy E .

PARTICLE ORBIT

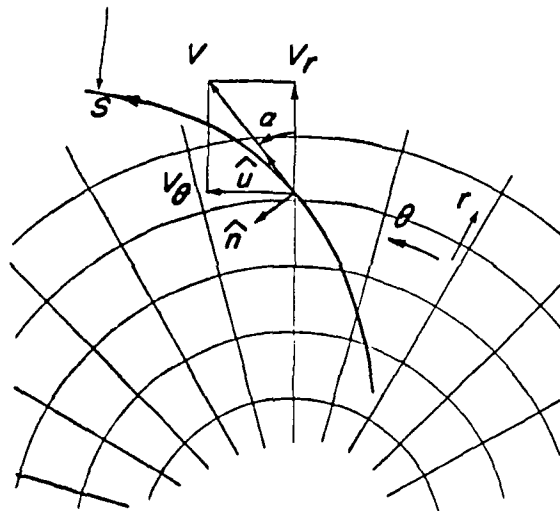


Fig. 4.1. Coordinate system and definitions for particle orbit integration.

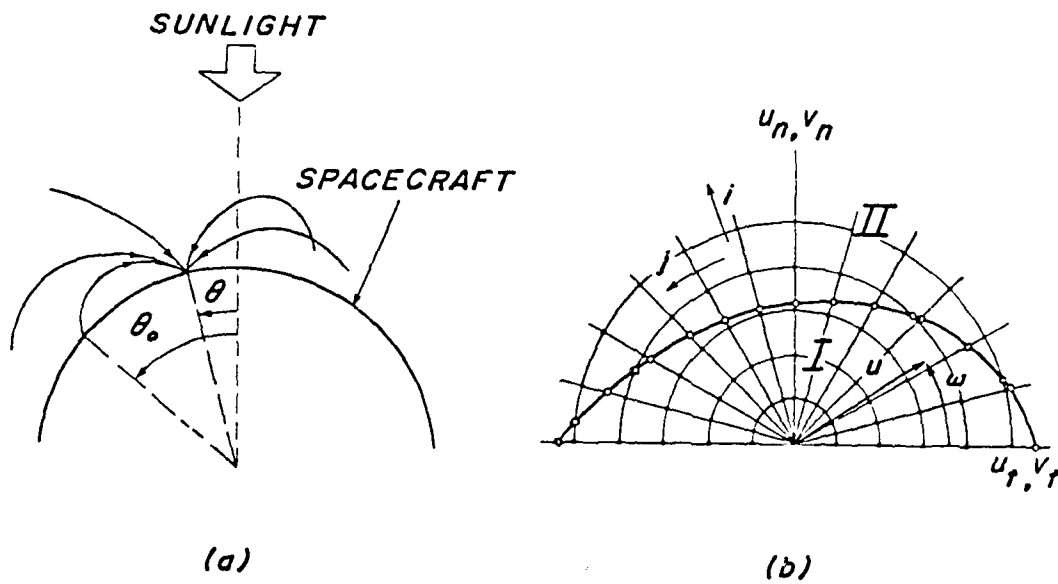


Fig. 4.2. Position-space (a) and velocity-space (b) coordinates for calculation of incident current density at a surface point. Figure 4.2a shows several particle orbits incident at a surface point θ , one of them having originated at the surface point θ_0 .

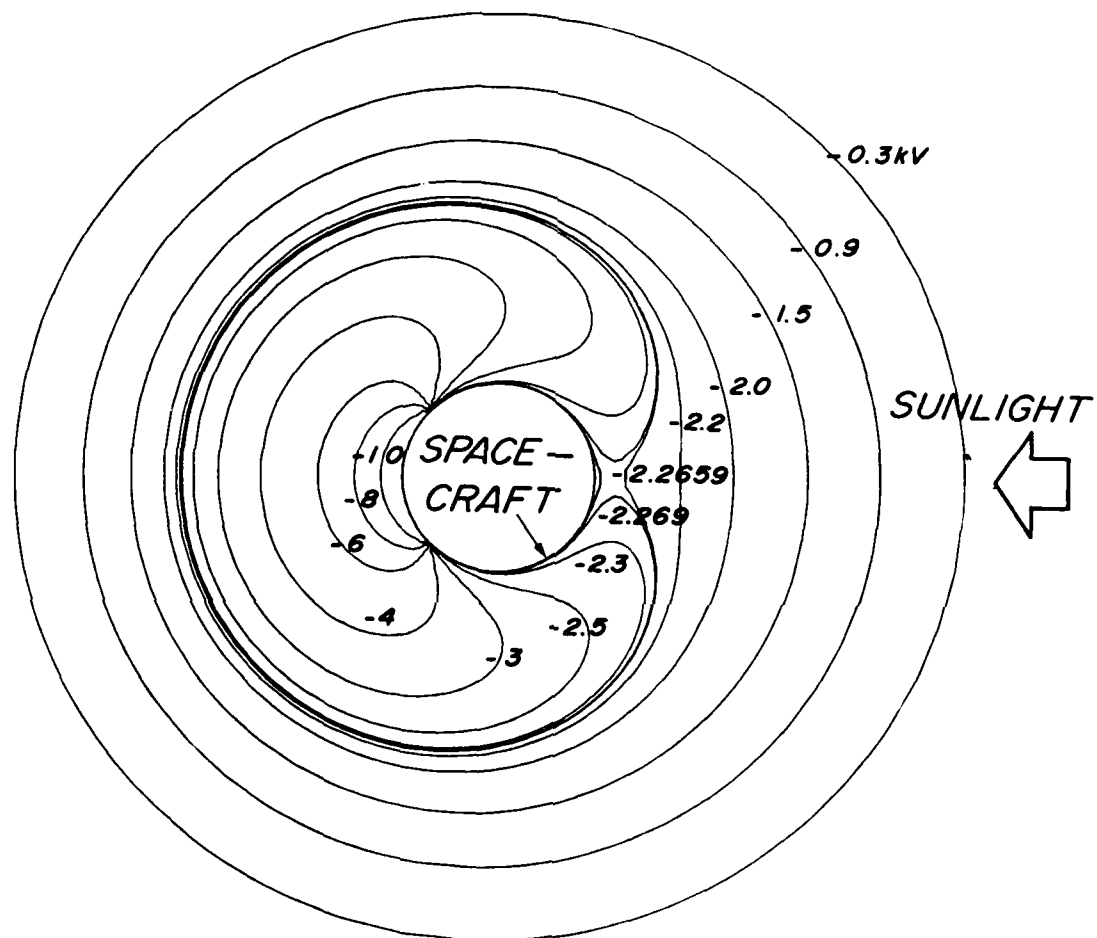


Fig. 4.3. Equipotential contours around a cylindrical spacecraft cross-section with two conductive sectors having angles of 270° and 90° . Sector potentials are -2.265 kV and -11.88 kV, respectively. Other data pertinent to this calculation are given in Sec. 4.5. The radial coordinate in Figs. 4.3 ~ 4.5, 4.8 and 4.9 is $1 + \ln(r/r_s)$ where r_s is spacecraft radius.

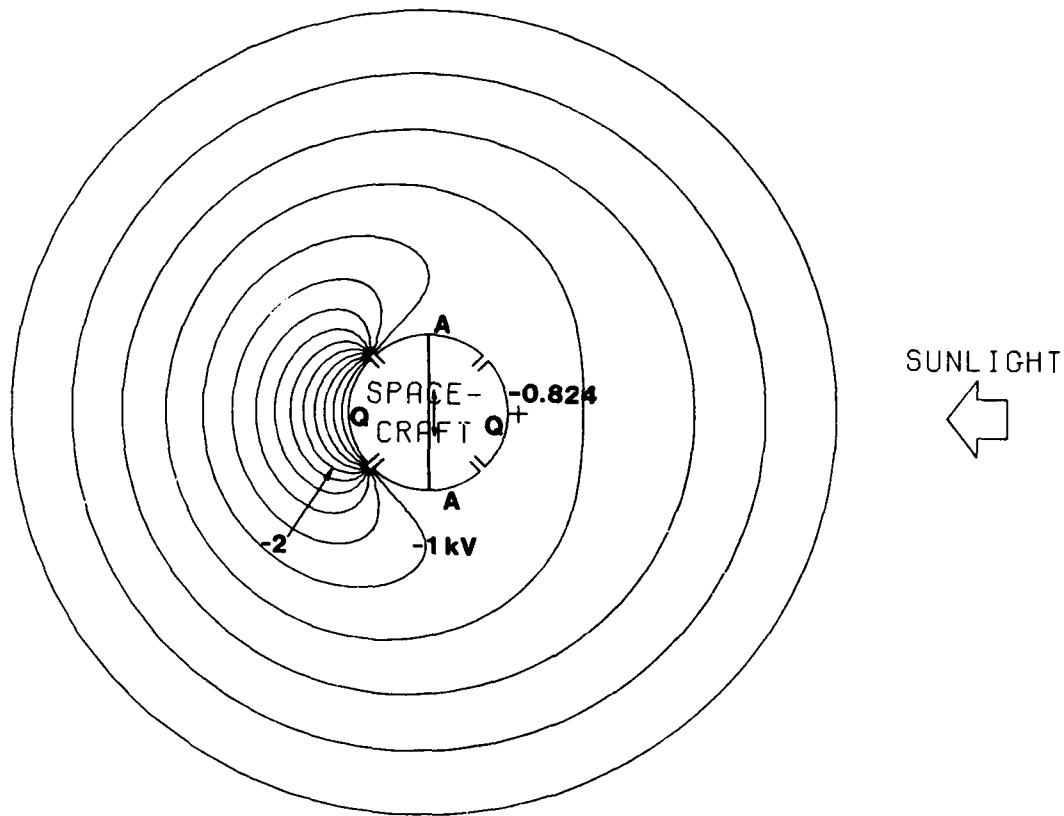


Fig. 4.4. CYLVIA calculation of equipotential contours around a cylindrical spacecraft cross-section with four sectors each having an angle of 90° . The two sectors labeled "A" are conductive, have the photoemission properties of aluminum, and are connected together electrically, as shown schematically in the figure. The two sectors labeled "Q" are nonconductive and have the photoemission properties of quartz. In this and subsequent figures, the symbol + indicates the location of a saddle point. Other data pertinent to this calculation are given in Sec. 4.5. The radial coordinate in this figure is as in Fig. 4.3. The floating surface potential distribution resulting from this calculation is shown in Fig. 4.6.

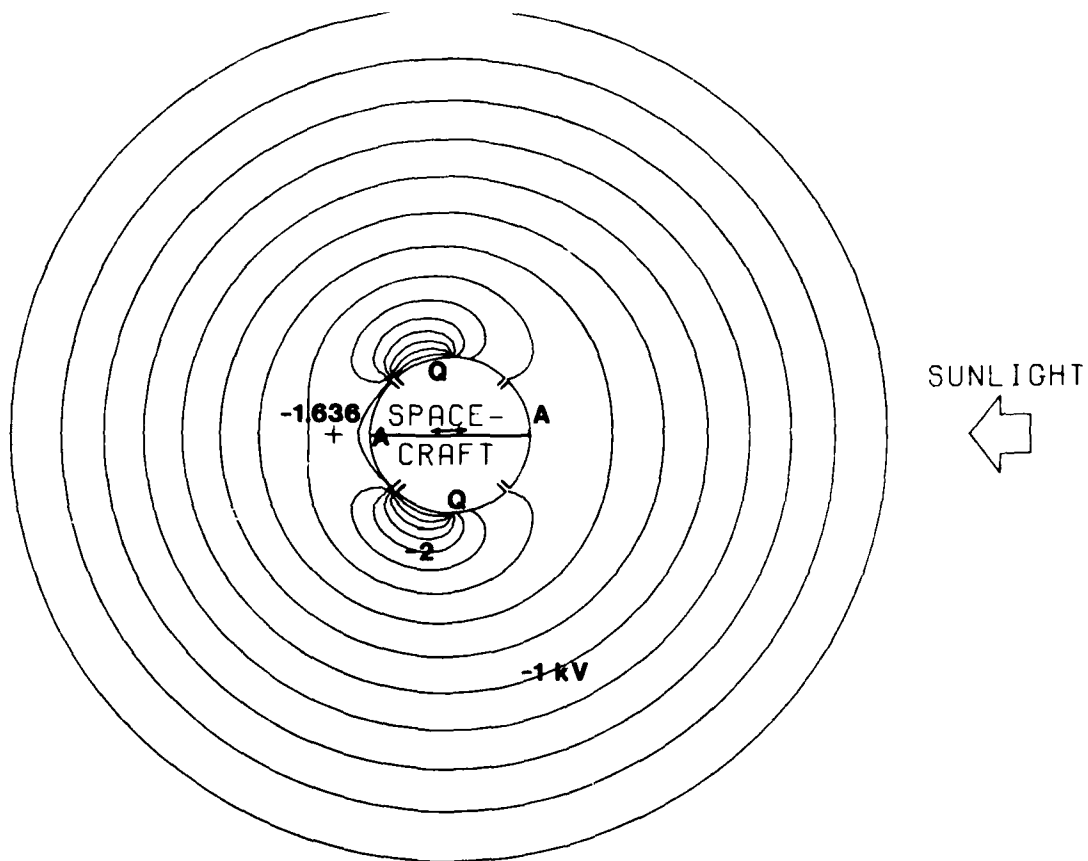


Fig. 4.5. Same as Fig. 4.4 except that the spacecraft has been rotated by 90°.

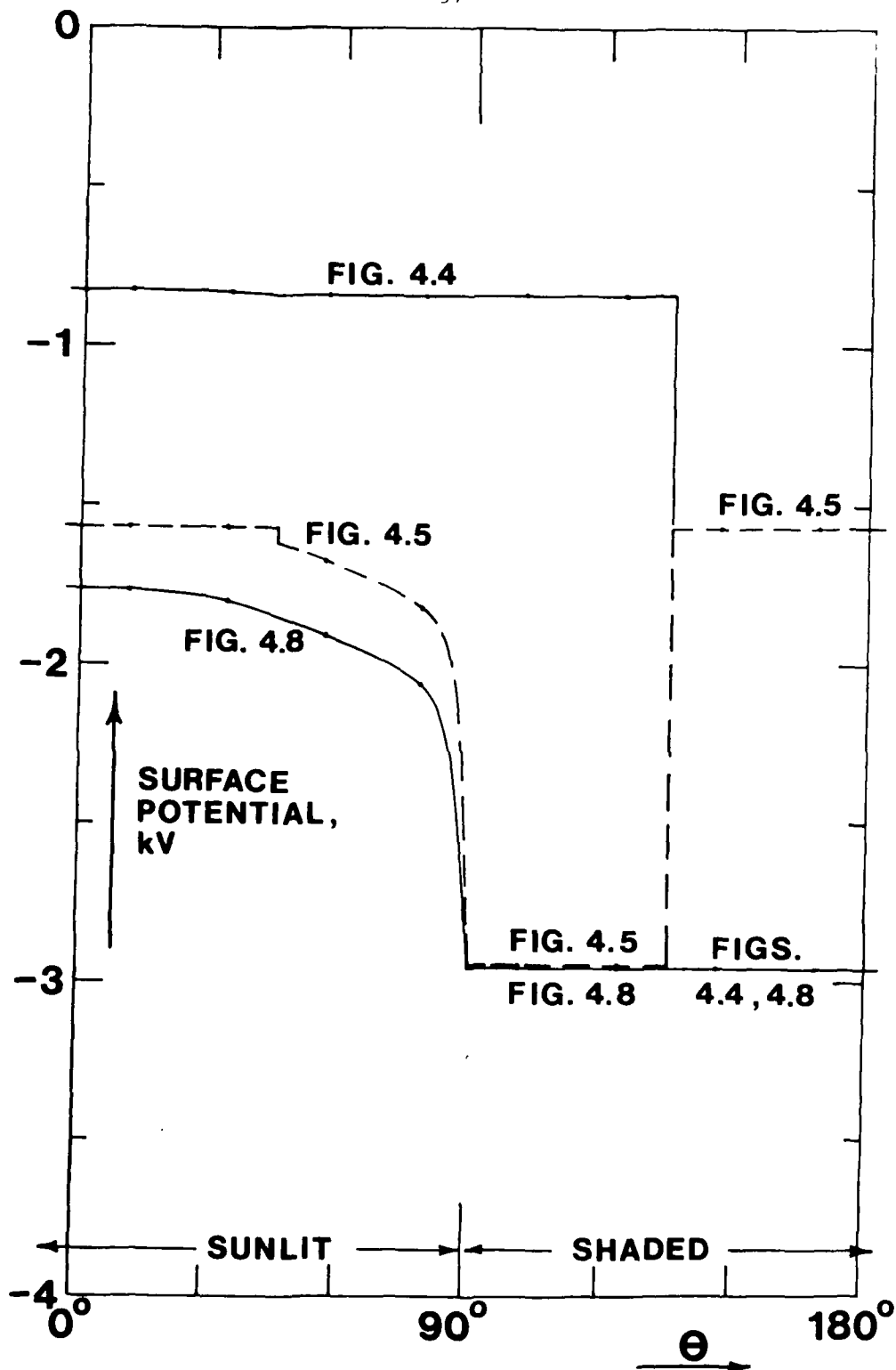


Fig. 4.6. Distributions of floating surface potential vs angle for the calculations shown in Figs. 4.4, 4.5, and 4.8.

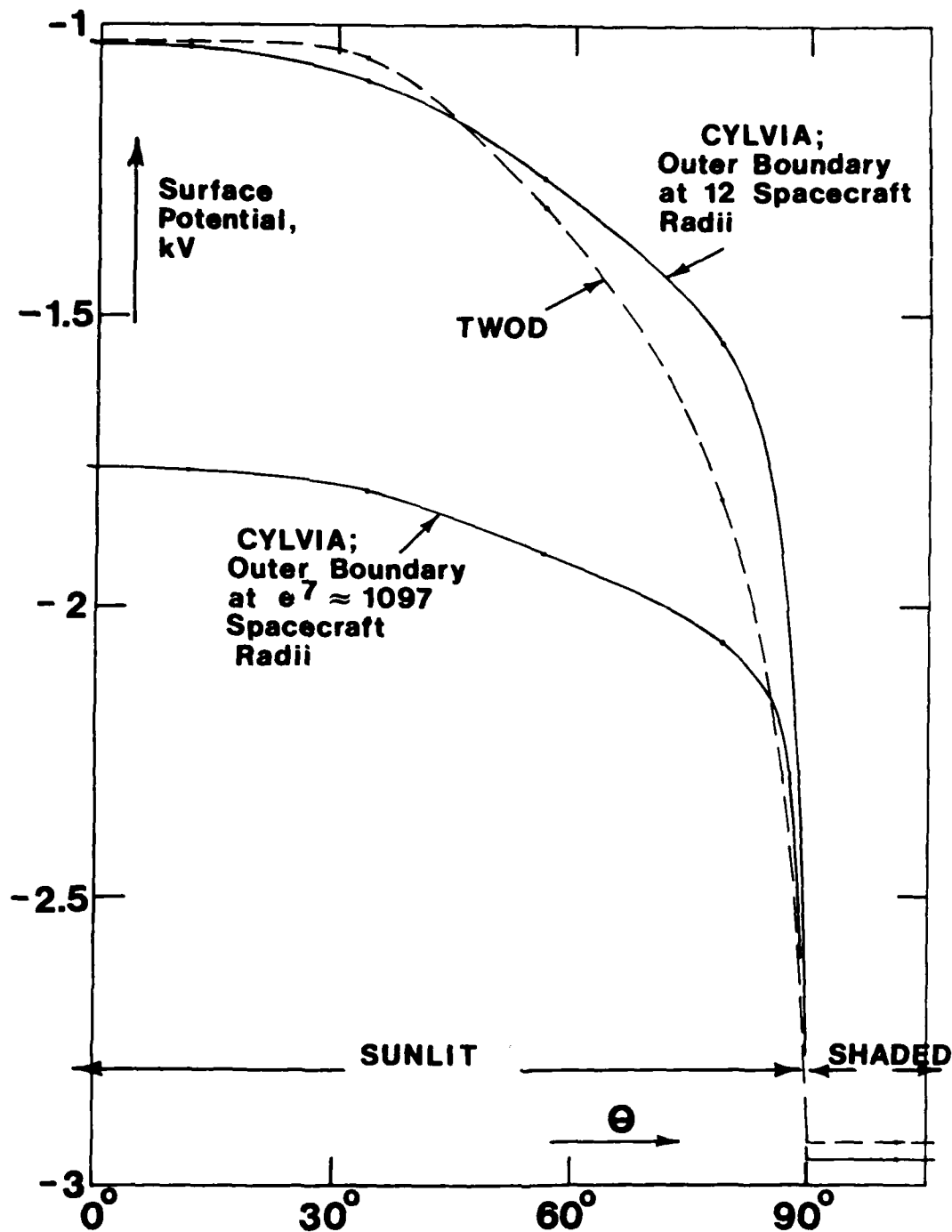


Fig. 4.7. Distributions of floating surface potentials vs angle for the calculation shown in Fig. 4.9, and also for another one which is the same except that the outer boundary of the calculation (which is held at space potential in all cases) is at $12r_s$ rather than e^7r_s . Also shown is another result for which the outer boundary is at $12r_s$, calculated using a program called TWOD, which combines NASCAP physical assumptions with circular cylindrical geometry (M. Mandell, Systems, Science and Software, Inc., private communication). Other data pertinent to these calculations are given in Sec. 4.5.

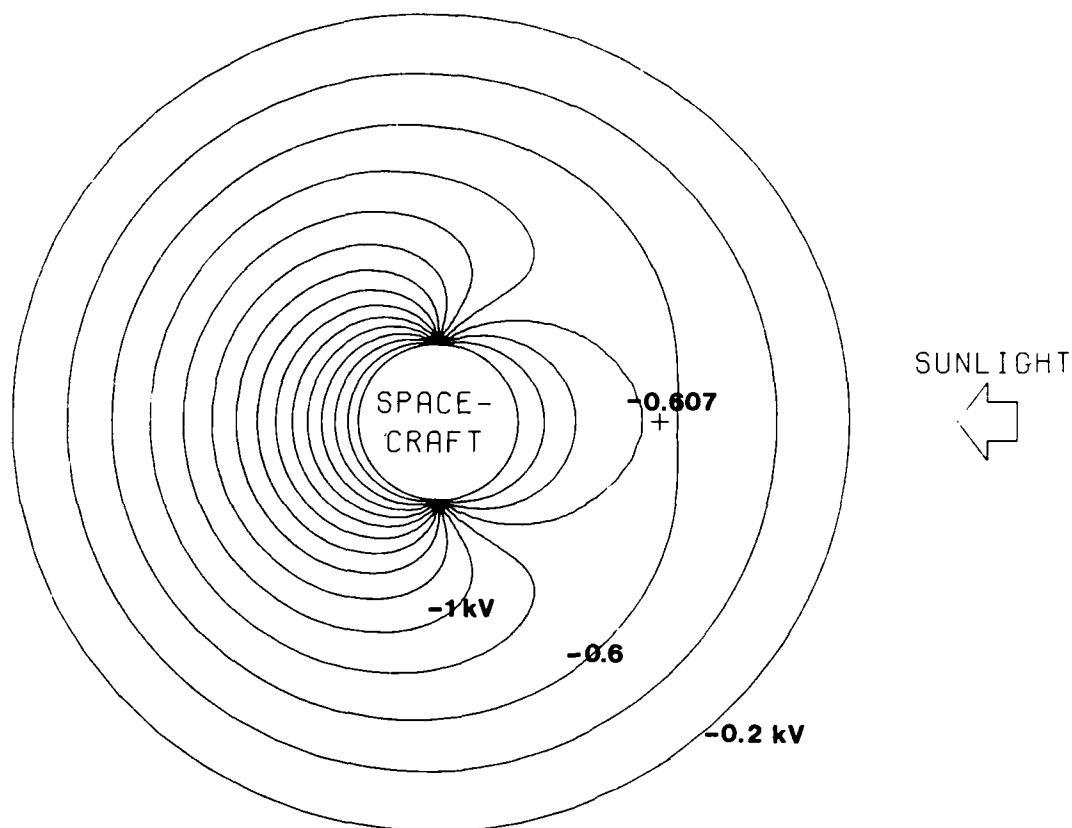


Fig. 4.8. CYLVIA calculation of equipotential contours around a cylindrical spacecraft cross-section having a nonconductive surface, corresponding to a surface potential distribution calculated assuming local current balance only (i.e., the presence of a potential barrier is ignored in calculating photoelectron escape). The symbol + indicates the location of a saddle point. The photoelectron charge flux $eJ_{ph} = 4.2 \times 10^{-5} \text{ A/m}^2$ at normal incidence.

$T_{ph} = 1.5 \text{ eV}$. Ambient ion and electron distributions are single Maxwellians, each with $n_p = 3 \text{ cm}^{-3}$ and $T = 1 \text{ keV}$. Secondary and backscattered electron fluxes are assumed zero. The polar-coordinate computation grids in position (r, θ) and in velocity space contain 65×16 and 8×16 intervals, respectively. Outer grid boundary radius r_B is e^7 times spacecraft radius r_s . Linearized ambient space charge (Eq. 4.3; Laframboise and Prokopenko, 1977), corresponding to a Debye length of $96 r_s$, is assumed. Radial coordinate in Figure is $1 + \ln(r/r_s)$.

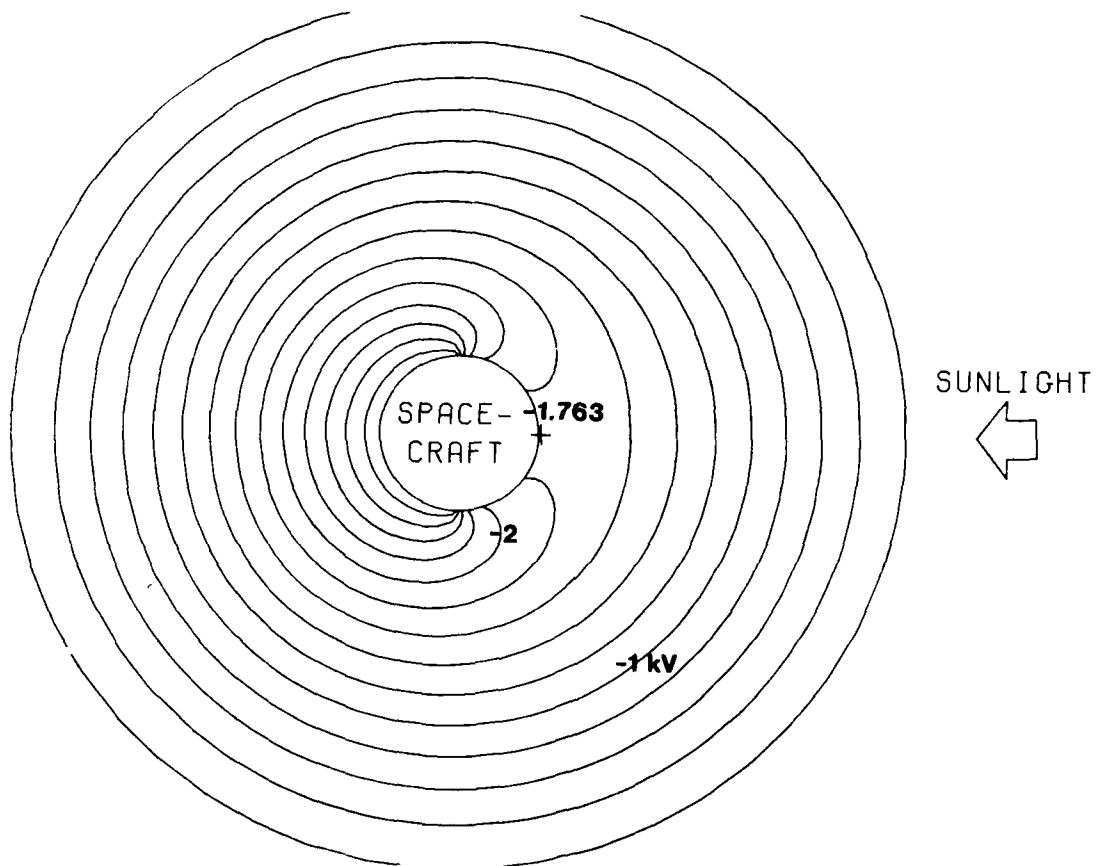


Fig. 4.9. Same as Figure 4.8 except that the calculation is now self-consistent including potential-barrier effects on photoelectron and other particle orbits.

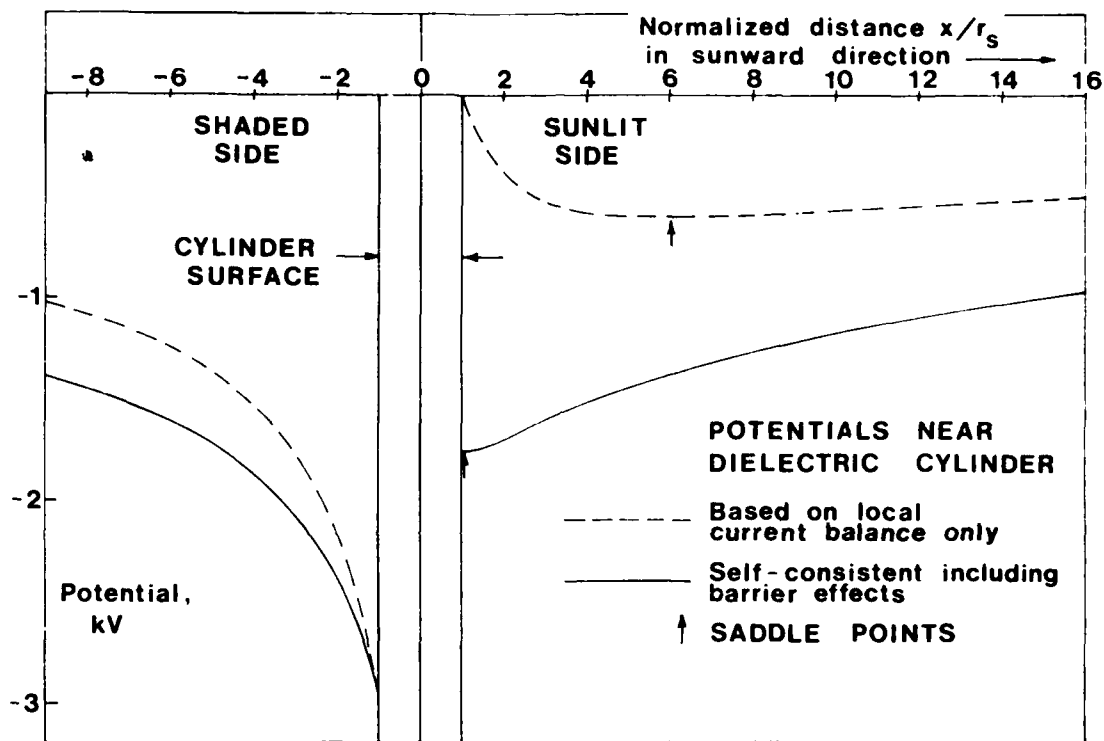


Fig. 4.10. Potentials vs distance along spacecraft-sun line for the situations shown in Figs. 4.8 and 4.9, showing the large decrease in differential charging which results when potential-barrier effects on particle (especially photoelectron) orbits are included. Without these effects, surface potentials at the sunward and anti-sunward points are 5.1V and -2.96 kV; with these effects, these potentials are -1.76 kV and -2.96 kV.

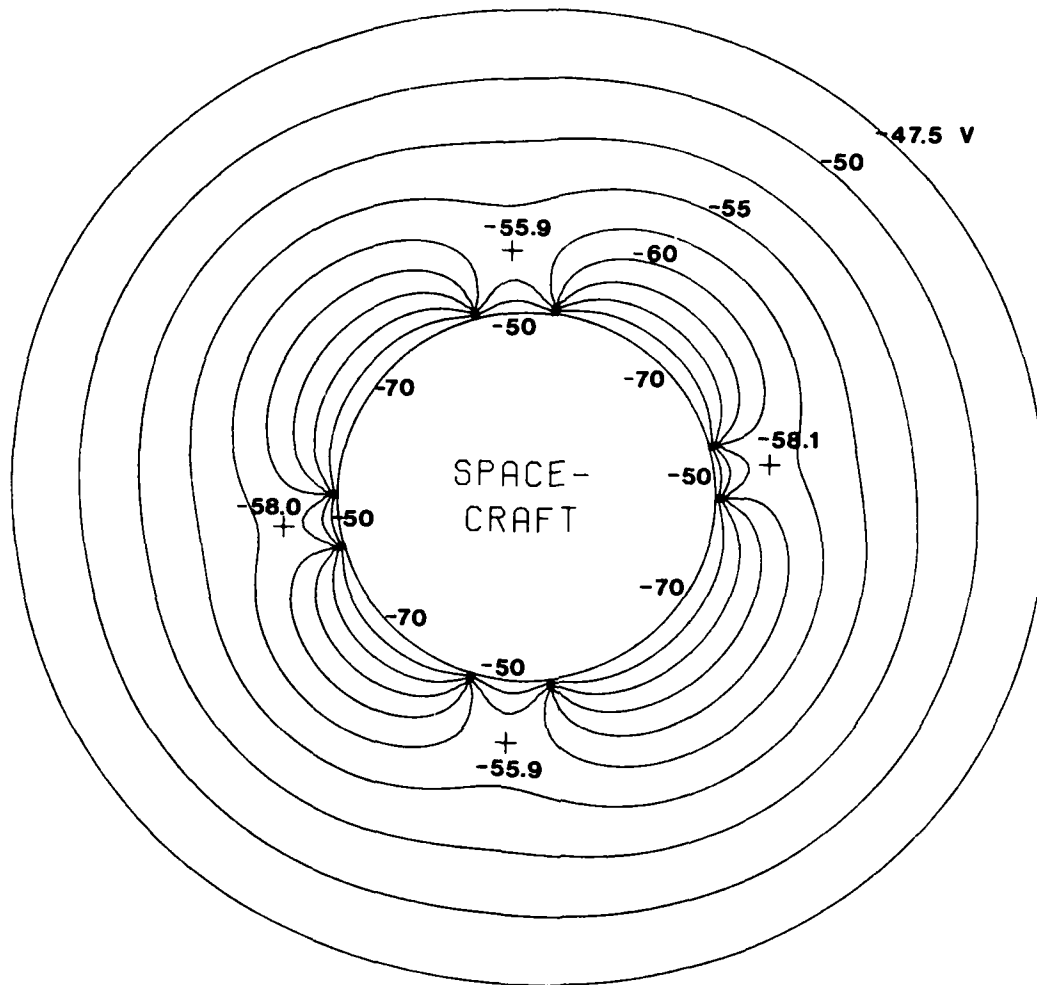


Fig. 4.11. CYLVIA calculation of equipotentials around a circular spacecraft cross-section with given rather than self-consistent surface potentials, as shown. In this Figure, the radial coordinate is proportional to radius. The computational grid in (r, θ) contains 65×180 intervals. The outer grid boundary is at $e^5 \approx 148$ spacecraft radii. Linear space charge corresponding to $\lambda_D = 32.5$ spacecraft radii is assumed. Other data pertinent to this calculation are given in Sec. 5.2. This calculation was done for the purpose of comparison with a XYCIC calculation shown in Fig. 5.1, and also with a similar but three-dimensional calculation done using NASCAP (Olsen, 1980, p. 190; Olsen and Whipple, 1980, Fig. 16). The results of this comparison are discussed in Sec. 5.2.

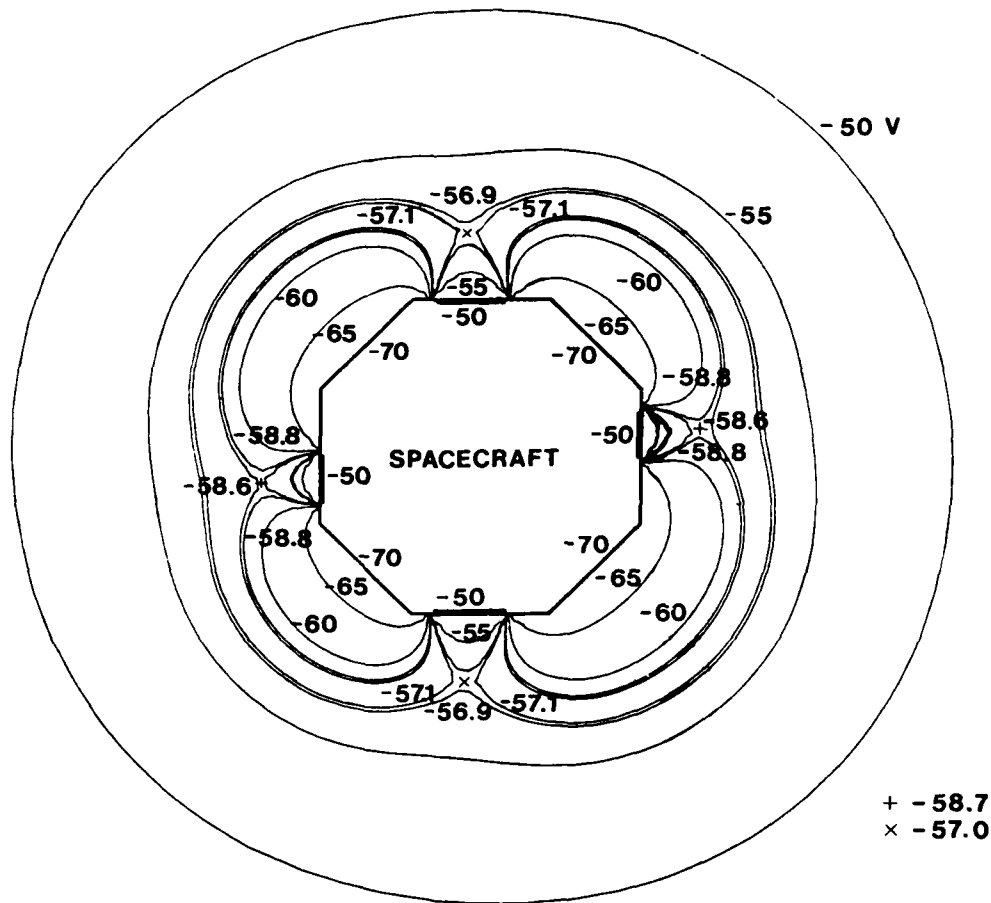


Fig. 5.1. XYCIC calculation of equipotentials, corresponding to the CYLVIA calculation shown in Fig. 4.11. One difference between these two calculations is that in the XYCIC calculation, zero space charge is assumed. The innermost grid used in the XYCIC calculation contains 40×40 intervals; the octagon has a dimension of 28×28 intervals and is centred in this grid. Six other grids surround the innermost grid; the outermost grid boundary is a centred square of side 19.2 times as large as the innermost grid boundary, i.e. located at 27.4 object half-widths.

Fig. 5.2. XYCIC calculation of equipotentials around a cross-section through a hypothetical antenna + spacecraft body combination. As in Figs. 4.11 and 5.1, surface potentials are imposed (in this case, also hypothetical) values. Zero space charge is assumed. The innermost grid used contains 32×32 intervals with the combined total width of the "object" being 24 intervals. Six other grids surround the innermost grid; the outermost grid boundary is a centred square of side 20 times the innermost grid boundary, i.e. located at 26.7 half-widths of the combined object.

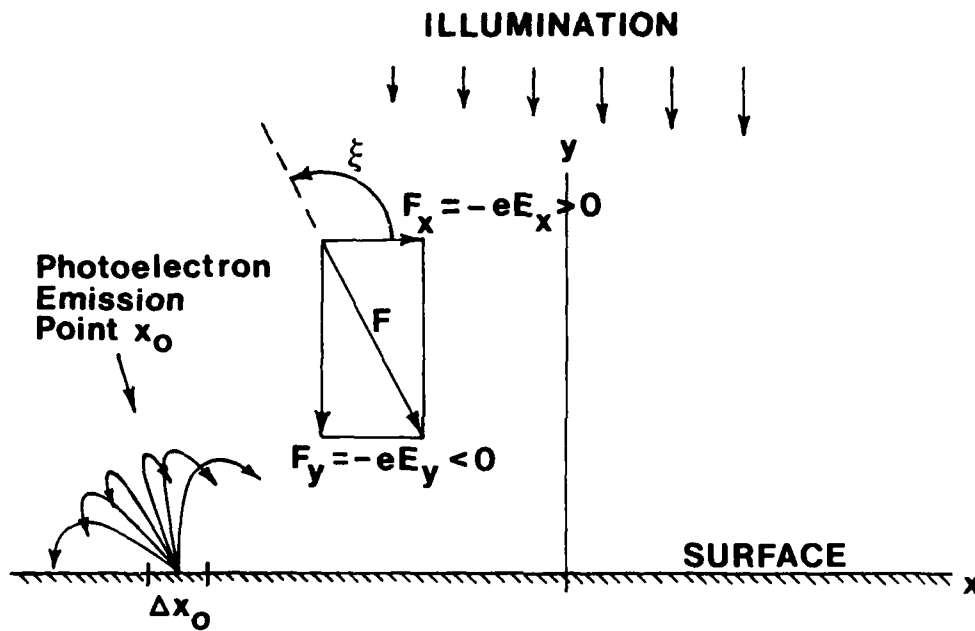


Fig. 6.1. Geometry for photocurrent sheet calculation. The illumination is assumed to vary linearly with x , producing a photoemission current density $J_{ph}(x_0) = J_{ph,0} + J_{ph}'x_0$. The electric field components E_x and E_y are assumed uniform, so that the surface potential varies linearly with x . The electron orbits are then tilted parabolas. Their impact points x can be found analytically (Eq. 6.1) for given values of emission position x_0 and emission velocity components v_{x0} and v_{y0} .

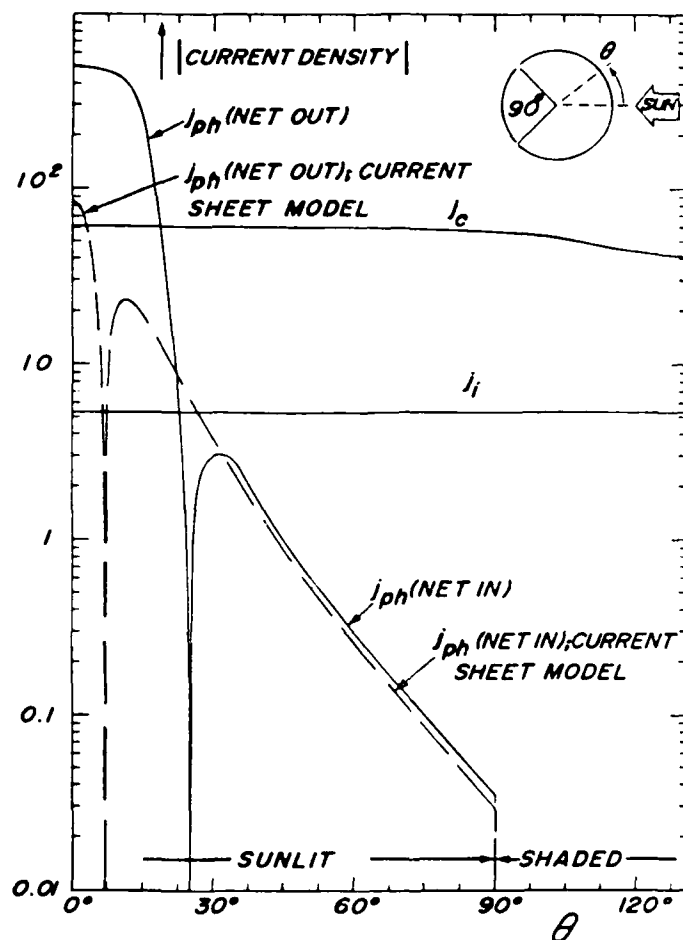


Fig. 6.2. Current densities vs surface position for the situation shown in Fig. 4.3 and described in Sec. 6.3. In this Figure, normalized current density j is defined as J/J_{ref} , where J_{ref} is the random flux of Maxwellian ions having a temperature and density of 1 keV and 1 cm^{-3} . Approximate photoelectron currents j_{ph} obtained using the approximate surface current ("current sheet") model given by Eqs. (6.7) and (6.8) are shown as dashed curves.

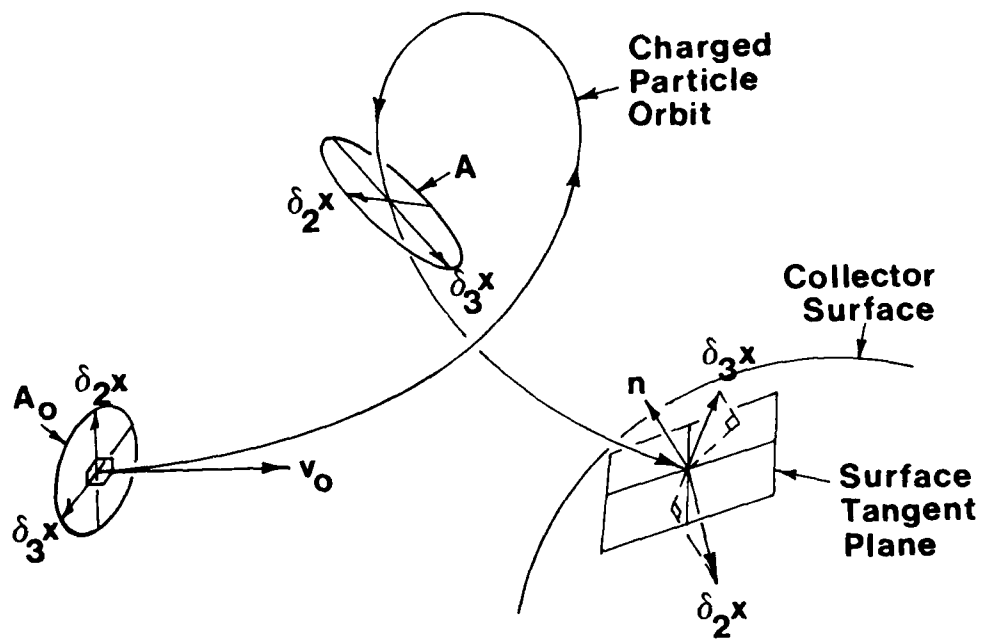


Fig. 7.1. Particle orbit geometry.

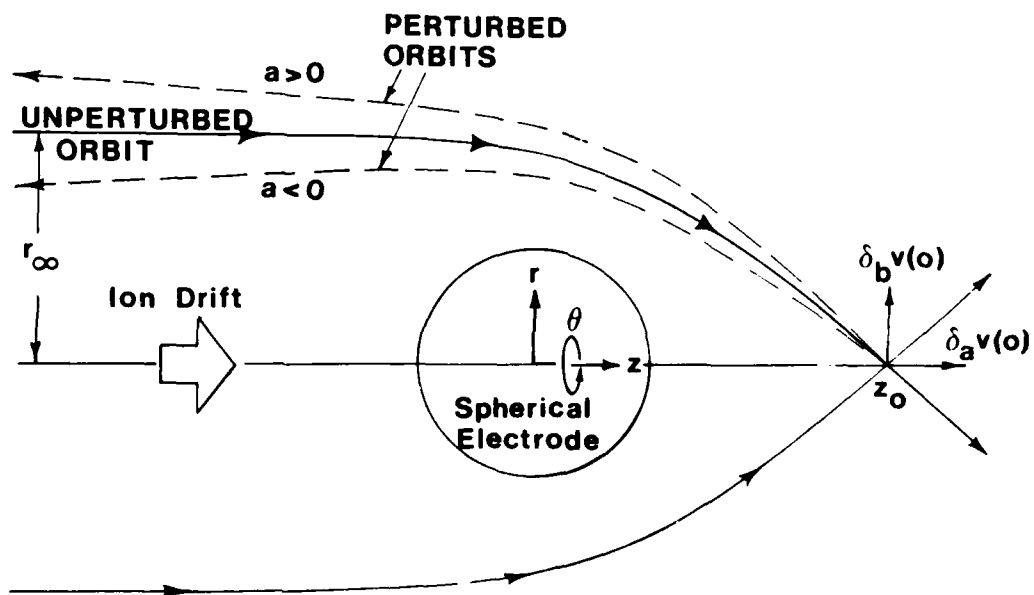


Fig. 7.2. Geometry for perturbation calculation of sphere axial defocusing.

[illegible]

```

100  KUN1=1+KUN10
KUN2=1+KUN11
KUN3=1+KUN12
KUN4=1+KUN13
KUN5=1+KUN14
KUN6=1+KUN15
KUN7=1+KUN16
KUN8=1+KUN17
KUN9=1+KUN18
KUN10=1+KUN19
KUN11=1+KUN20
KUN12=1+KUN21
KUN13=1+KUN22
KUN14=1+KUN23
KUN15=1+KUN24
KUN16=1+KUN25
KUN17=1+KUN26
KUN18=1+KUN27
KUN19=1+KUN28
KUN20=1+KUN29
KUN21=1+KUN30
KUN22=1+KUN31
KUN23=1+KUN32
KUN24=1+KUN33
KUN25=1+KUN34
KUN26=1+KUN35
KUN27=1+KUN36
KUN28=1+KUN37
KUN29=1+KUN38
KUN30=1+KUN39
KUN31=1+KUN40
KUN32=1+KUN41
KUN33=1+KUN42
KUN34=1+KUN43
KUN35=1+KUN44
KUN36=1+KUN45
KUN37=1+KUN46
KUN38=1+KUN47
KUN39=1+KUN48
KUN40=1+KUN49
KUN41=1+KUN50
KUN42=1+KUN51
KUN43=1+KUN52
KUN44=1+KUN53
KUN45=1+KUN54
KUN46=1+KUN55
KUN47=1+KUN56
KUN48=1+KUN57
KUN49=1+KUN58
KUN50=1+KUN59
KUN51=1+KUN60
KUN52=1+KUN61
KUN53=1+KUN62
KUN54=1+KUN63
KUN55=1+KUN64
KUN56=1+KUN65
KUN57=1+KUN66
KUN58=1+KUN67
KUN59=1+KUN68
KUN60=1+KUN69
KUN61=1+KUN70
KUN62=1+KUN71
KUN63=1+KUN72
KUN64=1+KUN73
KUN65=1+KUN74
KUN66=1+KUN75
KUN67=1+KUN76
KUN68=1+KUN77
KUN69=1+KUN78
KUN70=1+KUN79
KUN71=1+KUN80
KUN72=1+KUN81
KUN73=1+KUN82
KUN74=1+KUN83
KUN75=1+KUN84
KUN76=1+KUN85
KUN77=1+KUN86
KUN78=1+KUN87
KUN79=1+KUN88
KUN80=1+KUN89
KUN81=1+KUN90
KUN82=1+KUN91
KUN83=1+KUN92
KUN84=1+KUN93
KUN85=1+KUN94
KUN86=1+KUN95
KUN87=1+KUN96
KUN88=1+KUN97
KUN89=1+KUN98
KUN90=1+KUN99
KUN91=1+KUN100
KUN92=1+KUN101
KUN93=1+KUN102
KUN94=1+KUN103
KUN95=1+KUN104
KUN96=1+KUN105
KUN97=1+KUN106
KUN98=1+KUN107
KUN99=1+KUN108
KUN100=1+KUN109
KUN101=1+KUN110
KUN102=1+KUN111
KUN103=1+KUN112
KUN104=1+KUN113
KUN105=1+KUN114
KUN106=1+KUN115
KUN107=1+KUN116
KUN108=1+KUN117
KUN109=1+KUN118
KUN110=1+KUN119
KUN111=1+KUN120
KUN112=1+KUN121
KUN113=1+KUN122
KUN114=1+KUN123
KUN115=1+KUN124
KUN116=1+KUN125
KUN117=1+KUN126
KUN118=1+KUN127
KUN119=1+KUN128
KUN120=1+KUN129
KUN121=1+KUN130
KUN122=1+KUN131
KUN123=1+KUN132
KUN124=1+KUN133
KUN125=1+KUN134
KUN126=1+KUN135
KUN127=1+KUN136
KUN128=1+KUN137
KUN129=1+KUN138
KUN130=1+KUN139
KUN131=1+KUN140
KUN132=1+KUN141
KUN133=1+KUN142
KUN134=1+KUN143
KUN135=1+KUN144
KUN136=1+KUN145
KUN137=1+KUN146
KUN138=1+KUN147
KUN139=1+KUN148
KUN140=1+KUN149
KUN141=1+KUN150
KUN142=1+KUN151
KUN143=1+KUN152
KUN144=1+KUN153
KUN145=1+KUN154
KUN146=1+KUN155
KUN147=1+KUN156
KUN148=1+KUN157
KUN149=1+KUN158
KUN150=1+KUN159
KUN151=1+KUN160
KUN152=1+KUN161
KUN153=1+KUN162
KUN154=1+KUN163
KUN155=1+KUN164
KUN156=1+KUN165
KUN157=1+KUN166
KUN158=1+KUN167
KUN159=1+KUN168
KUN160=1+KUN169
KUN161=1+KUN170
KUN162=1+KUN171
KUN163=1+KUN172
KUN164=1+KUN173
KUN165=1+KUN174
KUN166=1+KUN175
KUN167=1+KUN176
KUN168=1+KUN177
KUN169=1+KUN178
KUN170=1+KUN179
KUN171=1+KUN180
KUN172=1+KUN181
KUN173=1+KUN182
KUN174=1+KUN183
KUN175=1+KUN184
KUN176=1+KUN185
KUN177=1+KUN186
KUN178=1+KUN187
KUN179=1+KUN188
KUN180=1+KUN189
KUN181=1+KUN190
KUN182=1+KUN191
KUN183=1+KUN192
KUN184=1+KUN193
KUN185=1+KUN194
KUN186=1+KUN195
KUN187=1+KUN196
KUN188=1+KUN197
KUN189=1+KUN198
KUN190=1+KUN199
KUN191=1+KUN200
KUN192=1+KUN201
KUN193=1+KUN202
KUN194=1+KUN203
KUN195=1+KUN204
KUN196=1+KUN205
KUN197=1+KUN206
KUN198=1+KUN207
KUN199=1+KUN208
KUN200=1+KUN209
KUN201=1+KUN210
KUN202=1+KUN211
KUN203=1+KUN212
KUN204=1+KUN213
KUN205=1+KUN214
KUN206=1+KUN215
KUN207=1+KUN216
KUN208=1+KUN217
KUN209=1+KUN218
KUN210=1+KUN219
KUN211=1+KUN220
KUN212=1+KUN221
KUN213=1+KUN222
KUN214=1+KUN223
KUN215=1+KUN224
KUN216=1+KUN225
KUN217=1+KUN226
KUN218=1+KUN227
KUN219=1+KUN228
KUN220=1+KUN229
KUN221=1+KUN230
KUN222=1+KUN231
KUN223=1+KUN232
KUN224=1+KUN233
KUN225=1+KUN234
KUN226=1+KUN235
KUN227=1+KUN236
KUN228=1+KUN237
KUN229=1+KUN238
KUN230=1+KUN239
KUN231=1+KUN240
KUN232=1+KUN241
KUN233=1+KUN242
KUN234=1+KUN243
KUN235=1+KUN244
KUN236=1+KUN245
KUN237=1+KUN246
KUN238=1+KUN247
KUN239=1+KUN248
KUN240=1+KUN249
KUN241=1+KUN250
KUN242=1+KUN251
KUN243=1+KUN252
KUN244=1+KUN253
KUN245=1+KUN254
KUN246=1+KUN255
KUN247=1+KUN256
KUN248=1+KUN257
KUN249=1+KUN258
KUN250=1+KUN259
KUN251=1+KUN260
KUN252=1+KUN261
KUN253=1+KUN262
KUN254=1+KUN263
KUN255=1+KUN264
KUN256=1+KUN265
KUN257=1+KUN266
KUN258=1+KUN267
KUN259=1+KUN268
KUN260=1+KUN269
KUN261=1+KUN270
KUN262=1+KUN271
KUN263=1+KUN272
KUN264=1+KUN273
KUN265=1+KUN274
KUN266=1+KUN275
KUN267=1+KUN276
KUN268=1+KUN277
KUN269=1+KUN278
KUN270=1+KUN279
KUN271=1+KUN280
KUN272=1+KUN281
KUN273=1+KUN282
KUN274=1+KUN283
KUN275=1+KUN284
KUN276=1+KUN285
KUN277=1+KUN286
KUN278=1+KUN287
KUN279=1+KUN288
KUN280=1+KUN289
KUN281=1+KUN290
KUN282=1+KUN291
KUN283=1+KUN292
KUN284=1+KUN293
KUN285=1+KUN294
KUN286=1+KUN295
KUN287=1+KUN296
KUN288=1+KUN297
KUN289=1+KUN298
KUN290=1+KUN299
KUN291=1+KUN300
KUN292=1+KUN301
KUN293=1+KUN302
KUN294=1+KUN303
KUN295=1+KUN304
KUN296=1+KUN305
KUN297=1+KUN306
KUN298=1+KUN307
KUN299=1+KUN308
KUN300=1+KUN309
KUN301=1+KUN310
KUN302=1+KUN311
KUN303=1+KUN312
KUN304=1+KUN313
KUN305=1+KUN314
KUN306=1+KUN315
KUN3
```

```

      KUN7=KORT(KON32KONWS2)
      F=X*(1-18*(KON18KONWS8828EXP(-KUN7)/KON68818*(KON10KONWS88828
      1EXP(-KUN7)/KON68828*(KON118KONWS18878EXP(-KUN7)/KON1883
      1*(KON18KONWS2828EXP(-KUN72)/KON62)
      F=XSUM=F+FXSUM
40  CONTINUE
      CSEC=FXSUM
      GO TO 6
5  KUN=0
      KUN1=10./8KON
      KON2=(CUTOFF+10.)/(CUTOFF-10.)
      KON3=2./8(CUTOFF-10.)/EMAX
      KON4=(CUTOFF+10.-2.8U)/(CUTOFF-10.)
      KUN10=4.58KON
      KUN30=18./EMAX
      KUN40=1./222222-U/4.5
      KON1=KON
      KON31=1./8/EMAX
      KON41=1./22222-U/.45
      KON12=25.8KON8/(1-CUTLOW)82
      KON22=(1+CUTLOW)/(1-CUTLOW)
      KON32=2./8(1-CUTLOW)/EMAX
      KON42=KON22-2.8U/(1-CUTLOW)
      KON8=2.8U/(CUTOFF-10.)
      KON80=U/4.5
      KON81=U/.45
      KON82=2.8U/(1-CUTLOW)
      KON13=1-5.58KON8(CUTLOW-U)883/CUTLOW
      KON13=(CUTLOW+U)/(CUTLOW-U)
      KON133=KON13/(CUTLOW-U)/EMAX
      DO 50 I=1,N
      KON5=Y(I)+KON4
      KON7=8ORT(KON38KONWS)
      KON50=Y(I)+KON40
      KON60=Y(I)+1.222222
      KON70=8ORT(KON38KONWS0)
      KON51=Y(I)+KON41
      KON61=Y(I)+1.222222
      KON71=8ORT(KON318KONWS1)
      KON52=Y(I)+KON42
      KON42=Y(I)+KON22
      KON72=8ORT(KON328KONWS2)
      KON53=Y(I)+1.
      KON63=Y(I)+KON23
      KON73=8ORT(KON338KONWS3)
      F=X*(1-18*(KON18KONWS8828EXP(-KUN7)/KON6883
      1*(KON108KONWS8828EXP(-KUN70)/KON68828*(KON118KONWS18828EXP(-KUN71)
      1/KON61883*(KON128KONWS2828EXP(-KUN72)/KON62)
      1*(KON138KONWS3828EXP(-KUN73)
      F=XSUM=F+FXSUM
50  CONTINUE
      CSEC=FXSUM
      GO TO 6
5  KON1=10./8KON
      KON2=(CUTOFF+10.)/(CUTOFF-10.)
      KON3=2./8(CUTOFF-10.)/EMAX
      KON4=(CUTOFF+10.-2.8U)/(CUTOFF-10.)
      KUN10=4.58KON
      KUN30=18./EMAX
      KUN40=1./22222-U/4.5
      KON1=KON
      KON31=1./8/EMAX
      KON41=1./22222-U/.45
      KON12=25.8KON8/(1-CUTLOW)82
      KON22=(1+CUTLOW)/(1-CUTLOW)
      KON32=2./8(1-CUTLOW)/EMAX
      KON42=KON22-2.8U/(1-CUTLOW)
      KON8=2.8U/(CUTOFF-10.)
      KON80=U/4.5
      KON81=U/.45
      KON82=2.8U/(1-CUTLOW)
      KON83=2.8U/CUTLOW
      KON13=12.58KON8(CUTLOW882
      KON133=2./CUTLOW/EMAX
      KON43=1.-2.8U/CUTLOW
      F=XSUM=0.
      DO 40 I=1,N
      KON5=Y(I)+KON4
      KON4=Y(I)+KON2
      KON7=8ORT(KON38KONWS)
      KON50=Y(I)+KON40
      KON60=Y(I)+1.222222
      KON70=8ORT(KON38KONWS0)
      KON51=Y(I)+KON41
      KON61=Y(I)+1.222222
      KON71=8ORT(KON318KONWS1)
      KON52=Y(I)+KON42
      KON42=Y(I)+KON22
      KON72=8ORT(KON328KONWS2)
      KON53=Y(I)+KON43
      KON73=8ORT(KON338KONWS3)
      KON63=Y(I)+1.
      IF (KONCHN.EQ.1)F=X*(1-18*(KON18KONWS8828EXP(-KUN7)/KON6883
      1*(KON108KONWS8828EXP(-KUN70)/KON68828*(KON118KONWS18828EXP(-KUN71)
      1/KON61883*(KON128KONWS2828EXP(-KUN72)/KON62)
      1*(KON138KONWS3828EXP(-KUN73)
      IF (KONCHN.EQ.1)F=X*(1-18*(KON18KONWS8828EXP(-KUN7)/KON6883
      1*(KON108KONWS8828EXP(-KUN70)/KON68828*(KON118KONWS18828EXP(-KUN71)
      1/KON61883*(KON128KONWS2828EXP(-KUN72)/KON62)
      1*(KON138KONWS3828EXP(-KUN73)
      IF (KONCHN.EQ.1)F=X*(1-18*(KON18KONWS8828EXP(-KUN7)/KON6883
      1*(KON108KONWS8828EXP(-KUN70)/KON68828*(KON118KONWS18828EXP(-KUN71)
      1/KON61883*(KON128KONWS2828EXP(-KUN72)/KON62)
      1*(KON138KONWS3828EXP(-KUN73)
      F=XSUM=F+FXSUM
60  CONTINUE
      IF (KONCHN.EQ.2)F=XSUM=.63661988FXSUM
      CSEC=FXSUM
      IF (U.L.T.0.)CALL RETARD(U,CSEC,TSEC)
      CSEC=CSEC/A
      B RETURN
      END

```

Appendix B: Listing of threshold temperatures program

```

PROGRAM THRESHOLD TEMPERATURES

```

```

PROGRAM TEMP

```

```

THIS SUBROUTINE COMPUTES THE CRITICAL TEMPERATURES FOR SPATIAL
MATERIALS INCLUDING ANGLE DEPENDENCE OF TFIELD.

```

```

DOUBLE PRECISION DZ
COMMON/CTRL/ENX(12),DNX(12),BSA(12),BSB(12),BSC(12),Z(12)
COMMON EM,DN,KEM,A,B,C,FZ,IFLG,ICNN,DINTG(10)
DIMENSION TC(12),DUMMY(12),IDUM(44),DDTS(12)
EQUIVALENCE (DUMMY,IDUM)
DATA EPS/1.0E-5/,DDTS/0.05/1.0/
DATA NUMS/17/,NUME/29/,IFLGE/3/,NP1/17/,NP2/29/
DATA LU/13/,ITRAC/20/,ISECT/0/

DO 500 N=NUMS,NUME
  WRITE(1,800) N
  800 FORMAT(5X, 'N=', I2)
  ENX(N)=0
  DNX(N)=0
  BSA(N)=0
  BSB(N)=0
  BSC(N)=0
  Z(N)=0
  500 NPART=NP1,NP2
  PAC=NPART/2
  DTS=DDTS(NPART)
  WRITE(1,804) NPART
  804 FORMAT(10X, 'NPART=', I2)
  DO 500 IFLG=1,IFLGE
    IF (IFLGE.EQ.2) GO TO 90
    A=0
    B=0
    C=0
    IF (NPART.EQ.1) TS=EM
    IF (NPART.EQ.2) TS=EM/2.0
    GO TO 10
  90 A=BSA(N)
    B=BSB(N)
    C=BSC(N)
    IF (IFLGE.EQ.2) GO TO 4
    DZ=DOUBLE(Z(N))
    BETAB=SNGL(7.37000D28*(0.5087500))
    FZ=(EXP(BETAB)-BETAB-1.0)/BETAB*282.0
    WRITE(1,201) Z(N),BETAB
    201 FORMAT(10X, 'Z=', F5.1, 'X', 'BETAB=', E15.7)
    GO TO 8
  6 FZ=1.0
  8 TS=TC(N,NPART)
  IF (NPART.EQ.1.AND.TS.LE.1.0E-4) TS=EM
  IF (NPART.EQ.2.AND.TS.LE.1.0E-4) TS=EM/2.0
  DT=DTS
  NPATH=1
  20 FL=RCUR(TS)
  30 TSS=TS+DT*FAC
  IF (TSS.LE.1.0E-4) GO TO 500
  FN=RCUR(TSS)
  WRITE(1,600) TS,FL,FN,DT
  600 FORMAT(4F15.7)
  IF (NPART.EQ.1.AND.TS.LE.1.0E-4) GO TO 500
  IF (NPART.EQ.2.AND.TS.LE.1.0E-4) GO TO 500
  IF (FL.FN) 50=50.40
  40 TS=TS+DT*FAC
  FL=FN
  GO TO (30,50),NPATH
  50 DT=DT/2.0
  NPATH=2
  IF (DT.EPS) 40=40.30
  60 NPAT=NPART+(IFLG-1)*2
  TC(N,NPAT)=TS
  WRITE(1,200) IFLG,TS
  200 FORMAT(5X, 'IFLG=', I1, 'X', 'TC=', F8.4)
  500 CONTINUE
  CALL EXEC(2,LU,ENX+64,ITRAC,ISECT)
  CALL EXEC(2,LU,DNX+64,ITRAC,ISECT+1)
  CALL EXEC(2,LU,BSA+64,ITRAC,ISECT+2)
  CALL EXEC(2,LU,BSB+64,ITRAC,ISECT+3)
  CALL EXEC(2,LU,BSC+64,ITRAC,ISECT+4)
  CALL EXEC(2,LU,Z+64,ITRAC,ISECT+5)
  DO 300 J=1+6
    ISECT=ISECT+J+5
    NO 310 I=1+32
    DUMMY(I)=TC(I,J)
  310 CONTINUE
  CALL EXEC(2,LU,DUMMY+64,ITRAC,ISECT)
  300 CONTINUE
  IDUM(1)=NUMS
  IDUM(2)=NUME
  CALL EXEC(2,LU,IDUM+64,ITRAC,ISECT+12)
  STOP
  END

```

```

BLOCK DATA
COMMON/CTRL/ENX(12),DNX(12),BSA(12),BSB(12),BSC(12),Z(12)
DATA ENX/0.8,0.3,0.3,0.42,0.33,0.35,0.3,0.4,0.3,0.15/
A0.25,0.8,0.25,0.4,0.8,0.35,0.36,0.33,0.39,0.85,0.15/
B0.41,0.15,0.15,0.15,0.72,0.48,0.59,0.3/
DATA DNX/1.45,0.97,2.6,2.3,3.46,0.73,2.2,5.0,3.0,2.1/
A1.8,1.4,0.92,4.0,1.0,2.55,2.39,2.35,1.52,6.38,2.1/
B2.05,2.1,2.1,2.1,1.03,1.49,1.86,1.0/
DATA Z/79.0,13.0,10.0,10.0,10.0,10.0,4.0,29.0,29.0,8.0,5.3/
A5.3,24.4,12.0,10.0,47.0,15.3,16.2,16.9,15.3,10.0,5.0/
B10.0,5.0,5.0,5.0,70.1,42.0,63.4,6.0/
DATA BSA/0.4802,0.1548,0.1238,0.1238,0.1238,0.06,0.3134/
A0.3134,0.09,0.07,0.07,0.275,0.146,0.1238,0.39,0.183,0.192/
B0.2,0.183,0.1238,0.06,0.1238,0.06,0.06,0.06,0.454,0.373/
C0.438,0.08/
DATA BSB/0.3544,0.0303,0.0172,0.0172,0.0172,0.0,0.0692/
A0.0692,0.0,0.0,0.0,0.04,0.025,0.0172,0.289,0.037,0.04/
B0.042,0.037,0.0172,0.0,0.0172,0.0,0.0,0.0,0.138,0.276/
C0.325,0.0/
DATA BSC/0.6103,0.3431,0.3435,0.3435,0.3435,0.0,0.6207/
A0.6207,0.0,0.0,0.0,0.56,0.34,0.3435,0.632,0.382,0.599/
B0.41,0.382,0.3435,0.0,0.3435,0.0,0.0,0.0,0.612,0.617/
C0.613,0.0/
END

```

```

SUBROUTINE INTG(EINTG)
COMMON EM,DN,KEM,A,B,C,FZ,IFLG,ICNN,DINTG(10)
DATA ERROR/1.0E-4/,EFCUT/1.0E-7/
ITER=0
DO 100 I=1,200
  CUTOFF=1
  EFCUT=EINTG(CUTOFF)
  IF (EFCUT.LE.EFCUT) GO TO 110
  100 CONTINUE
  WRITE(1,909)
  909 FORMAT('INSUFFICIENT # OF DOMAINS')
  110 DE=CUTOFF/10.0
  SUM1=0
  SUM2=0
  F=0

```

```

  SUM2=SUM2+INTG(E)
  E=E+DE
  IF (E.GT.1.0) CUTOFF=E*0.4
  4 SUM1=0.0
  E=DE/2.0
  10 SUM4=SUM4+INTG(E)
  E=E+DE
  IF (E.GT.1.0) CUTOFF=E*0.4
  20 EINTG=DE/6.0*(SUM1+2.0*SUM2+4.0*SUM4)
  ITER=ITER+1
  IF (ITER.EQ.1) GO TO 60
  DINTG(1)=EINTG
  GO TO 40
  60 DINTG(4)=DINTG(5)
  DINTG(5)=EINTG
  40 IF (ABS(EINTG-SUM4)/EINTG-ERROR) 50=50+10
  50 SUM2=SUM2+SUM4
  SUM4=EINTG
  IF (DE.GT.1.0)
    GO TO 4
  50 DINTG(1)=CUTOFF
  DINTG(2)=EFCUT
  DINTG(3)=DE
  IF (ITER.EQ.1) RETURN
  EINTG=(16.0*DINTG(5)-DINTG(4))/15.0
  RETURN
  END

FUNCTION RCUR(T)
COMMON EM,DN,KEM,A,B,C,FZ,IFLG,ICNN,DINTG(10)
KEM=EM/7
CALL INTG(EINTG)
RCUR=KEM*2*EXP(2.0)*DN*EINTG*(A-B/(1.0+C*BT)*2.0)*FZ-1.0
RETURN
END

FUNCTION FINTG(E)
COMMON EM,DN,KEM,A,B,C,FZ,IFLG,ICNN,DINTG(10)
P1=2.0*SQRT(E)-RENE
IF (IFLG.EQ.3) GO TO 10
IF (P1.GT.-20.0) GO TO 5
FINTG=0.0
RETURN
5 FINTG=E*2*EXP(P1)
RETURN
10 X=0.2755*(ALOG(E)-1.658)
Y=0.0228/(X*SQRT(X*240.0228))
BETAS=EXP(Y)
P2=P1+BETAS
IF (P1.GT.-20.0) GO TO 15
FINTG=(E/BETAS)*2*EXP(P2)*2.0
RETURN
15 FINTG=(E/BETAS)*2*EXP(P2)-EXP(P1)*(BETAS+1.0)*2.0
RETURN
END
END

```



```

C
C GENERATE INITIAL POTENTIAL MAPS
CALL EXEC(BNAME1)
INAM=0
C
C 1101 FORMAT (10X, NUMBER OF ITERATIONS= 1)
C
C COMPUTE NEW INDICES FOR CURRENT COLLECTION IF SYMMETRY
NN=N
IF (ISYM.EQ.2) NN=N/2
NN=NN-1
C
C BUILD POTENTIAL OF SECTORS FROM POTENTIAL AT GRID POINTS
C
L=0
DO 4000 I=1,NSECT
  P=PERSEC(I)
  N=L+N
  N1=L+1
  DO 4001 NJ=N1,N2
    J=SECIND(NJ)
    PSECTR(I)=PHE(J)
  4001 CONTINUE
  L=L+N
  4000 CONTINUE
C
C *****
C START ITERATION PROCESS
C
ITER=0
4010 NTOUR=0
C
C
C 4199 CONTINUE
C GENERATE GRID AND CALL POISON SOLVER
CALL EXEC(BNAME2)
9002 INAM=0
7211 FORMAT (10X, IPE12.5)
CALL EXEC(BNAME3)
7006 INAM=0
NTOUR=NTOUR+1
ITER=ITER+1
4100 FORMAT (17 SECTOR PSECTR CSECTR ELEC CUR)
C
C COMPUTE CURRENT COLLECTION FOR ALL SECTORS AND OBJECTIVE FUNCTION
C
C COMPUTE CURRENT COLLECTION DUE TO PRIMARY PARTICLES
C AND SECONDARY EMERGING PARTICLES
C BYPASS COMPUTATIONS IF FLAGS IDTL AND JDTL CONCERNING FINE DETAIL
C STRUCTURE ARE NOT SET TO ONE
L=0
IS=0
4200 IS=IS+1
IF (IDTL(IS).NE.1) GO TO 4200
N=PERSEC(IS)
N2=L+N
NJ=L
4201 NJ=NJ+1
J=SECIND(NJ)
JP=J
IF (JDTL(J).NE.1) GO TO 4201
IF (ISYM.EQ.0) GO TO 4210
IF (J.LE.NN) GO TO 4210
C IF THERE IS A SYMMETRY-SAVE COMPUTATIONS
C
CION(J)=CION(N-J+1)
CELEC(J)=CELEC(N-J+1)
CSEC(J)=CSEC(N-J+1)
CBSCAT(J)=CBSCAT(N-J+1)
SECPRI(J)=SECPRI(N-J+1)
GO TO 4202
C
4210 CONTINUE
CALL EXEC(BNAME3)
9003 INAM=0
CALL EXEC(BNAME13)
9013 INAM=13=0
4202 IF (NJ.LT.N2) GO TO 4201
L=L+N
IF (IS.LT.NSECT) GO TO 4200
C
C COMPUTE CURRENT COLLECTION DUE TO SECONDARY ARRIVING PARTICLES
C
L=0
IS=0
4250 IS=IS+1
IF (IDTL(IS).NE.1) GO TO 4250
N=PERSEC(IS)
N2=L+N
NJ=L
4251 NJ=NJ+1
J=SECIND(NJ)
JP=J
IF (JDTL(J).NE.1) GO TO 4251
IF (ISYM.EQ.0) GO TO 4260
IF (J.LE.NN) GO TO 4260
C IF THERE IS SYMMETRY-SAVE COMPUTATIONS
CPHOTO(J)=CPHOTO(N-J+1)
CSEC(J)=CSEC(N-J+1)
CBSCAT(J)=CBSCAT(N-J+1)
SECPRI(J)=SECPRI(N-J+1)
GO TO 4252
C
4260 CONTINUE
C COMPUTE SECONDARY CURRENTS
IF (IFAU1(5).EQ.1) CALL EXEC(BNAME4)
9004 INAM=0
IF (IFAU1(7).EQ.1) CALL EXEC(BNAME14)
9014 INAM=14=0
IF (IFAU1(8).EQ.1) CALL EXEC(BNAME15)
9015 INAM=15=0
IF (IFAU1(14).EQ.1) CALL EXEC(BNAME16)
9016 INAM=16=0
4252 IF (NJ.LT.N2) GO TO 4251
L=L+N
IF (IS.LT.NSECT) GO TO 4250
C
C COMPUTE TOTAL CURRENT AND SAVE TOTAL ELECTRON CURRENT FOR SECTOR
IS=0
WRITE(LUMP,4101)
4101 FORMAT (17 J POTENTIAL TOTCUR IONCUR ELEC CUR
1 PHOTCUR ENIPHOTCUR SECONDEUR EISECUR BSCATCUR
2 EMIASCAT ELE IND EMI ELEC IND)
WRITE(LUMP,1101) ITER
4270 IS=IS+1

```

```

C
C 1101 FORMAT (10X, NUMBER OF ITERATIONS= 1)
C
C COMPUTE NEW INDICES FOR CURRENT COLLECTION IF SYMMETRY
NN=N
IF (ISYM.EQ.2) NN=N/2
NN=NN-1
C
C BUILD POTENTIAL OF SECTORS FROM POTENTIAL AT GRID POINTS
C
L=0
DO 4000 I=1,NSECT
  P=PERSEC(I)
  N=L+N
  N1=L+1
  DO 4001 NJ=N1,N2
    J=SECIND(NJ)
    PSECTR(I)=PHE(J)
  4001 CONTINUE
  L=L+N
  4000 CONTINUE
C
C *****
C START ITERATION PROCESS
C
ITER=0
4010 NTOUR=0
C
C
C 4199 CONTINUE
C GENERATE GRID AND CALL POISON SOLVER
CALL EXEC(BNAME2)
9002 INAM=0
7211 FORMAT (10X, IPE12.5)
CALL EXEC(BNAME3)
7006 INAM=0
NTOUR=NTOUR+1
ITER=ITER+1
4100 FORMAT (17 SECTOR PSECTR CSECTR ELEC CUR)
C
C COMPUTE CURRENT COLLECTION FOR ALL SECTORS AND OBJECTIVE FUNCTION
C
C COMPUTE CURRENT COLLECTION DUE TO PRIMARY PARTICLES
C AND SECONDARY EMERGING PARTICLES
C BYPASS COMPUTATIONS IF FLAGS IDTL AND JDTL CONCERNING FINE DETAIL
C STRUCTURE ARE NOT SET TO ONE
L=0
IS=0
4200 IS=IS+1
IF (IDTL(IS).NE.1) GO TO 4200
N=PERSEC(IS)
N2=L+N
NJ=L
4201 NJ=NJ+1
J=SECIND(NJ)
JP=J
IF (JDTL(J).NE.1) GO TO 4201
IF (ISYM.EQ.0) GO TO 4210
IF (J.LE.NN) GO TO 4210
C IF THERE IS A SYMMETRY-SAVE COMPUTATIONS
C
CION(J)=CION(N-J+1)
CELEC(J)=CELEC(N-J+1)
CSEC(J)=CSEC(N-J+1)
CBSCAT(J)=CBSCAT(N-J+1)
SECPRI(J)=SECPRI(N-J+1)
GO TO 4202
C
4210 CONTINUE
CALL EXEC(BNAME3)
9003 INAM=0
CALL EXEC(BNAME13)
9013 INAM=13=0
4202 IF (NJ.LT.N2) GO TO 4201
L=L+N
IF (IS.LT.NSECT) GO TO 4200
C
C COMPUTE CURRENT COLLECTION DUE TO SECONDARY ARRIVING PARTICLES
C
L=0
IS=0
4250 IS=IS+1
IF (IDTL(IS).NE.1) GO TO 4250
N=PERSEC(IS)
N2=L+N
NJ=L
4251 NJ=NJ+1
J=SECIND(NJ)
JP=J
IF (JDTL(J).NE.1) GO TO 4251
IF (ISYM.EQ.0) GO TO 4260
IF (J.LE.NN) GO TO 4260
C IF THERE IS SYMMETRY-SAVE COMPUTATIONS
CPHOTO(J)=CPHOTO(N-J+1)
CSEC(J)=CSEC(N-J+1)
CBSCAT(J)=CBSCAT(N-J+1)
SECPRI(J)=SECPRI(N-J+1)
GO TO 4252
C
4260 CONTINUE
C COMPUTE SECONDARY CURRENTS
IF (IFAU1(5).EQ.1) CALL EXEC(BNAME4)
9004 INAM=0
IF (IFAU1(7).EQ.1) CALL EXEC(BNAME14)
9014 INAM=14=0
IF (IFAU1(8).EQ.1) CALL EXEC(BNAME15)
9015 INAM=15=0
IF (IFAU1(14).EQ.1) CALL EXEC(BNAME16)
9016 INAM=16=0
4252 IF (NJ.LT.N2) GO TO 4251
L=L+N
IF (IS.LT.NSECT) GO TO 4250
C
C COMPUTE TOTAL CURRENT AND SAVE TOTAL ELECTRON CURRENT FOR SECTOR
IS=0
WRITE(LUMP,4101)
4101 FORMAT (17 J POTENTIAL TOTCUR IONCUR ELEC CUR
1 PHOTCUR ENIPHOTCUR SECONDEUR EISECUR BSCATCUR
2 EMIASCAT ELE IND EMI ELEC IND)
WRITE(LUMP,1101) ITER
4270 IS=IS+1

```



```

      READ(LUM9,20) (IPANEL(I),I=1,NSECT)
      DO 100 I=1,NSECT
      IF(IPANEL(I))
      READ(LUM9,20) (PERFAN(I),I=1,NPOINT)
      WRITE(LUM9,20) (IPANEL(I),PERFAN(I),I=1,NPOINT)
100 CONTINUE
901 FORMAT(1X,SECTOR NUMBER 8,12,8 NUMBER OF PANELS 8,12,
1 8 NR OF GRID POINTS PER PANEL 8,414)
      READ(LUM9,20) (PANIND(I),I=1,NPOINT)
      IF(IPANEL(1).EQ.0) RETURN
      READ(LUM9,20) (IDTL(I),I=1,NSECT)
      WRITE(LUM9,20) (IDTL(I),I=1,NSECT)
900 FORMAT(1X,SECTORS WHERE WE WANT A FINE STRUCTURE(1614))
C
      READ(LUM9,20) (JDTL(J),J=1,NPOINT)
      WRITE(LUM9,20) (JDTL(J),J=1,NPOINT)
902 FORMAT(1X,8 GRID POINTS WHERE WE WANT A FINE STRUCTURE(1616))
      RETURN
99 WRITE(LUM9,30)
10 FORMAT(8,ERROR IN SECTOR DATA(,))
      WRITE(LUM9,35) NPOINT
15 FORMAT(8,NUMBER OF INDICES 8,13,8 IS NOT EQUAL
170 NUMBER OF POINTS 8,13)
C
      STOP
98 WRITE(LUM9,30)
      WRITE(LUM9,31) I,J,SECIND(J)
31 FORMAT(8,INDEX(8,13,8) 8,13,8 8,13)
C
      STOP
97 WRITE(LUM9,30)
      WRITE(LUM9,32) I,SECIND(I)
32 FORMAT(8,INDEX(8,13,8) 8,13,8 IS LESS THAN UNITY)
C
      STOP
96 WRITE(LUM9,30)
      WRITE(LUM9,33) I,SECIND(I),NPOINT
33 FORMAT(8,INDEX(8,13,8) 8,13,8 IS GREATER THAN
170 NUMBER OF POINTS 8,13)
C
      STOP
      END
      SUBROUTINE FINGERD
C
C PURPOSE:
C-----
C TO RESET ALL ARRAYS FOR A FINE DETAIL STRUCTURE OF SURFACE
C IN ORDER TO RESPECT GEOMETRY,INTERVALS ARE DIVIDED BY THREE.
C
      INTEGER PERSEC,SECIND,PERPAN,PANIND
      COMMON PSAVE(144,10),CSAVE(144,10),PSECTR(144),CSECTR(144),
1DELEC(20),DELMAX(144),ENAX(144),ETA(20),BSCAT(144),
2BSCAT2(144),BSCAT3(144),PHO(20,40),
1ANG(40),CPHORI(144),SUMANG,ANGD,BOUNDL(20,40),BOUNDI(20,40),
2ANGL(20,40),VIE(20,40),ICHECK(20,40),RATIO(13),IROOT(144),
3IFAU(14),JLOCAL(144),ICOM(144),
1VI(20),EV(8),NLEV,NFINES,ILEV,TIMIN(20),TIMAX(20),VINUM(20),
2A(144),B(144),C(144),BB(144),BM(144),TM(144),DM(144),
3EM(144),TWOCOS(700),
1IFLG,NPOINT,N,ICOM,IS/M,IPDIS,NSECT,NPEROD,NPEROD,IDINY,
2GAMMA,DVUX(70,48),DVUY(70,48),Y(144),DELTAK,DELTAY,
3YS(64,48),XS(64),XSS(70),
1VARIABLE(4),T,DELT,SBOUND,NDIR,POT,M,J1,RPI,RP12,RPINAF,SOTPI,
2SAY,TEMP1,TEMP2,DEME1,DEME2,DEMI1,DEMI2,TEMP11,TEMP12,
3TEMP,LUM3,LUM4,LUM5,LUM6,LUM7,LUM8,LUM9,LUM10,
1IDTL(144),JDTL(144),PERSEC(144),SECIND(144),IPANEL(144),
2PERPAN(144,4),PANIND(144),
1ICION(144),CELEC(144),CSECT(144),CSECI(144),CPHOTO(144),
2CPHOT1(144),CBSCAT(144),CBSCA1(144),SECPRI(144),SECPRI(144),
3PMI(144),CGUM(144),
1KASE,JOM,DPI,NANG,RAD,PBOUND,OMEGA,ALPHA,SO,JP,IS,ECS,
2XPU12(20),EFTVI(20),IERROR,TETMIN,TETMAX,BETA1,BETA2,JLESS,
3L2,CARRIV,CPH,XI,CSECEL,CSECI,CS,CB,CSI,CBI
      EQUIVALENCE (IROOT(1),IDUMY(1))
C
C=====
C
      IOLD=NSECT
      JOLD=NPOINT
      NPOINT=3*JOLD
      ANG=ANGD/3.0
      SUMANG=SUMANG/3.0
C
C FIND NEW FLAGS OF CORRESPONDING GRID POINTS
CFIRST SAVE OLD VALUES
C
      DO 100 J=1,JOLD
      IF(JDTL(J).EQ.0) GO TO 102
      IDUMY(J83-2)=1
      IDUMY(J83-1)=1
      IDUMY(J83)=1
      GO TO 100
102 IDUMY(J83-2)=0
      IDUMY(J83-1)=1
      IDUMY(J83)=0
100 CONTINUE
C
C
C
C NOW RESET ARRAY
      DO 110 J=1,NPOINT
      110 JDTL(J)=IDUMY(J)
C
C
C FIND NEW INDICES OF CORRESPONDING GRID POINTS
      L=0
      II=0
      DO 112 I=1,IOLD
      K=PERSEC(I)
      N2=L+K
      N1=L+1
      DO 113 N=1,N2
      J=PERIND(N)
      IF(ICOM(I).EQ.0.AND.ISYM.EQ.2) GO TO 1100
      IDUMY(NJ83-2)=J83-2
      IDUMY(NJ83-1)=J83-1
      IDUMY(NJ83)=J83
      II=II+3
      GO TO 113
1100 II=II+6
      IDUMY(II-5)=J83-2
      IDUMY(II-2)=PERIND(N)+1
C
      IDUMY(II-1)=J83-1
      IDUMY(II)=J83-1
      IDUMY(II+1)=J83-1
      IDUMY(II+2)=J83-1
      IDUMY(II+3)=J83-1
      IDUMY(II+4)=J83-1
      IDUMY(II+5)=J83-1
      IDUMY(II+6)=J83-1
      IDUMY(II+7)=J83-1
      IDUMY(II+8)=J83-1
      IDUMY(II+9)=J83-1
      IDUMY(II+10)=J83-1
      IDUMY(II+11)=J83-1
      IDUMY(II+12)=J83-1
      IDUMY(II+13)=J83-1
      IDUMY(II+14)=J83-1
      IDUMY(II+15)=J83-1
      IDUMY(II+16)=J83-1
      IDUMY(II+17)=J83-1
      IDUMY(II+18)=J83-1
      IDUMY(II+19)=J83-1
      IDUMY(II+20)=J83-1
      IDUMY(II+21)=J83-1
      IDUMY(II+22)=J83-1
      IDUMY(II+23)=J83-1
      IDUMY(II+24)=J83-1
      IDUMY(II+25)=J83-1
      IDUMY(II+26)=J83-1
      IDUMY(II+27)=J83-1
      IDUMY(II+28)=J83-1
      IDUMY(II+29)=J83-1
      IDUMY(II+30)=J83-1
      IDUMY(II+31)=J83-1
      IDUMY(II+32)=J83-1
      IDUMY(II+33)=J83-1
      IDUMY(II+34)=J83-1
      IDUMY(II+35)=J83-1
      IDUMY(II+36)=J83-1
      IDUMY(II+37)=J83-1
      IDUMY(II+38)=J83-1
      IDUMY(II+39)=J83-1
      IDUMY(II+40)=J83-1
      IDUMY(II+41)=J83-1
      IDUMY(II+42)=J83-1
      IDUMY(II+43)=J83-1
      IDUMY(II+44)=J83-1
      IDUMY(II+45)=J83-1
      IDUMY(II+46)=J83-1
      IDUMY(II+47)=J83-1
      IDUMY(II+48)=J83-1
      IDUMY(II+49)=J83-1
      IDUMY(II+50)=J83-1
      IDUMY(II+51)=J83-1
      IDUMY(II+52)=J83-1
      IDUMY(II+53)=J83-1
      IDUMY(II+54)=J83-1
      IDUMY(II+55)=J83-1
      IDUMY(II+56)=J83-1
      IDUMY(II+57)=J83-1
      IDUMY(II+58)=J83-1
      IDUMY(II+59)=J83-1
      IDUMY(II+60)=J83-1
      IDUMY(II+61)=J83-1
      IDUMY(II+62)=J83-1
      IDUMY(II+63)=J83-1
      IDUMY(II+64)=J83-1
      IDUMY(II+65)=J83-1
      IDUMY(II+66)=J83-1
      IDUMY(II+67)=J83-1
      IDUMY(II+68)=J83-1
      IDUMY(II+69)=J83-1
      IDUMY(II+70)=J83-1
      IDUMY(II+71)=J83-1
      IDUMY(II+72)=J83-1
      IDUMY(II+73)=J83-1
      IDUMY(II+74)=J83-1
      IDUMY(II+75)=J83-1
      IDUMY(II+76)=J83-1
      IDUMY(II+77)=J83-1
      IDUMY(II+78)=J83-1
      IDUMY(II+79)=J83-1
      IDUMY(II+80)=J83-1
      IDUMY(II+81)=J83-1
      IDUMY(II+82)=J83-1
      IDUMY(II+83)=J83-1
      IDUMY(II+84)=J83-1
      IDUMY(II+85)=J83-1
      IDUMY(II+86)=J83-1
      IDUMY(II+87)=J83-1
      IDUMY(II+88)=J83-1
      IDUMY(II+89)=J83-1
      IDUMY(II+90)=J83-1
      IDUMY(II+91)=J83-1
      IDUMY(II+92)=J83-1
      IDUMY(II+93)=J83-1
      IDUMY(II+94)=J83-1
      IDUMY(II+95)=J83-1
      IDUMY(II+96)=J83-1
      IDUMY(II+97)=J83-1
      IDUMY(II+98)=J83-1
      IDUMY(II+99)=J83-1
      IDUMY(II+100)=J83-1
      IDUMY(II+101)=J83-1
      IDUMY(II+102)=J83-1
      IDUMY(II+103)=J83-1
      IDUMY(II+104)=J83-1
      IDUMY(II+105)=J83-1
      IDUMY(II+106)=J83-1
      IDUMY(II+107)=J83-1
      IDUMY(II+108)=J83-1
      IDUMY(II+109)=J83-1
      IDUMY(II+110)=J83-1
      IDUMY(II+111)=J83-1
      IDUMY(II+112)=J83-1
      IDUMY(II+113)=J83-1
      IDUMY(II+114)=J83-1
      IDUMY(II+115)=J83-1
      IDUMY(II+116)=J83-1
      IDUMY(II+117)=J83-1
      IDUMY(II+118)=J83-1
      IDUMY(II+119)=J83-1
      IDUMY(II+120)=J83-1
      IDUMY(II+121)=J83-1
      IDUMY(II+122)=J83-1
      IDUMY(II+123)=J83-1
      IDUMY(II+124)=J83-1
      IDUMY(II+125)=J83-1
      IDUMY(II+126)=J83-1
      IDUMY(II+127)=J83-1
      IDUMY(II+128)=J83-1
      IDUMY(II+129)=J83-1
      IDUMY(II+130)=J83-1
      IDUMY(II+131)=J83-1
      IDUMY(II+132)=J83-1
      IDUMY(II+133)=J83-1
      IDUMY(II+134)=J83-1
      IDUMY(II+135)=J83-1
      IDUMY(II+136)=J83-1
      IDUMY(II+137)=J83-1
      IDUMY(II+138)=J83-1
      IDUMY(II+139)=J83-1
      IDUMY(II+140)=J83-1
      IDUMY(II+141)=J83-1
      IDUMY(II+142)=J83-1
      IDUMY(II+143)=J83-1
      IDUMY(II+144)=J83-1
      IDUMY(II+145)=J83-1
      IDUMY(II+146)=J83-1
      IDUMY(II+147)=J83-1
      IDUMY(II+148)=J83-1
      IDUMY(II+149)=J83-1
      IDUMY(II+150)=J83-1
      IDUMY(II+151)=J83-1
      IDUMY(II+152)=J83-1
      IDUMY(II+153)=J83-1
      IDUMY(II+154)=J83-1
      IDUMY(II+155)=J83-1
      IDUMY(II+156)=J83-1
      IDUMY(II+157)=J83-1
      IDUMY(II+158)=J83-1
      IDUMY(II+159)=J83-1
      IDUMY(II+160)=J83-1
      IDUMY(II+161)=J83-1
      IDUMY(II+162)=J83-1
      IDUMY(II+163)=J83-1
      IDUMY(II+164)=J83-1
      IDUMY(II+165)=J83-1
      IDUMY(II+166)=J83-1
      IDUMY(II+167)=J83-1
      IDUMY(II+168)=J83-1
      IDUMY(II+169)=J83-1
      IDUMY(II+170)=J83-1
      IDUMY(II+171)=J83-1
      IDUMY(II+172)=J83-1
      IDUMY(II+173)=J83-1
      IDUMY(II+174)=J83-1
      IDUMY(II+175)=J83-1
      IDUMY(II+176)=J83-1
      IDUMY(II+177)=J83-1
      IDUMY(II+178)=J83-1
      IDUMY(II+179)=J83-1
      IDUMY(II+180)=J83-1
      IDUMY(II+181)=J83-1
      IDUMY(II+182)=J83-1
      IDUMY(II+183)=J83-1
      IDUMY(II+184)=J83-1
      IDUMY(II+185)=J83-1
      IDUMY(II+186)=J83-1
      IDUMY(II+187)=J83-1
      IDUMY(II+188)=J83-1
      IDUMY(II+189)=J83-1
      IDUMY(II+190)=J83-1
      IDUMY(II+191)=J83-1
      IDUMY(II+192)=J83-1
      IDUMY(II+193)=J83-1
      IDUMY(II+194)=J83-1
      IDUMY(II+195)=J83-1
      IDUMY(II+196)=J83-1
      IDUMY(II+197)=J83-1
      IDUMY(II+198)=J83-1
      IDUMY(II+199)=J83-1
      IDUMY(II+200)=J83-1
      IDUMY(II+201)=J83-1
      IDUMY(II+202)=J83-1
      IDUMY(II+203)=J83-1
      IDUMY(II+204)=J83-1
      IDUMY(II+205)=J83-1
      IDUMY(II+206)=J83-1
      IDUMY(II+207)=J83-1
      IDUMY(II+208)=J83-1
      IDUMY(II+209)=J83-1
      IDUMY(II+210)=J83-1
      IDUMY(II+211)=J83-1
      IDUMY(II+212)=J83-1
      IDUMY(II+213)=J83-1
      IDUMY(II+214)=J83-1
      IDUMY(II+215)=J83-1
      IDUMY(II+216)=J83-1
      IDUMY(II+217)=J83-1
      IDUMY(II+218)=J83-1
      IDUMY(II+219)=J83-1
      IDUMY(II+220)=J83-1
      IDUMY(II+221)=J83-1
      IDUMY(II+222)=J83-1
      IDUMY(II+223)=J83-1
      IDUMY(II+224)=J83-1
      IDUMY(II+225)=J83-1
      IDUMY(II+226)=J83-1
      IDUMY(II+227)=J83-1
      IDUMY(II+228)=J83-1
      IDUMY(II+229)=J83-1
      IDUMY(II+230)=J83-1
      IDUMY(II+231)=J83-1
      IDUMY(II+232)=J83-1
      IDUMY(II+233)=J83-1
      IDUMY(II+234)=J83-1
      IDUMY(II+235)=J83-1
      IDUMY(II+236)=J83-1
      IDUMY(II+237)=J83-1
      IDUMY(II+238)=J83-1
      IDUMY(II+239)=J83-1
      IDUMY(II+240)=J83-1
      IDUMY(II+241)=J83-1
      IDUMY(II+242)=J83-1
      IDUMY(II+243)=J83-1
      IDUMY(II+244)=J83-1
      IDUMY(II+245)=J83-1
      IDUMY(II+246)=J83-1
      IDUMY(II+247)=J83-1
      IDUMY(II+248)=J83-1
      IDUMY(II+249)=J83-1
      IDUMY(II+250)=J83-1
      IDUMY(II+251)=J83-1
      IDUMY(II+252)=J83-1
      IDUMY(II+253)=J83-1
      IDUMY(II+254)=J83-1
      IDUMY(II+255)=J83-1
      IDUMY(II+256)=J83-1
      IDUMY(II+257)=J83-1
      IDUMY(II+258)=J83-1
      IDUMY(II+259)=J83-1
      IDUMY(II+260)=J83-1
      IDUMY(II+261)=J83-1
      IDUMY(II+262)=J83-1
      IDUMY(II+263)=J83-1
      IDUMY(II+264)=J83-1
      IDUMY(II+265)=J83-1
      IDUMY(II+266)=J83-1
      IDUMY(II+267)=J83-1
      IDUMY(II+268)=J83-1
      IDUMY(II+269)=J83-1
      IDUMY(II+270)=J83-1
      IDUMY(II+271)=J83-1
      IDUMY(II+272)=J83-1
      IDUMY(II+273)=J83-1
      IDUMY(II+274)=J83-1
      IDUMY(II+275)=J83-1
      IDUMY(II+276)=J83-1
      IDUMY(II+277)=J83-1
      IDUMY(II+278)=J83-1
      IDUMY(II+279)=J83-1
      IDUMY(II+280)=J83-1
      IDUMY(II+281)=J83-1
      IDUMY(II+282)=J83-1
      IDUMY(II+283)=J83-1
      IDUMY(II+284)=J83-1
      IDUMY(II+285)=J83-1
      IDUMY(II+286)=J83-1
      IDUMY(II+287)=J83-1
      IDUMY(II+288)=J83-1
      IDUMY(II+289)=J83-1
      IDUMY(II+290)=J83-1
      IDUMY(II+291)=J83-1
      IDUMY(II+292)=J83-1
      IDUMY(II+293)=J83-1
      IDUMY(II+294)=J83-1
      IDUMY(II+295)=J83-1
      IDUMY(II+296)=J83-1
      IDUMY(II+297)=J83-1
      IDUMY(II+298)=J83-1
      IDUMY(II+299)=J83-1
      IDUMY(II+300)=J83-1
      IDUMY(II+301)=J83-1
      IDUMY(II+302)=J83-1
      IDUMY(II+303)=J83-1
      IDUMY(II+304)=J83-1
      IDUMY(II+305)=J83-1
      IDUMY(II+306)=J83-1
      IDUMY(II+307)=J83-1
      IDUMY(II+308)=J83-1
      IDUMY(II+309)=J83-1
      IDUMY(II+310)=J83-1
      IDUMY(II+311)=J83-1
      IDUMY(II+312)=J83-1
      IDUMY(II+313)=J83-1
      IDUMY(II+314)=J83-1
      IDUMY(II+315)=J83-1
      IDUMY(II+316)=J83-1
      IDUMY(II+317)=J83-1
      IDUMY(II+318)=J83-1
      IDUMY(II+319)=J83-1
      IDUMY(II+320)=J83-1
      IDUMY(II+321)=J83-1
      IDUMY(II+322)=J83-1
      IDUMY(II+323)=J83-1
      IDUMY(II+324)=J83-1
      IDUMY(II+325)=J83-1
      IDUMY(II+326)=J83-1
      IDUMY(II+327)=J83-1
      IDUMY(II+328)=J83-1
      IDUMY(II+329)=J83-1
      IDUMY(II+330)=J83-1
      IDUMY(II+331)=J83-1
      IDUMY(II+332)=J83-1
      IDUMY(II+333)=J83-1
      IDUMY(II+334)=J83-1
      IDUMY(II+335)=J83-1
      IDUMY(II+336)=J83-1
      IDUMY(II+337)=J83-1
      IDUMY(II+338)=J83-1
      IDUMY(II+339)=J83-1
      IDUMY(II+340)=J83-1
      IDUMY(II+341)=J83-1
      IDUMY(II+342)=J83-1
      IDUMY(II+343)=J83-1
      IDUMY(II+344)=J83-1
      IDUMY(II+345)=J83-1
      IDUMY(II+346)=J83-1
      IDUMY(II+347)=J83-1
      IDUMY(II+348)=J83-1
      IDUMY(II+349)=J83-1
      IDUMY(II+350)=J83-1
      IDUMY(II+351)=J83-1
      IDUMY(II+352)=J83-1
      IDUMY(II+353)=J83-1
      IDUMY(II+354)=J83-1
      IDUMY(II+355)=J83-1
      IDUMY(II+356)=J83-1
      IDUMY(II+357)=J83-1
      IDUMY(II+358)=J83-1
      IDUMY(II+359)=J83-1
      IDUMY(II+360)=J83-1
      IDUMY(II+361)=J83-1
      IDUMY(II+362)=J83-1
      IDUMY(II+363)=J83-1
      IDUMY(II+364)=J83-1
      IDUMY(II+365)=J83-1
      IDUMY(II+366)=J83-1
      IDUMY(II+367)=J83-1
      IDUMY(II+368)=J83-1
      IDUMY(II+369)=J83-1
      IDUMY(II+370)=J83-1
      IDUMY(II+371)=J83-1
      IDUMY(II+372)=J83-1
      IDUMY(II+373)=J83-1
      IDUMY(II+374)=J83-1
      IDUMY(II+375)=J83-1
      IDUMY(II+376)=J83-1
      IDUMY(II+377)=J83-1
      IDUMY(II+378)=J83-1
      IDUMY(II+379)=J83-1
      IDUMY(II+380)=J83-1
      IDUMY(II+381)=J83-1
      IDUMY(II+382)=J83-1
      IDUMY(II+383)=J83-1
      IDUMY(II+384)=J83-1
      IDUMY(II+385)=J83-1
      IDUMY(II+386)=J83-1
      IDUMY(II+387)=J83-1
      IDUMY(II+388)=J83-1
      IDUMY(II+389)=J83-1
      IDUMY(II+390)=J83-1
      IDUMY(II+391)=J83-1
      IDUMY(II+392)=J83-1
      IDUMY(II+393)=J83-1
      IDUMY(II+394)=J83-1
      IDUMY(II+395)=J83-1
      IDUMY(II+396)=J83-1
      IDUMY(II+397)=J83-1
      IDUMY(II+398)=J83-1
      IDUMY(II+399)=J83-1
      IDUMY(II+400)=J83-1
      IDUMY(II+401)=J83-1
      IDUMY(II+402)=J83-1
      IDUMY(II+403)=J83-1
      IDUMY(II+404)=J83-1
      IDUMY(II+405)=J83-1
      IDUMY(II+406)=J83-1
      IDUMY(II+407)=J83-1
      IDUMY(II+408)=J83-1
      IDUMY(II+409)=J83-1
      IDUMY(II+410)=J83-1
      IDUMY(II+411)=J83-1
      IDUMY(II+412)=J83-1
      IDUMY(II+413)=J83-1
      IDUMY(II+414)=J83-1
      IDUMY(II+415)=J83-1
      IDUMY(II+416)=J83-1
      IDUMY(II+417)=J83-1
      IDUMY(II+418)=J83-1
      IDUMY(II+419)=J83-1
      IDUMY(II+420)=J83-1
      IDUMY(II+421)=J83-1
      IDUMY(II+422)=J83-1
      IDUMY(II+423)=J83-1
      IDUMY(II+424)=J83-1
      IDUMY(II+425)=J83-1
      IDUMY(II+426)=J83-1
      IDUMY(II+427)=J83-1
      IDUMY(II+428)=J83-1
      IDUMY(II+429)=J83-1
      IDUMY(II+430)=J83-1
      IDUMY(II+431)=J83-1
      IDUMY(II+432)=J83-1
      IDUMY(II+433)=J83-1
      IDUMY(II+434)=J83-1
      IDUMY(II+435)=J83-1
      IDUMY(II+436)=J83-1
      IDUMY(II+437)=J83-1
      IDUMY(II+438)=J83-1
      IDUMY(II+439)=J83-1
      IDUMY(II+440)=J83-1
      IDUMY(II+441)=J83-1
      IDUMY(II+442)=J83-1
      IDUMY(II+443)=J83-1
      IDUMY(II+444)=J83-1
      IDUMY(II+445)=J83-1
      IDUMY(II+446)=J83-1
      IDUMY(II+447)=J83-1
      IDUMY(II+448)=J83-1
      IDUMY(II+449)=J83-1
      IDUMY(II+450)=J83-1
      IDUMY(II+451)=J83-1
      IDUMY(II+452)=J83-1
      IDUMY(II+453)=J83-1
      IDUMY(II+454)=J83-1
      IDUMY(II+455)=J83-1
      IDUMY(II+456)=J83-1
      IDUMY(II+457)=J83-1
      IDUMY(II+458)=J83-1
      IDUMY(II+459)=J83-1
      IDUMY(II+460)=J83-1
      IDUMY(II+461)=J83-1
      IDUMY(II+462)=J83-1
      IDUMY(II+463)=J83-1
      IDUMY(II+464)=J83-1
      IDUMY(II+465)=J83-1
      IDUMY(II+466)=J83-1
      IDUMY(II+467)=J83-1
      IDUMY(II+468)=J83-1
      IDUMY(II+469)=J83-1
      IDUMY(II+470)=J83-1
      IDUMY(II+471)=J83-1
      IDUMY(II+472)=J83-1
      IDUMY(II+473)=J83-1
      IDUMY(II+474)=J83-1
      IDUMY(II+475)=J83-1
      IDUMY(II+476)=J83-1
      IDUMY(II+477)=J83-1
      IDUMY(II+478)=J83-1
      IDUMY(II+479)=J83-1
      IDUMY(II+480)=J83-1
      IDUMY(II+481)=J83-1
      IDUMY(II+482)=J83-1
      IDUMY(II+483)=J83-1
      IDUMY(II+484)=J83-1
      IDUMY(II+485)=J83-1
      IDUMY(II+486)=J83-1
      IDUMY(II+487)=J83-1
      IDUMY(II+488)=J83-1
      IDUMY(II+489)=J83-1
      IDUMY(II+490)=J83-1
      IDUMY(II+491)=J83-1
      IDUMY(II+492)=J83-1
      IDUMY(II+493)=J83-1
      IDUMY(II+494)=J83-1
      IDUMY(II+495)=J83-1
      IDUMY(II+496)=J83-1
      IDUMY(II+497)=J83-1
      IDUMY(II+498)=J83-1
      IDUMY(II+499)=J83-1
      IDUMY(II+500)=J83-1
      IDUMY(II+501)=J83-1
      IDUMY(II+502)=J83-1
      IDUMY(II+503)=J83-1
      IDUMY(II+504)=J83-1
      IDUMY(II+505)=J83-1
      IDUMY(II+506)=J83-1
      IDUMY(II+507)=J83-1
      IDUMY(II+508)=J83-1
      IDUMY(II+509)=J83-1
      IDUMY(II+510)=J83-1
      IDUMY(II+511)=J83-1
      IDUMY(II+512)=J83-1
      IDUMY(II+513)=J83-1
      IDUMY(II+514)=J83-1
      IDUMY(II+515)=J83-1
      IDUMY(II+516)=J83-1
      IDUMY(II+517)=J83-1
      IDUMY(II+518)=J83-1
      IDUMY(II+519)=J83-1
      IDUMY(II+520)=J83-1
      IDUMY(II+521)=J83-1
      IDUMY(II+522)=J83-1
      IDUMY(II+523)=J83-1
      IDUMY(II+524)=J83-1
      IDUMY(II+525)=J83-1
      IDUMY(II+526)=J83-1
      IDUMY(II+527)=J83-1
      IDUMY(II+528)=J83-1
      IDUMY(II+529)=J83-1
      IDUMY(II+530)=J83-1
      IDUMY(II+531)=J83-1
      IDUMY(II+532)=J83-1
      IDUMY(II+533)=J83-1
      IDUMY(II+534)=J83-1
      IDUMY(II+535)=J83-1
      IDUMY(II+536)=J83-1
      IDUMY(II+537)=J83-1
      IDUMY(II+538)=J83-1
      IDUMY(II+539)=J83-1
      IDUMY(II+540)=J83-1
      IDUMY(II+541)=J83-1
      IDUMY(II+542)=J83-1
      IDUMY(II+543)=J83-1
      IDUMY(II+544)=J83-1
      IDUMY(II+545)=J83-1
      IDUMY(II+546)=J83-1
      IDUMY(II+547)=J83-1
      IDUMY(II+548)=J83-1
      IDUMY(II+549)=J83-1
      IDUMY(II+550)=J83-1
      IDUMY(II+551)=J83-1
      IDUMY(II+552)=J83-1
      IDUMY(II+553)=J83-1
      IDUMY(II+554)=J83-1
      IDUMY(II+555)=J83-1
      IDUMY(II+556)=J83-1
      IDUMY(II+557)=J83-1
      IDUMY(II+558)=J83-1
      IDUMY(II+559)=J83-1
      IDUMY(II+560)=J83-1
      IDUMY(II+561)=J83-1
      IDUMY(II+562)=J83-1
      IDUMY(II+563)=J83-1
      IDUMY(II+564)=J83-1
      IDUMY(II+565)=J83-1
      IDUMY(II+566)=J83-1
      IDUMY(II+567)=J83-1
      IDUMY(II+568)=J83-1
      IDUMY(II+569)=J83-1
      IDUMY(II+570)=J83-1
      IDUMY(II+571)=J83-1
      IDUMY(II+572)=J83-1
      IDUMY(II+573)=J83-1
      IDUMY(II+574)=J83-1
      IDUMY(II+575)=J83-1
      IDUMY(II+576)=J83-1
      IDUMY(II+577)=J83-1
      IDUMY(II+578)=J83-1
      IDUMY(II+579)=J83-1
      IDUMY(II+580)=J83-1
      IDUMY(II+581)=J83-1
      IDUMY(II+582)=J83-1
      IDUMY(II+583)=J83-1
      IDUMY(II+584)=J83-1
      IDUMY(II+585)=J83-1
      IDUMY(II+586)=J83-1
      IDUMY(II+587)=J83-1
      IDUMY(II+588)=J83-1
      IDUMY(II+589)=J83-1
      IDUMY(II+590)=J83-1
      IDUMY(II+591)=J83-1
      IDUMY(II+592)=J83-1
      IDUMY(II+593)=J83-1
      IDUMY(II+594)=J83-1
      IDUMY(II+595)=J83-1
      IDUMY(II+596)=J83-1
      IDUMY(II+597)=J83-1
      IDUMY(II+598)=J83-1
      IDUMY(II+599)=J83-1
      IDUMY(II+600)=J83-1
      IDUMY(II+601)=J83-1
      IDUMY(II+602)=J83-1
      IDUMY(II+603)=J83-1
      IDUMY(II+604)=J83-1
      IDUMY(II+605)=J83-1
      IDUMY(II+606)=J83-1
      IDUMY(II+607)=J83-1
      IDUMY(II+608)=J83-1
      IDUMY(II+609)=J83-1
      IDUMY(II+610)=J83-1
      IDUMY(II+611)=J83-1
      IDUMY(II+612)=J83-1
      IDUMY(II+613)=J83-1
      IDUMY(II+614)=J83-1
      IDUMY(II+615)=J83-1
      IDUMY(II+616)=J83-1
      IDUMY(II+617)=J83-1
      IDUMY(II+618)=J83-1
      IDUMY(II+619)=J83-1
      IDUMY(II+620)=J83-1
```

```

IFANEL(I)=IDUMMY(I)
IP=IFANEL(I)
DO 295 I=1,IP
  PERPAN(I,L)=IDUMY(L)
295 CONTINUE
C
C CONDUCTIVITY OF NEW SECTORS
I1=0
DO 300 I=1,IOLD
  IF (ICOM(I),EQ,1) I1=I+1
  IF (ICOM(I),EQ,1) IDUMY(I1)=1
  IF (ICOM(I),EQ,1) GO TO 300
  I1=I+3
  IDUMY(I1-2)=0
  IDUMY(I1-1)=0
  IDUMY(I1)=0
300 CONTINUE
C
C NOW REORGANIZE ARRAYS
DO 310 I=1,MSECT
  ICOM(I)=IDUMY(I)
310 CONTINUE
C
C
C
C NOW RESET SURFACE PROPERTIES
C FIRST SAVE OLD VALUES
DO 450 J=1,JOLD
  IDUMY(J)=JLOCAL(J)
450 CONTINUE
C
DO 460 J=1,JOLD
  JLOCAL(J83-2)=IDUMY(J)
  JLOCAL(J83-1)=IDUMY(J)
  JLOCAL(J83)=IDUMY(J)
460 CONTINUE
C
C FIND NEW SURFACE PROPERTIES
C
DO 470 J=1,NPOINT
  REMIND LUN3
480 READ(LUN3,500) JFIRST
500 FORMAT(12)
  IF(JLOCAL(J),NE,JFIRST) GO TO 480
  READ(LUN3,301) DELMAX(J),EMAX(J),CPHOMX(J)
301 FORMAT(3X,3F10,3)
  READ(LUN3,301) BSCAT1(J),BSCAT2(J),BSCAT3(J)
  READ(LUN3,301) DELP(J),EXPP(J)
470 CONTINUE
C
WRITE(LUN9,900)
900 FORMAT(//10X,'THE FINAL DETAIL STRUCTURE IS NOW SET UP',10X,40
  1('B'))
C
C WRITE NEW VALUES
C
WRITE(LUN9,901) (JDTL(J),J=1,NPOINT)
C
WRITE(LUN9,902) (SECIND(J),J=1,NPOINT)
C
WRITE(LUN9,902) (PERSEC(I),I=1,MSECT)
C
WRITE(LUN9,902) (IDTL(I),I=1,MSECT)
C
WRITE(LUN9,902) (PANIND(J),J=1,NPOINT)
C
WRITE(LUN9,902) (ICOM(I),I=1,MSECT)
C
WRITE(LUN9,902)
902 FORMAT(//)
901 FORMAT(32I2)
DO 903 I=1,MSECT
  IP=IFANEL(I)
  WRITE(LUN9,902) (PERPAN(I,L),L=1,IP)
903 CONTINUE
C
C
C RETURN
END
SUBROUTINE INTPOL(DUMMY)
C *****
C PURPOSE: TO INTERPOLATE VARIABLES FOR FINEGRID STRUCTURE
C *****
C
C
C DIMENSION DUMMY(1)
C DIMENSION XX(144),YY(144),D(144)
C INTEGER PERSEC,SECIND,PERPAN,PANIND
C COMMON PBAVE(144,10),CSAVE(144,10),PBSECT(144),CSECT(144),
C 1DELET(20),DELMAX(144),EMAX(144),ETA(20),BSCAT3(144),
C 2BSCAT2(144),BSCAT3(144),PHO(20,40),
C 1AND(40),CPHOMX(144),BUNMD,AMD,BOUNDL(20,40),BOUNDI(20,40),
C 2ANGUL(20,40),VIL(20,40),ICHECK(20,40),RATIO(13),IROOT(144),
C 3IFAUT(14),JLOCAL(144),ICOM(144),
C 1VI(20),EV(B),MLEV,HTIME,ILEV,TIMIN(20),TIMAX(20),VINUM(20),
C 2A(144),B(144),C(144),BP(144),BU(144),TU(144),DU(144),
C 3EM(144),TMOCD(700)
C 1IFLG,NPOINT,N,IGCON,ISYH,IPDIS,MSECT,NPEROD,MPEROD,IDIY,
C 20ANNA,DVUX(70,48),DVDT(70,48),Y(144),DELTAX,DELTAY,
C 3YS(44,48),XS(44),XS(70),
C 1VARDLE(4),T,DELT,BOUNDL,NDIR,POT,N,J1,RP1,RP2,RPINAF,BOTPI,
C 2SAY,TEMP1,TEMP2,DEME1,DEME2,DEM11,DEM12,TEMP11,TEMP12,
C 3TEMPR,LUN3,LUN4,LUN5,LUN6,LUN7,LUN8,LUN9,LUN10,
C 1IDTL(144),JDTL(144),PERSEC(144),SECIND(144),IFANEL(144),
C 2PERPAN(144,4),PANIND(144),
C 1ICOM(144),CELEC(144),CSEC(144),CSEC(144),CPHOTD(144),
C 2CPHOT1(144),CBSCAT(144),CBSCAT(144),SECPRN(144),SECPR(144),
C 3PHI(144),COUN(144),
C 1RASE,JOML,BPHI,HAND,RAD,PBOUND,OMEGA,ALPHA,SO,JP,IS,ECS,
C 2EXPIV(20),EFPV(20),TERROR,TETIN,TETRA,BETA1,BETA2,JLESS,
C 3LC,CANIV,CPH,XI,CSECEL,CSECEL,CS,CP,CS1,C01
C EQUIVALENCE (XX(1),A(1)),(YY(1),B(1)),(D(1),DU(1))
C
C IF SECTORS ARE CONDUCTORS, INTERPOLATION IS DONE PER PANEL
C IF SECTORS ARE INSULATORS, INTERPOLATION IS DONE BETWEEN ADJACENT SECT
C
C DESCRIPTION OF VARIABLES
C JSTART=INDEX WHERE TO FIND FIRST GRID POINT OF SECTOR
C XX AND YY: TEMPORARY STORAGE FOR INTERPOLATION
C B,C,D: COEFFICIENT FOR SPLINE
C
JSTART=1
I=0
C
C LOOP OVER SECTORS
1000 I=I+1
C IF (I,GT,MSECT) RETURN
C DO DIFFERENT SECTORS IF INSULATORS OR CONDUCTORS
IF (ICOM(I),EQ,0) GO TO 10
C
C NOW DO INTERPOLATION FOR CONDUCTORS, FIND NO OF PANELS
C
IP=IFANEL(I)
C FIND NO OF GRID POINTS PER PANEL AND ACCUMULATE FUNCTION VALUES
C WHEN JDTL(I)=1
C
DO 2 I1=1,IP
  JP=PERPAN(I,I1)
  JEND=JP+JSTART-1
C
C NOW ACCUMULATE DATA
J1=0
DO 3 J1=JSTART,JEND
  I1=J1+1
  J1=PANIND(J1)
  IF (JDTL(J1),EQ,1) XX(J1)=DELTAY(J1-1)
  IF (JDTL(J1),EQ,1) YY(J1)=DUMMY(J1)
3 CONTINUE
C
C NOW CALL INTERPOLATION ROUTINE
C IF J1=JP, NO INTERPOLATION NEEDED FOR THAT PANEL
IF (J1,EQ,JP) GO TO 8
C
CALL SPLINE (J1,XX,YY,B,C,D)
C
DO 7 J1=JSTART,JEND
  J1=PANIND(J1)
  IF (JDTL(J1),EQ,0) DUMMY(J1)=SPIDER(J1,DELTAY(J1-1),XX,Y,B,C,D)
7 CONTINUE
C
8 JSTART=JEND+1
2 CONTINUE
GO TO 1000
C
C INTERPOLATION FOR INSULATORS
C
10 CONTINUE
C DO INTERPOLATION OF EXTRAPOLATION BETWEEN KNOWN SECTORS,
C TAKING INTO ACCOUNT THE SURFACE PROPERTIES OF SECTORS
C
IF (IDTL(I),EQ,1) JSTART=JSTART+PERSEC(I)
IF (IDTL(I),EQ,1) GO TO 1000
C
C SEE IF WE CAN DO AN INTERPOLATION
J1=JSTART
I1=1
11 I1=I1-1
IF (I1,LE,0) GO TO 20
J1=J1-PERSEC(I1)
IF (IDTL(I1),EQ,0) GO TO 11
I2=1
J2=JSTART
12 I2=I2+1
IF (I2,GT,MSECT) GO TO 30
J2=J2+PERSEC(I2-1)
IF (IDTL(I2),EQ,0) GO TO 12
C
C FUNCTION IS NOW KNOWN AT SECTORS I1 AND I2
C NOW CHECK IF SURFACE PROPERTIES ARE IDENTICAL AT I1 AND I2
IF (ICOM(I1),NE,0) GO TO 20
IF (ICOM(I2),NE,0) GO TO 30
J1=SECIND(I1)
J2=SECIND(I2)
IF (JLOCAL(J1),NE,JLOCAL(J2)) GO TO 20
IF (JLOCAL(J2),NE,JLOCAL(J1)) GO TO 30
40 DUMMY(J1)=(DUMMY(J2)-DUMMY(J1))/(Y(J2)-Y(J1))*Y(J1)+Y(J1)
1+DUMMY(J1)
IF (ISYH,EQ,2) DUMMY(NPOINT-JJ+1)=DUMMY(JJ)
JSTART=JSTART+PERSEC(I)
GO TO 1000
C
C DO EXTRAPOLATION FROM RIGHT OF I
20 I1=1
J1=JSTART
21 I1=I1+1
J1=J1+PERSEC(I1-1)
IF (ICOM(I1),EQ,0) GO TO 21
I2=11
J2=J1
22 I2=I2+1
J2=J2+PERSEC(I2-1)
IF (ICOM(I2),EQ,0) GO TO 22
GO TO 40
C
C DO EXTRAPOLATION FROM LEFT OF I
30 I1=1
J1=JSTART
31 I1=I1-1
J1=J1-PERSEC(I1)
IF (ICOM(I1),EQ,0) GO TO 31
I2=11
J2=J1
32 I2=I2-1
J2=J2-PERSEC(I2)
IF (ICOM(I2),EQ,0) GO TO 32
GO TO 40
C
C
C END
SUBROUTINE SPLINE(N,X,Y,B,C,D)
C REF: MALCOLM AND HOLLER
C DIMENSION X(N),Y(N),B(N),C(N),D(N)
C
C THE COEFFICIENTS B(I),C(I),AND D(I), I=1,2,...,N ARE COMPUTED
C FOR A CUBIC INTERPOLATING SPLINE
C
S(X)=Y(I)*B(I)*X(X-X(I))+C(I)*X(X-X(I))*X(X-X(I))+D(I)*X(X-X(I))
C
C FOR X(I),LE,X(I+1)
C
C INPUT
C N=NUMBER OF DATA POINTS
C X=ABSCISSA
C Y=ORDINATES
C
C OUTPUT
C B,C,D=ARRAYS OF SPLINE COEFFICIENTS
C
NRI=N-1
IF (N,LT,2) STOP
IF (N,LT,3) GO TO 50
C
C SET UP TRIDIAGONAL SYSTEM

```

```

C R=DIAGONAL, D=OFF DIAGONAL, C=RIGHT HAND SIDE
C

```

```

      D(1)=X(1)-X(1)
      C(1)=D(1)/D(1)
      DO 10 I=2,NM1
      D(I)=X(I)-X(I)
      C(I)=2.0*(D(I)-D(I-1))/D(I)
      C(I)=C(I)+C(I-1)
      C(I)=C(I)-C(I)
      10 CONTINUE
C END CONDITIONS, THIRD DERIVATIVES AT X(1) AND X(N)
C ARE OBTAINED FROM DIVIDED DIFFERENCES
      B(1)=D(1)
      B(N)=D(N-1)
      C(1)=0.
      C(N)=0.
      IF(N.EQ.3) GO TO 15
      C(1)=C(1)/(X(4)-X(2))-C(2)/(X(3)-X(1))
      C(N)=C(N-1)/(X(N)-X(N-2))-C(N-2)/(X(N-1)-X(N-3))
      C(1)=C(1)+D(1)*B(2)/(X(4)-X(1))
      C(N)=C(N)+D(N-1)*B(N-2)/(X(N)-X(N-3))

```

```

C FORWARD ELIMINATION
C

```

```

      15 DO 20 I=2,N
      I=I-1
      B(I)=B(I)-B(I-1)
      C(I)=C(I)-B(I-1)
      20 CONTINUE

```

```

C BACK SUBSTITUTION
C

```

```

      C(N)=C(N)/B(N)
      DO 30 I=N-1,NM1
      I=N-I
      C(I)=C(I)-B(I)*C(I+1)/B(I)
      30 CONTINUE

```

```

C COMPUTE POLYNOMIAL COEFFICIENTS
C

```

```

      B(N)=Y(N)-Y(NM1)/D(NM1)+D(NM1)*B(C(NM1)+2.0*B(C(N))
      DO 40 I=1,NM1
      B(I)=Y(I+1)-Y(I)/D(I)-D(I)*B(C(I)+2.0*B(C(I))
      D(I)=C(I+1)-C(I)/D(I)
      C(I)=3.0*B(C(I))
      40 CONTINUE
      C(N)=3.0*B(C(N))
      D(N)=D(N-1)
      RETURN

```

```

C
      50 B(1)=Y(2)-Y(1)/X(2)-X(1)
      C(1)=0.
      D(1)=0.
      B(2)=B(1)
      C(2)=0.
      D(2)=0.
      RETURN
      END
      FUNCTION SPIDER (N,U,X,Y,B,C,D)
      DIMENSION X(N),Y(N),B(N),C(N),D(N)

```

```

C THIS SUBROUTINE EVALUATE THE CUBIC SPLINE FUNCTION AT POINT U-USING
C HORNOR'S RULE
C IF U IS NOT IN THE PROPER INTERVAL, A BINARY SEARCH IS PERFORMED.
      10 I=1
      20 K=(I+J)/2
      IF(U.LT.X(K)) J=K
      IF(U.GE.X(K)) I=K
      IF(J.GT.I+1) GO TO 20

```

```

C EVALUATE SPLINE
C

```

```

      30 DX=U-X(I)
      SPIDER=Y(I)+DX*B(I)+DX*B(C(I))+DX*B(D(I))
      RETURN
      END
      SUBROUTINE GENRAT

```

PACKAGE 2

```

      GENERATE DIMENSIONLESS PARAMETERS
      GENERATE VELOCITY LEVELS
      GENERATE GRID
      GENERATE POTENTIAL DERIVATIVES

```

```

C PURPOSE
C TO GENERATE SCALING FACTORS WITH RESPECT TO TEMP REF AND DEN11.
C EXTERNALS
C NONE

```

```

C
      IMPLICIT REAL*8 (A-H,O-Z)
      INTEGER PERSEC,SECON,PERPAN,PANIND
      COMMON PSAVE(144,10),CSAVE(144,10),PBCTR(144),CBCTR(144),
      1DELEE(20),DELMAX(144),ENAX(144),ETA(20),BSCAT(144),
      2BSCAT2(144),BSCAT3(144),PHO(20,40),
      1ANG(40),CPHONX(144),SUNANG,ANGD,BOUND(20,40),BOUND1(20,40),
      2ANGL(20,40),V(1)(20,40),ICHECK(20,40),RATIO(13),IROOT(144),
      3IFAULT(144),JLOCAL(144),ICON(144),
      1VI(20),EV(8),M.EV,NTINES,ILEV,TIMIN(20),TIMAX(20),VIMIN(20),
      2A(144),B(144),C(144),B(144),BM(144),TM(144),DM(144),
      3EM(144),TMOCD(700),
      1IFLG,NPOINT,M,IGCON,ISYN,IPDIS,MSECT,NPEROD,NPEROD,IDIRY,
      2GAMMA,DUDX(70,40),DUDY(70,40),Y(144),DELTA,DELTA,
      3YS(44,40),XS(44,40),XSS(70),
      1VARIABLE(4),T,DELTA,SBOUND,NDIN,POT,M,J1,RP1,RP12,RP1MF,SGTP1,
      2SAY,TEMP1,TEMP2,DEME1,DEME2,DEMI1,DEMI2,TEMP11,TEMP12,
      3TEMPR,LUN3,LUN4,LUN5,LUN6,LUN7,LUN8,LUN9,LUN10,
      1PANEL(144,4),PANIND(144),PERSEC(144),SECON(144),IPANEL(144),
      2PANEL(144,4),PANIND(144),
      3PANEL(144,4),PANIND(144),
      4PANEL(144,4),PANIND(144),
      5PANEL(144,4),PANIND(144),
      6PANEL(144,4),PANIND(144),
      7PANEL(144,4),PANIND(144),
      8PANEL(144,4),PANIND(144),
      9PANEL(144,4),PANIND(144),
      10PANEL(144,4),PANIND(144),
      11PANEL(144,4),PANIND(144),
      12PANEL(144,4),PANIND(144),
      13PANEL(144,4),PANIND(144),
      14PANEL(144,4),PANIND(144),
      15PANEL(144,4),PANIND(144),
      16PANEL(144,4),PANIND(144),
      17PANEL(144,4),PANIND(144),
      18PANEL(144,4),PANIND(144),
      19PANEL(144,4),PANIND(144),
      20PANEL(144,4),PANIND(144),
      21PANEL(144,4),PANIND(144),
      22PANEL(144,4),PANIND(144),
      23PANEL(144,4),PANIND(144),
      24PANEL(144,4),PANIND(144),
      25PANEL(144,4),PANIND(144),
      26PANEL(144,4),PANIND(144),
      27PANEL(144,4),PANIND(144),
      28PANEL(144,4),PANIND(144),
      29PANEL(144,4),PANIND(144),
      30PANEL(144,4),PANIND(144),
      31PANEL(144,4),PANIND(144),
      32PANEL(144,4),PANIND(144),
      33PANEL(144,4),PANIND(144),
      34PANEL(144,4),PANIND(144),
      35PANEL(144,4),PANIND(144),
      36PANEL(144,4),PANIND(144),
      37PANEL(144,4),PANIND(144),
      38PANEL(144,4),PANIND(144),
      39PANEL(144,4),PANIND(144),
      40PANEL(144,4),PANIND(144),
      41PANEL(144,4),PANIND(144),
      42PANEL(144,4),PANIND(144),
      43PANEL(144,4),PANIND(144),
      44PANEL(144,4),PANIND(144),
      45PANEL(144,4),PANIND(144),
      46PANEL(144,4),PANIND(144),
      47PANEL(144,4),PANIND(144),
      48PANEL(144,4),PANIND(144),
      49PANEL(144,4),PANIND(144),
      50PANEL(144,4),PANIND(144),
      51PANEL(144,4),PANIND(144),
      52PANEL(144,4),PANIND(144),
      53PANEL(144,4),PANIND(144),
      54PANEL(144,4),PANIND(144),
      55PANEL(144,4),PANIND(144),
      56PANEL(144,4),PANIND(144),
      57PANEL(144,4),PANIND(144),
      58PANEL(144,4),PANIND(144),
      59PANEL(144,4),PANIND(144),
      60PANEL(144,4),PANIND(144),
      61PANEL(144,4),PANIND(144),
      62PANEL(144,4),PANIND(144),
      63PANEL(144,4),PANIND(144),
      64PANEL(144,4),PANIND(144),
      65PANEL(144,4),PANIND(144),
      66PANEL(144,4),PANIND(144),
      67PANEL(144,4),PANIND(144),
      68PANEL(144,4),PANIND(144),
      69PANEL(144,4),PANIND(144),
      70PANEL(144,4),PANIND(144),
      71PANEL(144,4),PANIND(144),
      72PANEL(144,4),PANIND(144),
      73PANEL(144,4),PANIND(144),
      74PANEL(144,4),PANIND(144),
      75PANEL(144,4),PANIND(144),
      76PANEL(144,4),PANIND(144),
      77PANEL(144,4),PANIND(144),
      78PANEL(144,4),PANIND(144),
      79PANEL(144,4),PANIND(144),
      80PANEL(144,4),PANIND(144),
      81PANEL(144,4),PANIND(144),
      82PANEL(144,4),PANIND(144),
      83PANEL(144,4),PANIND(144),
      84PANEL(144,4),PANIND(144),
      85PANEL(144,4),PANIND(144),
      86PANEL(144,4),PANIND(144),
      87PANEL(144,4),PANIND(144),
      88PANEL(144,4),PANIND(144),
      89PANEL(144,4),PANIND(144),
      90PANEL(144,4),PANIND(144),
      91PANEL(144,4),PANIND(144),
      92PANEL(144,4),PANIND(144),
      93PANEL(144,4),PANIND(144),
      94PANEL(144,4),PANIND(144),
      95PANEL(144,4),PANIND(144),
      96PANEL(144,4),PANIND(144),
      97PANEL(144,4),PANIND(144),
      98PANEL(144,4),PANIND(144),
      99PANEL(144,4),PANIND(144),
      100PANEL(144,4),PANIND(144),
      101PANEL(144,4),PANIND(144),
      102PANEL(144,4),PANIND(144),
      103PANEL(144,4),PANIND(144),
      104PANEL(144,4),PANIND(144),
      105PANEL(144,4),PANIND(144),
      106PANEL(144,4),PANIND(144),
      107PANEL(144,4),PANIND(144),
      108PANEL(144,4),PANIND(144),
      109PANEL(144,4),PANIND(144),
      110PANEL(144,4),PANIND(144),
      111PANEL(144,4),PANIND(144),
      112PANEL(144,4),PANIND(144),
      113PANEL(144,4),PANIND(144),
      114PANEL(144,4),PANIND(144),
      115PANEL(144,4),PANIND(144),
      116PANEL(144,4),PANIND(144),
      117PANEL(144,4),PANIND(144),
      118PANEL(144,4),PANIND(144),
      119PANEL(144,4),PANIND(144),
      120PANEL(144,4),PANIND(144),
      121PANEL(144,4),PANIND(144),
      122PANEL(144,4),PANIND(144),
      123PANEL(144,4),PANIND(144),
      124PANEL(144,4),PANIND(144),
      125PANEL(144,4),PANIND(144),
      126PANEL(144,4),PANIND(144),
      127PANEL(144,4),PANIND(144),
      128PANEL(144,4),PANIND(144),
      129PANEL(144,4),PANIND(144),
      130PANEL(144,4),PANIND(144),
      131PANEL(144,4),PANIND(144),
      132PANEL(144,4),PANIND(144),
      133PANEL(144,4),PANIND(144),
      134PANEL(144,4),PANIND(144),
      135PANEL(144,4),PANIND(144),
      136PANEL(144,4),PANIND(144),
      137PANEL(144,4),PANIND(144),
      138PANEL(144,4),PANIND(144),
      139PANEL(144,4),PANIND(144),
      140PANEL(144,4),PANIND(144),
      141PANEL(144,4),PANIND(144),
      142PANEL(144,4),PANIND(144),
      143PANEL(144,4),PANIND(144),
      144PANEL(144,4),PANIND(144),
      145PANEL(144,4),PANIND(144),
      146PANEL(144,4),PANIND(144),
      147PANEL(144,4),PANIND(144),
      148PANEL(144,4),PANIND(144),
      149PANEL(144,4),PANIND(144),
      150PANEL(144,4),PANIND(144),
      151PANEL(144,4),PANIND(144),
      152PANEL(144,4),PANIND(144),
      153PANEL(144,4),PANIND(144),
      154PANEL(144,4),PANIND(144),
      155PANEL(144,4),PANIND(144),
      156PANEL(144,4),PANIND(144),
      157PANEL(144,4),PANIND(144),
      158PANEL(144,4),PANIND(144),
      159PANEL(144,4),PANIND(144),
      160PANEL(144,4),PANIND(144),
      161PANEL(144,4),PANIND(144),
      162PANEL(144,4),PANIND(144),
      163PANEL(144,4),PANIND(144),
      164PANEL(144,4),PANIND(144),
      165PANEL(144,4),PANIND(144),
      166PANEL(144,4),PANIND(144),
      167PANEL(144,4),PANIND(144),
      168PANEL(144,4),PANIND(144),
      169PANEL(144,4),PANIND(144),
      170PANEL(144,4),PANIND(144),
      171PANEL(144,4),PANIND(144),
      172PANEL(144,4),PANIND(144),
      173PANEL(144,4),PANIND(144),
      174PANEL(144,4),PANIND(144),
      175PANEL(144,4),PANIND(144),
      176PANEL(144,4),PANIND(144),
      177PANEL(144,4),PANIND(144),
      178PANEL(144,4),PANIND(144),
      179PANEL(144,4),PANIND(144),
      180PANEL(144,4),PANIND(144),
      181PANEL(144,4),PANIND(144),
      182PANEL(144,4),PANIND(144),
      183PANEL(144,4),PANIND(144),
      184PANEL(144,4),PANIND(144),
      185PANEL(144,4),PANIND(144),
      186PANEL(144,4),PANIND(144),
      187PANEL(144,4),PANIND(144),
      188PANEL(144,4),PANIND(144),
      189PANEL(144,4),PANIND(144),
      190PANEL(144,4),PANIND(144),
      191PANEL(144,4),PANIND(144),
      192PANEL(144,4),PANIND(144),
      193PANEL(144,4),PANIND(144),
      194PANEL(144,4),PANIND(144),
      195PANEL(144,4),PANIND(144),
      196PANEL(144,4),PANIND(144),
      197PANEL(144,4),PANIND(144),
      198PANEL(144,4),PANIND(144),
      199PANEL(144,4),PANIND(144),
      200PANEL(144,4),PANIND(144),
      201PANEL(144,4),PANIND(144),
      202PANEL(144,4),PANIND(144),
      203PANEL(144,4),PANIND(144),
      204PANEL(144,4),PANIND(144),
      205PANEL(144,4),PANIND(144),
      206PANEL(144,4),PANIND(144),
      207PANEL(144,4),PANIND(144),
      208PANEL(144,4),PANIND(144),
      209PANEL(144,4),PANIND(144),
      210PANEL(144,4),PANIND(144),
      211PANEL(144,4),PANIND(144),
      212PANEL(144,4),PANIND(144),
      213PANEL(144,4),PANIND(144),
      214PANEL(144,4),PANIND(144),
      215PANEL(144,4),PANIND(144),
      216PANEL(144,4),PANIND(144),
      217PANEL(144,4),PANIND(144),
      218PANEL(144,4),PANIND(144),
      219PANEL(144,4),PANIND(144),
      220PANEL(144,4),PANIND(144),
      221PANEL(144,4),PANIND(144),
      222PANEL(144,4),PANIND(144),
      223PANEL(144,4),PANIND(144),
      224PANEL(144,4),PANIND(144),
      225PANEL(144,4),PANIND(144),
      226PANEL(144,4),PANIND(144),
      227PANEL(144,4),PANIND(144),
      228PANEL(144,4),PANIND(144),
      229PANEL(144,4),PANIND(144),
      230PANEL(144,4),PANIND(144),
      231PANEL(144,4),PANIND(144),
      232PANEL(144,4),PANIND(144),
      233PANEL(144,4),PANIND(144),
      234PANEL(144,4),PANIND(144),
      235PANEL(144,4),PANIND(144),
      236PANEL(144,4),PANIND(144),
      237PANEL(144,4),PANIND(144),
      238PANEL(144,4),PANIND(144),
      239PANEL(144,4),PANIND(144),
      240PANEL(144,4),PANIND(144),
      241PANEL(144,4),PANIND(144),
      242PANEL(144,4),PANIND(144),
      243PANEL(144,4),PANIND(144),
      244PANEL(144,4),PANIND(144),
      245PANEL(144,4),PANIND(144),
      246PANEL(144,4),PANIND(144),
      247PANEL(144,4),PANIND(144),
      248PANEL(144,4),PANIND(144),
      249PANEL(144,4),PANIND(144),
      250PANEL(144,4),PANIND(144),
      251PANEL(144,4),PANIND(144),
      252PANEL(144,4),PANIND(144),
      253PANEL(144,4),PANIND(144),
      254PANEL(144,4),PANIND(144),
      255PANEL(144,4),PANIND(144),
      256PANEL(144,4),PANIND(144),
      257PANEL(144,4),PANIND(144),
      258PANEL(144,4),PANIND(144),
      259PANEL(144,4),PANIND(144),
      260PANEL(144,4),PANIND(144),
      261PANEL(144,4),PANIND(144),
      262PANEL(144,4),PANIND(144),
      263PANEL(144,4),PANIND(144),
      264PANEL(144,4),PANIND(144),
      265PANEL(144,4),PANIND(144),
      266PANEL(144,4),PANIND(144),
      267PANEL(144,4),PANIND(144),
      268PANEL(144,4),PANIND(144),
      269PANEL(144,4),PANIND(144),
      270PANEL(144,4),PANIND(144),
      271PANEL(144,4),PANIND(144),
      272PANEL(144,4),PANIND(144),
      273PANEL(144,4),PANIND(144),
      274PANEL(144,4),PANIND(144),
      275PANEL(144,4),PANIND(144),
      276PANEL(144,4),PANIND(144),
      277PANEL(144,4),PANIND(144),
      278PANEL(144,4),PANIND(144),
      279PANEL(144,4),PANIND(144),
      280PANEL(144,4),PANIND(144),
      281PANEL(144,4),PANIND(144),
      282PANEL(144,4),PANIND(144),
      283PANEL(144,4),PANIND(144),
      284PANEL(144,4),PANIND(144),
      285PANEL(144,4),PANIND(144),
      286PANEL(144,4),PANIND(144),
      287PANEL(144,4),PANIND(144),
      288PANEL(144,4),PANIND(144),
      289PANEL(144,4),PANIND(144),
      290PANEL(144,4),PANIND(144),
      291PANEL(144,4),PANIND(144),
      292PANEL(144,4),PANIND(144),
      293PANEL(144,4),PANIND(144),
      294PANEL(144,4),PANIND(144),
      295PANEL(144,4),PANIND(144),
      296PANEL(144,4),PANIND(144),
      297PANEL(144,4),PANIND(144),
      298PANEL(144,4),PANIND(144),
      299PANEL(144,4),PANIND(144),
      300PANEL(144,4),PANIND(144),
      301PANEL(144,4),PANIND(144),
      302PANEL(144,4),PANIND(144),
      303PANEL(144,4),PANIND(144),
      304PANEL(144,4),PANIND(144),
      305PANEL(144,4),PANIND(144),
      306PANEL(144,4),PANIND(144),
      307PANEL(144,4),PANIND(144),
      308PANEL(144,4),PANIND(144),
      309PANEL(144,4),PANIND(144),
      310PANEL(144,4),PANIND(144),
      311PANEL(144,4),PANIND(144),
      312PANEL(144,4),PANIND(144),
      313PANEL(144,4),PANIND(144),
      314PANEL(144,4),PANIND(144),
      315PANEL(144,4),PANIND(144),
      316PANEL(144,4),PANIND(144),
      317PANEL(144,4),PANIND(144),
      318PANEL(144,4),PANIND(144),
      319PANEL(144,4),PANIND(144),
      320PANEL(144,4),PANIND(144),
      321PANEL(144,4),PANIND(144),
      322PANEL(144,4),PANIND(144),
      323PANEL(144,4),PANIND(144),
      324PANEL(144,4),PANIND(144),
      325PANEL(144,4),PANIND(144),
      326PANEL(144,4),PANIND(144),
      327PANEL(144,4),PANIND(144),
      328PANEL(144,4),PANIND(144),
      329PANEL(144,4),PANIND(144),
      330PANEL(144,4),PANIND(144),
      331PANEL(144,4),PANIND(144),
      332PANEL(144,4),PANIND(144),
      333PANEL(144,4),PANIND(144),
      334PANEL(144,4),PANIND(144),
      335PANEL(144,4),PANIND(144),
      336PANEL(144,4),PANIND(144),
      337PANEL(144,4),PANIND(144),
      338PANEL(144,4),PANIND(144),
      339PANEL(144,4),PANIND(144),
      340PANEL(144,4),PANIND(144),
      341PANEL(144,4),PANIND(144),
      342PANEL(144,4),PANIND(144),
      343PANEL(144,4),PANIND(144),
      344PANEL(144,4),PANIND(144),
      345PANEL(144,4),PANIND(144),
      346PANEL(144,4),PANIND(144),
      347PANEL(144,4),PANIND(144),
      348PANEL(144,4),PANIND(144),
      349PANEL(144,4),PANIND(144),
      350PANEL(144,4),PANIND(144),
      351PANEL(144,4),PANIND(144),
      352PANEL(144,4),PANIND(144),
      353PANEL(144,4),PANIND(144),
      354PANEL(144,4),PANIND(144),
      355PANEL(144,4),PANIND(144),
      356PANEL(144,4),PANIND(144),
      357PANEL(144,4),PANIND(144),
      358PANEL(144,4),PANIND(144),
      359PANEL(144,4),PANIND(144),
      360PANEL(144,4),PANIND(144),
      361PANEL(144,4),PANIND(144),
      362PANEL(144,4),PANIND(144),
      363PANEL(144,4),PANIND(144),
      364PANEL(144,4),PANIND(144),
      365PANEL(144,4),PANIND(144),
      366PANEL(144,4),PANIND(144),
      367PANEL(144,4),PANIND(144),
      368PANEL(144,4),PANIND(144),
      369PANEL(144,4),PANIND(144),
      370PANEL(144,4),PANIND(144),
      371PANEL(144,4),PANIND(144),
      372PANEL(144,4),PANIND(144),
      373PANEL(144,4),PANIND(144),
      374PANEL(144,4),PANIND(144),
      375PANEL(144,4),PANIND(144),
      376PANEL(144,4),PANIND(144),
      377PANEL(144,4),PANIND(144),
      378PANEL(144,4),PANIND(144),
      379PANEL(144,4),PANIND(144),
      380PANEL(144,4),PANIND(144),
      381PANEL(144,4),PANIND(144),
      382PANEL(144,4),PANIND(144),
      383PANEL(144,4),PANIND(144),
      384PANEL(144,4),PANIND(144),
      385PANEL(144,4),PANIND(144),
      386PANEL(144,4),PANIND(144),
      387PANEL(144,4),PANIND(144),
      388PANEL(144,4),PANIND(144),
      389PANEL(144,4),PANIND(144),
      390PANEL(144,4),PANIND(144),
      391PANEL(144,4),PANIND(144),
      392PANEL(144,4),PANIND(144),
      393PANEL(144,4),PANIND(144),
      394PANEL(144,4),PANIND(144),
      395PANEL(144,4),PANIND(144),
      396PANEL(144,4),PANIND(144),
      397PANEL(144,4),PANIND(144),
      398PANEL(144,4),PANIND(144),
      399PANEL(144,4),PANIND(144),
      400PANEL(144,4),PANIND(144),
      401PANEL(144,4),PANIND(144),
      402PANEL(144,4),PANIND(144),
      403PANEL(144,4),PANIND(144),
      404PANEL(144,4),PANIND(144),
      405PANEL(144,4),PANIND(144),
      406PANEL(144,4),PANIND(144),
      407PANEL(144,4),PANIND(144),
      408PANEL(144,4),PANIND(144),
      409PANEL(144,4),PANIND(144),
      410PANEL(144,4),PANIND(144),
      411PANEL(144,4),PANIND(144),
      412PANEL(144,4),PANIND(144),
      413PANEL(144,4),PANIND(144),
      414PANEL(144,4),PANIND(144),
      415PANEL(144,4),PANIND(144),
      416PANEL(144,4),PANIND(144),
      417PANEL(144,4),PANIND(144),
      418PANEL(144,4),PANIND(144),
      419PANEL(144,4),PANIND(144),
      420PANEL(144,4),PANIND(144),
      421PANEL(144,4),PANIND(144),
      422PANEL(144,4),PANIND(144),
      423PANEL(144,4),PANIND(144),
      424PANEL(144,4),PANIND(144),
      425PANEL(144,4),PANIND(144),
      426PANEL(144,4),PANIND(144),
      427PANEL(144,4),PANIND(144),
      428PANEL(144,4),PANIND(144),
      429PANEL(144,4),PANIND(144),
      430PANEL(144,4),PANIND(144),
      431PANEL(144,4),PANIND(144),
      432PANEL(144,4),PANIND(144),
      433PANEL(144,4),PANIND(144),
      434PANEL(144,4),PANIND(144),
      435PANEL(144,4),PANIND(144),
      436PANEL(144,4),PANIND(144),
      437PANEL(144,4),PANIND(144),
      438PANEL(144,4),PANIND(144),
      439PANEL(144,4),PANIND(144),
      440PANEL(144,4),PANIND(144),
      441PANEL(144,4),PANIND(144),
      442PANEL(144,4),PANIND(144),
      443PANEL(144,4),PANIND(144),
      444PANEL(144,4),PANIND(144),
      445PANEL(144,4),PANIND(144),
      446PANEL(144,4),PANIND(144),
      447PANEL(144,4),PANIND(144),
      448PANEL(144,4),PANIND(144),
      449PANEL(144,4),PANIND(144),
      450PANEL(144,4),PANIND(144),
      451PANEL(144,4),PANIND(144),
      452PANEL(144,4),PANIND(144),
      453PANEL(144,4),PANIND(144),
      454PANEL(144,4),PANIND(144),
      455PANEL(144,4),PANIND(144),
      456PANEL(144,4),PANIND(144),
      457PANEL(144,4),PANIND(144),
      458PANEL(144,4),PANIND(144),
      459PANEL(144,4),PANIND(144),
      460PANEL(144,4),PANIND(144),
      461PANEL(144,4),PANIND(144),
      462PANEL(144,4),PANIND(144),
      463PANEL(144,4),PANIND(144),
      464PANEL(144,4),PANIND(144),
      465PANEL(144,4),PANIND(144),
      466PANEL(144,4),PANIND(144),
      467PANEL(144,4),PANIND(144),
      468PANEL(144,4),PANIND(144),
      469PANEL(144,4),PANIND(144),
      470PANEL(144,4),PANIND(144),

```


[illegible]

CCC

```

C THIS SUBROUTINE CALCULATES THE SECONDARY CURRENT CSEC
C CSEC CONSISTS OF TWO PARTS: CSEC1=MAIN SECONDARY CURRENT
C LEAVING A LOCATION, AND CARRIV=SECONDARY
C CURRENT ARRIVING AT A LOCATION FROM OTHER PORTIONS OF THE CRAFT
C PHI IS POTENTIAL ON SURFACE
C N IS NUMBER OF GRID POINTS ON SPACECRAFT SURFACE
C NANG IS NUMBER OF INTERVALS THAT N=1/2 ANGLE (RPI/2) GRID FOR
C SECONDARIES IS DIVIDED INTO. NANG SHOULD BE ODD SO THAT THERE IS
C GRID POINT FOR RPI/2
C NLEV IS NUMBER OF VELOCITY LEVELS USED
C PHO IS ACTUAL CONTRIBUTION AT EACH POINT
C ANG IS LOCATION OF EACH GRID POINT. NOTE THAT ANG AND PHO ARE
C NLEV X NANG MATRICES.
C DATA DANG/0.017
C DATA FAC/1.0/DVI/0.01
C DATA XL/0
C GAMMA=RATIO(3)
C NDIM=3
C DELANG=.58RPI/FLOAT(NANG-1)
C L1=2*NANG-1
C L2=L1-1
C 1 PHO(I,L)=2.0*BCSEC1(J)/RESPI(POT-PHI(J))/RATIO(3)/
C 2 SOTPI
C IF (PHO(I,L).EQ.0.0) ICHECK(I,L)=1
C GO TO 190
180 PHO(I,L)=2.0*BCSEC1(J)/SOTPI
190 CONTINUE
191 CONTINUE
C 197 CONTINUE
C 197 L=1:L1
C DO 197 I=1:NLEV
C BOUNDL(I,L)=PHO(I,L)
C BOUNDI(I,L)=PHO(I,L)
C VI(I,L)=VI(I)
C ANG(I,L)=ANG(I)
197 CONTINUE
C IF (RL.EQ.0) GO TO 2100
C DO 200 I=1:NLEV
C DO 200 L=1:L1
C IF (ICHECK(I,L).EQ.1.OR.ICHECK(I,L+1).EQ.1) GO TO 200
C IF (PHO(I,L).EQ.0.0.AND.PHO(I,L+1).NE.0.0) GO TO 201
C IF (PHO(I,L).NE.0.0.AND.PHO(I,L+1).EQ.0.0) GO TO 202
C GO TO 200
201 LCUT=L
C ANGA=ANG(L)
C ANGB=ANG(L+1)
C GO TO 203
202 LCUT=L+1
C ANGA=ANG(L+1)
C ANGB=ANG(L)
203 ANGLE=0.5*(ANGA+ANGB)
204 AOLB=ANGLE
C VARIABLE(1)=50
C VARIABLE(2)=ANGLE
C VARIABLE(3)=Y(J)
C T=0
C BETAI=VI(I)/VE(I)+PHI(J)/GAMMA
C IF (BETAI.LT.0.0) BOUNDL(I,LCUT)=2.0*BCSEC1(J)/SOTPI
C IF (BETAI.LT.0.0) GO TO 207
C CALL ORBIT(SO,BETAI,J)
C IF (VARIABLE(1).GE.(SBOUND-DELTA)) GO TO 204
C IF (ABS((PHI(J)-POT)/GAMMA).LT.100.)
C 1 PHO(I,L)=2.0*BCSEC1(J)/RESPI(POT-PHI(J))/RATIO(3)/
C 2 SOTPI
C IF (PHO(I,L).EQ.0.0) ICHECK(I,L)=1
C GO TO 190
180 PHO(I,L)=2.0*BCSEC1(J)/SOTPI
190 CONTINUE
191 CONTINUE
C 197 CONTINUE
C 197 L=1:L1
C DO 197 I=1:NLEV
C BOUNDL(I,L)=PHO(I,L)
C BOUNDI(I,L)=PHO(I,L)
C VI(I,L)=VI(I)
C ANG(I,L)=ANG(I)
197 CONTINUE
C IF (RL.EQ.0) GO TO 2100
C DO 200 I=1:NLEV
C DO 200 L=1:L1
C IF (ICHECK(I,L).EQ.1.OR.ICHECK(I,L+1).EQ.1) GO TO 200
C IF (PHO(I,L).EQ.0.0.AND.PHO(I,L+1).NE.0.0) GO TO 201
C IF (PHO(I,L).NE.0.0.AND.PHO(I,L+1).EQ.0.0) GO TO 202
C GO TO 200
201 LCUT=L
C ANGA=ANG(L)
C ANGB=ANG(L+1)
C GO TO 203
202 LCUT=L+1
C ANGA=ANG(L+1)
C ANGB=ANG(L)
203 ANGLE=0.5*(ANGA+ANGB)
204 AOLB=ANGLE
C IF (ABS(ANGLE-AOLB).GT.DANG) GO TO 204
C ANGLE(I,LCUT)=ANGLE
200 CONTINUE
C 200 CONTINUE
C 200 L=1:L1
C DO 200 I=1:NLEV
C IF (ICHECK(I,L).EQ.1.OR.ICHECK(I,L+1).EQ.1) GO TO 200
C IF (PHO(I,L).EQ.0.0.AND.PHO(I,L+1).NE.0.0) GO TO 201
C IF (PHO(I,L).NE.0.0.AND.PHO(I,L+1).EQ.0.0) GO TO 202
C GO TO 200
201 LCUT=L
C ANGA=ANG(L)
C ANGB=ANG(L+1)
C GO TO 203
202 LCUT=L+1
C ANGA=ANG(L+1)
C ANGB=ANG(L)
203 ANGLE=0.5*(ANGA+ANGB)
204 AOLB=ANGLE
C IF (ABS(ANGLE-AOLB).GT.DANG) GO TO 204
C ANGLE(I,LCUT)=ANGLE
200 CONTINUE
C 200 CONTINUE
C 200 L=1:L1
C DO 200 I=1:NLEV
C IF (ICHECK(I,L).EQ.1.OR.ICHECK(I,L+1).EQ.1) GO TO 200
C IF (PHO(I,L).EQ.0.0.AND.PHO(I,L+1).NE.0.0) GO TO 201
C IF (PHO(I,L).NE.0.0.AND.PHO(I,L+1).EQ.0.0) GO TO 202
C GO TO 200
201 LCUT=L
C ANGA=ANG(L)
C ANGB=ANG(L+1)
C GO TO 203
202 LCUT=L+1
C ANGA=ANG(L+1)
C ANGB=ANG(L)
203 ANGLE=0.5*(ANGA+ANGB)
204 AOLB=ANGLE
C IF (ABS(ANGLE-AOLB).GT.DANG) GO TO 204
C ANGLE(I,LCUT)=ANGLE
200 CONTINUE
C 200 CONTINUE
C 200 L=1:L1
C DO 200 I=1:NLEV
C IF (ICHECK(I,L).EQ.1.OR.ICHECK(I,L+1).EQ.1) GO TO 200
C IF (PHO(I,L).EQ.0.0.AND.PHO(I,L+1).NE.0.0) GO TO 201
C IF (PHO(I,L).NE.0.0.AND.PHO(I,L+1).EQ.0.0) GO TO 202
C GO TO 200
201 LCUT=L
C ANGA=ANG(L)
C ANGB=ANG(L+1)
C GO TO 203
202 LCUT=L+1
C ANGA=ANG(L+1)
C ANGB=ANG(L)
203 ANGLE=0.5*(ANGA+ANGB)
204 AOLB=ANGLE
C IF (ABS(ANGLE-AOLB).GT.DANG) GO TO 204
C ANGLE(I,LCUT)=ANGLE
200 CONTINUE
C 200 CONTINUE
C 200 L=1:L1
C DO 200 I=1:NLEV
C IF (ICHECK(I,L).EQ.1.OR.ICHECK(I,L+1).EQ.1) GO TO 200
C IF (PHO(I,L).EQ.0.0.AND.PHO(I,L+1).NE.0.0) GO TO 201
C IF (PHO(I,L).NE.0.0.AND.PHO(I,L+1).EQ.0.0) GO TO 202
C GO TO 200
201 LCUT=L
C ANGA=ANG(L)
C ANGB=ANG(L+1)
C GO TO 203
202 LCUT=L+1
C ANGA=ANG(L+1)
C ANGB=ANG(L)
203 ANGLE=0.5*(ANGA+ANGB)
204 AOLB=ANGLE
C IF (ABS(ANGLE-AOLB).GT.DANG) GO TO 204
C ANGLE(I,LCUT)=ANGLE
200 CONTINUE
C 200 CONTINUE
C 200 L=1:L1
C DO 200 I=1:NLEV
C IF (ICHECK(I,L).EQ.1.OR.ICHECK(I,L+1).EQ.1) GO TO 200
C IF (PHO(I,L).EQ.0.0.AND.PHO(I,L+1).NE.0.0) GO TO 201
C IF (PHO(I,L).NE.0.0.AND.PHO(I,L+1).EQ.0.0) GO TO 202
C GO TO 200
201 LCUT=L
C ANGA=ANG(L)
C ANGB=ANG(L+1)
C GO TO 203
202 LCUT=L+1
C ANGA=ANG(L+1)
C ANGB=ANG(L)
203 ANGLE=0.5*(ANGA+ANGB)
204 AOLB=ANGLE
C IF (ABS(ANGLE-AOLB).GT.DANG) GO TO 204
C ANGLE(I,LCUT)=ANGLE
200 CONTINUE
C 200 CONTINUE
C 200 L=1:L1
C DO 200 I=1:NLEV
C IF (ICHECK(I,L).EQ.1.OR.ICHECK(I,L+1).EQ.1) GO TO 200
C IF (PHO(I,L).EQ.0.0.AND.PHO(I,L+1).NE.0.0) GO TO 201
C IF (PHO(I,L).NE.0.0.AND.PHO(I,L+1).EQ.0.0) GO TO 202
C GO TO 200
201 LCUT=L
C ANGA=ANG(L)
C ANGB=ANG(L+1)
C GO TO 203
202 LCUT=L+1
C ANGA=ANG(L+1)
C ANGB=ANG(L)
203 ANGLE=0.5*(ANGA+ANGB)
204 AOLB=ANGLE
C IF (ABS(ANGLE-AOLB).GT.DANG) GO TO 204
C ANGLE(I,LCUT)=ANGLE
200 CONTINUE
C 200 CONTINUE
C 200 L=1:L1
C DO 200 I=1:NLEV
C IF (ICHECK(I,L).EQ.1.OR.ICHECK(I,L+1).EQ.1) GO TO 200
C IF (PHO(I,L).EQ.0.0.AND.PHO(I,L+1).NE.0.0) GO TO 201
C IF (PHO(I,L).NE.0.0.AND.PHO(I,L+1).EQ.0.0) GO TO 202
C GO TO 200
201 LCUT=L
C ANGA=ANG(L)
C ANGB=ANG(L+1)
C GO TO 203
202 LCUT=L+1
C ANGA=ANG(L+1)
C ANGB=ANG(L)
203 ANGLE=0.5*(ANGA+ANGB)
204 AOLB=ANGLE
C IF (ABS(ANGLE-AOLB).GT.DANG) GO TO 204
C ANGLE(I,LCUT)=ANGLE
200 CONTINUE
C 200 CONTINUE
C 200 L=1:L1
C DO 200 I=1:NLEV
C IF (ICHECK(I,L).EQ.1.OR.ICHECK(I,L+1).EQ.1) GO TO 200
C IF (PHO(I,L).EQ.0.0.AND.PHO(I,L+1).NE.0.0) GO TO 201
C IF (PHO(I,L).NE.0.0.AND.PHO(I,L+1).EQ.0.0) GO TO 202
C GO TO 200
201 LCUT=L
C ANGA=ANG(L)
C ANGB=ANG(L+1)
C GO TO 203
202 LCUT=L+1
C ANGA=ANG(L+1)
C ANGB=ANG(L)
203 ANGLE=0.5*(ANGA+ANGB)
204 AOLB=ANGLE
C IF (ABS(ANGLE-AOLB).GT.DANG) GO TO 204
C ANGLE(I,LCUT)=ANGLE
200 CONTINUE
C 200 CONTINUE
C 200 L=1:L1
C DO 200 I=1:NLEV
C IF (ICHECK(I,L).EQ.1.OR.ICHECK(I,L+1).EQ.1) GO TO 200
C IF (PHO(I,L).EQ.0.0.AND.PHO(I,L+1).NE.0.0) GO TO 201
C IF (PHO(I,L).NE.0.0.AND.PHO(I,L+1).EQ.0.0) GO TO 202
C GO TO 200
201 LCUT=L
C ANGA=ANG(L)
C ANGB=ANG(L+1)
C GO TO 203
202 LCUT=L+1
C ANGA=ANG(L+1)
C ANGB=ANG(L)
203 ANGLE=0.5*(ANGA+ANGB)
204 AOLB=ANGLE
C IF (ABS(ANGLE-AOLB).GT.DANG) GO TO 204
C ANGLE(I,LCUT)=ANGLE
200 CONTINUE
C 200 CONTINUE
C 200 L=1:L1
C DO 200 I=1:NLEV
C IF (ICHECK(I,L).EQ.1.OR.ICHECK(I,L+1).EQ.1) GO TO 200
C IF (PHO(I,L).EQ.0.0.AND.PHO(I,L+1).NE.0.0) GO TO 201
C IF (PHO(I,L).NE.0.0.AND.PHO(I,L+1).EQ.0.0) GO TO 202
C GO TO 200
201 LCUT=L
C ANGA=ANG(L)
C ANGB=ANG(L+1)
C GO TO 203
202 LCUT=L+1
C ANGA=ANG(L+1)
C ANGB=ANG(L)
203 ANGLE=0.5*(ANGA+ANGB)
204 AOLB=ANGLE
C IF (ABS(ANGLE-AOLB).GT.DANG) GO TO 204
C ANGLE(I,LCUT)=ANGLE
200 CONTINUE
C 200 CONTINUE
C 200 L=1:L1
C DO 200 I=1:NLEV
C IF (ICHECK(I,L).EQ.1.OR.ICHECK(I,L+1).EQ.1) GO TO 200
C IF (PHO(I,L).EQ.0.0.AND.PHO(I,L+1).NE.0.0) GO TO 201
C IF (PHO(I,L).NE.0.0.AND.PHO(I,L+1).EQ.0.0) GO TO 202
C GO TO 200
201 LCUT=L
C ANGA=ANG(L)
C ANGB=ANG(L+1)
C GO TO 203
202 LCUT=L+1

```



```

190 PHO(I,L)=2.08ECSA1(J)/SOTPI
190 CONTINUE
191 IOML=0
DO 100 L=1,L1
IF (PHO(I,L).NE.0.0) IOML=IOML+1
300 CONTINUE
C
DO 197 L=1,L1
DO 197 I=1,MLEV
BOUNDL(I,L)=PHO(I,L)
BOUNDI(I,L)=PHO(I,L)
VII(I,L)=VI(I)
ANG(L,I,L)=ANG(L)
197 CONTINUE
C
IF (KL.EQ.0) GO TO 2100
DO 200 I=1,MLEV
DO 200 L=1,L2
IF (ICHECK(I,L).EQ.1.OR.ICHECK(I+1,L).EQ.1) GO TO 200
IF (PHO(I,L).EQ.0.0.AND.PHO(I+1,L).NE.0.0) GO TO 201
IF (PHO(I,L).NE.0.0.AND.PHO(I+1,L).EQ.0.0) GO TO 202
GO TO 200
201 LCUT=L
ANGA=ANG(L)
ANGB=ANG(L+1)
GO TO 203
202 LCUT=L+1
ANGA=ANG(L+1)
ANGB=ANG(L)
203 ANGLE=0.5*(ANGA+ANGB)
204 AOLD=ANGLE
VARIABLE(1)=50
VARIABLE(2)=ANGLE
VARIABLE(3)=Y(J)
T=0.0
BETA=VI(I)*VII(I)+PHI(J)/GAMMA
IF (BETA.LT.0.0) BOUNDL(I,LCUT)=2.08ECSA1(J)/SOTPI
IF (BETA.LT.0.0) GO TO 207
CALL ORBIT(SO,BETA,J)
IF (VARIABLE(1).GE.(SBOUND-DELTAX)) GO TO 204
IF (ABS(PHI(J)-POT)/GAMMA.LT.100.0)
1 BOUNDL(I,LCUT)=2.08ECSA1(J)*EXP((POT-PHI(J))/GAMMA)/SOTPI
204 ANGB=ANGLE
GO TO 205
205 ANGA=ANGLE
205 ANGLE=0.5*(ANGA+ANGB)
IF (ABS(ANGLE-AOLD).GT.DANG) GO TO 204
ANG(L,I,LCUT)=ANGLE
200 CONTINUE
C
MLEV1=MLEV-1
DO 210 L=1,L1
DO 210 I=1,MLEV1
IF (ICHECK(I,L).EQ.1.OR.ICHECK(I+1,L).EQ.1) GO TO 210
IF (PHO(I,L).EQ.0.0.AND.PHO(I+1,L).NE.0.0) GO TO 211
IF (PHO(I,L).NE.0.0.AND.PHO(I+1,L).EQ.0.0) GO TO 212
GO TO 210
211 ICUT=I
VIA=VI(I)
VIB=VI(I+1)
GO TO 213
212 ICUT=I+1
VIA=VI(I+1)
VIB=VI(I)
213 VIN=0.5*(VIA+VIB)
214 VIOLD=VIN
BETA=VIN*82*PHI(J)/GAMMA
IF (BETA.LT.0.0) BOUNDI(ICUT,L)=2.08ECSA1(J)/SOTPI
IF (BETA.LT.0.0) GO TO 217
VARIABLE(1)=50
VARIABLE(2)=ANG(L)
VARIABLE(3)=Y(J)
T=0.0
CALL ORBIT(SO,BETA,J)
IF (VARIABLE(1).GE.(SBOUND-DELTAX)) GO TO 214
IF (ABS(PHI(J)-POT)/GAMMA.LT.100.0)
1 BOUNDI(ICUT,L)=2.08ECSA1(J)*EXP((POT-PHI(J))/GAMMA)/SOTPI
217 VIB=VIN
GO TO 215
214 VIA=VIN
GO TO 215
215 VIN=0.5*(VIA+VIB)
IF (ABS(VIN-VIOLD).GT.DVIS(VI(I+1)-VI(I))) GO TO 214
VII(ICUT,L)=VIN
210 CONTINUE
C
2100 CONTINUE
C CALCULATE CBSCAT
CURRIN=0.
CURRAX=0.
CARRIV=0.
IF (IFAIL(18).EQ.0) GO TO 4000
CPH=0.0
DO 350 L=1,L1
IF (PHO(I,L).NE.0.0.OR.PHI(J).GT.0.0)
1 CPH=2.08ECSA1(J)/SOTPI
350 CONTINUE
WRITE (LUNG,4000) J
4000 FORMAT (/IX,50,SAMPLING IN VELOCITY SPACE FOR SCATTERERS AT J=8,
1 13/)
WRITE (LUNG,4001) (PHO(I,L),I=1,MLEV),L=1,L1
400 FORMAT (8(IX,1PE9.2))
CALL FIT(12,CARRIV,CURRIN,CURRAX,J,CPH,PHI,N,GAMMA)
4000 CONTINUE
401 FORMAT(/)
360 CBSCAT(J)=CBSAT(J)-CARRIV
400 CONTINUE
RETURN
END
SUBROUTINE FLPR(N,NANG,PHI,SECPH,ITER,IBCON,OMEGA,SO,J,SECPRI)
INTER=PERSEC*SECONB*PERPAN*PANIND
COMMON PSAVE(144,10),CSAVE(144,10),PSECTR(144),CSECTR(144),
IDLEE(20),DELMAX(144),EMAX(144),ETA(20),BSCAT(144),
2BSCAT2(144),BSCAT3(144),PHO(20,40),
1AND(40),CPHMAX(144),SUNANG,ANGB,BOUNDL(20,40),BOUNDI(20,40),
2ANGD(20,40),VII(20,40),ICHECK(20,40),RATIO(13),IROOT(144),
3IFAIL(144),JLOCAL(144),ICOM(144),
1VI(20),FV(8),MLEV,NTIME,LEV,TIN(20),TMAX(20),VINUN(20),
2AI(144),BI(144),C(144),BB(144),MU(144),TU(144),DU(144),
3FU(144),TUOCD(700),
11710,MPDINT,N,IBCON,ISYN,IPDIS,NSECT,NPEROD,NPEROD,IBIRY,
20ANNA,BUDY(70,40),BUDY(70,40),Y(144),DELTAX,DELTAY,
3Y(44,40),X(44),Y(70),
1VARB(4),T,DELT,SBOUND,NDIR,POT,N,J1,RP1,RP12,RP1HAF,SOTPI,
2DAY,TEMP1,TEMP2,DEHE1,DEHE2,DEH1,DEH2,TEMP11,TEMP12,
TEMP10,TEMP11,TEMP12,TEMP13,TEMP14,TEMP15,TEMP16,TEMP17,TEMP18,
1EDTL(144),IDTL(144),PERSEC(144),SECONB(144),IPANEL(144),
2PERPAN(144),PANIND(144),
1CIOM(144),CELEC(144),CSEC(144),CSECI(144),CPHOTO(144),
2CPHOTO(144),LBSCAT(144),CBSA1(144),SECPH(144),SECPRI(144),
3PHI(144),COMU(144),
1KASE=IOML*DPHI*HANG,RAD*FBOUND*OMEGA*ALPHA*SO*J*IS*ECS,
2KXPI(20),EIV(120),IERROR,TETIN,TETMAX,BETA1,BETA2,JL55,
3L2,CARRIV,CPH,XI,CSECEL,CSECE1,CS,CS1,CB1
C *****
C THIS SUBROUTINE CALCULATES THE SECONDARY CURRENT SECPH
C SECPH CONSISTS OF TWO PARTS:SECPH,MAIN SECONDARY CURRENT
C LEAVING A LOCATION,AND CARRIV,SECONDARY
C CURRENT ARRIVING AT A LOCATION FROM OTHER PORTIONS OF THE CRAFT
C PHI IS POTENTIAL ON SPACECRAFT SURFACE
C N IS NUMBER OF GRID POINTS ON SPACECRAFT SURFACE
C NANG IS NUMBER OF INTERVALS THAT HALF-ANGLE (RP1/2) GRID FOR
C SECONDARYS IS DIVIDED INTO. NANG SHOULD BE ODD SO THAT THERE IS
C A GRID POINT FOR RP1/2
C MLEV IS NUMBER OF VELOCITY LEVELS USED
C PHO IS ACTUAL CONTRIBUTION AT EACH POINT
C ANG IS LOCATION OF EACH GRID POINT. NOTE THAT ANG AND PHO ARE
C MLEV X NANG MATRICES.
C *****
DATA DANG/0.1/
DATA FAC/1.0/DUI/0.017/
DATA KL/0/
GAMMA=RATIO(13)
DELANG=58PI/FLOAT(NANG-1)
L1=2*NANG-1
L2=L1-1
NDIR=3
C GENERATE COEFFICIENTS PHO(I,L) AND ANG(L) FOR USE IN CALCULATING
C SECONDARY CURRENT DUE TO SECONDARYS ARRIVING FROM OTHER
C PORTIONS OF THE SPACECRAFT
IOML=1
DO 300 I=1,MLEV
DO 190 L=1,L1
IF (KL.EQ.0) ICHECK(I,L)=1
IF (KL.EQ.1) ICHECK(I,L)=0
PHO(I,L)=0.0
IF (IOML.EQ.0) GO TO 190
ANG(L)=DELANG*FLOAT(L-1)
BETA=VII(I)*82*PHI(J)/GAMMA
IF (BETA.LT.0.0) GO TO 180
VARIABLE(1)=50
VARIABLE(2)=ANG(L)
VARIABLE(3)=Y(J)
COSA=COS(ANG(L))
DISTAN=COSA*DUDX(I,J)/(2.0*VII(I)*82*GAMMA)+COSA
IF (L.EQ.1.AND.DBETA.LT.0.0) GO TO 180
IF (L.EQ.L1.AND.DBETA.GT.0.0) GO TO 180
T=0.
CALL ORBIT(SO,BETA,J)
IF (VARIABLE(1).GE.(SBOUND-DELTAX)) GO TO 190
IF (ABS(POT-PHI(J))/RATIO(13).LT.100.)
1 PHO(I,L)=2.08ECPRI(J)*EXP((POT-PHI(J))/RATIO(13))/
3 SOTPI
IF (PHO(I,L).EQ.0.0) ICHECK(I,L)=1
GO TO 190
180 PHO(I,L)=2.08ECPRI(J)/SOTPI
190 CONTINUE
IOML=0
DO 300 L=1,L1
IF (PHO(I,L).NE.0.0) IOML=IOML+1
300 CONTINUE
C
DO 197 L=1,L1
DO 197 I=1,MLEV
BOUNDL(I,L)=PHO(I,L)
BOUNDI(I,L)=PHO(I,L)
VII(I,L)=VI(I)
ANG(L,I,L)=ANG(L)
197 CONTINUE
C
IF (KL.EQ.0) GO TO 2100
DO 200 I=1,MLEV
DO 200 L=1,L2
IF (ICHECK(I,L).EQ.1.OR.ICHECK(I+1,L).EQ.1) GO TO 200
IF (PHO(I,L).EQ.0.0.AND.PHO(I+1,L).NE.0.0) GO TO 201
IF (PHO(I,L).NE.0.0.AND.PHO(I+1,L).EQ.0.0) GO TO 202
GO TO 200
201 LCUT=L
ANGA=ANG(L)
ANGB=ANG(L+1)
GO TO 203
202 LCUT=L+1
ANGA=ANG(L+1)
ANGB=ANG(L)
203 ANGLE=0.5*(ANGA+ANGB)
204 AOLD=ANGLE
VARIABLE(1)=50
VARIABLE(2)=ANGLE
VARIABLE(3)=Y(J)
T=0.0
BETA=VI(I)*VII(I)+PHI(J)/GAMMA
IF (BETA.LT.0.0) BOUNDL(I,LCUT)=2.08ECPRI(J)/SOTPI
IF (BETA.LT.0.0) GO TO 207
CALL ORBIT(SO,BETA,J)
IF (VARIABLE(1).GE.(SBOUND-DELTAX)) GO TO 204
IF (ABS(PHI(J)-POT)/GAMMA.LT.100.0)
1 BOUNDL(I,LCUT)=2.08ECPRI(J)*EXP((POT-PHI(J))/GAMMA)/SOTPI
GO TO 205
205 ANGB=ANGLE
205 ANGA=ANGLE
205 ANGLE=0.5*(ANGA+ANGB)
IF (ABS(ANGLE-AOLD).GT.DANG) GO TO 204
ANG(L,I,LCUT)=ANGLE
200 CONTINUE
C
MLEV1=MLEV-1
DO 210 L=1,L1
DO 210 I=1,MLEV1
IF (ICHECK(I,L).EQ.1.OR.ICHECK(I+1,L).EQ.1) GO TO 210
IF (PHO(I,L).EQ.0.0.AND.PHO(I+1,L).NE.0.0) GO TO 211
IF (PHO(I,L).NE.0.0.AND.PHO(I+1,L).EQ.0.0) GO TO 212
GO TO 210
211 ICUT=I
VIA=VI(I)
VIB=VI(I+1)
GO TO 213
212 ICUT=I+1
VIA=VI(I+1)
VIB=VI(I)
213 VIN=0.5*(VIA+VIB)
214 VIOLD=VIN
BETA=VIN*82*PHI(J)/GAMMA
IF (BETA.LT.0.0) BOUNDI(ICUT,L)=2.08ECPRI(J)/SOTPI
IF (BETA.LT.0.0) GO TO 217
VARIABLE(1)=50
VARIABLE(2)=ANG(L)
VARIABLE(3)=Y(J)
T=0.0
CALL ORBIT(SO,BETA,J)
IF (VARIABLE(1).GE.(SBOUND-DELTAX)) GO TO 214
IF (ABS(PHI(J)-POT)/GAMMA.LT.100.0)
1 BOUNDI(ICUT,L)=2.08ECPRI(J)*EXP((POT-PHI(J))/GAMMA)/SOTPI
217 VIB=VIN
GO TO 215
214 VIA=VIN
GO TO 215
215 VIN=0.5*(VIA+VIB)
IF (ABS(VIN-VIOLD).GT.DVIS(VI(I+1)-VI(I))) GO TO 214
VII(ICUT,L)=VIN
210 CONTINUE
C
2100 CONTINUE
C CALCULATE CBSCAT
CURRIN=0.
CURRAX=0.
CARRIV=0.
IF (IFAIL(18).EQ.0) GO TO 4000
CPH=0.0
DO 350 L=1,L1
IF (PHO(I,L).NE.0.0.OR.PHI(J).GT.0.0)
1 CPH=2.08ECSA1(J)/SOTPI
350 CONTINUE
WRITE (LUNG,4000) J
4000 FORMAT (/IX,50,SAMPLING IN VELOCITY SPACE FOR SCATTERERS AT J=8,
1 13/)
WRITE (LUNG,4001) (PHO(I,L),I=1,MLEV),L=1,L1
400 FORMAT (8(IX,1PE9.2))
CALL FIT(12,CARRIV,CURRIN,CURRAX,J,CPH,PHI,N,GAMMA)
4000 CONTINUE
401 FORMAT(/)
360 CBSCAT(J)=CBSAT(J)-CARRIV
400 CONTINUE
RETURN
END
SUBROUTINE FLPR(N,NANG,PHI,SECPH,ITER,IBCON,OMEGA,SO,J,SECPRI)
INTER=PERSEC*SECONB*PERPAN*PANIND
COMMON PSAVE(144,10),CSAVE(144,10),PSECTR(144),CSECTR(144),
IDLEE(20),DELMAX(144),EMAX(144),ETA(20),BSCAT(144),
2BSCAT2(144),BSCAT3(144),PHO(20,40),
1AND(40),CPHMAX(144),SUNANG,ANGB,BOUNDL(20,40),BOUNDI(20,40),
2ANGD(20,40),VII(20,40),ICHECK(20,40),RATIO(13),IROOT(144),
3IFAIL(144),JLOCAL(144),ICOM(144),
1VI(20),FV(8),MLEV,NTIME,LEV,TIN(20),TMAX(20),VINUN(20),
2AI(144),BI(144),C(144),BB(144),MU(144),TU(144),DU(144),
3FU(144),TUOCD(700),
11710,MPDINT,N,IBCON,ISYN,IPDIS,NSECT,NPEROD,NPEROD,IBIRY,
20ANNA,BUDY(70,40),BUDY(70,40),Y(144),DELTAX,DELTAY,
3Y(44,40),X(44),Y(70),
1VARB(4),T,DELT,SBOUND,NDIR,POT,N,J1,RP1,RP12,RP1HAF,SOTPI,
2DAY,TEMP1,TEMP2,DEHE1,DEHE2,DEH1,DEH2,TEMP11,TEMP12,
TEMP10,TEMP11,TEMP12,TEMP13,TEMP14,TEMP15,TEMP16,TEMP17,TEMP18,

```

```

      VARI(2)=ANG(L)
      VARI(3)=V(I)
      I=0
      CALL ORBIT(SO,RETAL,J)
      IF (VARI(1).GE.(SBOUND-DELTA)) GO TO 214
      VIR=VIR
      SECPN(1,0)=WEIGHT*SECPN(J)+WEIGHT*SECPN(J2)
      BOUND(1,CUT-L)=2.0*SECPNEXP(POT-PHI(J)/GAMMA)/SQRTI
      GO TO 215
214 VIA=VIR
      GO TO 215
215 VIR=0.5*(VIA+VIR)
      IF (ABS(VIR-VOLD).GT.DVIR*(V(I+1)-V(I))) GO TO 216
217 VII(CUT,L)=VIR
210 CONTINUE
C
C
C
2100 CONTINUE
C
C
C CALCULATE SECPN
      CURRINO=0.
      CURMAX=0.
      CARRIV=0.
      IF (IFAU(8).EQ.0) GO TO 4000
      CPH=0.0
      DO 350 L=1,L1
      IF (PHO(I,L).NE.0.0.DR.PHI(J).GT.0.0)
      1 CPH=2.0*SECPN(J)/SQRTI
350 CONTINUE
      WRITE (LUNG,6000) J
4000 FORMAT (1X,'SAMPLING IN VELOCITY SPACE FOR ELEC INDUCED AT J= ',
      1 13)
      WRITE (LUNG,6000) (PHO(I,L),I=1,NLEV),L=1,L1
400 FORMAT (81X,1PE9.2)
      CALL FIT(L2,CARRIV,CURRIN,CURMAX,J,CPH,PHI,N,GAMMA)
4000 CONTINUE
360 SECPN(J)=SECPN(J)+CARRIV
400 CONTINUE
      RETURN
      END
      SUBROUTINE GUM
      C=====
      C PURPOSE: TO COMPUTE THE CURRENT DUE TO THE EMISSION OF A GUM
      C=====
      COMMON /CUM/ CUM(144),CELEC(144),CSECT(144),CSECI(144),CHOTO(144)
      1 CPHOT(144),CBSCAT(144),CBSCAI(144),SECPN(144),SECPRI(144),
      2 PHI(144),CUM(144)
      RETURN
      END
      SUBROUTINE FIT(L2,CARRIV,CURRIN,CURMAX,J,PHO,PHI,N,GAMMA)
      C=====
      C THIS SUBROUTINE CALCULATES SECONDARY CURRENT FROM OTHER POINTS.
      C IT IS USED IN THE COMPUTATION OF PHOTOELECTRONS,SECONDARIES,AND
      C BACKSCATTERED ELECTRONS.
      C
      C PURPOSE
      C
      C TO COMPUTE THE CURRENT DENSITY=SUM OVER I(VELOCITY) AND SUM OVER L
      C (ANGLE) OF (A+B*ANG*E*VELOCITY+D*ANGLE*VELOCITY)*EXP(-VELOCITY**2)*
      C (VELOCITY**2)*SIN(ANGLE)*DB(ANGLE)*DB(VELOCITY)
      C TACKING INTO ACCOUNT THE FACT THAT FOR CERTAIN INCIDENT ENERGIES
      C AND CERTAIN DIRECTIONS, ELECTRON ORBITS DO CONNECT BACK TO THE AMBIENT
      C PLASMA.
      C DESCRIPTION OF THE VARIABLES
      C CARRIV: TOTAL ARRIVING SECONDARY CURRENT AT A GIVEN GRID POINT
      C CURRIN: ARRIVING CURRENT FOR ONE ELEMENTARY CELL IN VELOCITY SPACE
      C PHO(I,L): WEIGHTING FACTORS IN CURRENT INTEGRATION
      C A,B,C,D: COEFFICIENTS IN BILINEAR INTERPOLATION
      C ANGLE: SAMPLING ANGLE IN VELOCITY SPACE, ANGLES ARE SAMPLED FROM 0 TO
      C ZERO TO PI
      C VII: SAMPLING IN KINETIC VELOCITY
      C NLEV: NUMBER OF ENERGY LEVELS USED IN THE COMPUTATION
      C L2: NUMBER OF ANGLES IN VELOCITY SPACE USED IN THE COMPUTATION
      C
      INTEGER PERSEC,SECTNO,PERPAH,PAHIND
      COMMON /PAVE/ (144,10),CBAVE(144,10),PSPECTR(144),CSECT(144),
      1 DELEC(20),DELMAX(144),ENAX(144),ETA(20),BSCAT(144),
      2 BSCAT2(144),BSCAT3(144),PHO(20,40),
      1 ANGB(40),CPHOB(144),SUMANG,ANGD,BOUNDL(20,40),BOUNDI(20,40),
      2 ANGL(20,40),VUI(20,40),ICHECK(20,40),RATIO(13),IROOT(144),
      3 IFAU(14),LOCAL(144),ICON(144),
      4 IUI(20),EUI(8),NLEV,HTINES,ILEV,TININ(20),TINAX(20),VINUM(20),
      5 PA(144),BI(144),CI(144),BB(144),BU(144),TU(144),DU(144),
      6 SEU(144),THUCOS(700),
      7 IFLO,MPINT,N,ISEM,ISYN,IPDS,ISPECT,NPEROD,NPEROD,IDIHY,
      8 GAMMA,BUBX(70,40),BUBY(70,40),Y(144),DELTA,DELTA,
      9 YR(46,40),XR(46),XSR(70),
      10 VARI(4),T,DEL,BOUND,HDIN,POT,N,J1,RP1,RP12,RPINAF,SDPTI,
      11 DAY,TEMP1,TEMP2,BENI1,BENI2,BENI3,TEMP12,
      12 STEPFR,LUNG,LUNG,LUNG,LUNG,LUNG,LUNG,LUNG,LUNG,LUNG,LUNG,
      13 IDTL(144),JDTL(144),PERSEC(144),SECTNO(144),IPANEL(144),
      14 PERPAH(144,4),PAHIND(144),
      15 ICON(144),CELEC(144),CSECT(144),CSECI(144),CPHOTO(144),
      16 CPHOTI(144),CBSCAT(144),CBSCAI(144),SECPN(144),SECPRI(144),
      17 PHI(144),CUM(144),
      18 INASE,JOH,BPHI,HANG,RAD,PSOUB,ONEBA,ALPHA,BO,JP,IS,ECS,
      19 EXPVIZ(20),EFTUI(20),TERROR,TETIN,TETAX,BETA1,BETA2,A,EBB,
      20 CARRIV,CPH,XI,CSECEL,CSECI,CB,CB,CB,CB1
      C
      DATA KSTEP/5/
      C
      DO 390 I=1,NLEV
      DO 340 L=1,L2
      IF (I.GT.1) GO TO 320
      IF (PHI(J)/GAMMA.LT.0.0) GO TO 340
      IF (PHO(I,L).EQ.0.0.AND.PHO(I,L+1).EQ.0.0) GO TO 340
      DENOM=VUI(13)*(ANG(L)-ANG(L+1))
      A=PHO
      B=0.0
      C=(PHO(I,L+1)*BANG(L)-PHO(I,L)*BANG(L+1))+PHO(I,L)*BANG(L+1)-
      1 BANG(L+1)*DENOM
      D=(PHO(I,L+1)*BANG(L+1)-PHO(I,L+1)*BANG(L+1))/DENOM
      UPRI=(A+B*ANG(L))*SCOS(ANG(L))-(A+B*ANG(L+1))*
      1 COS(ANG(L+1))+B*SIN(ANG(L+1))-SIN(ANG(L))
      CURRENT=UPRI*(0.5*VUI(13)*EXPVIZ(13)+0.25*SDPTI*EFTUI(13))
      UPRI=0.5*(EXPVIZ(13)*EFTUI(13)+0.25*SDPTI*EFTUI(13))
      CURRENT=CURRENT*UPRI*(C1*(COS(ANG(L))-COS(ANG(L+1))+B*SIN(ANG(L))*SCOS(ANG(L))
      1 COS(ANG(L+1))-ANG(L+1)*SCOS(ANG(L+1))+SIN(ANG(L+1))-SIN(ANG(L))))
      CARRIV=CARRIV+CURRENT
      C
      GO TO 340
      C
      340 CONTINUE
      BETA=VUI(13)*0.5*PHI(J)/GAMMA
      IF (BETA.LT.0.0) GO TO 340
      DENOM=(ANG(L)-ANG(L+1))*VUI(13)-VUI(13)
      IF (PHO(I,L+1).EQ.0.0.AND.PHO(I,L+1).EQ.0.0.AND.PHO(I,L).EQ.0.0)
      1 (ANG.PHO(I,L).EQ.0.0) GO TO 340
      C
      CASE 1
      IF (PHO(I,L+1).EQ.0.0.AND.PHO(I,L+1).EQ.0.0.AND.PHO(I,L).EQ.0.0)
      1 (ANG.PHO(I,L).EQ.0.0.AND.ICHECK(I,L+1).EQ.0.0)
      GO TO 400
      C
      CASE 2
      IF (PHO(I,L+1).EQ.0.0.AND.PHO(I,L).EQ.0.0.AND.PHO(I,L+1).EQ.0.0)
      1 (ANG.PHO(I,L+1).EQ.0.0.AND.ICHECK(I,L+1).EQ.0.0.AND.
      2 ICHECK(I,L).EQ.0.0) GO TO 410
      C
      CASE 3
      IF (PHO(I,L+1).EQ.0.0.AND.PHO(I,L).EQ.0.0.AND.PHO(I,L+1).EQ.0.0)
      1 (ANG.PHO(I,L+1).EQ.0.0.AND.ICHECK(I,L+1).EQ.0.0.AND.
      2 ICHECK(I,L).EQ.0.0.AND.ICHECK(I,L+1).EQ.0.0) GO TO 420
      C
      CASE 4
      IF (PHO(I,L+1).EQ.0.0.AND.PHO(I,L).EQ.0.0.AND.PHO(I,L+1).EQ.0.0)
      1 (ANG.PHO(I,L+1).EQ.0.0.AND.ICHECK(I,L+1).EQ.0.0.AND.
      2 ICHECK(I,L).EQ.0.0.AND.ICHECK(I,L+1).EQ.0.0) GO TO 430
      C
      CASE 5
      IF (PHO(I,L+1).EQ.0.0.AND.PHO(I,L).EQ.0.0.AND.PHO(I,L+1).EQ.0.0)
      1 (ANG.PHO(I,L+1).EQ.0.0.AND.ICHECK(I,L).EQ.0.0) GO TO
      2 440
      C
      CASE 6
      IF (PHO(I,L+1).EQ.0.0.AND.PHO(I,L+1).EQ.0.0.AND.PHO(I,L).EQ.0.0)
      1 (ANG.PHO(I,L+1).EQ.0.0.AND.ICHECK(I,L+1).EQ.0.0.AND.
      2 ICHECK(I,L+1).EQ.0.0) GO TO 450
      C
      CASE 7
      IF (PHO(I,L+1).EQ.0.0.AND.PHO(I,L+1).EQ.0.0.AND.PHO(I,L).EQ.0.0)
      1 (ANG.PHO(I,L+1).EQ.0.0.AND.ICHECK(I,L+1).EQ.0.0.AND.
      2 ICHECK(I,L).EQ.0.0) GO TO 460
      C
      IF (PHO(I,L).EQ.0.0.AND.PHO(I,L+1).EQ.0.0.AND.PHO(I,L).
      1 (ANG.PHO(I,L+1).EQ.0.0) GO TO 9999
      GO TO 340
      C
      START COMPUTATION FOR THE REGULAR CASE
      9999 A=(PHO(I,L)*BANG(L+1)*VUI(13)-PHO(I,L)*BANG(L+1)*VUI(13)-PHO(I,
      1 L+1)*BANG(L)*VUI(13)+PHO(I,L+1)*BANG(L)*VUI(13))/DENOM
      B=(VUI(13)*(PHO(I,L)-PHO(I,L+1))-VUI(13)*(PHO(I,L)-PHO(I,L+1))
      1 /DENOM
      C=(ANG(L)*BANG(L+1)-PHO(I,L+1)-PHO(I,L+1)-ANG(L+1)*BANG(L+1)-PHO(
      1 I-L+1))/DENOM
      D=(PHO(I,L)-PHO(I,L+1)-PHO(I,L+1)+PHO(I,L+1))/DENOM
      UPRI=(A+B*ANG(L))*SCOS(ANG(L))-(A+B*ANG(L+1))*
      1 COS(ANG(L+1))+B*SIN(ANG(L+1))-SIN(ANG(L))
      CURRENT=UPRI*(0.5*VUI(13)*EXPVIZ(13)+0.25*SDPTI*EFTUI(13))
      UPRI=0.5*(EXPVIZ(13)*EFTUI(13)+0.25*SDPTI*EFTUI(13))
      CURRENT=CURRENT*UPRI*(C1*(COS(ANG(L))-COS(ANG(L+1))+B*SIN(ANG(L))*SCOS(ANG(L))
      1 COS(ANG(L+1))-ANG(L+1)*SCOS(ANG(L+1))+SIN(ANG(L+1))-SIN(ANG(L))))
      CARRIV=CARRIV+CURRENT
      GO TO 340
      C
      START COMPUTATIONS FOR THE NONREGULAR CASE
      C
      CASE NO 1-----
      400 CONTINUE
      PA=BOUNDI(I,L+1)
      PB=BOUNDL(I,L+1)
      PD=(PHO(I,L+1)-PHO(I,L))/(ANG(L+1)-ANG(L))
      1 (ANG(L+1)-ANG(L))+PHO(I,L)
      C
      REGION 1
      C-----
      D1=(PB-PD*PHO(I,L)+PHO(I,L+1))/(ANG(L+1)-ANG(L))*VUI(13)-
      1 VUI(13)
      C1=(ANG(L)*BANG(L+1)-PHO(I,L)-PHO(I,L+1)-ANG(L)*BANG(L+1))/
      1 (ANG(L+1)-ANG(L))*VUI(13)-VUI(13)
      D2=(PB-PD*PHO(I,L))/(ANG(L+1)-ANG(L))-D1*VUI(13)
      A1=PB-B1*ANG(L+1)-C1*VUI(13)-D1*ANG(L+1)*VUI(13)
      C
      REGION 2
      C-----
      VA=VUI(I,L+1)
      ANGB=ANG(L+1)
      D2=(PB-PD*PHO(I,L+1)-PA*PHO(I,L+1))*VUI(13)-VUI(13)
      1 (VA*VUI(13)-VUI(13)-VUI(13)-VUI(13)-VUI(13)-VUI(13)-
      2 (PB-PD)*BANG(L+1)*VUI(13)-PA*PHO(I,L+1)*BANG(L+1)*VUI(13)
      1 VUI(13))/(VA-VUI(13)-VUI(13)-VUI(13)-VUI(13)-VUI(13)-
      2 (PB-PD*PHO(I,L+1)-PA*PHO(I,L+1))-D2*VUI(13)-
      3 A2*PHO(I,L+1)-D2*ANG(L+1)-C2*VUI(13)-D2*VUI(13)*BANG(L+1)
      C
      UPRI=(A1+B1*ANG(L))*SCOS(ANG(L))-(A1+B1*ANG(L+1))*SCOS(ANG(L+1))
      1 B1*(SIN(ANG(L))-SIN(ANG(L+1)))
      CURRENT=UPRI*(0.5*VUI(13)*EXPVIZ(13)+0.25*SDPTI*EFTUI(13))
      UPRI=0.5*(EXPVIZ(13)*EFTUI(13)+0.25*SDPTI*EFTUI(13))
      CURRENT=CURRENT*UPRI*(C1*(COS(ANG(L))-COS(ANG(L+1))+B1*(SIN(ANG(L))*SCOS(ANG(L))
      1 COS(ANG(L+1))-ANG(L+1)*SCOS(ANG(L+1))+SIN(ANG(L+1))-SIN(ANG(L))))
      C
      STEP=(ANG(L+1)-ANG(L))/FLOAT(KSTEP)
      STEPA=ANG
      STEP=(VUI(I,L+1)-VUI(I))/FLOAT(KSTEP)
      STEPB=VUI(I)
      C
      DO 401 K=1,KSTEP
      STEPA=ANG+STEP
      UPRI=(A2+B2*ANG)*SCOS(STEPA)-(A2+B2*ANG)*SCOS(STEPA)+
      1 B2*(SIN(STEPA)-SIN(STEPA))
      CURRENT=CURRENT*UPRI*(0.5*VUI(13)*EXPVIZ(13)+0.25*SDPTI*EFTUI(13))
      UPRI=0.5*(EXPVIZ(13)*EFTUI(13)+0.25*SDPTI*EFTUI(13))
      CURRENT=CURRENT*UPRI*(C2*(COS(STEPA)-COS(STEPA))+
      1 B2*(STEP*SCOS(STEPA)-STEP*SCOS(STEPA)+SIN(STEPA)-SIN(STEPA)))
      STEPB=STEPS+STEP
      STEPA=STEPS
      401 CONTINUE
      CARRIV=CARRIV+CURRENT
      CUM=CUM+CUM
      901 FORMAT(9,901) J,I,L,CUM
      C
      GO TO 340
      C
      CASE NO 2-----
      410 D1=(BOUNDI(I,L+1)-PHO(I,L+1))*VUI(13)-VUI(13)-VUI(13)-
      1 VUI(13)-VUI(13)-VUI(13)-VUI(13)-VUI(13)-VUI(13)-
      2 (VUI(13)-VUI(13)-VUI(13)-VUI(13)-VUI(13)-VUI(13)-
      3 VUI(13)-VUI(13))
      C1=(BOUNDI(I,L+1)-PHO(I,L+1)+BANG(L)*VUI(13)-VUI(13))/VUI(13)
      1 VUI(13)
      B=(PHO(I,L)-PHO(I,L+1)-BANG(L+1)*VUI(13)-VUI(13))/ANG(L)-
      1 ANG(L+1)
      A=PHO(I,L+1)-BANG(L+1)-C1*VUI(13)-BANG(L+1)*VUI(13)
      CURRENT=0.0
      UPRI=(A1+B1*ANG(L+1)-C1*VUI(13)-BANG(L+1)*VUI(13))
      STEPA=ANG(I+1)+STEP
      STEPB=ANG(I+1)+STEP

```

[illegible]

```

1  PSAVE(144,10),CSAVE(144,10),PSECTR(144),CSECTR(144),
2  DELEE(20),DELMAX(144),EMAX(144),ETA(20),BSCAT(144),
3  BNA(2),144),BSCAT(144),PMU(20,40),
4  LANG(40),CPHONK(144),SUMANG,ANGD,BOUNDL(20,40),BOUNDI(20,40),
5  ANGL(20,40),VLI(20,40),ICHECK(20,40),RATIO(13),IROOT(144),
6  SIFAU(144),JLOCAL(144),ICOM(144),
7  IVE(20),EV(8),MLEV,NTINES,ILEV,TIMIN(20),TIMAX(20),VIMUN(20),
8  ZA(144),B(144),C(144),BB(144),BM(144),TM(144),DM(144),
9  YEM(144),TWOCS(700),
10 IFLG,NPOINT,M,IGEOM,ISYN,IPDIS,NSECT,NPEROD,NPEROD,INDIM,
11 GAMMA,DVUX(70,48),DVUY(70,48),Y(144),DELTA,DELTA,
12 SYS(66,48),XS(66),XSS(70),
13 IVARLE(4),T,DELTA,SBOUND,NDIN,PQT,M,J1,RP1,RP12,RPINAF,SOTPI,
14 2SAY,TEMPE1,TEMPE2,DEME1,DEME2,DEMI1,DEMI2,TEMPI1,TEMPI2,
15 STEPFR,LUN3,LUN4,LUN5,LUN6,LUN7,LUN8,LUN9,LUN10,
16 IDTL(144),JDTL(144),PERSEC(144),SECIND(144),IPANEL(144),
17 ZPERPAN(144,4),PANIND(144),
18 ICION(144),CELEC(144),CSECI(144),CSECI(144),CPHOTO(144),
19 2CPHOT(144),CBSCAT(144),CBSCAI(144),SECPRN(144),SECPRI(144),
20 3PHI(144),CGUM(144),
21 KASE,JOHL,DPHI,NANG,RAD,PBOUND,OMEGA,ALPHA,SO,JP,IS,ECS,
22 2EXPU(20),EFTVI(20),IERROR,TETHIN,TETMAX,BETA1,BETA2,JLESS,
23 3L2,CARRIV,CPM,XI,CSECEL,CSECEI,CS,CS,CS1,CB1
24 DATA DELMIN,ACCIN/18,1.E-2/
C
C
C
160 JLESS=0
2 JJJJ=0
3 KAAA=0
4 LLLL=0
5 TOLD=TETHIN
6 TOLD=TETMAX
7 VEL=SQRT(BETA2)
C
C
C
C CALCULATE THE ANGLES ZERO AND PIE AND RPIAF
C ANGLE ZERO
8 TETHIN=0
9 TETMAX=RP1
10 TETNE=RPINAF
C
C
11 DBETA=DVUX(1,J)/(2.0*BETA2*GAMMA)+1.0
12 IF(DBETA,LT,0.0) GO TO 1000
13 VARLE(1)=SO
14 VARLE(2)=0.0
15 VARLE(3)=Y(J)
16 VARLE(4)=VEL
17 T=0
18 DELT=H
19 CALL ORBIT(SO,BETA1,J)
20 501 FORMAT(1X,5F13.5,2I4,3F13.5)
21 IF(VARLE(1),GE,.(SBOUND-DELTA))KKKK=1
C
C
C
C ANGLE PIE
22 1000 VARLE(1)=SO
23 VARLE(2)=0.0
24 VARLE(3)=Y(J)
25 VARLE(4)=VEL
26 T=0
27 DELT=H
28 DBETA=DVUX(1,J)/(2.0*BETA2*GAMMA)-1.0
29 IF(DBETA,GT,0.0) GO TO 2000
30 CALL ORBIT(SO,BETA1,J)
31 IF(VARLE(1),GE,.(SBOUND-DELTA))JJJJ=1
C IF PARTICLE ESCAPES AT BOTH ZERO AND PIE, RETURN TO ION
32 IF(JJJJ,EG,1,AND,KKKK,EG,1)RETURN
C
C
C
C ANGLE RPI/2
C
2000 VARLE(1)=SO
3 VARLE(2)=VEL
4 VARLE(3)=Y(J)
5 VARLE(4)=0.0
6 T=0
7 DELT=H
8 CALL ORBIT(SO,BETA1,J)
9 IF(VARLE(1),GE,.(SBOUND-DELTA))LLLL=1
10 IF(LLLL,NE,1) GO TO 5000
11 TETHIN=RPINAF
12 TETLO=RPINAF
C
C PARTICLE ESCAPES AT RPIAF
C FIND MINIMUM ANGLE TETHIN BY BISECTION
C
13 IF(KKKK,EG,1) GO TO 4000
C
3000 TETHIN=(TETHIN+TETLO)/2.0
4 VARLE(1)=SO
5 VARLE(2)=VEL*BSIN(TETHIN)
6 VARLE(3)=Y(J)
7 VARLE(4)=VEL*CCOS(TETHIN)
8 T=0.0
9 DELT=H
10 CALL ORBIT(SO,BETA1,J)
11 IF(VARLE(1),GE,.(SBOUND-DELTA)) TETHIN=TETHIN
12 IF(VARLE(1),LT,0) TETHIN=TETHIN
13 IF(TETHIN-TETLO,GE,ACCIN) GO TO 3000
C
C FIND MAXIMUM ANGLE TETMAX BY BISECTION
C
14 IF(JJJJ,EG,1) RETURN
C
4000 CONTINUE
4500 TETMAX=(TETLO+TETMAX)/2.0
5 VARLE(1)=SO
6 VARLE(2)=VEL*BSIN(TETMAX)
7 VARLE(3)=Y(J)
8 VARLE(4)=VEL*CCOS(TETMAX)
9 T=0.0
10 DELT=H
11 CALL ORBIT(SO,BETA1,J)
12 IF(VARLE(1),GE,.(SBOUND-DELTA)) TETLO=TETMAX
13 IF(VARLE(1),LE,0) TETMAX=TETMAX
14 IF(TETMAX-TETLO,GE,ACCIN) GO TO 4500
15 TETMAX=TETLO
16 RETURN
C
C
C
5000 CONTINUE
C THIS SECTION ATTEMPTS TO FIND AT LEAST ONE ALLOWED ORBIT WHEN
C ALL RRRR,JJJJ,LLLL=0.
C DO ANGLE SCANNING FROM LEFT TO RIGHT EVERY 10 DEGREES
4999 DO 5001 L=1,17
1 TETHIN=RP1+DELTA(L)/DELTHIN
2 ADDH=L*H
3 VARLE(1)=SO
4 VARLE(2)=VEL*BSIN(TETHIN)
5 VARLE(3)=Y(J)
6 VARLE(4)=VEL*CCOS(TETHIN)
7 T=0.0
8 DELT=H
9 CALL ORBIT(SO,BETA1,J)
10 IF(VARLE(1),GE,.(SBOUND-DELTA)) GO TO 5002
11 IF(VARLE(1),LT,0) GO TO 5002
12 TETLO=TETHIN
13 TETMAX=TETHIN
14 GO TO 3000
C
C
C
5002 TETMIN=TETNE-RP1/DELTHIN
1 TETMAX=TETNE
2 TETLO=TETNE
3 GO TO 3000
C
C
C
END
3000 ROUTINE ORBIT(SO,BETA1,J)
C FOR MORE EFFICIENT SCHEME SEE BURDEN 7
C
C
C *****
C PURPOSE:
C 1 TO COMPUTE ORBITS NUMERICALLY USING RUNGE-KUTTA TECHNIQUES
C
C *****
C
C IMPLICIT DOUBLE PRECISION (A-H,O-Z)
C INTEGER PERSEC,SECIND,PERPAN,PANIND
C COMMON/BLK1/
1 PSAVE(144,10),CSAVE(144,10),PSECTR(144),CSECTR(144),
2 DELEE(20),DELMAX(144),EMAX(144),ETA(20),BSCAT(144),
3 BSCAT2(144),BSCAT3(144),PHO(20,40),
4 LANG(40),CPHONK(144),SUMANG,ANGD,BOUNDL(20,40),BOUNDI(20,40),
5 ANGL(20,40),VLI(20,40),ICHECK(20,40),RATIO(13),IROOT(144),
6 SIFAU(144),JLOCAL(144),ICOM(144),
7 IVE(20),EV(8),MLEV,NTINES,ILEV,TIMIN(20),TIMAX(20),VIMUN(20),
8 ZA(144),B(144),C(144),BB(144),BM(144),TM(144),DM(144),
9 YEM(144),TWOCS(700),
10 IFLG,NPOINT,M,IGEOM,ISYN,IPDIS,NSECT,NPEROD,NPEROD,INDIM,
11 GAMMA,DVUX(70,48),DVUY(70,48),Y(144),DELTA,DELTA,
12 SYS(66,48),XS(66),XSS(70),
13 IVARLE(4),T,DELTA,SBOUND,NDIN,PQT,M,J1,RP1,RP12,RPINAF,SOTPI,
14 2SAY,TEMPE1,TEMPE2,DEME1,DEME2,DEMI1,DEMI2,TEMPI1,TEMPI2,
15 STEPFR,LUN3,LUN4,LUN5,LUN6,LUN7,LUN8,LUN9,LUN10,
16 IDTL(144),JDTL(144),PERSEC(144),SECIND(144),IPANEL(144),
17 ZPERPAN(144,4),PANIND(144),
18 ICION(144),CELEC(144),CSECI(144),CSECI(144),CPHOTO(144),
19 2CPHOT(144),CBSCAT(144),CBSCAI(144),SECPRN(144),SECPRI(144),
20 3PHI(144),CGUM(144),
21 KASE,JOHL,DPHI,NANG,RAD,PBOUND,OMEGA,ALPHA,SO,JP,IS,ECS,
22 2EXPU(20),EFTVI(20),IERROR,TETHIN,TETMAX,BETA1,BETA2,JLESS,
23 3L2,CARRIV,CPM,XI,CSECEL,CSECEI,CS,CS,CS1,CB1
24 DATA TOL/1.0E-5/
25 BETA2=BETA1-Y(1,J)/GAMMA
26 DELT=H
27 IF(BETA2,NE,0.0) DELT=H/SQRT(BETA2)
C COMPUTE TIME TO TURNING POINT AND FIND BETTER TIME STEP
28 TAU=2.0*VARLE(2)*GAMMA/DVUX(1,J)
29 IF(TAU,GT,0.0,AND,TAU/20.0,LT,DELT) DELT=TAU
C
C
C
C PRINT(S)=0.0
C KDEC=0
C
C IRHO=0
C
C COMPUTE DERIVATIVES
C CALL FCT(DERY,BETA1,IRHO,IBETA1)
C
C SAVE VALUES OF PARAMETERS
11 DO 100 I=1,NDIN
2 VARLE(I)=VARLE(I)
3 SADV(I)=DERV(I)
100 CONTINUE
C
12 DO 1 I=1,NDIN
3 AK1(I)=DELTDERY(I)
4 VARLE(I)=0.5*AK1(I)+SAVE(I)
1 CONTINUE
C
C CALL OUTP(SO,PRINT)
C IF(PRINT(S),NE,0.0) RETURN
C CALL FCT(DERY,BETA1,IRHO,IBETA1)
C IF(1BETA1,EG,1) GO TO 10
C
C DO 2 I=1,NDIN
3 AK2(I)=DELTDERY(I)
4 VARLE(I)=0.5*AK2(I)+SAVE(I)
2 CONTINUE
C
C CALL OUTP(SO,PRINT)
C IF(PRINT(S),NE,0.0) RETURN
C CALL FCT(DERY,BETA1,IRHO,IBETA1)
C IF(1BETA1,EG,1) GO TO 10
C
C DO 3 I=1,NDIN
3 AK3(I)=DELTDERY(I)
4 VARLE(I)=AK3(I)+SAVE(I)
3 CONTINUE
C
C CALL OUTP(SO,PRINT)
C IF(PRINT(S),NE,0.0) RETURN
C CALL FCT(DERY,BETA1,IRHO,IBETA1)
C IF(1BETA1,EG,1) GO TO 10
C
C DO 4 I=1,NDIN
3 AK4(I)=DELTDERY(I)
4 CONTINUE
C
C COMPUTE THE NEW VALUES OF THE VARIABLES
C DO 5 I=1,NDIN
3 VARLE(I)=(AK1(I)+2.0*AK2(I)+AK3(I)+AK4(I))/4.0+SAVE(I)
5 CONTINUE
C
C CALL OUTP(SO,PRINT)
C IF(PRINT(S),NE,0.0) RETURN
C CALL FCT(DERY,BETA1,IRHO,IBETA1)
C IF(1BETA1,EG,1) GO TO 10
C
C COMPUTE TRUNCATION ERROR
C DO 6 I=1,NDIN
3 TE(I)=(AK1(I)+AK4(I)-2.0*AK3(I))/4.0
6 CONTINUE
C
C COMPUTE RELATIVE ERROR FOR EACH VARIABLE
C
C INT=0
C IRA=0
C DO 7 I=1,NDIN
3 RTE(I)=0.0
C IF(VARLE(I),NE,0.0) RTE(I)=TE(I)/VARLE(I)
C IF(ABS(RTE(I)),GT,TH) INT=INT+1

```

```

2 PERPAN(144),PANI(144),
3 I(TUM1(144),LELEU(144),LEUC(144),USEL(144),CPHUTU(144),
4 CPNPHI(144),CBSCAT(144),CBSCAT(144),SECPN(144),SECPN(144),
5 PHIT(144),IGUM(144),
6 J=JUM1,DPH1,NAHD,RAD,PROWD,ONG,GAL,PRNA,SO,J=15,EUS,
7 EXPIZ(20),EFTUI(20),TEERRD,ETETHIN,ETEMAX,MEI(2),MEI(2),JLS5,
8 J,2,CAKRV,CPH,XT,CSECEL,CSECEL,CS,CS,CS,CS,
9 IETAI=0
10 I A=1,NDIN
11 U=1-VARIABLE(1)
12 I=1-IFX(VARIABLE(1)/DELTA)*1
13 ORB=VARIABLE(3)
14 IF(ORB,LT,0.0) ORB=ORB+RP12
15 IF(ORB,GE,RP12) ORB=ORB-RP12
16 IF(ORB,LT,0.0,OR,ORB,GE,RP12) GO TO 11
17 DO 12 J=1,N
18 IF(ORB,LT,Y(J)) GO TO 13
19 IF(ORB,GE,Y(N)) GO TO 14
20 IF(ORB,GE,Y(J),AND,ORB,LT,Y(J+1)) GO TO 15
21 CONTINUE
22 GO TO 15
23 A=ORB+RP12
24 J=N
25 JP1=1
26 GO TO 14
27 J=N
28 JP1=1
29 A=ORB
30 GO TO 14
31 JP1=JP1
32 IF(J,EQ,N) JP1=1
33 A=ORB
34 CONTINUE
35 S=VARIABLE(1)
36 IP1=1
37 B=LINAR INTERPOLATION ON POTENTIAL DERIVATIVES
38 S=SI(1)/DELTA
39 BB=(A-Y(J))/DELTA
40 NP2=NP2
41 DO 32 II=1,NP2
42 IF(VARIABLE(1),GE,XSS(II),AND,VARIABLE(1),LT,XSS(II+1)) GO TO 32
43 II=II+1
44 AAA=(S-XSS(II))/(XSS(II+1)-XSS(II))
45 DXXA=(1.0-AAA)*S(1.0-DB)*SDVX(II),J)+SSS(1.0-AAA)*SDVX(II,J)+
46 AAA*(1.0-DB)*SDVX(II+1,J)+AAA*SSB*SDVX(II+1,J)
47 DO 33 J=1,N
48 IF(ORB,LT,Y(1)+0.5*DELTA)) GO TO 34
49 IF(ORB,GE,Y(N)+0.5*DELTA)) GO TO 35
50 J=J+1
51 IF(J,EQ,N) J=1
52 IF(ORB,GE,Y(J)+0.5*DELTA),AND,ORB,LT,
53 Y(J+1)+0.5*DELTA) GO TO 34
54 CONTINUE
55 J=N
56 J=1
57 A=ORB+RP12
58 GO TO 37
59 J=N
60 J=1
61 A=ORB
62 GO TO 37
63 A=ORB
64 SSB=(AD-Y(J)-0.5*DELTA)/DELTA
65 DXXA=EXP(1.0-DB)*SDVY(1,J)+SSB*(1.0-DB)*SDVY(1,J)+
66 AAA*(1.0-DB)*SDVY(1,J)+AAA*SSB*SDVY(1,J)
67 B=LINAR INTERPOLATION ON POTENTIAL
68 AA=EXP(S)-EXP(XB(1))/(EXP(XB(1+1))-EXP(XB(1)))
69 POT=(1.0-DB)*S(1.0-DB)*SDV(1,J)+SSB*(1.0-DB)*SDV(1,J)+
70 AAA*(1.0-DB)*SDV(1,J)+AAA*SSB*SDV(1,J)
71 EXPA=EXP(-VARIABLE(1))
72 PETA2=ETA1-POT/GAMMA
73 IF(PETA2,LE,0.0) IETAI=1
74 IF(PETA2,LE,0.0) RETURN
75 SEX=0.5*EXP(-2.0*VARIABLE(1))
76 DERY(1)=VARIABLE(2)
77 DERY(4)=VARIABLE(4)*SS2-VARIABLE(2)*SS2-SEX*SDXA/GAMMA
78 DERY(3)=-2.0*VARIABLE(2)*VARIABLE(4)-SEX*SDYA/GAMMA
79 DERY(4)=VARIABLE(4)
80 RETURN
81 END
82 SUBROUTINE GUESS(PHI,PSECTA,CSECTR,Y)
83
84
85
86
87
88
89
90
91
92
93
94
95
96
97
98
99
100
101
102
103
104
105
106
107
108
109
110
111
112
113
114
115
116
117
118
119
120
121
122
123
124
125
126
127
128
129
130
131
132
133
134
135
136
137
138
139
140
141
142
143
144
145
146
147
148
149
150
151
152
153
154
155
156
157
158
159
160
161
162
163
164
165
166
167
168
169
170
171
172
173
174
175
176
177
178
179
180
181
182
183
184
185
186
187
188
189
190
191
192
193
194
195
196
197
198
199
200
201
202
203
204
205
206
207
208
209
210
211
212
213
214
215
216
217
218
219
220
221
222
223
224
225
226
227
228
229
230
231
232
233
234
235
236
237
238
239
240
241
242
243
244
245
246
247
248
249
250
251
252
253
254
255
256
257
258
259
260
261
262
263
264
265
266
267
268
269
270
271
272
273
274
275
276
277
278
279
280
281
282
283
284
285
286
287
288
289
290
291
292
293
294
295
296
297
298
299
300
301
302
303
304
305
306
307
308
309
310
311
312
313
314
315
316
317
318
319
320
321
322
323
324
325
326
327
328
329
330
331
332
333
334
335
336
337
338
339
340
341
342
343
344
345
346
347
348
349
350
351
352
353
354
355
356
357
358
359
360
361
362
363
364
365
366
367
368
369
370
371
372
373
374
375
376
377
378
379
380
381
382
383
384
385
386
387
388
389
390
391
392
393
394
395
396
397
398
399
400
401
402
403
404
405
406
407
408
409
410
411
412
413
414
415
416
417
418
419
420
421
422
423
424
425
426
427
428
429
430
431
432
433
434
435
436
437
438
439
440
441
442
443
444
445
446
447
448
449
450
451
452
453
454
455
456
457
458
459
460
461
462
463
464
465
466
467
468
469
470
471
472
473
474
475
476
477
478
479
480
481
482
483
484
485
486
487
488
489
490
491
492
493
494
495
496
497
498
499
500
501
502
503
504
505
506
507
508
509
510
511
512
513
514
515
516
517
518
519
520
521
522
523
524
525
526
527
528
529
530
531
532
533
534
535
536
537
538
539
540
541
542
543
544
545
546
547
548
549
550
551
552
553
554
555
556
557
558
559
560
561
562
563
564
565
566
567
568
569
570
571
572
573
574
575
576
577
578
579
580
581
582
583
584
585
586
587
588
589
590
591
592
593
594
595
596
597
598
599
600
601
602
603
604
605
606
607
608
609
610
611
612
613
614
615
616
617
618
619
620
621
622
623
624
625
626
627
628
629
630
631
632
633
634
635
636
637
638
639
640
641
642
643
644
645
646
647
648
649
650
651
652
653
654
655
656
657
658
659
660
661
662
663
664
665
666
667
668
669
670
671
672
673
674
675
676
677
678
679
680
681
682
683
684
685
686
687
688
689
690
691
692
693
694
695
696
697
698
699
700
701
702
703
704
705
706
707
708
709
710
711
712
713
714
715
716
717
718
719
720
721
722
723
724
725
726
727
728
729
730
731
732
733
734
735
736
737
738
739
740
741
742
743
744
745
746
747
748
749
750
751
752
753
754
755
756
757
758
759
760
761
762
763
764
765
766
767
768
769
770
771
772
773
774
775
776
777
778
779
780
```

```

      2EXPV12(20),EFTV1(20),TERROR,TETMIN,TETMAX,METAI,BETA2,JLESS,
      3L2,CARRIV,CPH,XI,CSECEL,CSECE1,CS,CS,CBI,CBI
      4INTEGER I,J,N,L,N,N,T
      5DATA IXL,5,DE,3
      6DATA ISMITH,0
      7
      8DO I=1,NSECT
      9CURM(I)=0.0
     10CURP(I)=0.0
     11PHIN(I)=0
     12PHIP(I)=0
     13CONTINUE
     14
     15NTOUR=1
     16NTOUR=NTOUR+1
     17IF (NTOUR.GE.800) WRITE (9,400)
     18FORMAT (1X,4NO CONVERGENCE IN GUESS FIELD AFTER 800 ITER8)
     19IF (NTOUR.GE.800) STOP
     20L=0
     21DO 100 I=1,NSECT
     22ECS=0.0
     23CE1(I)=0.0
     24CN=0.0
     25N=PERSEC(I)
     26N=L*N
     27T=L*I
     28
     29DO 90 J=T,N
     30N=SECIND(J)
     31ECS=ECS+CURENT(N,PHI(N),Y(N),CE,CPH,CS,CB,CSECEL)
     32CET(I)=CET(I)+CE
     33PSECTR(I)=PHI(N)
     34CONTINUE
     35L=L+N
     36CSECTR(I)=ECS
     37CONTINUE
     38
     39C PREPARE DATA FOR REGULAR FALSI METHOD
     40IF (NTOUR-1) 201,401,401
     41DO 210 I=1,NSECT
     42IF (CSECTR(I).GT.0.0) GO TO 111
     43CURM(I)=CSECTR(I)
     44PHIN(I)=PSECTR(I)
     45PSECTR(I)=PSECTR(I)-0.0
     46GO TO 210
     47CURP(I)=CSECTR(I)
     48PHIP(I)=PSECTR(I)
     49PSECTR(I)=PSECTR(I)+0.0
     50CONTINUE
     51GO TO 500
     52
     53C BEGIN REGULA FALSI ITERATION
     54401 K=0
     55DO 410 I=1,NSECT
     56IF (ABS(CSECTR(I)).LE.TOLCET(I)) GO TO 410
     57IF (CURM(I).EQ.0.0) PHIN(I)=PSECTR(I)
     58IF (CURN(I).EQ.0.0) CURN(I)=CSECTR(I)
     59IF (CURP(I).EQ.0.0) PHIP(I)=PSECTR(I)
     60IF (CURM(I).EQ.0.0) CURP(I)=CSECTR(I)
     61K=K+1
     62IF (CURN(I)+CSECTR(I).GE.0.0) GO TO 420
     63CURP(I)=CSECTR(I)
     64PHIP(I)=PSECTR(I)
     65GO TO 430
     66CURN(I)=CSECTR(I)
     67PHIN(I)=PSECTR(I)
     68IF (CURN(I)+CURP(I).LE.0.0) GO TO 440
     69IF (CURN(I).GE.0.0) PSECTR(I)=PSECTR(I)+0.1
     70IF (CURP(I).LE.0.0) PSECTR(I)=PSECTR(I)-0.1
     71GO TO 410
     72PSECTR(I)=(PHIN(I)+CURP(I)-PHIP(I)+CURN(I))/(CURP(I)-CURN(I)
     731)
     74CONTINUE
     75IF (K.NE.0) GO TO 500
     76WRITE (9,401)
     77401 FORMAT (1X,0 OK PAST GUESS FIELD8)
     78WRITE (9,6001) (PHI(J),J=1,NPOINT)
     794001 FORMAT (6(1X,1PE12.3))
     80ISMITH=1
     81
     82C
     83500 L=0
     84DO 501 I=1,NSECT
     85PHINEM=PSECTR(I)
     86K=PERSEC(I)
     87N=L*K
     88T=L*I
     89DO 510 J=T,N
     90N=SECIND(J)
     91PHI(N)=PHINEM
     92CONTINUE
     93L=L+N
     94501 CONTINUE
     95IF (ISMITH.EQ.1) RETURN
     96GO TO 10
     97END
     98
     99FUNCTION CURENT (J,XI,YY,CE,CPH,CS,CB,CSECEL)
    100C PURPOSE: TO COMPUTE CURRENT COLLECTION AT GRID POINTS FOR GUESS FIELD.
    101C
    102C
    103C
    104C
    105C
    106C
    107C
    108C
    109C
    110C
    111C
    112C
    113C
    114C
    115C
    116C
    117C
    118C
    119C
    120C
    121C
    122C
    123C
    124C
    125C
    126C
    127C
    128C
    129C
    130C
    131C
    132C
    133C
    134C
    135C
    136C
    137C
    138C
    139C
    140C
    141C
    142C
    143C
    144C
    145C
    146C
    147C
    148C
    149C
    150C
    151C
    152C
    153C
    154C
    155C
    156C
    157C
    158C
    159C
    160C
    161C
    162C
    163C
    164C
    165C
    166C
    167C
    168C
    169C
    170C
    171C
    172C
    173C
    174C
    175C
    176C
    177C
    178C
    179C
    180C
    181C
    182C
    183C
    184C
    185C
    186C
    187C
    188C
    189C
    190C
    191C
    192C
    193C
    194C
    195C
    196C
    197C
    198C
    199C
    200C
    201C
    202C
    203C
    204C
    205C
    206C
    207C
    208C
    209C
    210C
    211C
    212C
    213C
    214C
    215C
    216C
    217C
    218C
    219C
    220C
    221C
    222C
    223C
    224C
    225C
    226C
    227C
    228C
    229C
    230C
    231C
    232C
    233C
    234C
    235C
    236C
    237C
    238C
    239C
    240C
    241C
    242C
    243C
    244C
    245C
    246C
    247C
    248C
    249C
    250C
    251C
    252C
    253C
    254C
    255C
    256C
    257C
    258C
    259C
    260C
    261C
    262C
    263C
    264C
    265C
    266C
    267C
    268C
    269C
    270C
    271C
    272C
    273C
    274C
    275C
    276C
    277C
    278C
    279C
    280C
    281C
    282C
    283C
    284C
    285C
    286C
    287C
    288C
    289C
    290C
    291C
    292C
    293C
    294C
    295C
    296C
    297C
    298C
    299C
    300C
    301C
    302C
    303C
    304C
    305C
    306C
    307C
    308C
    309C
    310C
    311C
    312C
    313C
    314C
    315C
    316C
    317C
    318C
    319C
    320C
    321C
    322C
    323C
    324C
    325C
    326C
    327C
    328C
    329C
    330C
    331C
    332C
    333C
    334C
    335C
    336C
    337C
    338C
    339C
    340C
    341C
    342C
    343C
    344C
    345C
    346C
    347C
    348C
    349C
    350C
    351C
    352C
    353C
    354C
    355C
    356C
    357C
    358C
    359C
    360C
    361C
    362C
    363C
    364C
    365C
    366C
    367C
    368C
    369C
    370C
    371C
    372C
    373C
    374C
    375C
    376C
    377C
    378C
    379C
    380C
    381C
    382C
    383C
    384C
    385C
    386C
    387C
    388C
    389C
    390C
    391C
    392C
    393C
    394C
    395C
    396C
    397C
    398C
    399C
    400C
    401C
    402C
    403C
    404C
    405C
    406C
    407C
    408C
    409C
    410C
    411C
    412C
    413C
    414C
    415C
    416C
    417C
    418C
    419C
    420C
    421C
    422C
    423C
    424C
    425C
    426C
    427C
    428C
    429C
    430C
    431C
    432C
    433C
    434C
    435C
    436C
    437C
    438C
    439C
    440C
    441C
    442C
    443C
    444C
    445C
    446C
    447C
    448C
    449C
    450C
    451C
    452C
    453C
    454C
    455C
    456C
    457C
    458C
    459C
    460C
    461C
    462C
    463C
    464C
    465C
    466C
    467C
    468C
    469C
    470C
    471C
    472C
    473C
    474C
    475C
    476C
    477C
    478C
    479C
    480C
    481C
    482C
    483C
    484C
    485C
    486C
    487C
    488C
    489C
    490C
    491C
    492C
    493C
    494C
    495C
    496C
    497C
    498C
    499C
    500C
    501C
    502C
    503C
    504C
    505C
    506C
    507C
    508C
    509C
    510C
    511C
    512C
    513C
    514C
    515C
    516C
    517C
    518C
    519C
    520C
    521C
    522C
    523C
    524C
    525C
    526C
    527C
    528C
    529C
    530C
    531C
    532C
    533C
    534C
    535C
    536C
    537C
    538C
    539C
    540C
    541C
    542C
    543C
    544C
    545C
    546C
    547C
    548C
    549C
    550C
    551C
    552C
    553C
    554C
    555C
    556C
    557C
    558C
    559C
    560C
    561C
    562C
    563C
    564C
    565C
    566C
    567C
    568C
    569C
    570C
    571C
    572C
    573C
    574C
    575C
    576C
    577C
    578C
    579C
    580C
    581C
    582C
    583C
    584C
    585C
    586C
    587C
    588C
    589C
    590C
    591C
    592C
    593C
    594C
    595C
    596C
    597C
    598C
    599C
    600C
    601C
    602C
    603C
    604C
    605C
    606C
    607C
    608C
    609C
    610C
    611C
    612C
    613C
    614C
    615C
    616C
    617C
    618C
    619C
    620C
    621C
    622C
    623C
    624C
    625C
    626C
    627C
    628C
    629C
    630C
    631C
    632C
    633C
    634C
    635C
    636C
    637C
    638C
    639C
    640C
    641C
    642C
    643C
    644C
    645C
    646C
    647C
    648C
    649C
    650C
    651C
    652C
    653C
    654C
    655C
    656C
    657C
    658C
    659C
    660C
    661C
    662C
    663C
    664C
    665C
    666C
    667C
    668C
    669C
    670C
    671C
    672C
    673C
    674C
    675C
    676C
    677C
    678C
    679C
    680C
    681C
    682C
    683C
    684C
    685C
    686C
    687C
    688C
    689C
    690C
    691C
    692C
    693C
    694C
    695C
    696C
    697C
    698C
    699C
    700C
    701C
    702C
    703C
    704C
    705C
    706C
    707C
    708C
    709C
    710C
    711C
    712C
    713C
    714C
    715C
    716C
    717C
    718C
    719C
    720C
    721C
    722C
    723C
    724C
    725C
    726C
    727C
    728C
    729C
    730C
    731C
    732C
    733C
    734C
    735C
    736C
    737C
    738C
    739C
    740C
    741C
    742C
    743C
    744C
    745C
    746C
    747C
    748C
    749C
    750C
    751C
    752C
    753C
    754C
    755C
    756C
    757C
    758C
    759C
    760C
    761C
    762C
    763C
    764C
    765C
    766C
    767C
    768C
    769C
    770C
    771C
    772C
    773C
    774C
    775C
    776C
    777C
    778C
    779C
    780C
    781C
    782C
    783C
    784C
    785C
    786C
    787C
    788C
    789C
    790C
    791C
    792C
    793C
    794C
    795C
    796C
    797C
    798C
    799C
    800C
    801C
    802C
    803C
    804C
    805C
    806C
    807C
    808C
    809C
    810C
    811C
    812C
    813C
    814C
    815C
    816C
    817C
    818C
    819C
    820C
    821C
    822C
    823C
    824C
    825C
    826C
    827C
    828C
    829C
    830C
    831C
    832C
    833C
    834C
    835C
    836C
    837C
    838C
    839C
    840C
    841C
    842C
    843C
    844C
    845C
    846C
    847C
    848C
    849C
    850C
    851C
    852C
    853C
    854C
    855C
    856C
    857C
    858C
    859C
    860C
    861C
    862C
    863C
    864C
    865C
    866C
    867C
    868C
    869C
    870C
    871C
    872C
    873C
    874C
    875C
    876C
    877C
    878C
    879C
    880C
    881C
    882C
    883C
    884C
    885C
    886C
    887C
    888C
    889C
    890C
    891C
    892C
    893C
    894C
    895C
    896C
    897C
    898C
    899C
    900C
    901C
    902C
    903C
    904C
    905C
    906C
    907C
    908C
    909C
    910C
    911C
    912C
    913C
    914C
    915C
    916C
    917C
    918C
    919C
    920C
    921C
    922C
    923C
    924C
    925C
    926C
    927C
    928C
    929C
    930C
    931C
    932C
    933C
    934C
    935C
    936C
    937C
    938C
    939C
    940C
    941C
    942C
    943C
    944C
    945C
    946C
    947C
    948C
    949C
    950C
    951C
    952C
    953C
    954C
    955C
    956C
    957C
    958C
    959C
    960C
    961C
    962C
    963C
    964C
    965C
    966C
    967C
    968C
    969C
    970C
    971C
    972C
    973C
    974C
    975C
    976C
    977C
    978C
    979C
    980C
    981C
    982C
    983C
    984C
    985C
    986C
    987C
    988C
    989C
    990C
    991C
    992C
    993C
    994C
    995C
    996C
    997C
    998C
    999C
    1000C
  
```

```

C CSEC N-D SEC CURRENT
C BSCAT BACA-SCATTER ELECTRON CURRENT
C CPHOTO N-D PHOTO ELECTRON CURRENT
C CETT NET CURRENT
C SECPRN N-D SEC ELECTRON CURRENT INDUCED BY PROTONS
C XI N-D POTENTIAL
C *****
C INTEGER PERSEC,SECIND,PERPAN,PANIND
C COMMON PSAVE(144,10),CSAVE(144,10),PSECTR(144),CSECTR(144),
C IDELEE(20),DELMAX(144),ENAX(144),ETA(20),BSCAT(144),
C BSCAT2(144),BSCAT3(144),PHO(20,40),
C IANG(40),CPHONX(144),SUMANG,ANGD,BOUNDL(20,40),BOUNDI(20,40),
C ZANGL(20,40),V1I(20,40),ICHECK(20,40),RATIO(13),IROOT(144),
C IFALT(144),JLDCAL(144),ICOW(144),
C IVE(20),EV(8),MLEV,NTINES,ILEV,TININ(20),TINAX(20),VINUM(20),
C ZA(144),B(144),C(144),BB(144),BM(144),TM(144),DM(144),
C JEM(144),TWCOS(700),
C IIFLG,NPOINT,N,IGDEM,ISYN,IPOIS,HSECT,NPEROD,NPEROD,INDIN,
C ZGAMMA,DVUX(70,48),DVUY(70,48),Y(144),DELTA,DELTAT,
C YS(46,48),XS(66),XSS(70),
C IVARBLE(4),T,DELT,SBOUND,NDIN,POT,H,J1,RPI,RP12,RP1MF,SOTPI,
C ZSAY,TEMP1,TEMP2,DEME1,DEME2,DENI1,DENI2,TEMP11,TEMP12,
C STEPR,LUN3,LUN4,LUN5,LUN6,LUN7,LUN8,LUN9,LUN10,
C IOTL(144),JOTL(144),PERSEC(144),SECIND(144),IPANEL(144),
C 2PERPAN(144,4),PANIND(144),
C ICION(144),CELEC(144),CSEC(144),CSEC1(144),CPHOTO(144),
C 2CPHOT(144),CBSCAT(144),CBSCA(144),SECPRN(144),SECPR1(144),
C 3PHI(144),COUN(144),
C IKASE,JOH,DPHI,HAND,RAD,PBOUND,OMEGA,ALPHA,SO,JP,IS,ECS,
C 2EXPVIZ(20),EFTVI(20),IERROR,TETMIN,TETMAX,BETA1,BETA2,JLESS,
C 3L2,CARRIV,CPH,XI,CSECEL,CSECE1,CB,CB,CB1,CB1
C *****
C IF (IFALT(1),EQ.0) CION(J)=0.0
C IF (IFALT(2),EQ.0) CELEC(J)=0.0
C IF (IFALT(3),EQ.0) CSEC(J)=0.0
C IF (IFALT(4),EQ.0) CBSCAT(J)=0.0
C IF (IFALT(5),EQ.0) CPHOTO(J)=0.0
C CPHOTO(J)=CPHOTO(J)/RATIO(9)
C CPHOTO(J)=CPHOTO(J)/RATIO(9)
C IF (IFALT(9),EQ.0) SECPRN(J)=0.0
C CETT=CION(J)+CELEC(J)+CSEC(J)+CBSCAT(J)+CPHOTO(J)+SECPRN(J)
C WRITE (LUN4,400) J,PHI(J),CETT,CION(J),CELEC(J),CPHOTO(J),CPHOT(J)
C 1,CSEC(J),CSEC1(J),CBSCAT(J),CBSCA(J),SECPRN(J),SECPR1(J)
C 400 FORMAT(13,12) (PE10,3)
C RETURN
C *****
C SUBROUTINE CBS(XI,J,CB,CB1,CB1)
C *****
C C PURPOSE IS TO FIND THE CONTRIBUTION OF SEC AND BACKS ELECTRONS TO THE
C GUESS FIELD.
C *****
C *****
C INTEGER PERSEC,SECIND,PERPAN,PANIND
C COMMON PSAVE(144,10),CSAVE(144,10),PSECTR(144),CSECTR(144),
C IDELEE(20),DELMAX(144),ENAX(144),ETA(20),BSCAT(144),
C BSCAT2(144),BSCAT3(144),PHO(20,40),
C IANG(40),CPHONX(144),SUMANG,ANGD,BOUNDL(20,40),BOUNDI(20,40),
C ZANGL(20,40),V1I(20,40),ICHECK(20,40),RATIO(13),IROOT(144),
C IFALT(144),JLDCAL(144),ICOW(144),
C IVE(20),EV(8),MLEV,NTINES,ILEV,TININ(20),TINAX(20),VINUM(20),
C ZA(144),B(144),C(144),BB(144),BM(144),TM(144),DM(144),
C JEM(144),TWCOS(700),
C IIFLG,NPOINT,N,IGDEM,ISYN,IPOIS,HSECT,NPEROD,NPEROD,INDIN,
C ZGAMMA,DVUX(70,48),DVUY(70,48),Y(144),DELTA,DELTAT,
C YS(46,48),XS(66),XSS(70),
C IVARBLE(4),T,DELT,SBOUND,NDIN,POT,H,J1,RPI,RP12,RP1MF,SOTPI,
C ZSAY,TEMP1,TEMP2,DEME1,DEME2,DENI1,DENI2,TEMP11,TEMP12,
C STEPR,LUN3,LUN4,LUN5,LUN6,LUN7,LUN8,LUN9,LUN10,
C IOTL(144),JOTL(144),PERSEC(144),SECIND(144),IPANEL(144),
C 2PERPAN(144,4),PANIND(144),
C ICION(144),CELEC(144),CSEC(144),CSEC1(144),CPHOTO(144),
C 2CPHOT(144),CBSCAT(144),CBSCA(144),SECPRN(144),SECPR1(144),
C 3PHI(144),COUN(144),
C IKASE,JOH,DPHI,HAND,RAD,PBOUND,OMEGA,ALPHA,SO,JP,IS,ECS,
C 2EXPVIZ(20),EFTVI(20),IERROR,TETMIN,TETMAX,BETA1,BETA2,JLESS,
C 3L2,CARRIV,CPH,XI,CSECEL,CSECE1,CB,CB,CB1,CB1
C *****
C DO 710 J=1,2
C IF (J,NE.1) GO TO 711
C GAMMA=RATIO(2)
C TEMPE=TEMP1
C RATE=RATIO(4)
C DEN=DENI1/DENI1
C GO TO 712
C 711 GAMMA=RATIO(10)
C TEMPE=TEMP2
C RATE=RATIO(11)
C DEN=DENI2/DENI1
C 712 CONTINUE
C IF (DEN,EQ.0.0) GO TO 710
C NUM=1
C VZERO=0.0
C IF (XI,NE.0.0)
C VZERO=MAX1(0.0,-XI/GAMMA*SORT(ABS(XI/GAMMA)))/ABS(XI/GAMMA)
C 1)
C DO 705 I=1,MLEV,ILEV
C BETA1=VI(1)882
C BETA2=BETA1-XI/GAMMA
C IF (BETA2,LE.0.0) GO TO 705
C NUM=NUM+1
C VINUM(NUM)=SORT(BETA2)
C DELEE(NUM)=7.48DELMAX(J)*BETA2*TEMP1EXP(-2.08SORT(BETA2*TEMP1/
C 1 ENAX(J))/ENAX(J)
C BSC=BSCAT3(J)*BETA2*GAMMA
C ETA(NUM)=BSCAT1(J)
C IF (BSC,LE.100.0)
C 1 ETA(NUM)=BSCAT1(J)-BSCAT2(J)EXP(-BSC)
C 705 CONTINUE
C IF (NUM,EQ.1) GO TO 710
C VINUM(1)=VZERO
C BETA2=VZERO882
C DELEE(1)=7.48DELMAX(J)*BETA2*TEMP1EXP(-2.08SORT(BETA2*TEMP1/
C 1 ENAX(J))/ENAX(J)
C BSC=BSCAT3(J)*BETA2*GAMMA
C ETA(1)=BSCAT1(J)
C IF (BSC,LE.100.0)
C 1 ETA(1)=BSCAT1(J)-BSCAT2(J)EXP(-BSC)
C NUM1=NUM-1
C CUR2=0.0
C CUR3=0.0
C COEF1=EXP(-XI/GAMMA)/SOTPI
C ABEL0=0.0
C BDEL0=0.0
C ASCA0=0.0
C BSCA0=0.0
C *****
C DO 814 I=1,NUM1
C DENOM=VINUM(I+1)-VINUM(I)
C ABEL1=(DELEE(I+1)-DELEE(I))/DENOM
C BDEL1=(DELEE(I)-ABEL1)/VINUM(I)
C ABEL1=2.08ABEL1
C BDEL1=2.08BDEL1
C CUR2=CUR2+EXP(-VINUM(I)882)*((ABEL1-ABEL0)/(1.0+VINUM(I)882)
C 1 + (BDEL1-BDEL0)/(VINUM(I)+COEFF(VINUM(I))))
C ABEL0=ABEL1
C BDEL0=BDEL1
C 814 CONTINUE
C CUR2=CUR2
C CUR3=CUR3
C IF (XI,LE.0.0) GO TO 817
C CUR2=(2.08SAY8(SORT(-XI/RATIO(13)))+COEFF(SORT(-XI/RATIO(13))))*
C 1 CUR2EXP(XI/RATIO(13))
C CUR3=(2.08SAY8(SORT(-XI/RATIO(4)))+COEFF(SORT(-XI/RATIO(4))))*
C 1 CUR3EXP(XI/RATIO(4))
C 817 CONTINUE
C IF (IFALT(3),EQ.0.0) CUR2=0.0
C IF (IFALT(4),EQ.0.0) CUR3=0.0
C CS=RATE*COEF1CUR2DEN+CS
C CB=RATE*COEF1CUR3DEN+CB
C CB1=CS1+RATE*COEF1CUR2DEN
C CB1=CB1+RATE*COEF1CUR3DEN
C 710 CONTINUE
C RETURN
C *****
C SUBROUTINE BECEL(XI,CSECEL,CSECE1)
C *****
C C *****
C C PURPOSE *****
C C TO COMPUTE SECONDARY ELECTRONS INDUCED BY PROTONS FOR THE
C C GUESS FIELD
C *****
C *****
C C EXTERNALS NONE
C *****
C *****
C INTEGER PERSEC,SECIND,PERPAN,PANIND
C COMMON PSAVE(144,10),CSAVE(144,10),PSECTR(144),CSECTR(144),
C IDELEE(20),DELMAX(144),ENAX(144),ETA(20),BSCAT(144),
C BSCAT2(144),BSCAT3(144),PHO(20,40),
C IANG(40),CPHONX(144),SUMANG,ANGD,BOUNDL(20,40),BOUNDI(20,40),
C ZANGL(20,40),V1I(20,40),ICHECK(20,40),RATIO(13),IROOT(144),
C IFALT(144),JLDCAL(144),ICOW(144),
C IVE(20),EV(8),MLEV,NTINES,ILEV,TININ(20),TINAX(20),VINUM(20),
C ZA(144),B(144),C(144),BB(144),BM(144),TM(144),DM(144),
C JEM(144),TWCOS(700),
C IIFLG,NPOINT,N,IGDEM,ISYN,IPOIS,HSECT,NPEROD,NPEROD,INDIN,
C ZGAMMA,DVUX(70,48),DVUY(70,48),Y(144),DELTA,DELTAT,
C YS(46,48),XS(66),XSS(70),
C IVARBLE(4),T,DELT,SBOUND,NDIN,POT,H,J1,RPI,RP12,RP1MF,SOTPI,
C ZSAY,TEMP1,TEMP2,DEME1,DEME2,DENI1,DENI2,TEMP11,TEMP12,
C STEPR,LUN3,LUN4,LUN5,LUN6,LUN7,LUN8,LUN9,LUN10,
C IOTL(144),JOTL(144),PERSEC(144),SECIND(144),IPANEL(144),
C 2PERPAN(144,4),PANIND(144),
C ICION(144),CELEC(144),CSEC(144),CSEC1(144),CPHOTO(144),
C 2CPHOT(144),CBSCAT(144),CBSCA(144),SECPRN(144),SECPR1(144),
C 3PHI(144),COUN(144),
C IKASE,JOH,DPHI,HAND,RAD,PBOUND,OMEGA,ALPHA,SO,JP,IS,ECS,
C 2EXPVIZ(20),EFTVI(20),IERROR,TETMIN,TETMAX,BETA1,BETA2,JLESS,
C 3L2,CARRIV,CPH,XI,CSECEL,CSECE1,CB,CB,CB1,CB1
C *****
C CSECE1=0.0
C CSECEL=0.0
C DO 710 J=1,2
C IF (J,NE.1) GO TO 711
C GAMMA=RATIO(8)
C TEMPI=TEMP11
C DEN=DENI2/DENI1
C RATE=RATIO(12)
C GO TO 712
C 711 CONTINUE
C GAMMA=RATIO(1)
C TEMPI=TEMP12
C DEN=DENI2/DENI1
C RATE=RATIO(12)
C 712 CONTINUE
C IF (TEMPI,EQ.0.0) GO TO 710
C NUM=1
C VZERO=0.0
C IF (XI,NE.0.0)
C 1 VZERO=MAX1(0.0,-XI/GAMMA*SORT(ABS(XI/GAMMA)))/
C 2 ABS(XI/GAMMA)
C *****
C DO 700 I=1,MLEV,ILEV
C BETA1=VI(1)882
C BETA2=BETA1-XI/GAMMA
C IF (BETA2,LE.0.0) GO TO 700
C NUM=NUM+1
C VINUM(NUM)=SORT(BETA2)
C DELEE(NUM)=BETP(J)*SORT(0.0018BETA2*TEMP1)/(1.0+BETA2*TEMP1/
C 1 EXP(J))
C 700 CONTINUE
C *****
C IF (NUM,EQ.1) GO TO 710
C VINUM(1)=VZERO
C BETA2=VINUM(1)882
C DELEE(1)=BETP(J)*SORT(0.0018BETA2*TEMP1)/(1.0+BETA2*TEMP1/
C 1 EXP(J))
C *****
C CUR2=0.0
C COFF1=EXP(-XI/GAMMA)/SOTPI
C ABEL0=0.0
C BDEL0=0.0
C NUM1=NUM-1
C DO 814 I=1,NUM1
C DENOM=VINUM(I+1)-VINUM(I)
C ABEL1=(DELEE(I+1)-DELEE(I))/DENOM
C BDEL1=(DELEE(I)-ABEL1)/VINUM(I)
C ABEL1=2.08ABEL1
C BDEL1=2.08BDEL1
C CUR2=CUR2+EXP(-VINUM(I)882)*((ABEL1-ABEL0)/(1.0+VINUM(I)882)
C 1 + (BDEL1-BDEL0)/(VINUM(I)+COEFF(VINUM(I))))
C ABEL0=ABEL1
C BDEL0=BDEL1
C 814 CONTINUE
C CUR2=CUR2
C CUR3=0.0
C CUR2=(2.08SAY8(SORT(-XI/RATIO(13)))+
C 1 COEFF(SORT(-XI/RATIO(13))))*EXP(XI/RATIO(13))
C CSECEL=CSECEL+COFF1CUR2RATESDEN
C CSECE1=CSECE1+COFF1CUR3RATESDEN
C 710 CONTINUE
C RETURN
C *****
C SUBROUTINE POT(IIFLG,NPEROD,N,NPEROD,H,A,B,C,INDIN,Y,IERROR,U)
C *****

```

210 CONTINUE
CALL PUT4(CFIN,MPFBOH,M,MPFBOH,M,A,B,C,INTRY,VS,11,BBBO,1,MPBO)

[illegible]

```

      INI=J-1
      IF (J.EQ.1) JMI=N
      O=((YS(I,J)-YS(I,JMI))/(2.0*DELTA Y))
      PX=((YS(I,J)-2.0*YS(I,JMI)+YS(I-1,J))/(DELTA X*DELTA X))
      OY=((YS(I,J)-2.0*YS(I,JMI)+YS(I,JMI))/(DELTA Y*DELTA Y))
      PY=((YS(I,J)-YS(I-1,J)-YS(I+1,JMI)+YS(I-1,JMI))/(
      1 (DELTA X*DELTA Y*4.0)
      2 OX=PX
      C
      DEN=PX*OY-OX*PY
      IF (DEN.NE.0.0) SX(I,J)=(O*PY-P*OY)/DEN
      IF (DEN.NE.0.0) SY(I,J)=(P*OX-O*PX)/DEN
      IF (ABS(SX(I,J)).LT.DELTA X.AND.ABS(SY(I,J)).LT.DELTA Y)
      1 GO TO 2
      SX(I,J)=999.
      C
      2 CONTINUE
      C
      C IF THERE IS NO SADDLE POINT, RETURN
      C
      ICH=0
      DO 10 J=1,N
      DO 10 I=2,NP1
      IF (SX(I,J).EQ.999.0) ICH=ICH+1
      10 CONTINUE
      IF (ICH.NE.0) GO TO 11
      WRITE(4,900)
      900 FORMAT(1X,'NO SADDLE POINT FOUND')
      RETURN
      C
      C FIND ACCURATE LOCATION OF SADDLE POINTS
      C
      11 DO 20 J=1,N
      JPI=J+1
      IF (J.EQ.N) JPI=1
      DO 20 I=1,NP1
      C
      C CHECK IF A SADDLE POINT HAS BEEN OBSERVED IN THE GRID CELL ABOVE
      C AND TO THE RIGHT OF THE POINT(I,J).
      C
      ANDYX=0.0
      ANDY=0.0
      AN=0.0
      JMI=J-1
      IF (I.EQ.1) GO TO 22
      IF (SX(I,J).EQ.999.0.OR.SX(I,J).LT.0.0.OR.SY(I,J).LT.0.0)
      1 GO TO 21
      AN=AN+1.0
      ANDYX=ANDYX+SX(I,J)
      ANDY=ANDY+SY(I,J)
      21 IF (SX(I,JPI).EQ.999.0.OR.SX(I,JPI).LT.0.0.OR.SY(I,JPI).GT.0.0)
      1 GO TO 22
      AN=AN+1.0
      ANDYX=ANDYX+SX(I,JPI)
      ANDY=ANDY+SY(I,JPI)+DELTA Y
      C
      22 IF (I.EQ.NP1) GO TO 24
      IF (SX(I+1,J).EQ.999.0.OR.SX(I+1,J).GT.0.0.OR.SY(I+1,J).LT.0.0)
      1 GO TO 23
      AN=AN+1.0
      ANDYX=ANDYX+SX(I+1,J)+DELTA X
      ANDY=ANDY+SY(I+1,J)
      23 IF (SX(I+1,JPI).EQ.999.0.OR.SX(I+1,JPI).GT.0.0.OR.SY(I+1,JPI).GT.
      1 0.0) GO TO 24
      AN=AN+1.0
      ANDYX=ANDYX+SX(I+1,JPI)+DELTA X
      ANDY=ANDY+SY(I+1,JPI)+DELTA Y
      24 CONTINUE
      IF (AN.EQ.0.0) GO TO 20
      AX=ANDYX/AN
      AY=ANDY/AN
      MAXX=ABS(AX)
      MAYY=ABS(AY)
      XSB=ABS(DELTA X)
      YSB=ABS(DELTA Y)
      SADDPT=((YS(I+1,J)+XSB+YS(I,J)+S(1.0-XSB))*S(1.0-YSB)
      1+((YS(I+1,JPI)+XSB+YS(I,JPI)+S(1.0-XSB))*YSB)
      C
      SARRAB=EXP(AUX)
      SARRB=EXP(1.0/MP1)
      WRITE(4,401) I,J,SARRAB,SARRB,SADDPT,AN
      401 FORMAT(1X,'SADDLE POINT DETECTED IN CELL',213,' RAD/RS= ',
      1 A7.3,' DEGREES= ',F7.3,' POTENTIAL(KV)= ',F12.5,
      1 ' NUMBER OF DETECTIONS= ',F4.1)
      IF (AN.LT.4.0) GO TO 20
      IF (ISCALE.EQ.0) SRRAB=EXP(1.0+MAXX)
      IF (ISCALE.EQ.1) SRRAB=EXP(1.0+MAXX)
      SARR=SPRAB*SCUS(MAYY)
      SARY=SPRAB*SCUS(MAYY)
      IF (ABS(SARY).GT.5.25) GO TO 20
      IF (ABS(SARR).GT.5.0) GO TO 20
      CALL SYNDL(SARR,SARY,0.20,4.45,0.0)
      20 CONTINUE
      CALL FINISH
      RETURN
      END
      SUBROUTINE SPOTS
      C
      C THIS SUBROUTINE GETS THE SURFACE POTENTIAL VALUES PHI(1,2,.....N)
      C IN A MANNER DEPENDING ON THE VALUE OF KSPOTS.
      C
      COMMON/CP01BA/N,N,KSPOTS,NR0CNS
      COMMON/BLK2/PHI(100),RELPHI(100),CH(20),NCH,ISCALE
      C
      IF (KSPOTS.GT.2) GO TO 900
      C
      IF (N.NE.100) GO TO 900
      DO 11 J=1,N
      PHI(J)=0.07
      IF (J.GE.1.AND.J.LE.8) PHI(J)=-0.05
      IF (J.GE.42.AND.J.LE.53) PHI(J)=-0.05
      IF (J.GE.91.AND.J.LE.98) PHI(J)=-0.05
      IF (J.GE.128.AND.J.LE.139) PHI(J)=-0.05
      11 CONTINUE
      RETURN
      C
      900 WRITE(4,901) N,KSPOTS
      901 FORMAT(1X,'SPOTS CALLED INCORRECTLY. N = ',I3,
      1 ' KSPOTS = ',I3)
      RETURN
      END

```

E1

FIN4

54

SCHOLARSHIP

```

SUBROUTINE UNIT
  COMMON AEMAI,XQ(2560),YQ(2560),IQ(2560,4),IL(53,51),
  ICH(53,53),ICK(52,52)
  CENDW/CMSW/INSHW,WSHIN,INSHAK,MSWAK,INO,JNO,BE,BY
  COMMON GBJI/MUR,K1,MSEG(15),ISPA(164),JSPACE(64),YSEB(64),
  YSEL(64),XSEF(64),YSEL(64),ISLP(64),IVEC(64),SLPSEG(64),
  ZGHI(5),CGGY(5)
  COMMON BLRB/MS,ME,I,DUM1,I,DUM2,I,DUM3,I,DUM4,I,DUM5,I,DUM6

  DO 100 N=MS,ME
    IS=ISLP(N)
    IV=IVEC(N)
    I1=IABS(IS+1)
    NTO=ISPACE(N)+INO
    NYO=JSPACE(N)+JNO
    IF(II,EO,4) GO TO 110
    NI=NKO
    N=N+1
    IF(N,EO,ME) N=MS
    M2=ISPACE(N)+INO
    GO TO 120
  110 N1=NYO
    N=N+1
    IF(N,EO,ME) N=MS
    M2=JSPACE(N)+JNO
  120 N=1
    IF(II,EO,2) N=2
    M1=IABS(N1-M2)/N
    ID=1
    IF(II,EO,2) ID=2

  130 N=1,M1
    IF(II,EO,4) GO TO 140
    IO=MXO+ID*IVS(N-1)
    JO=NYO+ISB(IO-MXO)/2
    GO TO 150
  140 IO=NO
    JO=NYO+IVS(N-1)
  150 IO=(IO,J)-3
    GO TO (160,180,220,240,250),II

  160 I1=IO+IV
    J1=JO+IV
    IF(ICH(10,J1),GT,-2) ICH(10,J1)=-1
    IF(ICH(11,J1),GT,-2) ICH(11,J1)=-1
    GO TO 130

  180 IF(IS,LT,0) GO TO 200
    I1=IO+IV
    J1=JO+IV
    J1=JO+IV
    IF(ICH(10,J1),GT,-2) ICH(10,J1)=-1
    IF(ICH(11,J1),GT,-2) ICH(11,J1)=-1
    IF(ICH(11,J0),NE,-3) ICH(11,J0)=-2
    IF(ICH(12,J0),NE,-3) ICH(12,J0)=-2
    IF(IV,EO,-1) GO TO 190
    ICK(10,J0)=5
    ICK(11,J0)=5
    GO TO 130
  190 ICK(11,J1)=7
    ICK(12,J1)=7
    GO TO 130

  200 I1=IO+IV
    J1=JO+IV
    J1=JO+IV
    IF(ICH(11,J0),GT,-2) ICH(11,J0)=-1
    IF(ICH(12,J0),GT,-2) ICH(12,J0)=-1
    IF(ICH(11,J1),NE,-3) ICH(11,J1)=-2
    IF(ICH(10,J1),NE,-3) ICH(10,J1)=-2
    IF(IV,EO,-1) GO TO 210
    ICK(10,J1)=6
    ICK(11,J1)=6
    GO TO 130
  210 ICK(12,J0)=8
    ICK(11,J0)=8
    GO TO 130

  220 IF(IS,LT,0) GO TO 230
    I1=IO+IV
    J1=JO+IV
    IF(ICH(10,J1),GT,-2) ICH(10,J1)=-1
    IF(ICH(11,J0),NE,-3) ICH(11,J0)=-2
    IF(IV,EO,-1) ICK(10,J0)=1
    IF(IV,EO,-1) ICK(11,J1)=3
    GO TO 130
  230 I1=IO+IV
    J1=JO+IV
    IF(ICH(11,J0),GT,-2) ICH(11,J0)=-1
    IF(ICH(10,J1),NE,-3) ICH(10,J1)=-2
    IF(IV,EO,-1) ICK(10,J1)=2
    IF(IV,EO,-1) ICK(11,J0)=4
    GO TO 130

  240 I1=IO+IV
    J1=JO+IV
    IF(ICH(11,J0),GT,-2) ICH(11,J0)=-1
    IF(ICH(11,J1),GT,-2) ICH(11,J1)=-1
    GO TO 130

  250 IF(IS,LT,0) GO TO 270
    I1=IO+IV
    J1=JO+IV
    J2=J1+IV
    IF(ICH(10,J1),GT,-2) ICH(10,J1)=-1
    IF(ICH(10,J2),GT,-2) ICH(10,J2)=-1
    IF(ICH(11,J1),NE,-3) ICH(11,J1)=-2
    IF(ICH(11,J0),NE,-3) ICH(11,J0)=-2
    IF(IV,EO,-1) GO TO 260
    ICK(10,J0)=9
    ICK(10,J1)=9
    GO TO 130
  260 ICK(11,J1)=11
    ICK(11,J2)=11
    GO TO 130

  270 I1=IO+IV
    J1=JO+IV
    J2=J1+IV
    IF(ICH(11,J0),GT,-2) ICH(11,J0)=-1
    IF(ICH(11,J1),GT,-2) ICH(11,J1)=-1
    IF(ICH(10,J1),NE,-3) ICH(10,J1)=-2
    IF(ICH(10,J2),NE,-3) ICH(10,J2)=-2
    IF(IV,EO,-1) GO TO 280
    J2=J1+IV
    ICK(10,J1)=10
    ICK(10,J2)=10
    GO TO 130
  280 ICK(11,J0)=12
    ICK(11,J1)=12
  130 CONTINUE
  140 CONTINUE
  150 CONTINUE

```

WE TURN
END
ENDS

```

C
      10
      11
      12
      13
      14
      15
      16
      17
      18
      19
      20
      21
      22
      23
      24
      25
      26
      27
      28
      29
      30
      31
      32
      33
      34
      35
      36
      37
      38
      39
      40
      41
      42
      43
      44
      45
      46
      47
      48
      49
      50
      51
      52
      53
      54
      55
      56
      57
      58
      59
      60
      61
      62
      63
      64
      65
      66
      67
      68
      69
      70
      71
      72
      73
      74
      75
      76
      77
      78
      79
      80
      81
      82
      83
      84
      85
      86
      87
      88
      89
      90
      91
      92
      93
      94
      95
      96
      97
      98
      99
      100
      101
      102
      103
      104
      105
      106
      107
      108
      109
      110
      111
      112
      113
      114
      115
      116
      117
      118
      119
      120
      121
      122
      123
      124
      125
      126
      127
      128
      129
      130
      131
      132
      133
      134
      135
      136
      137
      138
      139
      140
      141
      142
      143
      144
      145
      146
      147
      148
      149
      150
      151
      152
      153
      154
      155
      156
      157
      158
      159
      160
      161
      162
      163
      164
      165
      166
      167
      168
      169
      170
      171
      172
      173
      174
      175
      176
      177
      178
      179
      180
      181
      182
      183
      184
      185
      186
      187
      188
      189
      190
      191
      192
      193
      194
      195
      196
      197
      198
      199
      200
      201
      202
      203
      204
      205
      206
      207
      208
      209
      210
      211
      212
      213
      214
      215
      216
      217
      218
      219
      220
      221
      222
      223
      224
      225
      226
      227
      228
      229
      230
      231
      232
      233
      234
      235
      236
      237
      238
      239
      240
      241
      242
      243
      244
      245
      246
      247
      248
      249
      250
      251
      252
      253
      254
      255
      256
      257
      258
      259
      260
      261
      262
      263
      264
      265
      266
      267
      268
      269
      270
      271
      272
      273
      274
      275
      276
      277
      278
      279
      280
      281
      282
      283
      284
      285
      286
      287
      288
      289
      290
      291
      292
      293
      294
      295
      296
      297
      298
      299
      300
      301
      302
      303
      304
      305
      306
      307
      308
      309
      310
      311
      312
      313
      314
      315
      316
      317
      318
      319
      320
      321
      322
      323
      324
      325
      326
      327
      328
      329
      330
      331
      332
      333
      334
      335
      336
      337
      338
      339
      340
      341
      342
      343
      344
      345
      346
      347
      348
      349
      350
      351
      352
      353
      354
      355
      356
      357
      358
      359
      360
      361
      362
      363
      364
      365
      366
      367
      368
      369
      370
      371
      372
      373
      374
      375
      376
      377
      378
      379
      380
      381
      382
      383
      384
      385
      386
      387
      388
      389
      390
      391
      392
      393
      394
      395
      396
      397
      398
      399
      400
      401
      402
      403
      404
      405
      406
      407
      408
      409
      410
      411
      412
      413
      414
      415
      416
      417
      418
      419
      420
      421
      422
      423
      424
      425
      426
      427
      428
      429
      430
      431
      432
      433
      434
      435
      436
      437
      438
      439
      440
      441
      442
      443
      444
      445
      446
      447
      448
      449
      450
      451
      452
      453
      454
      455
      456
      457
      458
      459
      460
      461
      462
      463
      464
      465
      466
      467
      468
      469
      470
      471
      472
      473
      474
      475
      476
      477
      478
      479
      480
      481
      482
      483
      484
      485
      486
      487
      488
      489
      490
      491
      492
      493
      494
      495
      496
      497
      498
      499
      500
      501
      502
      503
      504
      505
      506
      507
      508
      509
      510
      511
      512
      513
      514
      515
      516
      517
      518
      519
      520
      521
      522
      523
      524
      525
      526
      527
      528
      529
      530
      531
      532
      533
      534
      535
      536
      537
      538
      539
      540
      541
      542
      543
      544
      545
      546
      547
      548
      549
      550
      551
      552
      553
      554
      555
      556
      557
      558
      559
      560
      561
      562
      563
      564
      565
      566
      567
      568
      569
      570
      571
      572
      573
      574
      575
      576
      577
      578
      579
      580
      581
      582
      583
      584
      585
      586
      587
      588
      589
      590
      591
      592
      593
      594
      595
      596
      597
      598
      599
      600
      601
      602
      603
      604
      605
      606
      607
      608
      609
      610
      611
      612
      613
      614
      615
      616
      617
      618
      619
      620
      621
      622
      623
      624
      625
      626
      627
      628
      629
      630
      631
      632
      633
      634
      635
      636
      637
      638
      639
      640
      641
      642
      643
      644
      645
      646
      647
      648
      649
      650
      651
      652
      653
      654
      655
      656
      657
      658
      659
      660
      661
      662
      663
      664
      665
      666
      667
      668
      669
      670
      671
      672
      673
      674
      675
      676
      677
      678
      679
      680
      681
      682
      683
      684
      685
      686
      687
      688
      689
      690
      691
      692
      693
      694
      695
      696
      697
      698
      699
      700
      701
      702
      703
      704
      705
      706
```

```

DO 90 I=INMS,INME
DO 90 J=JNMS,JNME
IF (ICM(I,J).LE.-1.OR.ICM(I,J).GE.1) GO TO 90
1 ICM(I,J).LE.-1.OR.ICM(I,J).GE.1) GO TO 90
2 ICM(I,J).LE.-1.OR.ICM(I,J).GE.1) GO TO 90
3 ICM(I,J).LE.-1.OR.ICM(I,J).GE.1) GO TO 90
90 CONTINUE

92 DO 95 I=INMS,INME
DO 95 J=JNMS,JNME
J1=ICM(I,J)
IF (J1.LE.-1.OR.J1.GE.1) GO TO 95
MS1=MS1+1
IL(I,J)=MS1
YG(MS1)=FLOAT(I-INO)DBY
YG(MS1)=FLOAT(J-JNO)DBY
95 CONTINUE
MODINS=MS1+1

DO 100 I=INMS,INME
DO 110 J=JNMS,JNME
J1=ICM(I,J)
IF (J1.EQ.-1) GO TO 120
IF (J1.EQ.0) GO TO 110
MS1=MS1+1
IL(I,J)=MS1
YG(MS1)=FLOAT(I-INO)DBY
YG(MS1)=FLOAT(J-JNO)DBY
GO TO 130
120 IL(I,J)=1
130 IF (I.EQ.INMS.OR.I.EQ.INME) GO TO 110
IF (J.EQ.JNMS.OR.J.EQ.JNME) GO TO 110
I1=ICK(I-1,J)
I2=ICK(I,J)
IF (I1.EQ.5.AND.I1.LE.0) GO TO 140
GO TO 110
140 IF (I2.EQ.5.AND.I2.LE.0) GO TO 150
GO TO 110
150 MS1=MS1+1
YG(MS1)=FLOAT(I-INO)DBY
YG(MS1)=FLOAT(J-JNO)DBY
H1=H1+1
H=(H1-1)DBY
IB1(M1)=1
IB1(M2)=J
IB1(M3)=MS1
110 CONTINUE

IF (I.EQ.INME) GO TO 100

C
DO 160 J=JNMS,JNME
J1=ICK(I,J-1)
J2=ICK(I,J)
IF (J1.EQ.9.AND.J1.LE.12) GO TO 170
GO TO 160
170 IF (J2.EQ.9.AND.J2.LE.12) GO TO 180
GO TO 160
180 MS1=MS1+1
YG(MS1)=FLOAT(I-INO)DBY
YG(MS1)=FLOAT(J-JNO)DBY
HJ=HJ+1
H=(HJ-1)DBY
IBJ(M1)=1
IBJ(M2)=J
IBJ(M3)=MS1
160 CONTINUE
MAXNO=MS1
KE(1)=MS1
KAT(1)=KE(1)-KE(1)+1

C
WRITE(LUN,123) MAXNO
123 FORMAT('00 MAXNO='//I4)

C
K=KELOUT
DO 200 I=1,INMSH
DO 210 J=1,JNMSH
MM=ICK(I,J)
IF (MM.EQ.-1) GO TO 210
K=K+1
IF (MM.GT.0) GO TO 220

IK(K,1)=IL(I,J)
IK(K,2)=IL(I+1,J)
IK(K,3)=IL(I+1,J+1)
IK(K,4)=IL(I+1,J+2)
GO TO 270

220 IF (MM.EQ.5.AND.MM.LE.0) GO TO 200
IF (MM.EQ.9.AND.MM.LE.12) GO TO 240
GO TO (230,240,250,260),MM

230 IK(K,1)=IL(I,J)
IK(K,2)=IL(I+1,J)
IK(K,3)=IL(I+1,J+1)
GO TO 270

240 IK(K,1)=IL(I,J)
IK(K,2)=IL(I+1,J)
IK(K,3)=IL(I+1,J+1)
GO TO 270

250 IK(K,1)=IL(I,J)
IK(K,2)=IL(I+1,J+1)
IK(K,3)=IL(I+1,J+2)
GO TO 270

260 IK(K,1)=IL(I+1,J)
IK(K,2)=IL(I+1,J+1)
IK(K,3)=IL(I+1,J+2)
GO TO 270

270 ICK(I,J)=1
GO TO 210

C
DO 290 I=1,NI
MM=(I-1)DBY
IF (IB1(MM+1).NE.1) GO TO 290
IF (IB1(MM+2).NE.1) GO TO 290
IS=IB1(MM+3)
GO TO 300
290 CONTINUE
300 NI=NI+4
GO TO (310,320,330,340),NI

110 IK(K,1)=IL(I,J)
IK(K,2)=IL(I+1,J)
IK(K,3)=IS
K=K+1
IK(K,1)=IL(I+1,J)
IK(K,2)=IL(I+2,J)
IK(K,3)=IS
K=K+1

IK(K,1)=15
IK(K,2)=IL(I+1,J)
IK(K,3)=IL(I+2,J)
GO TO 350
150 IK(K,1)=IL(I,J)
IK(K,2)=15
IK(K,3)=IL(I+1,J)
GO TO 350
350 IK(K,1)=IL(I,J)
IK(K,2)=15
IK(K,3)=IL(I+1,J)
K=K+1
IK(K,1)=IL(I+1,J)
IK(K,2)=15
IK(K,3)=IL(I+2,J)
GO TO 350
360 IK(K,1)=IL(I+1,J)
IK(K,2)=15
IK(K,3)=IL(I+2,J)
K=K+1
IK(K,1)=IL(I+1,J)
IK(K,2)=15
IK(K,3)=IL(I+2,J)
GO TO 350
370 ICK(I,J)=1
ICK(I+1,J)=1
GO TO 210

C
DO 370 M=1,MJ
MM=(M-1)DBY
IF (IBJ(MM+1).NE.1) GO TO 370
IF (IBJ(MM+2).NE.1) GO TO 370
IS=IBJ(MM+3)
GO TO 380
370 CONTINUE

C
380 NI=NI+4
GO TO (390,400,410,420),NI

C
390 IK(K,1)=IL(I,J)
IK(K,2)=IL(I+1,J)
IK(K,3)=IS
K=K+1
IK(K,1)=IL(I+1,J)
IK(K,2)=IL(I+1,J)
IK(K,3)=IL(I+1,J+1)
K=K+1
IK(K,1)=IL(I,J)
IK(K,2)=15
IK(K,3)=IL(I+1,J)
GO TO 430
400 IK(K,1)=IL(I,J)
IK(K,2)=IL(I+1,J)
IK(K,3)=15
K=K+1
IK(K,1)=IL(I,J)
IK(K,2)=15
IK(K,3)=IL(I+1,J)
K=K+1
IK(K,1)=IL(I+1,J)
IK(K,2)=15
IK(K,3)=IL(I+1,J+2)
GO TO 430
410 IK(K,1)=IL(I,J)
IK(K,2)=15
IK(K,3)=IL(I+1,J)
K=K+1
IK(K,1)=IL(I+1,J)
IK(K,2)=15
IK(K,3)=IL(I+1,J)
GO TO 430
420 IK(K,1)=IL(I+1,J)
IK(K,2)=IL(I+1,J)
IK(K,3)=15
K=K+1
IK(K,1)=15
IK(K,2)=IL(I+1,J)
IK(K,3)=IL(I+1,J+2)
K=K+1
IK(K,1)=15
IK(K,2)=IL(I+1,J)
IK(K,3)=IL(I+1,J+2)
GO TO 430
430 ICK(I,J)=1
ICK(I+1,J)=1

C
210 CONTINUE
260 CONTINUE
KAT=K-KELOUT
MAXLE=K

C
C
MM=1
IF (MM.EQ.1) GO TO 1302
DO 1301 J=1,JNMSH
J1=JNMSH+1-J
WRITE(LUN,1350) (ICM(I,J),I=1,INMSH)
CONTINUE
1301 ICASE=1
IF (INMSH.GT.25) ICASE=2
DO 440 I=1,ICASE
IF (I.EQ.2) GO TO 450
I1=1
I2=INMSH-INMSH+25
GO TO 460
450 I1=25
I2=INMSH
WRITE(LUN,979)
979 FORMAT('////')
460 DO 470 J=1,JNMSH
J1=JNMSH+1-J
WRITE(LUN,982) (IL(I,J),I=1,12)
982 FORMAT('2515')
470 CONTINUE

```

```

440 CONTINUE
150 CONTINUE
WRITE(LUN,73) NMAX,NODINO,NODINS
* 1. UNMAT. 8 OF CELLS IN AN INNERMOST NEST = 15/
1 88 NODINO = 15/ 88 NODINS = 15/
DO 500 J=1,NMAX
DO 500 J=1,NMAX
JJ=JCM(1,J)
IF(JJ.EQ.1.OR.JJ.EQ.-4) JCM(1,J)=0
500 CONTINUE
C
CALL EXEC(1,LU,IBUF,64,ITRACS+2,55)
IBUF(26)=NODINO
IBUF(27)=NODINS
IBUF(28)=NODINS-NODINO
CALL EXEC(2,LU,IBUF,64,ITRACS+2,55)
CALL EXEC(8,NAME)
C
STOP
END
END8

```

FTN4
BENA(AEN1,0)
PROGRAM ASSIN(5,150)

C THIS S/P DOES RENUMBERING OF NODES AT THE SURFACE OF OBJECT
C SO THAT LAST 'NSURF' NODES ARE ALWAYS CORRESPONDING TO THE
C SURFACE NODES, WHERE 'NSURF' IS A TOTAL 8 OF SURFACE NODE.

C
COMMON/AEN1/XD(2560),YD(2560),ID(2560,4),JL(53,53),
JCM(53,53),JCK(52,52)
COMMON/CRESH/INSHIN,JSMIN,INSMX,JSMX,INO,JNO,BX,BY
COMMON/CHST2/NEBMX,MAXMOD,MAXELE,NODOUT,NODIN,KELOUT,
IAELIN,NODINS
COMMON/IDAT/LUN,LU,ITRACS
COMMON/OBJ1/MODJCT,NSEGO(5),ISPACE(64),JSPACE(64),XSSEG(64),
LYSSEG(64),XSEGO(64),YESGO(64),ISLP(64),IVEC(64),SLPSEG(64),
2CDOX(5),CDOY(5)
COMMON/OBJ2/YSP(128),YSP(128),XEP(128),YEP(128),NSP(128),
INEP(128),NMP(128),MPAT(5),MAXPAT
COMMON/BLK1/XS(15,6),YS(15,6),XE(15,6),YE(15,6),TY(15,7),
LYYI(15,5),YYI2(15,5)
COMMON/BLK4/IBUF1(25),IBUF2(25),NODE(25),IBUF4(25)
DIMENSION NSURF(128),IBUF(64),NAME(3),IAUX(128)
EQUIVALENCE (ICK,IAUX)
C
DATA NAME/2SH,2HAD,2HE /
DATA NAME/2HDL,2HRT,2HI /
C
IFLG=0
WRITE(LUN,999)
999 FORMAT(//20,' ',5X,'ASSIN' STARTS',5X,20,' ')
NABA=0
IF(NABA.EQ.0) GO TO 690
ICASE=1
IF(INSMX.GT.25) ICASE=2
DO 400 I=1,ICASE
IF(I1.EQ.2) GO TO 610
I=1
I2=NINO(INSMX,25)
GO TO 620
610 I=25
I2=INSMX
WRITE(LUN,999)
999 FORMAT(//4)
420 DO 630 J=1,NMAX
JI=INSMX+1-J
WRITE(LUN,992) (IL(I,JI),I=1,I2)
992 FORMAT(25I3)
630 CONTINUE
400 CONTINUE
C
WRITE(LUN,670) ((I0(I,J),J=1,4),I=KELIN,MAXELE)
WRITE(LUN,680) (I,XG(I),YB(I),I=NODIN,MAXMOD)
670 FORMAT(24I5)
680 FORMAT(8I4,2F6,2)
690 IPAT=0
L=NODINS
LB=MAXMOD
MAXSEG=NSEGO(NODJCT)
DO 1000 N=1,MAXSEG
M=0
IS=ISLP(N)
IU=IVEC(N)
MI=XSEGO(N)
MI2=XSEGO(N)
MJ1=YSEGO(N)
MJ2=YSEGO(N)
IF(I1.EQ.0) GO TO 40
IF(I5.EQ.3) GO TO 40
O=FLOAT(IS)/2.0
IF(IU.EQ.1) GO TO 20
IF(I5.LT.0) GO TO 10
DO 100 L=LA,LB
IF(XG(L).GE.MI1.AND.XG(L).LE.MI2) GO TO 110
GO TO 100
110 IF(YB(L).GE.MJ1.AND.YB(L).LE.MJ2) GO TO 120
GO TO 100
120 IF(ABS(GB(XG(L)-MI1)+HJ1-YB(L)).LE.0.018BY) GO TO 125
GO TO 100
125 N=N+1
NODE(N)=L
100 CONTINUE
N2=1
GO TO 400
10 DO 130 L=LA,LB
IF(XG(L).GE.MI1.AND.XG(L).LE.MI2) GO TO 140
GO TO 130
140 IF(YB(L).GE.MJ1.AND.YB(L).LE.MJ2) GO TO 145
GO TO 130
145 IF(ABS(GB(XG(L)-MI1)+HJ1-YB(L)).LE.0.018BY) GO TO 147
GO TO 130
147 N=N+1
NODE(N)=L
130 CONTINUE
N2=2
GO TO 400
20 IF(I5.GT.0) GO TO 30
DO 150 L=LA,LB
IF(XG(L).GE.MI2.AND.XG(L).LE.MI1) GO TO 160
GO TO 150
160 IF(YB(L).GE.MJ1.AND.YB(L).LE.MJ2) GO TO 170
GO TO 150
170 IF(ABS(GB(XG(L)-MI1)+HJ1-YB(L)).LE.0.018BY) GO TO 175
GO TO 150
175 N=N+1
NODE(N)=L
140 CONTINUE

```

N2=3  
GO TO 400  
30 DO 180 L=LA,LB  
IF(XG(L).GE.MI2.AND.XG(L).LE.MI1) GO TO 185  
GO TO 180  
185 IF(YB(L).GE.MJ2.AND.YB(L).LE.MJ1) GO TO 190  
GO TO 180  
190 IF(ABS(GB(XG(L)-MI1)+HJ1-YB(L)).LE.0.018BY) GO TO 195  
GO TO 180  
195 N=N+1  
NODE(N)=L  
180 CONTINUE  
N2=4  
GO TO 400  
40 IF(IU.EQ.1) GO TO 50  
DO 200 L=LA,LB  
IF(YB(L).GE.MJ1) GO TO 210  
GO TO 200  
210 IF(XG(L).GE.MI1.AND.XG(L).LE.MI2) GO TO 220  
GO TO 200  
220 N=N+1  
NODE(N)=L  
200 CONTINUE  
N2=5  
GO TO 400  
50 DO 250 L=LA,LB  
IF(YB(L).GE.MJ1) GO TO 240  
GO TO 250  
240 IF(XG(L).GE.MI2.AND.XG(L).LE.MI1) GO TO 270  
GO TO 250  
270 N=N+1  
NODE(N)=L  
250 CONTINUE  
N2=6  
GO TO 400  
60 IF(IU.EQ.1) GO TO 70  
DO 300 L=LA,LB  
IF(XG(L).GE.MI1) GO TO 310  
GO TO 300  
310 IF(YB(L).GE.MJ1.AND.YB(L).LE.MJ2) GO TO 320  
GO TO 300  
320 N=N+1  
NODE(N)=L  
300 CONTINUE  
N2=7  
GO TO 400  
70 DO 350 L=LA,LB  
IF(XG(L).GE.MI1) GO TO 340  
GO TO 350  
340 IF(YB(L).GE.MJ2.AND.YB(L).LE.MJ1) GO TO 370  
GO TO 350  
370 N=N+1  
NODE(N)=L  
350 CONTINUE  
N2=8  
400 NMAX=N  
DO 410 N=1,NMAX  
IBUF2(N)=N  
IBUF4(N)=NODE(N)  
IF(NZ.EQ.7) GO TO 420  
IBUF1(N)=IBUF4(N)+81000.0  
GO TO 410  
420 IBUF1(N)=YB(1+IBUF4(N))+81000.0  
410 CONTINUE  
C  
CALL SORT(NMAX)  
C  
L=(NMAX+1)*(1-IV)/2  
DO 430 N=1,NMAX  
LL=L+IVN  
NODE(N)=IBUF4(1+IBUF2(LL))  
430 CONTINUE  
NMAX=NMAX-1  
DO 440 N=1,NMAX  
IPAT=IPAT+1  
NSP(IPAT)=NODE(N)  
NEP(IPAT)=NODE(N+1)  
440 CONTINUE  
IF(IFLG.EQ.0) GO TO 1000  
NSP(N)=IPAT  
DO 450 N=1,NODJCT  
IF(N.NE.NSEGO(N)) GO TO 450  
IF(N.EQ.1) GO TO 440  
NPAT(N)=IPAT-NPAT(N-1)  
GO TO 450  
440 NPAT(N)=IPAT  
450 CONTINUE  
1000 CONTINUE  
IF(IFLG.EQ.1) GO TO 480  
IAUX(1)=IPAT  
DO 470 I=1,IPAT  
IAUX(I+1)=NSP(I)  
470 CONTINUE  
IFLG=1  
CALL NSURF  
GO TO 470  
480 MAXPAT=IPAT  
NSURF=MAXPAT  
DO 490 N=1,MAXPAT  
L=NSP(N)  
LL=NEP(N)  
NSURF(N)=L  
XSP(N)=XG(L)  
YSP(N)=YB(L)  
XEP(N)=XG(LL)  
YEP(N)=YB(LL)  
490 CONTINUE  
NODS=MAXMOD-NSURF  
C  
CALL EXEC(1,LU,IBUF,64,ITRACS+2,55)  
IBUF(9)=NODS  
IBUF(10)=MAXELE  
IBUF(11)=MAXMOD  
IBUF(12)=MAXPAT  
IBUF(13)=NSURF  
CALL EXEC(2,LU,IBUF,64,ITRACS+2,55)  
CALL EXEC(2,LU,XSP,256,ITRACS+3,0)  
CALL EXEC(2,LU,YSP,256,ITRACS+3,0)  
CALL EXEC(2,LU,XEP,256,ITRACS+3,16)  
CALL EXEC(2,LU,YEP,256,ITRACS+3,16)  
CALL EXEC(2,LU,NSP,128,ITRACS+3,32)  
CALL EXEC(2,LU,NEP,128,ITRACS+3,36)  
CALL EXEC(2,LU,NSURF,128,ITRACS+3,40)  
DO 510 I=1,32  
IBUF(I)=NMP(I)  
510 CONTINUE  
DO 520 I=1,5  
IBUF(I)=MPAT(I)  
520 CONTINUE  
CALL EXEC(1,LU,IBUF,64,ITRACS+3,44)  
CALL EXEC(8,NAME)

```

```

      N1=NSURF-1
      M=1
      1 N1=M+1
      2 IF (NSURF(M).LE.NSURF(M1)) GO TO 3
      I1=NSURF(M)
      NSURF(M)=NSURF(M1)
      NSURF(M1)=I1
      3 M1=M+1
      IF (M1.LE.NSURF) GO TO 2
      M=M+1
      IF (M1.LE.M1) GO TO 1

C
      DO 100 M=1,NSURF
      MM=NSURF(M)
      BUFX(M)=XG(MM)
      BUFY(M)=YG(MM)
      DO 120 I=1,INSMNX
      DO 120 J=1,INSMNY
      LL=IL(I,J)
      IF (LL.EQ.MM) GO TO 140
120 CONTINUE
      GO TO 140
140 IL(I,J)=LL
160 DO 180 I=KELIN,MAXELE
      DO 180 J=1,4
      LL=IG(I,J)
      IF (LL.EQ.MM) IG(I,J)=LL
180 CONTINUE
190 CONTINUE

C
      DO 200 M=1,NSURF
      M1=NSURF(M)+1
      IF (M.NE.NSURF) M2=NSURF(M+1)-1
      IF (M.EQ.NSURF) M2=MAXMOD
      MSHFT=M
      IF (M1.GT.M2) GO TO 200
      DO 220 MM=M1,M2
      NEW=MM-MSHFT
      XG(NEW)=XG(MM)
      YG(NEW)=YG(MM)
      DO 240 I=1,INSMNX
      DO 240 J=1,INSMNY
      LL=IL(I,J)
      IF (LL.EQ.MM) GO TO 260
240 CONTINUE
      GO TO 280
260 IL(I,J)=NEW
280 DO 300 I=KELIN,MAXELE
      DO 300 J=1,4
      LL=IG(I,J)
      IF (LL.EQ.MM) IG(I,J)=NEW
300 CONTINUE
320 CONTINUE
340 CONTINUE

C
      MO=MAXMOD-BSURF
      DO 320 M=1,NSURF
      NEW=MO+M
      BUFX(NEW)=BUFX(M)
      YG(NEW)=BUFY(M)
      MM=NSURF(M)
      DO 340 I=1,INSMNX
      DO 340 J=1,INSMNY
      LL=IL(I,J)
      IF (LL.GE.-1) GO TO 340
      IF (IABS(LL).EQ.MM) GO TO 360
340 CONTINUE
      GO TO 380
360 IL(I,J)=NEW
380 DO 400 I=KELIN,MAXELE
      DO 400 J=1,4
      LL=IG(I,J)
      IF (LL.GE.0) GO TO 400
      IF (IABS(LL).EQ.MM) IG(I,J)=NEW
400 CONTINUE
320 CONTINUE
      RETURN
      END
      ENDS

FTM4
SERNAI(AEN1,0)
      PROGRAM MESTR(5,150)

C THIS S/P GENERATES A MESH OF RECTANGULAR FINITE ELEMENTS
C OUTSIDE THE HOST ONE AND DEFINE THE NUMBERS OF THE FOUR NODES
C OF EACH ELEMENT.

      COMMON/AEN1/XG(2540),YG(2540),IG(2540,4),IL(53,53),
      ICH(5,53),ICK(52,52)
      COMMON/CHBSM/INSHN,INSHN1,INSMNX,INSMNY,IHO,JHO,BX,BY
      COMMON/CMST/NESTR(10),NM1(10),NMJ(10),NOUTER(10),KS(10),
      IREL(10),KAME(10),KAMAX,MAXMOD,MAXELE,NODOUT,NODIN,KELOUT,
      IREL IN,NODINS
      COMMON/CONV/MCONV(10,4,4)
      COMMON/IDATA/LUN,LU,ITRACS
      COMMON/PSOLV/ISYH,IPDIS,IPBOT,RDEBY,CPOIS
      COMMON/BLR4/IBUF1(25),IBUF2(25),IBUF3(25),IBUF4(25)
      DIMENSION BMSTR(10,2),BMSTR1(10,2),BUF(44),IBUF(44),NAME(3)
      DIMENSION JBUF(254),MCONV(4,40),MINNER(200)
      EQUIVALENCE (JBUF,BUF,IBUF),BUF,ICK,MINNER
      DATA NAME/2NME,2NMA,2NI /

C
      WRITE(LUN,999)
      999 FORMAT('//20','5X','MESTR' STARTS,'5X,20',' )
      NS=0
      I=NS-NSMAX-1
      XPT=XT/I (INSMNX,INSMNY)
      YPT=Y/I (INSMNY,INSMNX)
      BMSTR(1,1)=XPT
      BMSTR(1,2)=YPT
      BMSTR(1,3)=YPT
      BMSTR(1,4)=YPT
      NM=7
      IF (I.YM.FI).NM=1

```

```

DO 40 J=1,NMESJ
XB=XB1
YB=YB1
DO 60 J=2,J1
XB=XB+DX$FLOAT(288(J-1)*NMEST(J))
YB=YB+DY$FLOAT(288(J-1)*NMEST(J))
60 CONTINUE
NMSTX(J,1)=XB
NMSTX(J,2)=XB
NMSTY(J,1)=-YB
NMSTY(J,2)=YB
NI=NI1(J1)
NJ=NJ1(J1)

C
IF(J1.LT.NESMAX) GO TO 75
IF(ISYN.EQ.1) GO TO 72
NOUTER(1)=1
NOUTER(2)=NI
NOUTER(3)=NI+NJ-1
NOUTER(4)=NI+2*NJ-2
NOUTER(5)=(NI+NJ)*2-4
DO 45 J=1,5
NOUTER(J+5)=NOUTER(J)+J-1
45 CONTINUE
GO TO 75
72 NOUTER(2)=1
NOUTER(3)=NJ
NOUTER(4)=NI+NJ-1
NOUTER(5)=NOUTER(4)

C
75 J2=NMEST(J1)
HX=DY$FLOAT(288(J1-1))
HY=DY$FLOAT(288(J1-1))
AS(J1)=NB+1
DO 50 J=1,J2
XI=XB-HX$FLOAT(J-1)
YI=YB-HY$FLOAT(J-1)
NN=2
IF(ISYN.EQ.1) NN=1
NI=N1-NNB(J-1)
N2=N1-NNB(J-1)
IF(ISYN.EQ.1) NI=N1+1
IF(ISYN.EQ.1) GO TO 85
DO 80 N=1,NI
NS=NB+1
XS(NS)=XI+NX$FLOAT(N-1)
YS(NS)=-YI
80 CONTINUE
85 DO 90 N=1,N2
NS=NB+1
XS(NS)=XI
YS(NS)=-YI+$FLOAT(ISYN/3)+NY$FLOAT(N-1)
90 CONTINUE
DO 100 N=1,NI
NS=NB+1
XS(NS)=XI-HX$FLOAT(N-1)
YS(NS)=YI
100 CONTINUE
IF(ISYN.EQ.1) GO TO 50
DO 110 N=1,N2
NS=NB+1
XS(NS)=-XI
YS(NS)=YI-HY$FLOAT(N-1)
110 CONTINUE
120 CONTINUE
KE(J1)=NB
KAM(J1)=KE(J1)-KB(J1)+1
40 CONTINUE

C
WRITE(LUN,125) (N,XO(N),YO(N),N=1,NAXNO)
C 125 FORMAT(7(I5,2F6.2))
WRITE(LUN,127) ((KS(I),KE(I),KAM(I),I=1,NESMAX)
127 FORMAT('8',1BX,' KS KE KAM'/14X,'NEST 0 '=12,5X,3IS))
WRITE(LUN,128) (NOUTER(I),I=1,5)
128 FORMAT('88 NOUTER/SX,S1S)

C
N=0
DO 600 I=1,10
DO 600 J=1,2
N=N+1
BUF(N)=BNMSTX(I,J)
NOUTER(I,J)
600 CONTINUE
CALL EXEC(2,LU,BUF,128,ITRACS+4,64)
CALL EXEC(1,LU,BUF,64,ITRACS+2,55)
DO 610 I=1,10
IBUF(I*20)=NOUTER(I)
610 CONTINUE
CALL EXEC(2,LU,BUF,64,ITRACS+2,55)
DO 620 I=1,NESMAX
IBUF(I)=KS(I)
IBUF(I+10)=KE(I)
IBUF(I+20)=KAM(I)
620 CONTINUE
CALL EXEC(2,LU,BUF,64,ITRACS+4,64)

C
N=0
NI=0
IF(ISYN.EQ.1) GO TO 142
DO 140 I=1,INSMIX-2
N=N+1
NINNER(N)=IL(I+1)
IF(IL(EQ.INSMIX)) GO TO 140
NI=N1+1
NCONNA(1,NI)=IL(I+1,1)
140 CONTINUE
GO TO 145
142 N=N+1
NINNER(N)=IL(INSMIX,1)
145 NI=0
DO 150 J=3,INSMIX-2
N=N+1
NI=N1+1
NINNER(N)=IL(INSMIX,J)
NCONNA(2,NI)=IL(INSMIX,J-1)
150 CONTINUE
NI=0
DO 160 I=3,INSMIX-2
N=N+1
NI=N1+1
I1=INSMIX+1-I
NINNER(N)=IL(I1,INSMIX)
NCONNA(3,NI)=IL(I1,I1,INSMIX)
160 CONTINUE
IF(ISYN.EQ.1) GO TO 172
JI=INSMIX-2
NI=0
DO 170 J=3,JI-2
N=N+1
NI=N1+1
I1=INSMIX+1-I
```

[illegible]

```

N=0
MS=1
IF (I SYN.EQ.1) MS=0
DO 200 I=1,NES
  I1=MS*2-1-I
  N1=NN1(I1)
  N2=NN2(I1)
  IF (I SYN.EQ.1) GO TO 240
  N1=N1
  IG(A,1)=MS
  IG(A,2)=MS+1
  IG(A,3)=MS+(N1+N2)*2
  IG(A,4)=IG(A,3)-1
240 J1=NEST(I1)
  DO 250 J=1,J1
    NN=2
    IF (I SYN.EQ.1) NN=1
    N1=N1-NN*J
    R2=N2-NN*J
    IF (I.EQ.NES.AND,J.EQ.J1) GO TO 340
    IF (J.EQ.J1) GO TO 270
    JUMP=1
    GO TO 280
270 JUMP=2
280 IF (J.EQ.J1) GO TO 290

```

```

K=K+1
IF (ISYM.EQ.1) GO TO 292
IG(K,1)=IG(K-1,1)+1
IG(K,2)=IG(K,1)+1
IG(K,3)=IG(K,1)+1
IG(K,4)=IG(K,3)+1
292 IG(K,1)=IG(K-1,1)+1
IG(K,2)=IG(K-1,4)+1
IG(K,3)=IG(K,2)+1
IG(K,4)=IG(K,1)+1 JUMP
IF (J.NE.J1) GO TO 307
NCDNN(11,2,1)=K
NCDNN(11,2,3)=IG(K,1)+1
GO TO 307
IF ISYM.EQ.1) GO TO 306
IF (J.NE.J1) GO TO 295
NCDNN(11,1,1)=K+1
NCDNN(11,1,3)=IG(K,1)+1

```

```

295 DO 300 N=1,M1
      K=N+1
      IG(K,1)=IG(K,1)+1
      IG(K,2)=IG(K,1)+2+1
      IG(K,3)=IG(K,1)+3+JUMP
      IG(K,4)=IG(K,3)-JUMP
300 CONTINUE
      IF(J,NE,J1) GO TO 305
      NCONN(1,1:4)=IG(K,4)+1
305 K=N+1
      IG(K,1)=IG(K,1)+1
      IG(K,2)=IG(K,1)+1
      IG(K,3)=IG(K,2)+1
      IG(K,4)=IG(K,1)+3
      IF(J,NE,J1) GO TO 308
      NCONN(1,1:4)=K
      NCONN(1,1:3)=IG(K,4)+1
      GO TO 308

```

```

306 K=K+1
      IB(K,1)=MS+2*NI+NJ
      IB(K,2)=MS+1
      IB(K,3)=MS+2
      IB(K,4)=IB(K,1)+JUMP
      IF(J.NE.J1) GO TO 307
      NCONN(I1,2,1)=K
      NCONN(I1,2,3)=IB(K,1)+1
307 N2=N2-1

```

```

308 DO 310 N=1,M2
      K=K+1
      I(K,1)=I(K-1,4)
      I(K,2)=I(K-1,2)+1
      I(K,3)=I(K-1,3)+1
      I(K,4)=I(K-1,4)+JUMP
310 CONTINUE
      IF (J.NE.J1) GO TO 315
      NCONH(1,2,2)=K
      NCONH(1,2,4)=I(K,1)+1
315 K=K+1
      I(K,1)=I(K-1,4)
      I(K,2)=I(K-1,2)+1
      I(K,3)=I(K-1,3)+1
      I(K,4)=I(K-1,4)+1
      IF (J.NE.J1) GO TO 310
      NCONH(1,3,1)=K+1
      NCONH(1,3,3)=I(K,1)+1

```

```

310 DO 320 M=1,M1
   A=X(1)
   I(GR-1)=I(GR-1,1)+JUMP
   I(GR-2)=I(GR-1,2)+JUMP
   I(GR-3)=I(GR-1,3)+JUMP
   I(GR-4)=I(GR-3,1)
   JZ C,CONTINUE
   IF (J.ME.J1) GO TO 325
   MCORRG((1,3+2)*N
   MCORRG((1,3+4)+I(GR,2))
325 IF (ISYN.EQ.1) GO TO 250
   A=X(1)
   I(GR-1)=I(GR-1,4)+2
   I(GR-2)=I(GR-1,2)+JUMP
   I(GR-3)=I(GR-1,3)+J
   I(GR-4)=I(GR-3,1)
   IF (J.ME.J1) GO TO 320
   MCORRG((1,4+1)+X(1)
   MCORRG((1,4+3)+I(GR,2))

```

```

170 M2=M2-1
180 J30 M=1:M2
190 A=0
200 I0(A,1)=I0(A-1,1)+1
210 I0(A,2)=I0(A,1,2)+N*MP
220 I0(A,3)=I0(A,1,2)
230 I0(A,4)=I0(A,1,4)+1

```

```

500 CONTINUE
      P=K+1
      IG(K,1)=IG(K-1,1)+1
      IG(K,2)=IG(K,1)+1
      IG(K,3)=IG(K,1)+2
      IG(K,4)=IG(K,1)+3+1
      IF (J.NE.J1) GO TO 250
      MCONC(11,4,2)=K
      MCONC(11,4,4)=IG(K,3)+1
250 CONTINUE
      MS=IG(K,2)
      IF (ISYM.EQ.1) MS=IG(K,4)
200 CONTINUE

340 M=0
      DO 630 I=1,4
      DO 630 J=1,40
      M=M+1
      JBUF(I)=MCONC(I,J)
630 CONTINUE
      CALL EXEC(2,LU,JBUF,256,ITRACS+4,54)

```

```

IF (ISYN.EQ.1) GO TO 352
MS=IG(K+2)
K=K+1
IG(K,1)=MS
IG(K,2)=MS+1
IG(K,3)=NINNER(1)
IG(K,4)=IG(K,3)+1
NCONW(1,1,1)=K+1
DO M=1,M1
K=K+1
IG(K,1)=IG(K,1+2)
IG(K,2)=IG(K,1+2)
IG(K,3)=NINNER(M+1)
IG(K,4)=IG(K,1+3)
350 CONTINUE
NCONW(1,1,2)=K
K=K+1
IG(K,1)=IG(K,1+2)
IG(K,2)=IG(K,1+2)
IG(K,3)=IG(K,2+1)
IG(K,4)=IG(K,1+1)
NCONW(1,1,2)=K+1

```

```

352 M4=M1+1
IF (15*Y,EG,4) GO TO 355
R=K+1
IG(K,1)=MINNER(1)
IG(K,2)=IG(K,1+4)+1
IG(K,3)=IG(K,2)+1
IG(K,4)=MINNER(2)
NCON=11,2,1)=R
M4=2
M2=M2-1
355 DO 360 M=1,M2
R=K+1
M3=M4+N
IG(K,1)=IG(K,1+4)
IG(K,2)=IG(K,1+3)
IG(K,3)=IG(K,2)+1
IG(K,4)=MINNER(M3)

```

```

360 CONTINUE
      MCONM(I1,2)=K
      K=K+1
      IG(K,1)=IG(K-1,4)
      IG(K,2)=IG(K-1,3)
      IG(K,3)=IG(K-2)+4
      IG(K,4)=IG(K-1,3)+1
      MCONM(I1,3,1)=K+1

      N4=M1+M2+1
      IF(ISTN.EQ.1) N4=M2+2
      DO 370 M1=1,M1
      K=K+1
      M3=N4+M
      IG(K,1)=MINOR(M3)
      IG(K,2)=IG(K-1,4)
      IG(K,3)=IG(K-1,4)
      IG(K,4)=IG(K-1,4)

```

```

370 CONTINUE
NCOMM(I1,3,2)=K
IF(18YN.EQ.1) GO TO 382
K=K+1
IO(K,1)=IO(K-1,4)+2
IO(K,2)=IO(K-1,1)
IO(K,3)=IO(K-1,4)
IO(A,4)=IO(K,3)+1
NCOMM(I1,4,1)=K+1

```

```

M4=M12+M2+1
M2=M2-1
DO 300 N=1,M2
K=K+1
M3=M4+M
IG(K,1)=IG(K-1,1)+1
IG(K,2)=WINNER(M3)
IG(K,3)=IG(K-1,2)
IG(K,4)=IG(K-1,1)
300 CONTINUE
K=K+1
IG(K,1)=IG(K-1,1)+1
IG(K,2)=WINNER(1)
IG(K,3)=IG(K-1,2)
IG(K,4)=IG(K-1,1)
MCDOWN(1,4,2)=K

```

```

382 KELOUT=K
      WRITE(LUN,385) ((I8(K,M),M=1,4),K=1,KELOUT)
385 FORMAT(20I5)
      WRITE(LUN,387) ((I,J,(NCONM(I,J,K),K=1,4),J=1,4),I=2,NESMAX)
387 FORMAT('00 NCONM'/2X,' I J K=1 K=2 K=3 K=4'/
          A(215,4I6))

```

```

      RI=RELOUT+1
      WRITE(LUN,395) ((IG(K,M),M=1,4),K=R1,MAXELE)
395  FORMAT(20I5)
      RETURN

```

```

      N=0
      DO 440 J=1,10
      DO 440 J=1,4
      DO 440 K=1,4
      N=N+1
      (JUR(J),NCONW(J),J,R)
440 CONTINUE
      CALL REFCIT(LU,JJUR,256,ITRACS+4,50

```

```
CALL EXEC(B-NAME)

STOP
END
ENDS
```



```

FTN4
      VERN(AERAT,0)
      PROGRAM AERAT(150)
C
C THIS S/P WRITES AERAT PARAMETERS ON DISC.
C
      COMMON AERAT/AM(4096),JA(4096),IA(512),IG(2560),YB(2560),
     1IG(2560),YBC(512),JBC(512),IBC(512),NCOMU(128),
     2NCONV(128),NCONV(256)
      COMMON/CHST1/ROUTER(10)
      COMMON/CHST2/MESMAX,MAXMOD,MAXELE,MODFS,MODINS
      COMMON/CONV/NCONU,NCONA(4,48),NCONM(10,4,4)
      COMMON/ELER/STA(10),SMA(10),SXB(10),SYD(10),
     1SMB(10),SXC(15),SYC(15),SMC(15),SXL(10),SYL(10),
     2SNC(10),SXC(15),SYC(15),SMC(15),SXD(10),SYD(10),
     3SND(10),SXE(15),SYE(15),SME(15),SXE(20),SYE(20),
     4SNE(20),SXF(30),SYF(30),SNF(30)
      COMMON/IDAT/LUN,LU,ITRACS
      COMMON/PSOLV/ISTH,IPDIS,IPOT,RDEBY,CPOIS
      COMMON/BLK1/ELMAT(9,9)
      COMMON/BLK4/IBUF(25),IBUF(25),IGA(25),IGG(25)
      COMMON/BLK6/A1,A2,A3,DEMOM,AA1,AA2
      COMMON/BLK7/NOMB,NVAR,JPMAX,NBC,A,A1,A2,A3,AA,J,MES,N
      COMMON/BLB/NWB,NZ,NZ1,NZ2,NZ3,NCTYP
      DIMENSION NAME(3)
      DATA NAME/2ND,2HAT,2NC /

      WRITE(LUN,999)
999 FORMAT(//20,'.5X','AERAT' STARTS '.5X,20')
      CALL EXEC(2,LU,IBUF1,256,ITRACS+8,ISECT)
      CALL EXEC(2,LU,IBUF2,256,ITRACS+9,ISECT)
      ISECT=ISECT+4
      ISTART=ISTART+128
100 CONTINUE
C
      NSTOP=2560/256
      ISECT=0
      DO 200 J=1,2
      N=J+2
      ISTART=0
      DO 210 N=1,NSTOP
      DO 220 I=1,256
      II=ISTART+I
      IBUF1(I)=IG(II,J)
      IBUF2(I)=IG(II,N)
220 CONTINUE
      CALL EXEC(2,LU,IBUF1,256,ITRACS+10,ISECT)
      CALL EXEC(2,LU,IBUF2,256,ITRACS+11,ISECT)
      ISECT=ISECT+4
      ISTART=ISTART+256
210 CONTINUE
200 CONTINUE
C
      DO 250 I=1,INSHMX
      IBUF1(I)=IL(I,1)
      IBUF2(I)=IL(I,INSHMX)
250 CONTINUE
      DO 260 J=1,INSHMX
      IBUF1(J)=IL(1,J)
      IBUF2(J)=IL(1,INSHMX,J)
260 CONTINUE
      CALL EXEC(2,LU,IBUF1,256,ITRACS+12,ISECT)
      CALL EXEC(2,LU,IBUF2,256,ITRACS+13,ISECT)
      ISECT=ISECT+4
      N=0
310 CONTINUE
300 CONTINUE
C
      WRITE(LUN,781)
781 FORMAT(//)
      STOP
      END
      ENDS

```

```

FTN4
      VERN(AERAT,0)
      PROGRAM GLMAT(150)
C
C THIS IS THE MAIN ROUTINE FOR THE GLOBAL MATRIX SECTION
C OF AYTIC
C
      COMMON AERAT/AM(4096),JA(4096),IA(512),IG(2560),YB(2560),
     1IG(2560),YBC(512),JBC(512),IBC(512),NCOMU(128),
     2NCONV(128),NCONV(256)
      COMMON/CHST1/ROUTER(10)
      COMMON/CHST2/MESMAX,MAXMOD,MAXELE,MODFS,MODINS
      COMMON/CONV/NCONU,NCONA(4,48),NCONM(10,4,4)
      COMMON/ELER/STA(10),SMA(10),SXB(10),SYD(10),
     1SMB(10),SXC(15),SYC(15),SMC(15),SXL(10),SYL(10),
     2SNC(10),SXC(15),SYC(15),SMC(15),SXD(10),SYD(10),
     3SND(10),SXE(15),SYE(15),SME(15),SXE(20),SYE(20),
     4SNE(20),SXF(30),SYF(30),SNF(30)
      COMMON/IDAT/LUN,LU,ITRACS
      COMMON/PSOLV/ISTH,IPDIS,IPOT,RDEBY,CPOIS
      COMMON/BLK1/ELMAT(9,9)
      COMMON/BLK4/IBUF1(25),IBUF2(25),IGA(25),IGG(25)
      COMMON/BLK6/A1,A2,A3,DEMOM,AA1,AA2
      COMMON/BLK7/NOMB,NVAR,JPMAX,NBC,A,A1,A2,A3,AA,J,MES,N
      COMMON/BLB/NWB,NZ,NZ1,NZ2,NZ3,NCTYP
      DIMENSION NAME(3)
      DATA NAME/2ND,2HAT,2NC /

      WRITE(LUN,999)
999 FORMAT(//20,'.5X','GLMAT' STARTS '.5X,20')
      CALL EXEC(8,NAME)
      STOP
      END
      BLOCK DATA
      COMMON/CHST1/ROUTER(10)
      COMMON/CHST2/MESMAX,MAXMOD,MAXELE,MODFS,MODINS
      COMMON/CONV/NCONU,NCONA(4,48),NCONM(10,4,4)
      COMMON/ELER/STA(10),SMA(10),SXB(10),SYD(10),
     1SMB(10),SXC(15),SYC(15),SMC(15),SXL(10),SYL(10),
     2SNC(10),SXC(15),SYC(15),SMC(15),SXD(10),SYD(10),
     3SND(10),SXE(15),SYE(15),SME(15),SXE(20),SYE(20),
     4SNE(20),SXF(30),SYF(30),SNF(30)
      COMMON/IDAT/LUN,LU,ITRACS
      COMMON/PSOLV/ISTH,IPDIS,IPOT,RDEBY,CPOIS
      COMMON/BLK1/ELMAT(9,9)
      COMMON/BLK4/IBUF1(25),IBUF2(25),IGA(25),IGG(25)
      COMMON/BLK6/A1,A2,A3,DEMOM,AA1,AA2
      COMMON/BLK7/NOMB,NVAR,JPMAX,NBC,A,A1,A2,A3,AA,J,MES,N
      COMMON/BLB/NWB,NZ,NZ1,NZ2,NZ3,NCTYP
      DATA LUN/4,LU/51,ITRACS/0
      DATA NVAR/0,JPMAX/0,NBC/0
      END
      SUBROUTINE SORT(N)
      COMMON/BLK4/IGA(25),IBB(25),IBF3(25),IBUF4(25)
C
      N1=N-1
      N=1
      1 N1=N+1
      2 IF(IAA(N).LE.IGG(N1)) GO TO 3
      I1=IAA(N)
      I2=IBB(N)
      IAA(N)=IAA(N1)
      IBB(N)=IBB(N1)
      IAA(N1)=I1
      IBB(N1)=I2
      3 N1=N1+1
      IF(N1.LE.N) GO TO 2
      N=N+1
      IF(N1.LE.N1) GO TO 1
      RETURN
      END
      ENDS

FTN4
      VERN(AERAT,0)
      PROGRAM GLHT2(150)
C
C THIS S/P FORMS GLOBAL MATRIX FOR POTENTIAL SOLVER AND
C APPLIES BOUNDARY CONDITIONS.
C
      COMMON AERAT/AM(4096),JA(4096),IA(512),IG(2560),YB(2560),
     1IG(2560),YBC(512),JBC(512),IBC(512),NCOMU(128),
     2NCONV(128),NCONV(256)
      COMMON/CHST1/ROUTER(10)
      COMMON/CHST2/MESMAX,MAXMOD,MAXELE,MODFS,MODINS
      COMMON/CONV/NCONU,NCONA(4,48),NCONM(10,4,4)
      COMMON/IDAT/LUN,LU,ITRACS
      COMMON/PSOLV/ISTH,IPDIS,IPOT,RDEBY,CPOIS
      COMMON/BLK1/ELMAT(9,9)
      COMMON/BLK4/IBUF1(25),IBUF2(25),IGA(25),IGG(25)
      COMMON/BLK6/A1,A2,A3,DEMOM,AA1,AA2
      COMMON/BLK7/NOMB,NVAR,JPMAX,NBC,A,A1,A2,A3,AA,J,MES,N
      COMMON/BLB/NWB,NZ,NZ1,NZ2,NZ3,NCTYP
      DIMENSION NAME(3)
      DATA NAME/2HNE,2HNA,2NC /

      WRITE(LUN,999)
999 FORMAT(//20,'.5X','GLHT2' STARTS '.5X,20')
      NAME=1
      IF(NAME.EQ.0) GO TO 333
      MES1=NAME(MESMAX-1,1)
      DO 160 MES=MES1,MESMAX
      AA=MESMAX+1-MES
      N1=1
      IF(AA.NE.MESMAX) N1=NCONV(AA+1,4,2)+1
      A2=MAXELE
      IF(AA.NE.1) A2=NCONV(AA,1,1)-1
      WRITE(LUN,971) MES,AA,N1,A2
971 FORMAT('9 MES= ',2,5X,'AA= ',2,5X,'N1= ',4,5X,'A2= ',4)
      DO 170 A=A1,A2
      IG1=IGA(A,1)
      IG2=IGA(A,2)
      IG3=IGA(A,3)
      IF(IG1.EQ.0) GO TO 220
C
      NNB=4
      NB=IG1(IG2)-IG1(IG3)
      NY=IG1(IG3)-YB(IG2)
      A1=NY,NB
      A2=NY,NB
      A3=NCONV(NB,1,1)
C
      IF(AA.NE.1) GO TO 210
      IF(NCONV.EQ.0) GO TO 210
      DO 190 I=1,NCONV
      1 I=I

```

```

100 CONTINUE
    GO TO 110
110 MTYPE=0
    CALL FELMT
    GO TO 150
C
220 NMD=1
    IGA(1)=IG1
    IGA(2)=IG2
    IGA(3)=IG3
    MA=(IG(IG1)+IG(IG3)+IG(IG1)+IG(IG2)+
    IGA(IG3)+IG(IG1)+IG(IG2)+IG(IG1)+IG(IG3))*
    YG(IG2)+AG(IG1)+YG(IG3))
    K1=YG(IG1)+IG(IG3)
    K2=YG(IG1)+YG(IG1)
    K3=YG(IG1)+YG(IG2)
    A1=XG(IG1)+XG(IG2)
    A2=XG(IG1)+XG(IG3)
    A3=XG(IG2)+YG(IG1)
    C1=MA*B2/12.08CFOIS
    C2=MA*B2.0
    DENOM=C2
    ELMAT(1,1)=(B2*B2+A1*B2-2.08C1)
    ELMAT(1,2)=(B2*B1+A2*B1-C1)
    ELMAT(1,3)=(B3*B1+A3*B1-C1)
    ELMAT(2,2)=(B2*B2+A2*B2-2.08C1)
    ELMAT(2,3)=(B3*B2+A3*B2-C1)
    ELMAT(3,3)=(B3*B2+A3*B2-2.08C1)
C
230 CALL FILE
170 CONTINUE
C
235 CONTINUE
    WRITE(LUN,973) KK
973 FORMAT('  KK=',I2)
    IF(KK.EQ.1) GO TO 160
    DO 240 J=1,4
    K1=NCONH(KK,J,1)
    K2=NCONH(KK,J,2)
    N2=J+2-J/384
    IF(KK.NE.2) K3=NCONH(KK,J,3)
    N=0
    DO 250 K=K1,K2
    N=N+1
    IF(KK.NE.2) IGG(S)=K3+(N-1)*2
    IF(KK.EQ.2) IGG(S)=NCONH(K,J,N)
    MCTYP=-1
    CALL FELMT
250 CONTINUE
    IF(J.EQ.4) GO TO 240
    K=K2+1
    MCTYP=0
    CALL FELMT
240 CONTINUE
160 CONTINUE
C
    IA(NVAR+1)=JPMAX+1
    DO 270 M=1,NUAR
    II=IA(N)
    I2=IA(N+1)-1
    NO=MODINS+M-1
    DO 280 I=1,I2
    II=I
    IF(KK(II).EQ.NO) GO TO 290
280 CONTINUE
    WRITE(LUN,980)
980 FORMAT('ERROR IS DETECTED')
    STOP
290 IF(II.EQ.I1) GO TO 270
    MN=JA(II)
    A=AN(II)
    I3=I1+1
    DO 300 I=I3,I1
    IO=I3+II-1
    JA(IO)=JA(IO-1)
    AN(IO)=AN(IO-1)
300 CONTINUE
    JA(I1)=MN
    AN(I1)=A
270 CONTINUE
C
C *****APPLY THE BOUNDARY CONDITIONS
C IBPOT IS THE FLAG INDICATING THE TYPE OF BOUNDARY CONDITIONS
C IMPOSED ON THE OUTERMOST EDGES.
C IBPOT=1: PHI=0.0
C IBPOT=2: PHI=h/R
C IBPOT=3: PHI=h*EXP(-R/RDEBY)
C IBPOT=4: PHI=h*EXP(-R/RDEBY)/R
C
    WRITE(LUN,546) K,(AN(IA(I)),I=1,64)
333 IF(IBPOT.EQ.1) GO TO 510
    NMDB=0
    DEBA=RDEBY*2.0
    NMD=4
    DENOM=1.0
    DO 330 M=1,4
    DO 330 N=1,2
    K1=NDOUTER(M)
    K2=NDOUTER(N+1)
    IF(N.NE.4) K2=K2-1
    WRITE(LUN,547) M,K1,K2
547 FORMAT('M=',I3,5X,'K1=',I3,5X,'K2=',I3)
    L=0
    DO 340 K=K1,K2
    L=L+1
    MZ=M
    DO 350 I=1,4
    IGA(I)=IG(K,I)
    DO 350 J=1,4
    ELMAT(I,J)=0.0
350 CONTINUE
    IG1=IGA(1)
    IG2=IGA(2)
    IG3=IGA(3)
    IG4=IGA(4)
    MX=XG(IG2)+XG(IG1)
    MY=YG(IG3)+YG(IG2)
    MFG=0
    IF(A.EQ.R1.OR.A.EQ.A2) MFG=1
    IF(A.EQ.A1) MFG=1
340 GO TO 170,180,190,400,MZ
170 B1=XG(IG1)
    B2=MY
    K1=MX+YG(IG1)
    K2=IG1-410

```

```

01 R1=TO(IG,9)
R1=M
R3=ABS(XG(IG,1))
GO TO 410
190 R1=XG(IG,8)
R1=MZ
R1=ARS(TG(IG,4))
GO TO 410
400 R1=TO(IG,1)
R1=MZ
R3=ABS(XG(IG,1))
410 F1=P2*B7
IF(I*POT(EQ,1)-GO TO 430
R1=ATAM(B,BB)/N1A+KBB*2*(P1+B2)
D1=ALOG((1.0+R2/C).08B1B2)-(K1B2/K1B8B2)
F1=((R1+B2)*B2-B3B2)*B1B1B2-(K1B2/K1B8B2)*
F2=((R1+B2)/2.0)*B2-B2)*B3B2-K3B2-B3B2-B3B2-
F1*(B2-B3B2)*B1B1B2+(B2-B3B2)*B3B2
IF(IPOT(EQ,2)-GO TO 440
IF(IPOT(EQ,4)-GO TO 430
420 P1=+0
P2=+0
P3=+0
430 B4=SQRT(1.0+(B1B2/B3)*B2)
B5=SQRT(1.0+(B1/B3)*B2)
B6=B2/(B4*B5)*(B2/2.0B1/R3)
R7=B2*B3B4
R3=ACOS(1.0+(B2+B6)/(R1*B5B3))
F1=P1*(B7-(3.08B1+.08B2)*B6*(2.0B1-B2)*B2-B3B2)*B3B2
I/DEBA
P2=P2*((3.08B1+2.08B2)*B6-B7*(2.08B1*(B1-B2)+B3B2)*B3B2)
P3=P3*(B7-(3.08B1B6*(2.08B1B2-B3B2)*B3B2)/DEBA
440 P1=P1/E1
P2=P2/E1
P3=P3/E1
M1=MZ
M2=MZ+1-MZ/484
IF(MZ.LE.2)-GO TO 450
M1=MZ
M2=MZ
450 ELMAT(M1,M1)=ELMAT(M1,M1)+P1
ELMAT(M1,M2)=ELMAT(M1,M2)+P2
ELMAT(M2,M2)=ELMAT(M2,M2)+P3
IF(MZ.EQ.3)-ELMAT(3,4)=ELMAT(4,3)
WRITE(LUN,88B) L,P1,P2,P3
88B FORMAT('L=',I3,5X,'P1=',IPE12,5,
'5X','P3=',IPE12,5)
IF(MZ.EQ.0)-GO TO 500
NFLB=0
IF(K,EQ,K1) MZ=(MZ+1)+(5-NZ)/484
IF(K,EQ,K2) MZ=(MZ+1)-NZ/484
GO TO 360
500 CONTINUE
IF(K,NE,K1) BDIA(N,L)=BDIA(N,L)+ELMAT(N,M)
IF(K,EQ,K1) BDIA(N,L)=ELMAT(N,M)
IF(K,NE,K2) BDIA(N,L)=BDIA(N,L+1)+ELMAT(N+1,M)
IF(K,EQ,K2) BDIA(N,L)=BDIA(N+1,M)
DOFF(N,L)=ELMAT(N,M)
WRITE(LUN,507) K,(IGA(I),I=1,4)
507 FORMAT(5X,'K=',I3,5X,'IGA=',4I6)
WRITE(LUN,509)((ELMAT(I,J),J=1,4),I=1,4)
509 FORMAT(IPAE13,5)
CALL FILE
WRITE(LUN,568) K,(AN(IA(I)),I=1,64)
568 FORMAT('BK='//I3//IP10E13,5)
340 CONTINUE
330 CONTINUE
WRITE(LUN,732)
732 FORMAT('88 BDIA')
WRITE(LUN,733)((BDIA(N,L),L=1,20),N=1,2)
733 FORMAT(IP10E13,5)
WRITE(LUN,777)
777 FORMAT('88 DOFF')
WRITE(LUN,734)((DOFF(N,L),L=1,20),N=1,2)
734 FORMAT(IP10E13,5)
DO 1000 I=1,NMAX
I1=IA(I)
I2=IA(I+1)-1
WRITE(LUN,1001) I,(JA(J),J=1,I2)
1001 FORMAT(I3,3X,I2V)
WRITE(LUN,1002)(AK(J),J=1,I2)
1002 FORMAT(6X,I2V,4)
1000 CONTINUE
CALL EXEC(2,LU,BDIA,I2B,ITRACS+4,B1)
CALL EXEC(2,LU,DOFF,I2B,ITRACS+4,B3)
STOP
GO TO 800
510 NOMB=NOUTER(S)
NA=NOMB+1
DO 600 N=NA,NOMFS
IP1=IA(N)
IP2=IA(N+1)-1
DO 610 I=IP1,IP2
JP=JA(I)
IF(JP.GT.NOMB) GO TO 610
JA(I)=J
LAST=N
CONTINUE
600 CONTINUE
NC=1
IA(I)=1
NUM=0
DO 650 N=NA,LAST
IP1=IA(N)
IP2=IA(N+1)-1
DO 660 I=IP1,IP2
JP=JA(I)
IF(JP.EQ.-1) GO TO 660
NUM=NUM+1
JA(NUM)=JP
AK(NUM)=AK(I)
CONTINUE
NC=NC+1
IA(NC)=NUM+1
650 CONTINUE
ND=IP2+1
NB=LAST+1
NSUB=IA(NB)-IA(NC)
DB=NB+1
DO 700 N=NB,NOMFS
NC=NC+1
IA(NC)=IA(N)-NSUB
700 CONTINUE
NUM=NC
DO 10 I=N,NB,NPMAX
I=N-NSUB
AK(I)=AK(N)
JA(I)=IA(N)

```

[illegible]

1 104
 2 104
 3 104

[illegible]

6. 7. 8. 9. 10. 11. 12. 13. 14. 15. 16. 17. 18. 19. 20. 21. 22. 23. 24. 25. 26. 27. 28. 29. 30. 31. 32. 33. 34. 35. 36. 37. 38. 39. 40. 41. 42. 43. 44. 45. 46. 47. 48. 49. 50. 51. 52. 53. 54. 55. 56. 57. 58. 59. 60. 61. 62. 63. 64. 65. 66. 67. 68. 69. 70. 71. 72. 73. 74. 75. 76. 77. 78. 79. 80. 81. 82. 83. 84. 85. 86. 87. 88. 89. 90. 91. 92. 93. 94. 95. 96. 97. 98. 99. 100. 101. 102. 103. 104. 105. 106. 107. 108. 109. 110. 111. 112. 113. 114. 115. 116. 117. 118. 119. 120. 121. 122. 123. 124. 125. 126. 127. 128. 129. 130. 131. 132. 133. 134. 135. 136. 137. 138. 139. 140. 141. 142. 143. 144. 145. 146. 147. 148. 149. 150. 151. 152. 153. 154. 155. 156. 157. 158. 159. 160. 161. 162. 163. 164. 165. 166. 167. 168. 169. 170. 171. 172. 173. 174. 175. 176. 177. 178. 179. 180. 181. 182. 183. 184. 185. 186. 187. 188. 189. 190. 191. 192. 193. 194. 195. 196. 197. 198. 199. 200. 201. 202. 203. 204. 205. 206. 207. 208. 209. 210. 211. 212. 213. 214. 215. 216. 217. 218. 219. 220. 221. 222. 223. 224. 225. 226. 227. 228. 229. 230. 231. 232. 233. 234. 235. 236. 237. 238. 239. 240. 241. 242. 243. 244. 245. 246. 247. 248. 249. 250. 251. 252. 253. 254. 255. 256. 257. 258. 259. 260. 261. 262. 263. 264. 265. 266. 267. 268. 269. 270. 271. 272. 273. 274. 275. 276. 277. 278. 279. 280. 281. 282. 283. 284. 285. 286. 287. 288. 289. 290. 291. 292. 293. 294. 295. 296. 297. 298. 299. 300. 301. 302. 303. 304. 305. 306. 307. 308. 309. 310. 311. 312. 313. 314. 315. 316. 317. 318. 319. 320. 321. 322. 323. 324. 325. 326. 327. 328. 329. 330. 331. 332. 333. 334. 335. 336. 337. 338. 339. 340. 341. 342. 343. 344. 345. 346. 347. 348. 349. 350. 351. 352. 353. 354. 355. 356. 357. 358. 359. 360. 361. 362. 363. 364. 365. 366. 367. 368. 369. 370. 371. 372. 373. 374. 375. 376. 377. 378. 379. 380. 381. 382. 383. 384. 385. 386. 387. 388. 389. 390. 391. 392. 393. 394. 395. 396. 397. 398. 399. 400. 401. 402. 403. 404. 405. 406. 407. 408. 409. 410. 411. 412. 413. 414. 415. 416. 417. 418. 419. 420. 421. 422. 423. 424. 425. 426. 427. 428. 429. 430. 431. 432. 433. 434. 435. 436. 437. 438. 439. 440. 441. 442. 443. 444. 445. 446. 447. 448. 449. 450. 451. 452. 453. 454. 455. 456. 457. 458. 459. 460. 461. 462. 463. 464. 465. 466. 467. 468. 469. 470. 471. 472. 473. 474. 475. 476. 477. 478. 479. 480. 481. 482. 483. 484. 485. 486. 487. 488. 489. 490. 491. 492. 493. 494. 495. 496. 497. 498. 499. 500. 501. 502. 503. 504. 505. 506. 507. 508. 509. 510. 511. 512. 513. 514. 515. 516. 517. 518. 519. 520. 521. 522. 523. 524. 525. 526. 527. 528. 529. 530. 531. 532. 533. 534. 535. 536. 537. 538. 539. 540. 541. 542. 543. 544. 545. 546. 547. 548. 549. 550. 551. 552. 553. 554. 555. 556. 557. 558. 559. 560. 561. 562. 563. 564. 565. 566. 567. 568. 569. 570. 571. 572. 573. 574. 575. 576. 577. 578. 579. 580. 581. 582. 583. 584. 585. 586. 587. 588. 589. 590. 591. 592. 593. 594. 595. 596. 597. 598. 599. 600. 601. 602. 603. 604. 605. 606. 607. 608. 609. 610. 611. 612. 613. 614. 615. 616. 617. 618. 619. 620. 621. 622. 623. 624. 625. 626. 627. 628. 629. 630. 631. 632. 633. 634. 635. 636. 637. 638. 639. 640. 641. 642. 643. 644. 645. 646. 647. 648. 649. 650. 651. 652. 653. 654. 655. 656. 657. 658. 659. 660. 661. 662. 663. 664. 665. 666. 667. 668. 669. 670. 671. 672. 673. 674. 675. 676. 677. 678. 679. 680. 681. 682. 683. 684. 685. 686. 687. 688. 689. 690. 691. 692. 693. 694. 695. 696. 697. 698. 699. 700. 701. 702. 703. 704. 705. 706. 707. 708. 709. 710. 711. 712. 713. 714. 715. 716. 717. 718. 719. 720. 721. 722. 723. 724. 725. 726. 727. 728. 729. 730. 731. 732. 733. 734. 735. 736. 737. 738. 739. 740. 741. 742. 743. 744. 745. 746. 747. 748. 749. 750. 751. 752. 753. 754. 755. 756. 757. 758. 759. 760. 761. 762. 763. 764. 765. 766. 767. 768. 769. 770. 771. 772. 773. 774. 775. 776. 777. 778. 779. 780. 781. 782. 783. 784. 785. 786. 787. 788. 789. 790. 791. 792. 793. 794. 795. 796. 797. 798. 799. 800. 801. 802. 803. 804. 805. 806. 807. 808. 809. 810. 811. 812. 813. 814. 815. 816. 817. 818. 819. 820. 821. 822. 823. 824. 825. 826. 827. 828. 829. 830. 831. 832. 833. 834. 835. 836. 837. 838. 839. 840. 841. 842. 843. 84

Philosophy 310 21 x 3 = 1500

THIS IS THE MAIN ROUTINE FOR THE CURRENT COLLECTION SECTION
OF SYCLIC.

[illegible][illegible]

```

C      DOUBLE PRECISION FUNCTION ERFC(X)
C
C.....PURPOSE.....
C
C THIS F/P COMPUTES THE COMPLEMENTARY ERROR FUNCTION USING
C  "ORDER"TH CHEBYSHEV EXPANSION.
C
C.....DESCRIPTION OF THE VARIABLES.....

```

```

C
C CCMB(I):CMEDYSHEV COEFFICIENTS.
C CNB(I):CMEDYSHEV POLYNOMIALS.

```

```

C      DOUBLE PRECISION CMB,CMB+X,T,SUM
C      CMMW/CMB/CMB(31),IORDER
C      DIMENSION CMB(31)

C      T=(X-3.75D0)/(X+3.75D0)
C      CMB(1)=1.0D0
C      CMB(2)=T
C      DO 100 I=3,IORDER
C      CMB(I)=2.0D0*TCMB(I-1)-CMB(I-2)
100    CONTINUE
C      SUM=0.0D0
C      DO 150 I=1,IORDER
C      SUM=CMB(I)+CMB(I)
150    CONTINUE
C      ERFC=SUM/(1.0D0+2.0D0X)*DEXP(-XX)
C      RETURN
C      END
C      FUNCTION ATTR(XO,N)

```

```

C
C.....
C
C THIS F/P COMPUTES THE FOLLOWING
C ATTR(X,1)=F(X) FOR N=1
C ATTR(X,2)=F(X)*SORT(PI)/2.0 FOR N=2
C WHERE F(X)=2.0/SORT(PI)*SORT(X)*EXP(-X)*ERFC(SORT(X)).
C

```

```

C
DOUBLE PRECISION ERFC(X,Y),SUM,SGP12,MSGP12
DATA SGP12,MSGP12/1.12837916099531300,0.8462269254527500-1/

GO TO (10,20),N
IF(X0.EQ.0.0) GO TO 40
IF(X0.GT.34.0) GO TO 60
X=DBLE(X0)
Y=DBDR7(X)
SUM=SGP12*Y*DEXP(-X)+ERFC(Y)
GO TO 30
20 IF(X0.EQ.0.0) GO TO 50
IF(X0.GT.6.0) GO TO 60
Y=DBLE(X0)
X=Y*Y
SUM=Y*DEXP(-X)+MSGP12*ERFC(Y)
30 ATTN=SHDL(SUM)
RETURN
40 ATTN=1.0
RETURN
50 ATTN=SHDL(MSGP12)
RETURN
60 ATTN=0.0
RETURN
END
ENDS

```

FTN4
PROGRAM CNTRL(S.150)

```

C THIS CONTROLS 'XYCIC' RUNSTREAM.
C
COMMON/GENRL/LUMJ,NBPT,ICENTL,NFOUR,ITER,ACTIVE,
1,ITL,ITLJF,ITLINS(3)
COMMON/LODAI/LUM1,LUM2,LU,ITRACS,NTRACK(32),NITER
1
DIMENSION NAME1(3),NAME2(3),NAME3(3),NAME4(3),NAME5(3),
1,NAME6(3),NAME7(3),NAME8(3),ITLINS(3),ATLINS(3),BUP(32)
DATA NAME1/2NH0,2NH1,2NH1 // NAME2/2NH0,2NH5,2NH //
1 NAME3/2NH1,2NH0,2NH1 // NAME4/2NH0,2NH1,2NH //
2 NAME5/2NH0,2NH1,2NH1 // NAME6/2NH1,2NH1,2NH //
3 NAME7/2NH0,2NH1,2NH1 // NAME8/2NH0,2NH1,2NH //
DATA ITRIT/0/
C
IF (ICENTL.EQ.0) GO TO 10
IF (IFORROR.EQ.1) GO TO 1700
GO TO (100,110,130,150,170,200,220,230,240),ICENTR
C
F
R
C REAR ALL NECESSARY DATA.
10 WRITE (LUMJ,11)
11 FORMAT('====O =50= "PSYCHE" STARTS. =50=O =50=')
ICENTL=1
CALL INCBUS(1)
101 WRITE (LUMJ,101)
102 FORMAT(3,' FINISHED READING ALL DATA. ')

```

WRITE (UNIT=10)

[illegible]

```

IPI0ISS=1
NSTOP=NVAR/256+1
ISECT=0
ISTART=0
DO 40 N=1,NSTOP
CALL EXEC(1,U,BUFR*,1)*NTRACK(9),ISECT)
DO 50 I=1,256
AY(ISTART+I)=BUFR(I)
50 CONTINUE
ISECT=ISECT+8
ISTART=ISTART+256
40 CONTINUE
WRITE(LUNI,753) (AY(I),I=1,NVAR)
C 753 FORMAT(' * '(1P10F13.5))
NSTOP=NBC/256+1
ISECT=0
ISTART=0
DO 60 N=1,NSTOP
CALL EXEC(1,U,BUFR*256+NTRACK(9),ISECT)
CALL EXEC(1,U,JBUFR*256+NTRACK(9),ISECT(1674))
DO 70 I=1,256
II=ISTART+I
JBC(II)=JBURF(I)
JBC(II)=JBURF(I)
70 CONTINUE
ISTART=ISTART+256
ISECT=ISECT+4
60 CONTINUE
ISECT=48
ISTART=0
DO 80 N=1,NSTOP
CALL EXEC(1,U,BUFR*512+NTRACK(9),ISECT)
DO 90 I=1,256
YBC(ISTART+I)=BUFR(I)
90 CONTINUE
ISTART=ISTART+256
ISECT=ISECT+8
80 CONTINUE
WRITE(LUNI,738) NBC
C 738 FORMAT('NBC=',I5)
WRITE(LUNI,739) (IBC(I),I=1,NBC)
C 739 FORMAT('IBC'/'2515')
WRITE(LUNI,740) (JBC(I),I=1,NBC)
C 740 FORMAT('JBC'/'2515'))
DO 100 I=1,NBC
N=IBC(I)+1-NODINS
N=IBC(I)
NODE=JBC(I)
AY(N)=AY(N)-YBC(I)*POT(NODE)
100 CONTINUE
WRITE(LUNI,753) (AY(I),I=1,NVAR)
C 753 FORMAT(' * '(1P10F13.5))
NSTOP=NMOD/256+1
ISECT=0
ISTART=0
DO 110 N=1,NSTOP
DO 120 I=1,256
BUFR(I)=POT(I)*ISTART)
120 CONTINUE
CALL EXEC(2,U,BUFR*512+NTRACK(11),ISECT)
ISTART=ISTART+256
ISECT=ISECT+8
110 CONTINUE
DO TO(200,300),IP0ISB
FOR DOB=NMOD
C 200 CALL EXEC(S,NAME1)
FOR ICCB=METHOD
300 NSTOP=(NVAR+1)/256+1
ISECT=0
ISTART=0
DO 310 N=1,NSTOP
CALL EXEC(1,U,BUFR*256+NTRACK(6),ISECT)
DO 320 I=1,256
IA(ISTART+I)=BUFR(I)
320 CONTINUE
DO 340 I=1,256
BUFR(I)=AY(ISTART+I)
340 CONTINUE
CALL EXEC(2,U,BUFR*512+NTRACK(7),ISECT82)
ISECT=ISECT+4
310 CONTINUE
NSTOP=JPNAK/256+1
ITRACK=NTRACK(5)
ISECT=0
ISTART=0
DO 350 N=1,NSTOP
CALL EXEC(1,U,BUFR*256+ITRACK*ISECT)
DO 360 I=1,256
JA(ISTART+I)=BUFR(I)
360 CONTINUE
ISECT=ISECT+4
ISTART=ISTART+256
IF(MOD(N-24),NE.0) GO TO 350
ITRACK=ITRACK+1
ISECT=0
350 CONTINUE
WRITE(LUNI,753) (POT(I),I=1,NVAR)
C 753 FORMAT('POT'/'2515'))
WRITE(LUNI,753) (AP(I),I=1,NVAR)
C 753 FORMAT('AP'/'2515'))
WRITE(LUNI,800) (JA(I),I=1,NVAR)
C 800 FORMAT('JB'/'2515'))
WRITE(LUNI,800) (IB(I),I=1,NVAR)
C 800 FORMAT('IB'/'2515'))
IF(IP0ISS.EQ.2) CALL EXEC(S,NAME2)
ITRACK=NTRACK(3)
ISECT=0
ISTART=0
DO 400 N=1,NSTOP
CALL EXEC(1,U,BUFR*512+ITRACK*ISECT)
DO 410 I=1,256
AB(ISTART+I)=BUFR(I)
410 CONTINUE
ISECT=ISECT+8
ISTART=ISTART+256
IF(MOD(N-12),NE.0) GO TO 400
ITRACK=ITRACK+1
ISECT=0
400 CONTINUE
NSTOP=NMODIN/8+1
ISECT=0
ISTART=0
DO 420 N=1,NSTOP
CALL EXEC(1,U,BUFR*64+ITRACK*5*ISECT)
N=N
DO 430 I=1,N
II=INSTANT+I
NI 430 J=1,N
N=N+1
NI 430 II=1,NM(R)
END

```

FOR THE OUTERMOST BOUNDARIES.

$\rho = 2$
 $\mu = 101 + 0.0102$
 $\sigma(10) = 1.0102$
 $\sigma(10) = 1.0102$
 $\sigma(10) = 1.0102$

```

100 DO 200 J=1,4
101   I=MAX(J,1)-1
102   I=MAX(J,2)-1
103   I=MAX(J,3)-1
104   I=MAX(J,4)-1
105   CONTINUE
106   N=MIN(J,4)
107   DO 200 I=1,MAX(J,4)-1
108     FOR THE INTERIOR SPACE OF GRID.
109
110     DO 200 I=1,4
111       A=MAX(J,MAX(I,1))
112       N=N+1
113       IF (J.EQ.1) GO TO 200
114       K=START+1
115       SUM=A*(2)*8*(POT(L+1)+POT(L-1)+POT(N+1)+POT(N-1))+
116       I*(13)*8*(POT(L)+POT(N)+POT(N+1)+POT(N-1))
117       GO TO 270
118     200 K=START+3
119       L=L+3
120       SUM=A*(12)*8*(POT(L+1)+POT(L-1)+POT(N)+POT(L-3))+
121       I*(13)*8*(POT(L)+POT(L-2)+POT(N+1)+POT(N-1))
122       RES=SUM-POT(N)
123       POT(N)=POT(N)+OMEGA*RES
124       EPS=EPS+ABS(RES)
125       N=N+1
126       L=L+1
127       SUM=A*(12)*8*(POT(L+1)+POT(L-1)+POT(N+1)+POT(N-2))+
128       I*(13)*8*(POT(L)+POT(N)+POT(N+1)+POT(N-1))
129       270 POT(N)=POT(N)
130       POT(N)=POT(N)+OMEGA*RES
131       EPS=EPS+ABS(RES)
132       DO 280 K=K+START+MAX
133         N=N+1
134         N=N+1
135         L=L+1
136         NS=N+1
137         IF (J.EQ.4.AND.N.EQ.AMAX) NS=N+2
138         SUM=A*(12)*8*(POT(L+1)+POT(L-1)+POT(NS)+POT(N-1))+
139         I*(13)*8*(POT(L)+POT(N)+POT(N+1)+POT(N-1))
140         RES=SUM-POT(N)
141         POT(N)=POT(N)+OMEGA*RES
142         EPS=EPS+ABS(RES)
143         CONTINUE
144         N=N+1
145         N=N+1
146         L=L+1
147         NS=N+1
148         IF (J.EQ.4) GO TO 285
149         SUM=A*(12)*8*(POT(L+1)+POT(L-1)+POT(N+2)+POT(N-1))+
150         I*(13)*8*(POT(L)+POT(N)+POT(N+1)+POT(N-1))
151       GO TO 290
152     285 SUM=A*(12)*8*(POT(L+1)+POT(L-1)+POT(L+3)+POT(N-1))+
153       I*(13)*8*(POT(L)+POT(N)+POT(N+1)+POT(L+2)+POT(N-1))
154     290 RES=SUM-POT(N)
155       POT(N)=POT(N)+OMEGA*RES
156       EPS=EPS+ABS(RES)
157     250 CONTINUE
158       GO TO 230
159 C
160 C
161 FOR THE INNER EDGE OF GRID.
162
163 300 CONTINUE
164   IF (J.EQ.1) GO TO 345
165   DO 310 J=1,4
166     A=MAX(J,MAX(I,1))
167     N=N+1
168     IF (J.EQ.1) GO TO 320
169     I=(POT(L)+POT(N)+POT(N+1)+POT(L-1)+POT(N-2))+A*(13)*8
170     RES=SUM-POT(N)
171     POT(N)=POT(N)+OMEGA*RES
172     EPS=EPS+ABS(RES)
173     N=N+1
174     N=N+1
175     L=L+1
176     SUM=A*(12)*8*(POT(L+1)+POT(L-1)+POT(N-1))+A*(13)*8
177     I*(POT(L)+POT(N+1)+POT(N-1))+A*(14)*8POT(N)+A*(15)*8POT(N+1)+
178     2A*(16)*8POT(N+2)
179     GO TO 330
180   310 L=L+3
181     SUM=A*(12)*8*(POT(L+1)+POT(L-1)+POT(N)+POT(L-3))+A*(13)*8
182     I*(POT(L)+POT(N-2)+POT(N+1)+POT(N-1))
183     RES=SUM-POT(N)
184     POT(N)=POT(N)+OMEGA*RES
185     EPS=EPS+ABS(RES)
186     N=N+1
187     L=L+1
188     SUM=A*(12)*8*(POT(L+1)+POT(L-1)+POT(N-2))+A*(13)*8
189     I*(POT(L)+POT(N+1)+POT(N-1))+A*(14)*8POT(N)+A*(15)*8POT(N+1)+
190     2A*(16)*8POT(N+2)
191     330 RES=SUM-POT(N)
192     POT(N)=POT(N)+OMEGA*RES
193     EPS=EPS+ABS(RES)
194     DO 340 K=3+MAX
195       N=N+1
196       N=N+2
197       L=L+1
198       NS=N+2
199       IF (J.EQ.4.AND.K.EQ.AMAX) NS=N+2
200       SUM=A*(12)*8*(POT(L+1)+POT(L-1)+POT(N-1))+A*(13)*8
201       I*(POT(L)+POT(N+1)+POT(N-1))+A*(14)*8POT(N)+A*(15)*8POT(N+1)+
202       2A*(16)*8POT(N+2)
203       340 RES=SUM-POT(N)
204       POT(N)=POT(N)+OMEGA*RES
205       EPS=EPS+ABS(RES)
206       CONTINUE
207       N=N+1
208       N=N+2
209       L=L+1
210       IF (J.EQ.4) GO TO 342
211       SUM=A*(12)*8*(POT(L+1)+POT(L-1)+POT(N+2))+A*(13)*8
212       I*(POT(L)+POT(N+1)+POT(N-1))+A*(14)*8POT(N)+A*(15)*8POT(N+1)+
213       2A*(16)*8POT(N+2)
214       GO TO 344
215     342 SUM=A*(12)*8*(POT(L+1)+POT(L-1)+POT(L+3))+A*(13)*8
216       I*(POT(L)+POT(L+2)+POT(N-1))+A*(14)*8POT(N+1)+
217       2A*(15)*8POT(N-1)+A*(16)*8POT(N-2)
218     344 RES=SUM-POT(N)
219       POT(N)=POT(N)+OMEGA*RES
220       EPS=EPS+ABS(RES)
221   170 CONTINUE
222   100 CONTINUE
223
224 FOR THE INNERMOST GRID.
225
226 345 CONTINUE
227   M=MIN(M,N)-1
228   IF (M
229     DO 350 N=MIN(M,N)+MAX
230     L=L+1
231     M=M+1
232     IF (M
233     END

```

```

      SUM1=SUM1+POT*(X(1)-1)
      SUM2=SUM2+POT*(X(1)-1)
140 CONTINUE
      J=J+1
      IF (X(1)-1) 150,140,140
      IF (X(1)-1) 150,140,140
      IF (X(1)-1) 150,140,140
      IF (X(1)-1) 150,140,140
150 CONTINUE
C
      DO 170 N=1,NMAX
      IO=I+M
      II=IO+1
      I2=I+M+1
      NO=MOD(I2-1,N)
      SUM=0.0
      DO 160 J=1,I2
      SUM=SUM+AM*(I)POT*(I+J)
160 CONTINUE
      SUM=IAT*(N)-SUM/AM*(IO)
      RES=SUM-POT*(NO)
      POT=(NO)+SUM
      EPS=EPS+ABS(RES)
170 CONTINUE
C
      WRITE(LUNI,988) ITER,EPS
C 988 FORMAT('ITER=',I3,'X',EPS='IPE13.5)
      IF (ITER.GE.ITMAX) GO TO 510
      IF (EPS.LT.EPS) GO TO 510
      GO TO 2000
500 CALL EXEC(B,NAME,10,ITER)
C
510 CONTINUE
      CALL EXEC(B,NAME,20,ITER)
      STOP
      END
      ENDS

```

FTN4

```

      SENAI=AMN3(0)
      PROGRAM MENAR(5,150)
      DIMENSION I(10,2540),IMORA(254),CIOM(128),CELE(128),CPRO(128),
      2CPROM(128),CSEC(128),CSECM(128),CBSC(128),CBSCM(128),
      3CPH(128),CPHOM(128),PSECT(128),CSECT(128),PENIT(128),
      4XSP(128),YSP(128),XEP(128),YEP(128),XSEG(64),YSEG(64),
      5ISECT(64),YISECT(64),SLPSEC(64),IROOT(128),IDM(128),
      6MODBT(128),NCOM(128),NCOMV(128),NCOMM(128),NCON(128),
      7NEMTS(128),NEMTE(128),NSECT(128),NCOND(128),NPPAN(64),
      8NHSUP(128),ISLP(64),IUEC(64),MPAT(64),MCP(128),MCNA(128),
      9MCP(384),MCMC(128),MSP(128),MEP(128),MSUP(128),
      10COMMON/CHIST/MESNA,MAXMOD,MAXLE,MODOUT,MODIN,AELOUT,AEIN,
      11COMMON/IDAT/LUM1,LUM2,LU,ITRACS,NTRACK(32),ITER
      12COMMON/PSOLV/ISYN,IPOISS,IPOT,RDEBY,CPOIS,MMAR,JPMAR,NBC,
      13INORA,MODFS,MODINO,MODINS,MODINH
      DIMENSION IO(2540),YQ(2540)
      DIMENSION BUFR(254),IBUFR(128)
      DIMENSION NAME(3),LIST(5)
      EQUIVALENCE (AM(1),XQ),(AM(254),YQ)
      DATA NAME/2HDA,2HTA,2H3 /
C
      CALL RHPAR(LIST)
      WRITE(LUNI,999)
C 999 FORMAT(20,'X',MENAR(5),STARTS',5X,20',)
      ICODE=LIST(1)
      CALL EXEC(1,LU,IBUFR,128,NTRACK(19),16)
      IBUFR(ITER)=LIST(2)
      CALL EXEC(2,LU,IBUFR,128,NTRACK(19),16)
      NSTOP=MAXMOD/254+1
      ISECT=0
      DO 100 N=1,NSTOP
      DO 100 I=1,254
      BUFR(I)=POT(I+ISTART)
100 CONTINUE
      CALL EXEC(2,LU,IBUFR,512,NTR(1),ISECT)
      ISTART=ISTART+254
      ISECT=ISECT+8
100 CONTINUE
      IF (ICODE.EQ.10) GO TO 300
C
      WRITE(LUNI,151) (POT(I),I=1,MAXMOD)
C 151 FORMAT('P10E13.5)
      NSTOP=MAXMOD/254+1
      ISTART=0
      ISECT=0
      DO 140 N=1,NSTOP
      DO 140 I=1,254
      BUFR(I)=POT(I+ISTART)
140 CONTINUE
      CALL EXEC(2,LU,IBUFR,512,NTRACK(11),ISECT)
      CALL EXEC(1,LU,IBUFR,512,NTRACK(14),ISECT)
      DO 180 I=1,254
      XQ(I+ISTART)=BUFR(I)
180 CONTINUE
      CALL EXEC(1,LU,IBUFR,512,NTRACK(15),ISECT)
      DO 190 I=1,254
      YQ(I+ISTART)=BUFR(I)
190 CONTINUE
      ISTART=ISTART+254
      ISECT=ISECT+8
160 CONTINUE
      NSTOP=MAXLE/128+1
      DO 200 J=1,2
      ISTART=0
      ISECT=0
      IF (J.EQ.2) ISECT=40
      DO 210 N=1,NSTOP
      CALL EXEC(1,LU,IBUFR,128,NTRACK(16),ISECT)
      DO 220 I=1,128
      IG(I+ISTART)=IBUFR(I)
220 CONTINUE
      ISECT=ISECT+2
      ISTART=ISTART+128
210 CONTINUE
200 CONTINUE
      I=128+J+1
      ISTART=0
      ISECT=0
      IF (J.EQ.4) ISECT=60
      DO 240 N=1,NSTOP
      CALL EXEC(1,LU,IBUFR,128,NTRACK(16),ISECT)
      DO 250 I=1,128
      IG(I+ISTART)=IBUFR(I)
250 CONTINUE
      I=128+J+1
      ISTART=ISTART+128
      ISECT=ISECT+2
      IF (J.EQ.6) ISECT=80

```



```

      K=1000000
      DO 430 N=1,3
      IF(N.EQ.1) GO TO 435
      IF(N.EQ.2) GO TO 440
      IF(N.EQ.3) GO TO 445
      430 CONTINUE
      DO 435 L=1,3
      IF(L.EQ.1) GO TO 435
      IF(L.EQ.2) GO TO 435
      IF(L.EQ.3) GO TO 435
      435 CONTINUE
      DO 440 L=1,3
      IF(L.EQ.1) GO TO 440
      IF(L.EQ.2) GO TO 440
      IF(L.EQ.3) GO TO 440
      440 CONTINUE
      DO 445 L=1,3
      IF(L.EQ.1) GO TO 445
      IF(L.EQ.2) GO TO 445
      IF(L.EQ.3) GO TO 445
      445 CONTINUE
      DO 450 L=1,3
      IF(L.EQ.1) GO TO 450
      IF(L.EQ.2) GO TO 450
      IF(L.EQ.3) GO TO 450
      450 CONTINUE
      IF(N.EQ.1) GO TO 440
      CALL PLOT(XP(1),YP(1),3)
      CALL PLOT(XP(2),YP(2),2)
      440 CONTINUE
      410 CONTINUE
      475 IF(N.EQ.1) GO TO 50
      DO 480 M=1,MAX
      N1=IPLOT(M)
      N2=IG(N1,1)
      ZP(1,1)=POT(N2)*SCZ
      N3=IG(N1,4)
      ZP(1,2)=POT(N3)*SCZ
      N4=IG(N1,2)
      ZP(1,3)=POT(N4)*SCZ
      N5=IG(N1,3)
      ZP(1,4)=POT(N5)*SCZ
      XP(1)=XO(IG(N1,1))*SC
      XP(2)=XO(IG(N1,2))*SC
      YP(1)=YO(IG(N1,1))*SC
      YP(2)=YO(IG(N1,4))*SC
      DO 490 L=1,NCN
      CN=CNP(L)
      CALL CHTOUR(XP,2,YP,2,ZP,1DIRX,CN,SEP,CN)
      490 CONTINUE
      480 CONTINUE
      50 CONTINUE
      IF(N.EQ.1) GO TO 500
      CALL FINISH
      500 STOP
      END
      SUBROUTINE PAPLY(NCN,CNP)
      DIMENSION CNP(10)
      DATA NCN/2/
      DATA CNP/50.0,55.0/
      RETURN
      END
      INDS

```

FILM

7-